



PACIFIC EARTHQUAKE ENGINEERING RESEARCH CENTER

Van Nuys Hotel Building Testbed Report: Exercising Seismic Performance Assessment

Helmut Krawinkler
Editor

Department of Civil and Environmental Engineering
Stanford University

Van Nuys Hotel Building Testbed Report: Exercising Seismic Performance Assessment

Helmut Krawinkler

Editor

Department of Civil and Environmental Engineering
Stanford University

PEER Report 2005/11
Pacific Earthquake Engineering Research Center
College of Engineering
University of California, Berkeley

October 2005

Contributing authors:

Hesaam Aslani	Stanford U.
Jack Baker	Stanford U.
C. Allin Cornell	Stanford U.
Jon Heintz	Degenkolb Engineers
Tara Hutchinson	UC Irvine
Ufuk Ince	U. of Washington
Helmut Krawinkler	Stanford U.
Steven Kramer	U. of Washington
Bruce Kutter	UC Davis
Laura Lowes	U. of Washington
Geoffrey Martin	USC
Jack Meszaros	U. of Washington
Eduardo Miranda	Stanford U.
Takuya Nagae	Stanford U.
Robert Pekelnicky	Degenkolb Engineers
Keith Porter	California Institute of Technology
Kim Shoaf	UCLA
Hope Seligson	ABS Consulting
Paul Somerville	URS Greiner
Farzin Zareian	Stanford U.

ABSTRACT

Beginning with the Year 5 Research Program, PEER established a series of PEER Methodology Testbeds. The testbeds are real facilities, inventories of facilities, or networks to which the PEER performance-based earthquake engineering assessment methodologies can be applied. The primary purpose of the testbeds is to assess the applicability of the methodologies and foster their refinement. The testbeds serve supplementary purposes such as further focusing and integrating the research, promoting multi-disciplinary research interactions, emphasizing systems-level research, and involving interested earthquake professionals and decision makers.

The testbed study documented in this report is concerned with a hotel building in Southern California for which the primary performance issues are (a) financial losses due to structural and nonstructural damage and (b) the probability of collapse, which will dominate the life-safety issue. The building is an older reinforced concrete building representative of a class of buildings constructed in the 1960s in the western U.S. Instrumental records and damage from past earthquakes make it suitable for verifying analytical models and simulation platforms, while its seismic deficiencies make it suitable for rigorous implementation of the assessment methodology.

An attempt is made to illustrate how individual parts of a seismic performance assessment process can be executed in order to provide information that is needed downstream for decision making based on predicted performance. What sets the illustrated process apart from presently employed engineering approaches is the explicit consideration of important uncertainties and their propagation through the performance assessment process. The study did disclose that there are gaps in knowledge, tools, and data that need to be filled in order to permit widespread implementation of probabilistic performance assessment, but that the proposed methodology is sound and will lead to performance interpretations of much value in decision making and risk management.

ACKNOWLEDGMENTS

This report summarizes selected results from a series of research projects in which methods and tools for performance assessment were developed and tested. Only one project was concerned specifically with the testbed building, whereas in all other projects the researchers made a commitment to apply their research ideas and concepts to specific aspects of the performance assessment of the testbed building. Participation in the testbed was a collaborative activity that required a commitment on the part of the participating PEER researchers to define and deliver milestones, coordinate research activities, share results with other testbed participants, and participate in a series of testbed meetings.

The Van Nuys testbed study became a true team effort in which investigators sacrificed parts of their individual research plans and objectives for the good of the testbed study. Researchers and authors of this report made compromises in their approaches to accommodate the needs of the testbed for a consistent methodology to the various aspects of performance assessment. The editor exercised a heavy hand in rewording manuscripts so that they became parts of a, hopefully, consistent story. All other authors tolerated this heavy hand, for which the editor is most grateful. Thus, the credit goes to the authors of individual sections, who are listed at the beginning of this report.

This work was supported by the Earthquake Engineering Research Centers Program of the National Science Foundation under award number EEC-9701568 through the Pacific Earthquake Engineering Research Center (PEER). Any opinions, findings, and conclusions or recommendations expressed in this material are those of the author(s) and do not necessarily reflect those of the National Science Foundation.

CONTENTS

ABSTRACT.....	iii
ACKNOWLEDGMENTS	iv
TABLE OF CONTENTS	v
LIST OF FIGURES	vii
LIST OF TABLES	ix
1 THE PEER PERFORMANCE ASSESSMENT METHODOLOGY AND ITS APPLICATION TO THE VAN NUYS HOTEL BUILDING	1
1.1 Background	1
1.2 Objectives and Scope	2
1.3 The PEER PBEE Methodology	3
1.4 Report Outline	7
2 THE VAN NUYS HOTEL BUILDING.....	9
2.1 Building Description	9
2.2 Structural System	11
2.3 Architectural Finishes and MEP Components	17
2.4 Site Conditions	17
2.5 Fundamental Period of the Structure	18
3 HAZARD ANALYSIS AND REPRESENTATION OF GROUND MOTIONS	19
3.1 The Role of Hazard Analysis in Performance Assessment.....	19
3.2 Free-Field Ground Motion Hazard Analysis.....	20
3.3 Variability and Uncertainty in the Ground Motion Hazard	27
3.4 IM Selection for the Van Nuys Building and Its Implications	30
3.5 Effects of Site Soil Profile on IMs and Ground Motions.....	37
4 ENGINEERING ANALYSIS AND PREDICTION OF EDPs.....	49
4.1 Foundation Modeling and Effects of SSI on EDPs.....	49
4.2 Analytical Models of Structural System	52
4.3 Validation of Numerical Models.....	59
4.4 Prediction of EDPs for Damage Assessment.....	72
4.5 Prediction of Probability of Collapse.....	85

5	PREDICTION OF LOSSES.....	95
5.1	Connecting Structural Analysis with Damage and Loss Analysis.....	95
5.2	Damage Estimation	97
5.3	Loss Estimation.....	101
5.4	Application of Loss Estimation Methodology.....	103
6	PROPAGATION OF UNCERTAINTIES FROM IM TO DV	113
6.1	Sources of Uncertainties	113
6.2	Tornado Diagram Analysis	115
6.3	Monte Carlo Simulation for Studying the Body of a DV Distribution.....	118
6.4	FOSM for Estimating the First Two Moments of DV.....	121
6.5	Consideration of Correlations	123
6.6	Reliability Methods for Modeling Low-Probability Events	125
7	RELATION TO PRESENTLY ACCEPTED ENGINEERING APPROACHES....	127
7.1	Current Practice of Seismic Evaluation and Strengthening.....	127
7.2	Engineering Evaluation of the Van Nuys Testbed Building.....	132
7.3	FEMA 356 Rehabilitation Design.....	150
7.4	Engineering Assessment of the PEER PBEE Methodology	160
8	PBEE ADOPTION AND DECISION MAKING	163
8.1	Introduction.....	163
8.2	Past Investment Decisions	164
8.3	Enabling a PBEE Mind-Set.....	168
8.4	A PBEE-Enabled Seismic Investment Decision Support System.....	172
8.5	Lessons for PBEE Implementation and Diffusion.....	181
	APPENDIX A. PAST EARTHQUAKE DAMAGE IN VAN NUYS BUILDING.....	183
	APPENDIX B. COMPONENT FRAGILITY FUNCTIONS	193
	APPENDIX C. SUMMARY OF LOSS ESTIMATION METHODOLOGY	207
	APPENDIX D. FATALITY MODEL FOR NON-DUCTILE CONCRETE FRAME STRUCTURES DEVELOPED FROM GÖLCÜK POPULATION SURVEY DATA	217
	REFERENCES.....	237

LIST OF FIGURES

Fig. 1.1	Overview of PEER performance assessment methodology	4
Fig. 2.1	Location of the testbed building (near center of map).....	10
Fig. 2.2	Tested building (star) relative to 1971 and 1994 earthquakes (EERI, 1994)	10
Fig. 2.3	Column layout (three bays in transverse direction, eight in long. direction)	11
Fig. 2.4	Floor beam and floor spandrel beam plans.....	12
Fig. 2.5	South frame elevation with element numbers	13
Fig. 2.6	Arrangement of column steel (Riesman and Riesman Associates, 1965).....	13
Fig. 3.1	Uniform hazard spectra for the Van Nuys site for three levels of annual accidence probability.....	22
Fig. 3.2	Hazard Curve for the 1.5 sec S_a for the Van Nuys Site, based on the USGS website results and modified for local site conditions	23
Fig. 3.3	Disaggregation of the hazard for $S_a(T = 1.5 \text{ s}) \geq 0.53g$ at the Van Nuys site.....	24
Fig. 3.4	Variability in the spectral accelertions of each set of ten scaled recordings for the longitudinal component for each of three ground-motion levels.....	28
Fig. 3.5	Epistemic uncertainty in the 1.5 sec S_a hazard curve at the Van Nuys site.....	29
Fig. 3.6	Boring logs for Van Nuys testbed site.....	39
Fig. 3.7	Base case shear wave velocity profile	41
Fig. 3.8	Rock outcrop response spectra for 10%/50 yr hazard level (a) spectra for individual motions, and (b) mean and mean $\pm \sigma$ spectra	42
Fig. 3.9	Response of SDOF structure with $T_l = 1.5 \text{ sec}$, $R = 4$, and $\alpha = 0.05$	43
Fig. 3.10	Results of Monte Carlo simulations for Motion 6	47
Fig. 3.11	Results of Monte Carlo simulations for Motion 13	47
Fig. 4.1	Illustration of probabilistic seismic demand analysis (Krawinkler & Miranda, 2004)	51
Fig. 4.2	Example of drift hazard curve (Krawinkler et al., 2003).....	51
Fig. 4.3	Foundation plan and primary types of pile-pile-cap combinations	53
Fig. 4.4	Results of p - y pushover analysis compared to stiffness of uncoupled elastic spring	56
Fig. 4.5	Elevation of Van Nuys building exterior frame with piles and p - y springs	57
Fig. 4.6	Comparison of spectra of original surface motions, deconvolved motion at 13 m, and surface motion output from nonlinear soil column analysis.....	58
Fig. 4.7	Base shear versus roof displacement for baseline OpenSees1 model	65

Fig. 4.8	Base shear versus roof displacement for baseline OpenSees2 model	65
Fig. 4.9	Roof displacement during the Northridge earthquake (1994), as computed from sensor data (“observed”) and as predicted using the OpenSees1 model	67
Fig. 4.10	Frame member curvature ductility demands under Northridge earthquake ground motion as predicted using the OpenSees1 model	67
Fig. 4.11	Roof displacement during the Northridge earthquake (1994), as computed from sensor data (observed) and as predicted using the OpenSees2 model.....	68
Fig. 4.12	Frame member curvature ductility demands under Northridge earthquake ground motion as predicted using the OpenSees2 model	68
Fig. 4.13	Base shear versus roof displacement pushover curves for different models	72
Fig. 4.14	Maximum interstory drifts for 50/50 ground motion records.....	73
Fig. 4.15	Maximum interstory drifts for 10/50 ground motion records.....	73
Fig. 4.16	Maximum interstory drifts for 2/50 ground motion records.....	74
Fig. 4.17	Impact of global system modeling parameters on EDP prediction	75
Fig. 4.18	Impact of element model parameters on EDP prediction	76
Fig. 4.19	Impact of column failure model parameters on EDP prediction	78
Fig. 4.20	Impact of material model parameters on EDP prediction	79
Fig. 4.21	Maximum interstory drift at the 50/50 hazard level for different models	82
Fig. 4.22	Maximum interstory drift ratio from IDAs, “Drain T ₁ =1.5sec.” model	83
Fig. 4.23	Maximum roof drift ratio from IDAs, “Drain T ₁ =1.5sec.” model.....	83
Fig. 4.24	Impact of period variation on EDP prediction.....	84
Fig. 4.25	Collapse fragility curve based on “OpenSees1” model	86
Fig. 4.26	Collapse fragility curve based on “Drain T=1.5sec.” model	86
Fig. 4.27	Collapse fragility curve based on a bilinear nondegrading hinge model, MCB.....	87
Fig. 4.28	Comparison of collapse fragility curves for the testbed structure with and without considering the possibility of having a collapse triggered by the loss of vertical carrying capacity in structural elements	88
Fig. 4.29	Collapse fragility curve based on “Drain T=1.1sec.” model	90
Fig. 4.30	Mean annual S_a hazard curves and annual probability of collapse for “Drain T ₁ =1.5sec.” and “Drain T ₁ =1.1sec.” models	90
Fig. 5.1	Fragility functions corresponding to damage measures dm_1 and dm_2 in slab-column connections	99
Fig. 5.2	Fragility surface for punching shear failure in slab-column connection as a function of the interstory drift ratio and normalized gravity shear force	100
Fig. 5.3	Distribution of cost of nonstructural components in the building	100

Fig. 5.4	Fragility functions of metal stud gypsum board partitions.....	101
Fig. 5.5	Loss functions of metal stud gypsum board partitions.....	102
Fig. 5.6	Graphic representation of the computation of expected losses (in millions of dollars) as a function of the ground motion intensity.....	106
Fig. 5.7	(a) Dollar loss in the testbed structure associated with a 20% probability of exceedance in ground motion with an intensity of 0.32g; (b) Probability of experiencing a loss larger than 4 million dollars in an event with a ground motion intensity of 0.32g.....	108
Fig. 5.8	Dollar losses in the testbed structure associated with a 10% probability of being exceeded for two levels of ground motion intensity.....	108
Fig. 5.9	Loss curve computed for the Van Nuys testbed structure.....	109
Fig. 5.10	Graphic representation of the computation of expected downtime (in days) as a function of the ground motion intensity.....	111
Fig. 6.1	Tornado diagram analysis of Van Nuys testbed by Porter et al. (2002a).....	117
Fig. 6.2	Results of MCS analysis.....	120
Fig. 7.1	Site specific response spectra.....	136
Fig. 7.2	Modal load pattern.....	139
Fig. 7.3	Uniform load pattern.....	139
Fig. 7.4	Typical FEMA 356 backbone curve.....	141
Fig. 7.5	Shear controlled backbone curve.....	141
Fig. 7.6	Column splice hinge backbone curve.....	141
Fig. 7.7	Nonlinear pushover curves for two load patterns.....	143
Fig. 7.8	Annotated modal pattern pushover curve.....	144
Fig. 7.9	Annotated uniform pattern pushover curve.....	145
Fig. 7.10	Scheme 1 — Shear wall elevation.....	152
Fig. 7.11	Scheme 2 — Shear wall elevation.....	153
Fig. 7.12	Scheme 2 — Concrete frame upgrade details.....	153
Fig. 7.13	Scheme 3 — Typical floor plan.....	154
Fig. 7.14	Scheme 3 — Shear wall and fiber-wrap elevation.....	155
Fig. 7.15	Scheme 3 — New shear wall pier detail.....	156
Fig. 7.16	Scheme 3 — New shear wall spandrel beam detail.....	156
Fig. 7.17	Scheme 3 — Foundation plan.....	158
Fig. 7.18	Scheme 3 — Typical new wall foundation.....	158
Fig. 7.19	Strengthened building pushover curve.....	159

Fig. 8.1	The process of creating a PBEE decision support system.....	172
Fig. 8.2	Repair cost loss curve and its variations under two retrofit assumptions.....	175
Fig. 8.3	Financial decision metrics for two different mitigation levels	178
Fig. 8.4	Decision/trade-off table presenting financial and non-financial DVs	178
Fig. 8.5	Simulated structural loss net present value distributions.....	179
Fig. A.1	Instrument locations in 1971 San Fernando earthquake.....	184
Fig. A.2	Spectral acceleration, 1971 ground-floor motions, longitudinal (left) and transverse (right).....	184
Fig. A.3	Instrument locations after 1980	186
Fig. A.4	Spectral acceleration of ground-floor motions, 1994 longitudinal (left) and transverse (right).....	188
Fig. A.5	Structural damage in 1994 Northridge earthquake, south frame (Trifunac et al., 1999).....	190
Fig. A.6	Structural damage in 1994 Northridge earthquake, north frame (Trifunac et al., 1999).....	190
Fig. A.7	Shearwalls added to south (left) and north frames (right) after the 1994 Northridge earthquake. (Left: lines A-3, 7 and 8 from near to far. Right: lines D-8, 7, 5, and 3).....	191
Fig. B.1	Fragility functions corresponding to damage measures dm_1 and dm_2 in slab-column connections	195
Fig. B.2	Fragility surface for punching shear failure in slab-column connection as a function of the interstory drift ratio and normalized gravity shear force	196
Fig. B.3	Fragility function corresponding to damage measure dm_1 in columns.....	197
Fig. B.4	Fragility surface for axial failure in columns	197
Fig. B.5	Fragility functions corresponding to damage measures in interior beam-column connections	199
Fig. B.6	Fragility functions corresponding to damage measures in interior beam-column connections	200
Fig. B.7	Sensitivity chart of nonstructural components in Van Nuys building.....	201
Fig. B.8	Fragility functions of metal stud gypsum board partitions.....	202
Fig. B.9	Fragility curves of sliding windows	203
Fig. B.10	Fragility curves of acoustical suspended ceilings.....	204

LIST OF TABLES

Table 2.1	Column reinforcement schedule.....	14
Table 2.2	Spandrel beam reinforcement schedule, floors 3 through 7	15
Table 2.3	Roof and second-floor spandrel beam reinforcement schedule.....	16
Table 2.4	Computed fundamental period for Van Nuys Building at the beginning of the Northridge earthquake	18
Table 3.1	Disaggregation of the mean annual frequency of exceedance of three levels of the IM (see footnote 6) at the Van Nuys building soil	24
Table 3.2	Standard deviations of natural logs of EDPs for several IMs. Three models of the Van Nuys building and three sets of recordings, for two EDPs: max. IDR and max. PFA	34
Table 3.3	Interpreted soil profile for Van Nuys building site from available subsurface information	40
Table 3.4	Assumed coefficients of variation for rock, soil, and structural properties.....	44
Table 4.1	Preliminary recommendations for elastic vertical, horizontal and rotational spring stiffnesses	56
Table 4.2	Data and statistics of modeling parameter study — pushover analyses.....	80
Table 4.3	Data and statistics of modeling parameter study — dynamic analyses using Northridge earthquake ground motion	80
Table 5.1	Definition of damage measures, <i>DM</i> , in structural components	99
Table 6.1	Examples of sources of uncertainty in PBEE analysis.....	114
Table 6.2	Parameters of the sensitivity study	117
Table 7.1	Summary of reference codes, standards, and guidelines used in practice.....	129
Table 7.2	Modal periods and participating mass ratios	142
Table 7.3	Target displacements for various hazard levels.....	146
Table 8.1	Potential private and public benefits from PBEE in case of major earthquakes	163
Table 8.2	Consortium owners’ repair and retrofit considerations	166
Table 8.3	Current owner’s EQ preparation considerations	168
Table 8.4	Contrasts in “mind-sets” associated with code- vs. performance-based earthquake engineering practice	171
Table 8.5	Summaries of engineering-based, interdisciplinary discussions of client needs and PEER-PBEE capabilities	173
Table A.1	Approximate fundamental building periods (Islam, 1996)	185

Table A.2	Events causing strong motion (Trifunac et al., 1999; CSMIP, 1994)	187
Table A.3	Recorded peak displacements and story drift ratios	189
Table B.1	Definition of damage measures, <i>DM</i> , for structural components.....	194
Table B.2	Statistical parameters for fragility and loss functions of slab-column connections	195
Table B.3	Statistical parameters for fragility and loss functions of columns	197
Table B.4	Statistical parameters for fragility and loss functions of interior beam-column connections	198
Table B.5	Statistical parameters for fragility functions of interior beam-column connections	199
Table B.6	List of main nonstructural components in the testbed building	200
Table B.7	Parameters of fragility and loss functions of gypsum-board partitions.....	201
Table B.8	Parameters of fragility and loss functions for sliding windows	202
Table B.9	Description and parameters of fragility curves of acoustical ceilings.....	204
Table B.10	Statistical parameters for fragility and loss functions of generic nonstructural drift sensitive components.....	205
Table B.11	Statistical parameters for fragility and loss functions of generic nonstructural acceleration sensitive components	205
Table D.1	Age distribution of individuals in sample	218
Table D.2	Distribution of construction of buildings	219
Table D.3	Distribution of injury/death across age categories	220
Table D.4	Survey responses used to categorize buildings as having suffered “Partial Collapse” and “Total Collapse”.....	222
Table D.5	Characteristics of the sample subset ($n = 517$).....	225
Table D.6	Fatality rates by partial or total building collapse	226
Table D.7	Fatality rates by gender and type of building collapse	227
Table D.8	Fatality rates by age group and type of building collapse	227
Table D.9	Fatality rates by movement during the earthquake and type of building collapse	228
Table D.10	Fatality rates by movement during the earthquake and type of building collapse	228
Table D.11	Fatality rates by building height and by type of building collapse.....	229
Table D.12	Fatality rates by occupant’s floor location within building and type of building collapse	229
Table D.13	Fatality rates by occupant’s floor location, conditional on building height and type of building collapse	230

Table D.14	Fatality odds ratio for age.....	231
Table D.15	Fatality rates by age group conditional on occupant’s floor location within a 5–10 floor building that totally collapsed.....	232
Table D.16	ATC-13 injury and death rates* (after Table 9.3, ATC, 1985)	233
Table D.17	HAZUS® Earthquake loss estimation methodology casualty rates (HAZUS®99, SR-2).....	234
Table D.18	HAZUS® Earthquake loss estimation methodology injury severity class definitions (HAZUS®99, SR-2).....	234
Table D.19	Comparison of PEER NDCF fatality model to published models	236

1 The PEER Performance Assessment Methodology and Its Application to the Van Nuys Hotel Building

Authors: H. Krawinkler, K. Porter

1.1 BACKGROUND

Since its inception in 1997, PEER has focused on the development of methodologies and tools for performance-based earthquake engineering. Performance-based earthquake engineering (PBEE) implies design, evaluation, and construction of engineered facilities whose performance under common and extreme loads responds to the diverse needs and objectives of owners-users and society. It is based on the premise that performance can be predicted and evaluated with quantifiable confidence in order to make, together with the client, intelligent and informed trade-offs based on life-cycle considerations rather than construction costs alone. So far, PEER has focused on methods of performance assessment, with due consideration given to the effects of all important uncertainties that enter the performance prediction process, from earthquake occurrence modeling to the assessment of earthquake consequences such as dollar losses or casualties.

If it were not for uncertainties, the performance prediction process would be rather straightforward and would mimic what good engineering companies practice today. Present practice is to describe the earthquake intensity deterministically at discrete hazard levels, develop a deterministic model of the structure, and predict, deterministically, response parameters such as story drifts, which are compared to deterministic limits (e.g., story drift ≤ 0.02) in order to judge adequacy of a design. It is well established that uncertainties in each part of this process make

performance assessment so much more complex, but also so much more realistic. The PEER PBEE methodology tries to face up to these complexities.

Much of the PEER development effort has been directed towards individual parts of the complex process of probabilistic performance assessment. It needs to be found out how the parts of this methodology fit together to make a whole that (1) leads to consistent, understandable, and repeatable end results, (2) has most of the important parts in place, (3) can be put in perspective with respect to presently employed engineering approaches, (4) can be implemented by the profession, and (5) can be interpreted by all stakeholders in an understandable manner that helps individuals and organizations to make informed decisions.

1.2 OBJECTIVES AND SCOPE

To address the aforementioned questions, PEER has created a testbed program in which different parts of the PBEE methodology have been applied, tested, and modified as needed, on several testbed structures. In the building domain, two testbed structures have been utilized, one the UC Berkeley Science Building and the other the Van Nuys Hotel Building. This report is concerned with the latter.

There are many parts and variations to the PBEE methodology being developed in PEER, which is briefly summarized in Section 1.3. The testbeds were selected so that their location, site condition, structural configuration, use, and decision impact differ to the extent that complementary parts of the PBEE methodology can be tested in the performance assessment process. For the Van Nuys hotel building, the primary performance issues are dollar losses due to structural and nonstructural damage, and the probability of collapse that will dominate the life safety issue. The building is a relatively old reinforced concrete frame building (built in the 60-ies) but is located on firm soil and in an area in which near-fault ground motions are not prevalent. On the other hand, the UC Berkeley Science Building is a relatively new frame structure, but is located in an area in which near-fault ground motions dominate the long return period hazard, and its use as a science building makes content performance the dominant behavior issue.

For the Van Nuys hotel building the emphasis is on loss estimation and collapse prediction. The seismic hazard and ground motion issues are relatively straightforward, and so

are the soil-foundation-structure interaction issues. The challenges are in the prediction of engineering demand parameters (EDPs), which are needed for damage assessment and collapse prediction, and on the loss estimation side in the need to develop damage state fragility functions and loss functions that permit rational loss estimation, considering structural and important nonstructural components and systems. These issues will receive much attention in this report.

In addition to testing the processes developed within PEER, engineering practitioners involved in the testbed project have compared the PEER methodology with current practice to identify strengths and development needs relative to other approaches. This comparison should help to guide our research and ensure that it meets practitioner expectations and capabilities, and that the PEER methodology contributes materially to the value practitioners can offer to users and society.

1.3 THE PEER PBEE METHODOLOGY

The PEER performance assessment methodology has been summarized in various publications; the following ones serve as references for the interested reader: Cornell and Krawinkler, 2000, Krawinkler, 2002, Deierlein et al., 2003, Krawinkler and Miranda, 2004, Moehle and Deierlein, 2004. This summary discussion is concerned with performance assessment of buildings.

The PEER performance assessment methodology is illustrated in Figure 1.1. As shown in the figure, the methodology embodies four stages: hazard analysis (the quantification of the frequency and intensity of earthquakes and of the ground motions that represent the effects of earthquakes at a particular site), structural analysis (the quantification of the response quantities needed for loss, downtime, collapse and casualty evaluation [i.e., collapse analysis, shown separately in Figure 1.1, can be viewed part of structural analysis]), damage analysis (the quantification of damage states and their relation to response parameters), and the evaluation of losses, downtime and casualties, and their consequences for the owner and society.

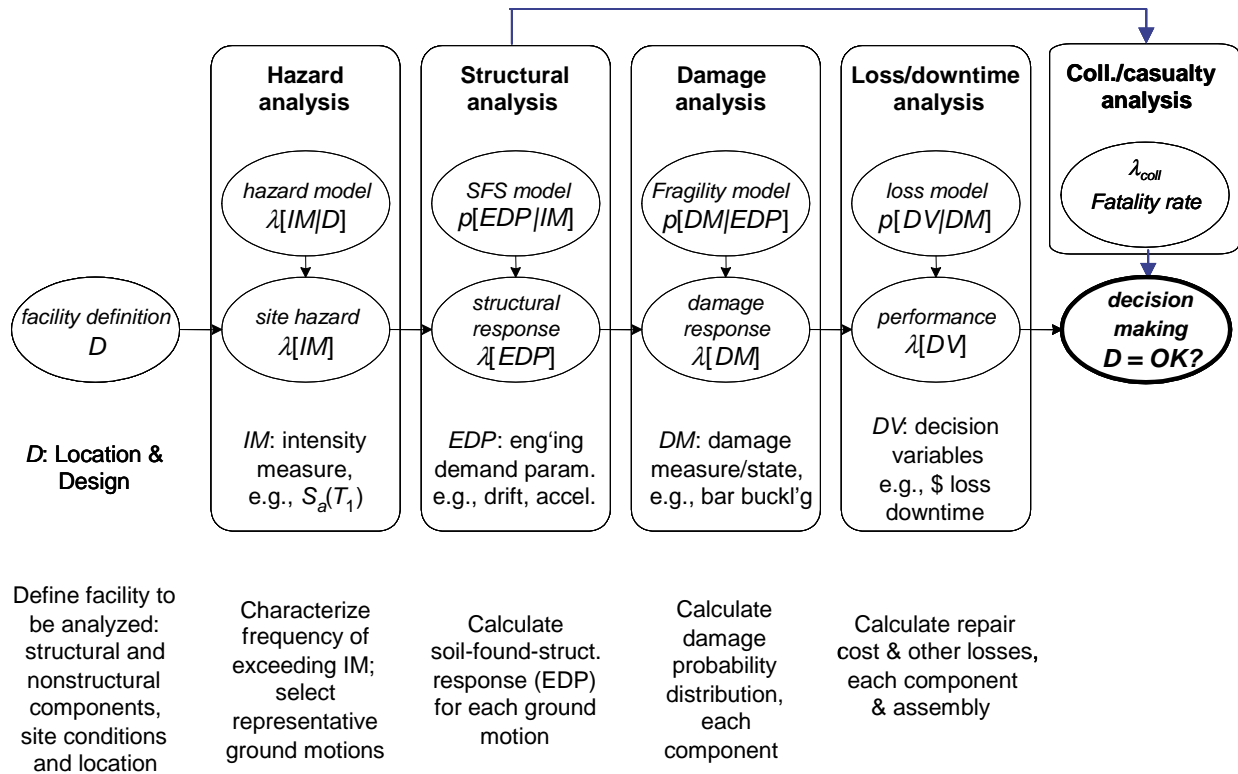


Fig. 1.1 Overview of PEER performance assessment methodology

The end of the process is a consequence analysis, which necessitates the quantification (in probabilistic terms) of variables that can be employed to judge consequences. These variables are denoted as **decision variables, DVs**. Examples are dollar losses, length of downtime, or number of casualties. The task at hand is to compute these *DVs*, given that all relevant building systems, i.e., the soil/foundation/structure system as well as the nonstructural and content systems, are known and that sufficient information is available to quantify seismic input, structural response, damage, cost of repair, length of business interruptions (downtime), and the probability of collapse, which then needs to be related to the expected number of casualties. In the assessment process the key issue is to identify and quantify, with due consideration to all important uncertainties, decision variables of primary interest to the decision makers. The components of the assessment process can be briefly summarized as follows.

Hazard analysis. The first step is to calculate the seismic hazard, quantified here as the frequency with which specific values of a relevant scalar or vector **intensity measure (IM)** are exceeded. If a scalar *IM* is used, such as the 5% damped spectral acceleration at the first mode

period, $S_a(T_I)$, the hazard usually is defined in terms of a seismic hazard curve. The outcome of a probabilistic seismic hazard analysis (PSHA), which forms part of the input to structural analysis, is usually expressed in terms of a mean annual frequency (MAF) of exceedance of $IM(s)$, i.e., $\lambda(IM)$, as shown in the lower half of the first box of Figure 1.1. A challenge that will be discussed in Chapter 3 is the selection of ground motions, which, when scaled to the selected IM, provide an efficient and sufficient means to represent the ground motion effects on the structure associated with the selected IM.

Structural analysis. Given the ground motion hazard, a vector of **Engineering Demand Parameters, EDPs**, (second box in Fig. 1.1) needs to be computed, which defines the response of the building in terms of parameters that can be related to *DMs* and *DVs*. The *EDP* vector should include all parameters of relevance for damage and losses to the soil/foundation/structure system as well as to the nonstructural and content systems. Interstory drift is an example of a relevant *EDP*. Relationships between *EDPs* and *IMs* are typically obtained through inelastic dynamic analyses, which should incorporate, to the extent feasible, the complete structural, geotechnical, SFSI (soil-foundation-structure-interaction), and non-structural systems. The outcome of this process, which may be referred to as probabilistic seismic demand analysis, can be expressed as $p(EDP|IM)$, or more specifically as $P[EDP \geq y | IM = x]$, which is the probability that the *EDP* exceeds a specified value y , given (i.e., conditional) that the *IM* (e.g., $S_a(T_I)$) is equal to particular value x . When integrated over the appropriate *IM* hazard curve, the MAF of exceedance of *EDP(s)*, i.e., $\lambda(EDP)$, as shown in the lower half of the second box of Figure 1.1 is obtained.

Damage analysis. To close the loop, *EDPs* have to be related to the *DVs* of interest. In most (but not all) cases an intermittent variable, called a **Damage Measure, DM**, has to be inserted between the *EDP* and the *DV*, simply to facilitate the computation of *DVs* from *EDPs*. A *DM* describes the damage and consequences of damage to the structure or to a component of the structural, nonstructural, or content system, and the term $P(DM|EDP)$ can be viewed as a fragility function for a specific damage (failure) state (probability of being in or exceeding a specific damage state, given a value of *EDP*). The *DMs* include, for example, descriptions of necessary repairs to structural or nonstructural components. Section 5.2 and Appendix B summarize fragility functions of specific interest to this testbed study. If the fragility functions for all relevant damage states of all relevant components are known, the *DVs* of interest can be

evaluated either directly or by means of cost functions that relate the damage states to repair/replacement costs.

Loss analysis. The goal of the loss analysis is to estimate the frequency with which various levels of performance are exceeded. Performance can be parameterized via one or more decision variables (DV). DVs are defined at the system level, such as total repair cost, number of casualties, or repair duration (sometimes called “dollars, deaths, and downtime”). DVs can be expressed in terms of expected annual values (most meaningful for cost-benefit analysis), probability of exceeding certain intolerable levels (relevant to risk-of-ruin analysis and for purchasing insurance), or mean values conditioned on a meaningful scenario event. In this testbed study, the DV of primary interest is dollar loss, with an additional focus on collapse probability (but without taking the step from collapse to casualties). Only preliminary consideration is given to the downtime problem, which remains a challenge to be addressed in the future.

The framework equation for performance assessment. The aforementioned steps, which form the basis of performance assessment, can be expressed in the following equation for a desired realization of the DV , such as the MAF of the DV , $\lambda(DV)$, in accordance with the total probability theorem:

$$\lambda(DV) = \iiint G\langle DV|DM \rangle dG\langle DM|EDP \rangle dG\langle EDP|IM \rangle d\lambda(IM) \quad (1.1)$$

This equation, which often is referred to as the framework equation for performance assessment, suggests a generic structure for coordinating, combining and assessing the many considerations implicit in performance-based seismic assessment. Inspection of Eq. (1.1) reveals that it “de-constructs” the assessment problem into the four basic elements of hazard analysis, structural analysis (demand prediction), damage analysis, and loss estimation, by introduction of the three “intermediate variables,” IM , EDP , and DM . Then it re-couples the elements via integration over all levels of the selected intermediate variables. This integration implies that in principle one must assess the conditional probabilities $G(EDM|IM)$, $G(DM|EDP)$ and $G(DV|DM)$ parametrically over a suitable range of DM , EDP , and IM levels.

In the form written, the assumption is that appropriate intermittent variables ($EDPs$ and DMs) are chosen such the conditioning information need not be “carried forward” (e.g., given EDP , the DMs (and DVs) are conditionally independent of IM ; otherwise IM should appear after

the *EDP* in the first factor.) So, for example, the *EDPs* should be selected so that the *DMs* (and *DVs*) do not *also* vary with intensity, once the *EDP* is specified. Similarly one should choose the intensity measures (*IM*) so that, once it is given, the dynamic response (*EDP*) is not also further influenced by, say, magnitude or distance to the source (which have already been integrated into the determination of $\lambda(IM)$) (Krawinkler and Miranda, 2004).

The role of uncertainties. The performance assessment process described herein would be routine were it not for the presence of uncertainties. We identify the major sources of uncertainty in $\lambda[DV]$, quantifying the contribution at each step from *IM*, *GM*, *EDP*, and *DM* to *DV*, considering propagation and correlation. We identify the sources of uncertainty that are most significant *in this situation*, and those that can be neglected. Of the major contributors, we identify opportunities for reducing uncertainty by additional data-gathering or by changes in modeling. In other situations, such as a similar commercial building on liquefiable soil, a newer building, or a bridge, different sources of uncertainty may be more important. The larger PEER effort will seek to categorize a variety of such situations and identify important sources of uncertainty in each.

1.4 REPORT OUTLINE

This report attempts to summarize, on hand of a testbed building, the implementation and testing of the PEER performance assessment methodology as performed by a team of researchers and practicing engineers. The objective of the testbed studies was to exercise the methodology to illustrate its feasibility and to identify gaps in methodology, data, and tools. This report is structured in keeping with this objective, and attempts to show the information flow throughout the execution of the performance assessment process. Chapter 2 provides a documentation of relevant properties of the testbed building with a focus on the structural system. Chapter 3 summarizes case specific hazard analysis, which results in a quantification of relevant intensity measures, *IMs*, and of ground motion records that represent the “details” of the ground shaking hazard associated with various levels of *IMs*. Chapter 4 illustrates how this hazard information is utilized to quantify the response of the building system in terms of engineering demand parameters, *EDPs*, that provide the link to downstream variables that ultimately result in probabilistic expressions of the seismic performance of the building articulated in terms of

decision variables, DVs. The process of relating EDPs to DVs is illustrated in Chapter 5, using direct dollar losses as the primary DV.

The primary aspect that distinguished the PEER performance assessment approach from presently employed engineering evaluation approaches is the explicit and rigorous treatment of aleatory and epistemic uncertainties in all phases of the performance assessment. Issues associated with the identification, quantification, and propagation of uncertainties are summarized in Chapter 6, with various approaches for propagating uncertainties being contrasted.

In Chapter 7 the aim is to relate the PEER assessment methodology to presently employed engineering practice. Evaluation methods used in current practice are summarized, and a discussion is presented on the presently employed means of communicating performance to owners. A FEMA 356 evaluation of the testbed building is illustrated and a conceptual FEMA 356 rehabilitation design is documented for further use by PEER researchers. The chapter concludes with an engineering assessment of the PEER PBEE methodology and a summary of the impediments the methodology may encounter in implementation in engineering practice.

Chapter 8 addresses challenges that have to be addressed in order to make a reliability-based seismic performance assessment methodology attractive to owners. It points out the kinds of investment decisions an owner is faced with and what options he/she may choose for his property. The conclusion is that the owner will favor a performance-based design over a code based design only if the advantages are clearly articulated and expressed in terms that fit into his/her investment decision vocabulary.

The report concludes with four appendices, which provide a description of past earthquake damage in the testbed building (Appendix A), a compendium of fragility curves useful for the testbed building (Appendix B), a documentation of the loss estimation methodology implemented in Chapter 5 (Appendix C), and the process and results of a fatality survey following the 1999 Kocaeli (Turkey) earthquake, which was used to develop a fatality model for collapsed non-ductile reinforced concrete frame structures (Appendix D).

2 The Van Nuys Hotel Building

Author: Keith A. Porter

2.1 BUILDING DESCRIPTION

This text summarizes the structural and architectural features of the Van Nuys hotel building as it existed just prior to the 1994 Northridge earthquake. Additional information is provided in Appendix A.

The testbed building is a 7-story, 66,000 sf (6,200 m²) hotel in Van Nuys, California, at 34.221° north latitude, 118.471° west longitude, in the San Fernando Valley of Los Angeles County. The building is located near the center of the map shown in Figure 2.1. The building has been studied extensively, e.g., by Jennings (1971), Scholl et al. (1982), Islam (1996a, 1996b), Islam et al. (1998), Li and Jirsa (1998), Trifunac et al. (1999). To date, no researcher has assessed the seismic vulnerability of the building in terms of repair cost as a function of shaking intensity.

The hotel was designed in 1965 according to the 1964 Los Angeles City Building Code, and built in 1966. The building was lightly damaged in the M6.6 1971 San Fernando event, approximately 20 km to the northeast, and severely damaged in the M6.7 1994 Northridge earthquake, whose epicenter was approximately 4.5 km to the southwest (Figure 2.2). After the 1994 earthquake, the building was retrofitted with new reinforced concrete shear walls, but we examine it as it existed just before the earthquake.

The architect/engineer designer is Rissman and Rissman Associates (1965). In plan, it is 63 ft by 150 ft, 3 bays by 8 bays, 7 stories tall. The long direction is oriented east-west. The building is approximately 65 ft tall: the first story is 13 ft, 6 in; stories 2 through 7 are 8 ft, 6 in. The ground floor, as it existed prior to the 1994 Northridge earthquake, contains a lobby, dining

room, tavern, banquet room, and various hotel support services. Upper floors are arranged with 22 hotel suites accessed via a central corridor running the longitudinal axis of the building.



Fig. 2.1 Location of the testbed building (near center of map)

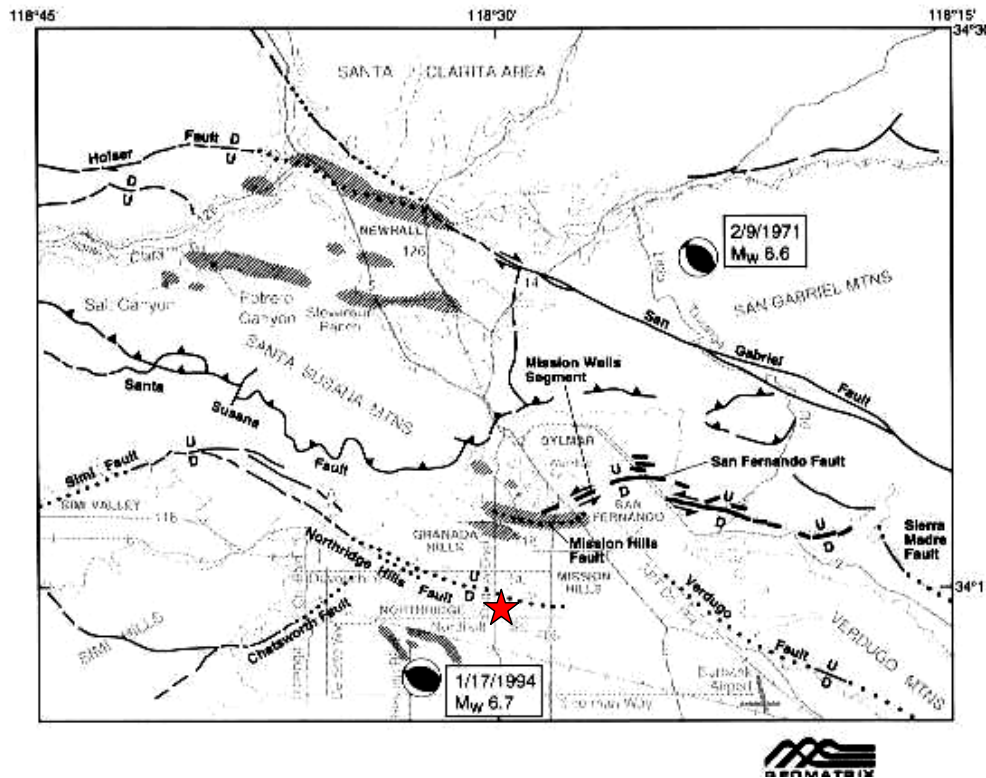


Fig. 2.2 Testbed building (star) relative to 1971 and 1994 earthquakes (EERI, 1994)

2.2 STRUCTURAL SYSTEM

The structural system is a cast-in-place reinforced-concrete moment-frame building with nonductile column detailing. Lateral force resistance is provided primarily by the perimeter moment frames, although the interior columns and flat slabs also contribute to lateral stiffness. The gravity system comprises 2-way reinforced-concrete flat slabs supported by square columns at the interior and the rectangular columns of the perimeter frame. Slabs are 10-in.-deep at the 2nd floor, 8½ in. at the 3rd through 7th floors, and 8 in. at the roof. The roof also has lightweight concrete topping varying in thickness between 3-1/4 in. and 8 in. The building is founded on 24-in.-diameter drilled piers in groups of two, three, and four piers per pile cap, and columns centered on the pile cap. The three-pier configuration on a triangular arrangement is used for most of the perimeter columns. Interior columns are supported on 4-pier pile caps.

The column plan (with the designer's column numbers) is shown in Figure 2.3. Floor and roof beams and spandrel beams are shown in Figure 2.4. Frames are regular in elevation; the south frame elevation is shown in Figure 2.5. These figures show the designer's notation for beam and column numbering. Columns in the south frame are 14 in. wide by 20 in. deep, i.e., oriented to bend in their weak direction when resisting lateral forces in the plane of the frame. Spandrel beams in the south frame are generally 16 in. wide by 30 in. deep at the 2nd floor, 16 in. wide by 22-½ in. deep at the 3rd to 7th floors, and 16 in. wide by 22 in. deep at the roof. The ground floor has some masonry infill walls, but above the 2nd floor there are no other stiff elements between the columns that might produce a short-column effect.

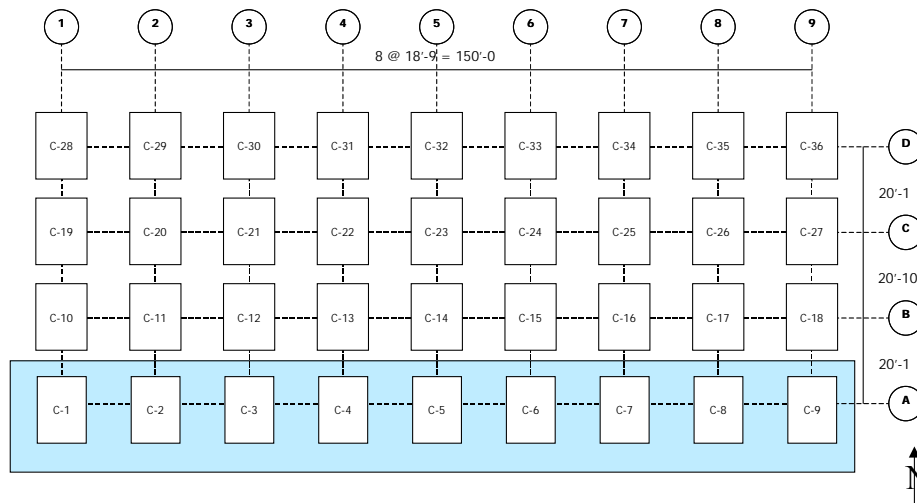


Fig. 2.3 Column layout (three bays in transverse direction, eight in longitudinal direction)

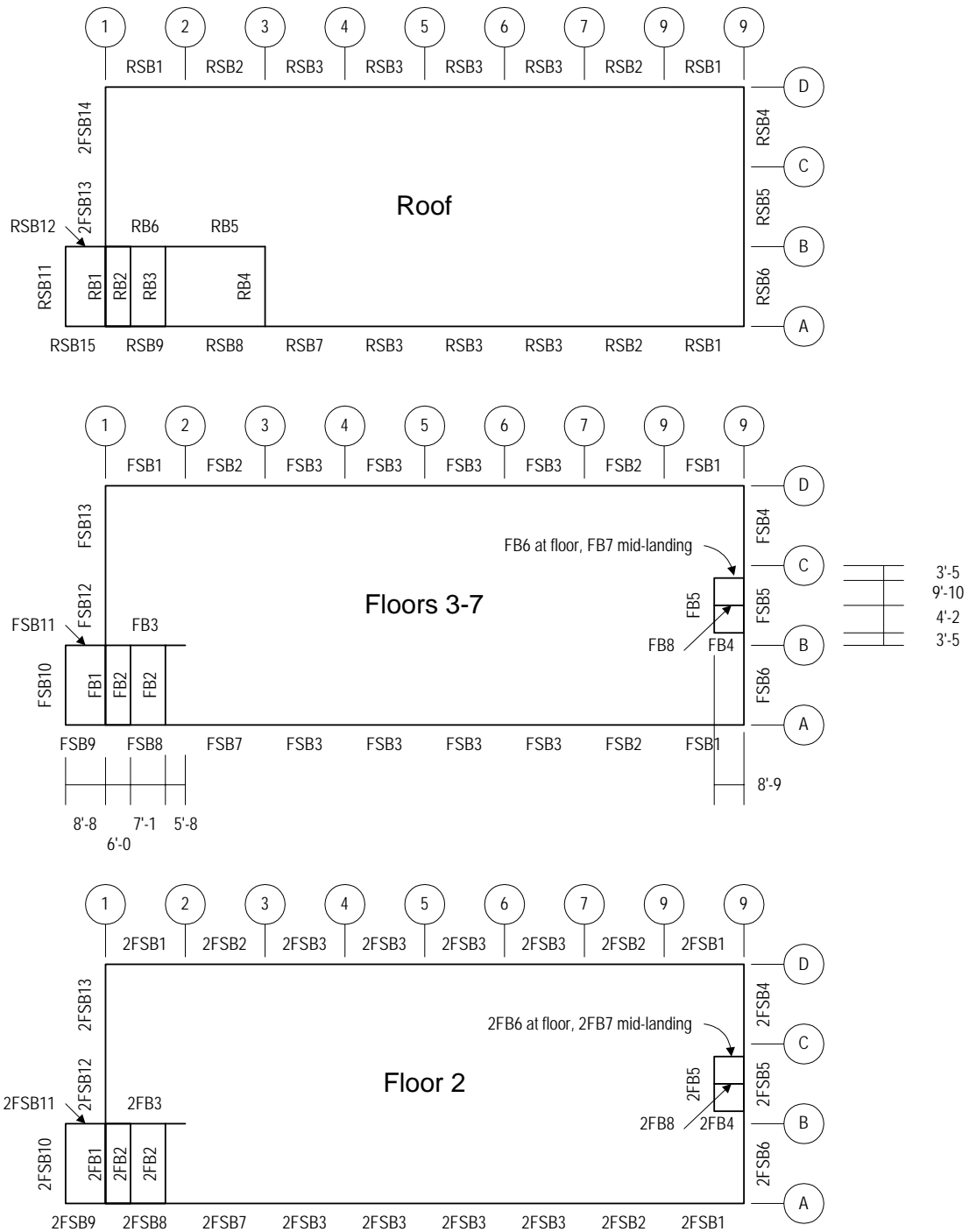


Fig. 2.4 Floor beam and floor spandrel beam plans

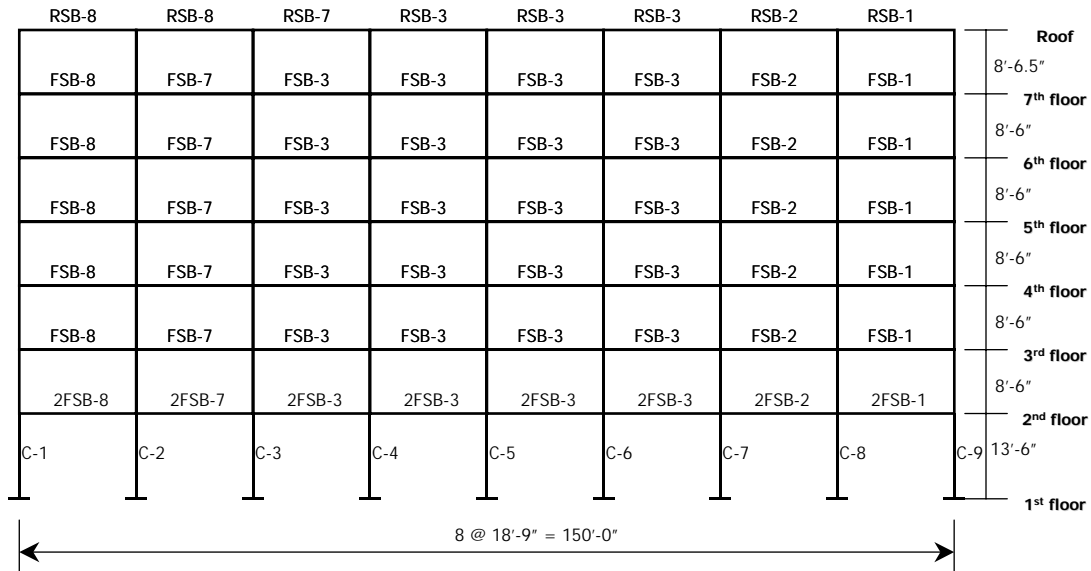


Fig. 2.5 South frame elevation with element numbers

Column concrete has nominal strength of $f'_c = 5$ ksi for the first story, 4 ksi for the second story, and 3 ksi from the third story to the seventh. Beam and slab concrete is nominally $f'_c = 4$ ksi at the second floor and 3 ksi from the third floor to the roof. Column reinforcement steel is scheduled as A432-62T (Grade 60) for billet bars. Beam and slab reinforcement is scheduled as ASTM A15-62T and A305-56T (Grade 40) for intermediate grade, deformed billet bars. Column reinforcement is arranged as shown in Figure 2.6. The column reinforcement schedule is shown in Table 2.1. The reinforcement of floor spandrel beams for floors 3 through 7 is shown in Table 2.2, and the reinforcement of floor spandrel beams for roof and second floor is shown in Table 2.3.

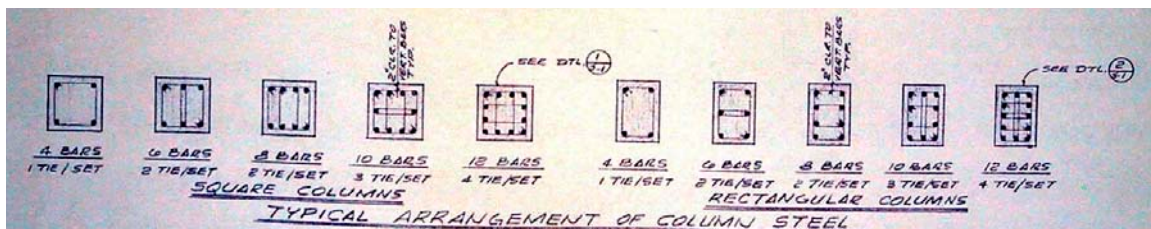


Fig. 2.6 Arrangement of column steel (Rissman and Rissman Associates, 1965)

Table 2.1 Column reinforcement schedule

		Column mark							
		C-13 to C-17, C-21 to C-26	C-11, C-12, C-20	C-30 to C-34	C-10, C-18, C-19, C-27	C-2, C-3, C- 8, C-29, C-35	C-1, C-9, C-28, C-36	C-1A, C-10A	C-17A, C-26A
Level	Col size	18"x18"	18"x18"	14"x20"	14"x20"	14"x20"	14"x20"	10"x12"	10"x12"
7th floor	Vert. bars	6-#7	6-#7	6-#7	6-#7	6-#7	6-#7	4-#5	
	Ties	#2@12"	#2@12"	#2@12"	#2@12"	#2@12"	#2@12"	#2@10"	
6th floor	Vert. bars	6-#7	6-#7	6-#7	6-#7	6-#7	6-#7	4-#5	4-#5
	Ties	#2@12"	#2@12"	#2@12"	#2@12"	#2@12"	#2@12"	#2@10"	#2@10"
5th floor	Vert. bars	6-#7	6-#8	6-#7	6-#7	6-#7	6-#7	4-#5	4-#5
	Ties	#2@12"	#3@12"	#2@12"	#2@12"	#2@12"	#2@12"	#2@10"	#2@10"
4th floor	Vert. bars	6-#8	8-#9	6-#7	6-#9	6-#7	6-#7	4-#5	4-#5
	Ties	#3@12"	#3@12"	#2@12"	#3@12"	#2@12"	#2@12"	#2@10"	#2@10"
3rd floor	Vert. bars	8-#9	12-#9	6-#9	8-#9	8-#9	6-#7	4-#6	4-#5
	Ties	#3@12"	#3@12"	#3@12"	#3@12"	#3@12"	#2@12"	#2@10"	#2@10"
2nd floor	Vert. bars	10-#9	12-#9	6-#9	8-#9	8-#9	6-#7	4-#6	4-#5
	Ties	#3@12"	#3@12"	#3@12"	#3@12"	#3@12"	#2@12"	#2@10"	#2@10"
1st floor	Col size	20"x20"	20"x20"						
	Vert. bars	10-#9	12-#9	10-#9	12-#9	10-#9	8-#9	4-#8	4-#6
	Ties	#3@12"	#3@12"	#3@12"	#3@12"	#3@12"	#3@12"	#3@10"	#2@10"

Table 2.2 Spandrel beam reinforcement schedule, floors 3 through 7

Beam mark	Width	Height	Top bars					Bottom bars	#3 ties
			7F	6F	5F	4F	3F		
FSB-1	16"	22-½"	①⑨ 2#7	2#9	2#9	3#8	3#8	2#7 (2#8 @ 3F, 4F)	①⑨ 3@5", 5@6", rest @10", 3F- 5F
			②⑧ FSB-2 top bars						②⑧ 6@4", 5@6", 3F-5F
FSB-2	16"	22-½"	②⑧ 2#9	3#8	3#8	3#8	3#9	2#6	8@5", 5@6" ea end
			③⑦ FSB-3 top bars						Rest @ 10" 3F-5F
FSB-3	16"	22-½"	2#8	2#9	3#8	3#8	3#9	2#6	3@5", 5@6" ea end
									Rest @ 10" 3F-5F
FSB-7	16"	22-½"	③ FSB-3 top bars					2#7	3@5", 5@6" ea end
			② FSB-8 top bars						Rest @ 10" 3F-5F
FSB-8	16"	22-½"	② 2#8	2#9	2#9	3#8	3#8	2#7 (2#8 @ 5F, 2#9 @ 3F, 4F)	① 3@5", 5@6", rest@10" 3F-5F
			① 2#7	2#8	2#9	2#9	3#8		② 6@4", 5@6" 3F-5F

①, ②, etc.: column lines
 3F, 4F, etc: floor levels

Table 2.3 Roof and second-floor spandrel beam reinforcement schedule

Beam mark	Width	Height	Top bars	Bottom bars	#3 ties
RSB-1	16"	22"	①⑨ 2#6 ②⑧ 2#8	2#7	#3@10"
RSB-2	16"	22"	②⑧ RSB-1 top bars ③⑦ RSB-3 top bars	2#6	Same
RSB-3	16"	22"	2#8	2#6	Same
RSB-7	16"	22"	④ RSB-3 top bars ③ 2#9	2#6	Same
RSB-8	16"	22"	③ 2#9 ② 3#9	2#9	Same
2FSB-1	16"	30"	①⑨ 2#9 ②⑧ 2FSB-2 top bars	2#8	4 @ 6", 2 @ 8", ea end, rest @ 13"
2FSB-2	16"	30"	②⑧ 3#8 ③⑦ 2FSB-3 top bars	2#6	Same
2FSB-3	16"	30"	2#9	2#6	Same
2FSB-7	16"	30"	③ 2FSB-3 top bars ② 2FSB-8 top bars	2#7	Same
2FSB-8	16"	30"	② 2#9 ① 2#9	2#8	Same

2.3 ARCHITECTURAL FINISHES AND MEP COMPONENTS

The building is clad on the north and south facades with aluminum window wall, comprising 3/16-in. heavy sheet glass in sliding frames, and 1/4-in. cement asbestos board panels with an ornamental site-obscuring mesh of baked enamel or colored vinyl. Interior partitions are constructed of 5/8-in. gypsum wallboard on 3-5/8 in. metal studs at 16-in. centers. Ceilings in hotel rooms at the 2nd through 7th floors are a textured coating applied to the soffit of the concrete slab above; at the first floor, ceilings are suspended wallboard or lath and plaster. Ceilings in the hallways at the 2nd through 7th floors are suspended ceilings in an exposed 2-ft x 4-ft tee-bar grid, suspended only far enough from the soffit to accommodate the depth of fluorescent lighting fixtures (about 2 in.). The east and west end walls are finished on the inside with gypsum wallboard and on the outside with stucco.

Through-wall air-conditioning units are mounted in the waist panels below the windows and provide ventilation to the suites. Central HVAC is provided only for hallway and ground-floor spaces. Central HVAC equipment—fans for the kitchen, one cooling tower for the lobby, and two packaged AC units for hallways—are located on the roof, along with a 1000-gal water tank. The cooling tower is anchored. Two 3500-lb hydroelectric elevators provide vertical transport; these are located in the southwest corner of the building, with motors (anchored) located on the roof. Building service equipment located on the ground floor includes switchgear and transformer (both unanchored and unbraced), hot water heater (anchored), washers, dryers, and water softener (unanchored). An unanchored transformer and an anchored diesel generator are located in the south parking area on mechanical pads a few feet from the south façade.

2.4 SITE CONDITIONS

Soil conditions at the site are found in Tinsley and Fumal (1985), who map surficial soil deposits in the Los Angeles region using a variety of sources. They describe the site soil as Holocene fine-grained sediment (silt and clay) with a mean shear-wave velocity of 200 m/sec (and a standard deviation of 20 m/sec), corresponding to site class D, stiff soil, as defined by the International Code Council (2000), and soil profile type S_D according to the Structural Engineers

Association of California (1999). California Geosystems (1994) performed four soil borings at the site, and report that site soils are “mostly brown silty fine sand and sandy silts with some clay binder. The composition of soils is fairly consistent.” While soil densification during an earthquake is possible, the geotechnical engineers do not find liquefaction, lateral spreading, or other ground failures to be significant perils. In his study of the same building, Islam (1996b) reaches the conclusion that the “site coefficient factor [is] S2 or greater.”

2.5 FUNDAMENTAL PERIOD OF THE STRUCTURE

Prior to the 1971 San Fernando earthquake, the building was instrumented with three self-contained triaxial accelerographs; the instrumentation was upgraded to a 16-channel recording system comprising uniaxial, bi-axial and triaxial instruments prior to the 1987 Whittier-Narrows earthquake. Acceleration data provided by these instruments have been analyzed by others to determine the fundamental period of the structure at the beginning of the Northridge earthquake. Table 2.4 lists the fundamental period of the building in the longitudinal (EW) and transverse (NS) directions at the beginning of the Northridge earthquake as computed by a series of different research teams. On the basis of the data listed in Table 2.4, the fundamental period of the building in the longitudinal direction at the beginning of the Northridge earthquake was assumed to be 1.5 sec.

Table 2.4 Computed fundamental period for Van Nuys Building at the beginning of the Northridge earthquake

Research Team	Fundamental Period of the Building	
	Longitudinal / EW	Transverse / NS
Trifunac et al. (2001)	1.05 sec	1.11 sec
Gilmartin et al. (1998)	1.5 sec	1.6 sec
Islam (1996)	1.5 sec	--

3 Hazard Analysis

3.1 THE ROLE OF HAZARD ANALYSIS IN PERFORMANCE ASSESSMENT

In the context of performance assessment, hazard analysis quantifies the last term in the framework equation (1.1), i.e., $\lambda(IM)$, the mean annual frequency (MAF) of exceedance of $IM(s)$, and provides sets of ground motions, which represent, when scaled to specific values of the intensity measure IM , the “details” (frequency content, duration, etc.) of the seismic input at the hazard level associated with the selected IM value. This chapter addresses the following aspects of the hazard analysis performed for the Van Nuys building:

- Free-field hazard analysis and ground motion selection, with the word free-field implying that the results represent the hazard at the ground surface, i.e., they do not account for soil-foundation-structure interaction effects. Neither do they account for specifics of the soil profile below the building.
- The process of accounting for aleatory and epistemic uncertainties in the development of site specific hazard curves and ground motion representations.
- Considerations that enter in the selection of appropriate IMs , which constitute the link between the shaking hazard and the response of the structure represented by various $EDPs$, which then provide the link to downstream evaluation of appropriate DVs .
- Effects of the local site soil profile on IMs and free-field ground motions, including a sensitivity study of this effect to variations in the soil properties.

Here, as throughout this report, the emphasis is on the identification, quantification, and propagation of uncertainties. Thus, the emphasis is *not* on the determination of a single uniform hazard spectrum, which then could be used as a deterministic spectrum for design or evaluation. The emphasis is on descriptions that permit the carrying forward of all important uncertainties through the whole performance assessment process and evaluation of their effect on the DVs .

3.2 FREE-FIELD GROUND MOTION HAZARD ANALYSIS

Authors: C.A. Cornell, P. Somerville

3.2.1 Background

The first step in estimation of future building performance is the assessment and characterization of the seismic threat at the site. The seismic threat, or “hazard” in the colloquial sense of the word, to the Van Nuys testbed structure is strong ground shaking. The process of assessment and characterization this hazard requires an integration of regional earth science information into a form most effective for use in the subsequent PBEE steps of prediction of structural behavior and building performance. This objective implies here the development of a curve of mean annual frequency¹ of exceedance (or “hazard” in the special sense of PSHA) versus level for the chosen Intensity Measure (IM), and selection of a sample of representative ground motions for use in conducting the structural dynamic analyses to predict in probabilistic terms the Engineering Demand Parameters (EDPs). This chapter describes how this phase of PBEE has been done for this application.

For this structure it has been judged that the appropriate set of EDPs for estimation of the Decision Variables (DVs) (e.g., economic loss) is the set consisting of the peak Interstory Drift Ratio (IDR) and Peak Floor Acceleration (PFA) for each of the seven floors. (The current application restricts attention to the longitudinal direction only, implying a total vector of 14 EDPs.) As we shall discuss later (Section 3.4), it has been concluded here that the $S_d(T_1)$, the 5% damped spectral acceleration at a period in the vicinity of that of the first mode (taken here at 1.5 sec), is the appropriate IM for this particular application, because it is an effective predictor of building displacements such as IDRs and an adequate predictor of PFAs. Therefore this hazard assessment focus is on this spectral acceleration and on the records that can be expected to accompany it.

This section will first discuss the seismic threat at the site in general terms, and then more specifically in terms of $S_d(T_1)$, the IM of choice, and finally how the sample of specific, representative accelerograms was chosen for this application.

¹ The mean annual frequency will be used interchangeably here with the simpler term “annual probability” as the two are numerically equal in the range of interest.

3.2.2 General Ground Motion Hazard

This section describes the general assessment of the seismic threat to a site. The analysis includes a representation of the surrounding sources of earthquakes, their likelihoods of producing magnitudes of different levels and the ground motion effects that these events will produce at the site. This assessment is conventionally done today in terms of a Probabilistic Seismic Hazard Assessment (PSHA) which produces curves of annual probabilities of exceedance versus level for the spectral acceleration at a specified period. A set of such curves can be used to produce also Uniform Hazard (Response) Spectra (UHS) for different specified levels of annual probabilities of exceedance. The formal description of this method, which integrates probabilistic representations of the potential magnitudes on each source and of their effects at the site, is widely available (e.g., Kramer, 1996). In this application we have adopted for the most part the PSHA conducted by the USGS² as reported by Frankel et al., 1997, 2001. The USGS website describes the detailed input assumptions used.

The Van Nuys Testbed is located on a soil site (NEHRP Class D) in the San Fernando Valley which has both a variety of faults lying beneath it and the large San Andreas fault passing some 50 kilometers to the northeast. The net effect of the combined threats of all these faults is conventionally represented by suites of UHS; three such UHS for mean annual frequencies of 0.014, 0.0021, 0.0004 (or 50%, 10% and 2% per 50 years) are shown in Figure 3.1. Tabulated versions of these results and their bases are described in a report by Somerville and Collins (2002), available on the PEER website. In brief they were obtained from the USGS UHS, which are reported for rock sites (NEHRP B-C), by multiplying those spectral ordinates by the ratio of soil to rock spectral ordinates for the Abrahamson and Silva (1997) ground motion model³.

² The 1996 USGS PSHA (Frankel et al., 1997) results used as the newer results were not available at the beginning of the project.

³ These ratios are somewhat dependent on magnitude and distance; the values used here for these variables are those from the disaggregation of hazard defined in Table 3.1. The results are representative of Class D soil conditions, which is its NEHRP category based on blow count data. As will be discussed in Section 3.4.4.1, the rock results would have been used had a site-specific soil amplification analysis been called for.

Soil UHS for Van Nuys Site

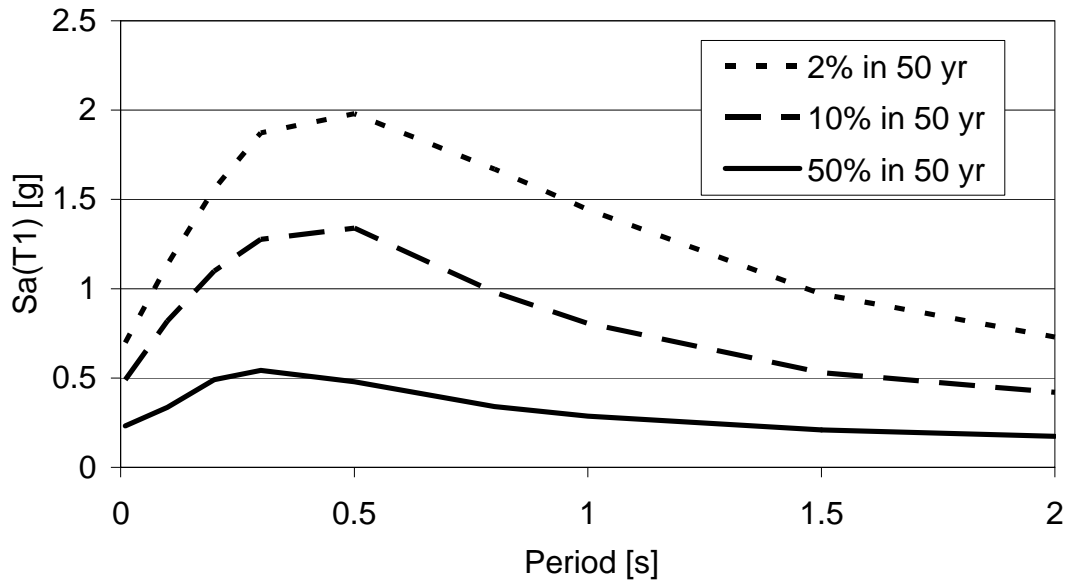


Fig. 3.1 Uniform hazard spectra for the Van Nuys site for three levels of annual exceedance probability, based on the 1996 USGS website results and modified for local site conditions

It is important to point out that, although the site is located near active faults in map view (i.e., when viewed from above, the site is located near the traces of active faults), none of the faults that dominate the seismic hazard at the site are oriented in such a way that the site will experience strong rupture directivity effects. For example, the fault that caused the 1994 Northridge earthquake is located about 10 km below the site, but it dips up to the north-northeast and focuses forward rupture directivity toward the northern part of the San Fernando Valley. (Therefore modification to account for near-fault rupture directivity effects, and the use of separate response spectra for the fault normal and fault parallel components of ground motion, are not be required.)

3.2.3 IM-Focused Ground Motion Hazard

In this sub-section we turn attention to the more detailed characterization of the Van Nuys Testbed IM hazard characterization. The USGS estimate of the hazard curve for $S_a(T_1)$ (i.e., 1.5 sec) is shown in Figure 3.2. The previous UHS provide just three of the points on this curve but

the entire curve is needed for the PBBE here as all ground motion levels contribute to, for example, the expected economic loss.

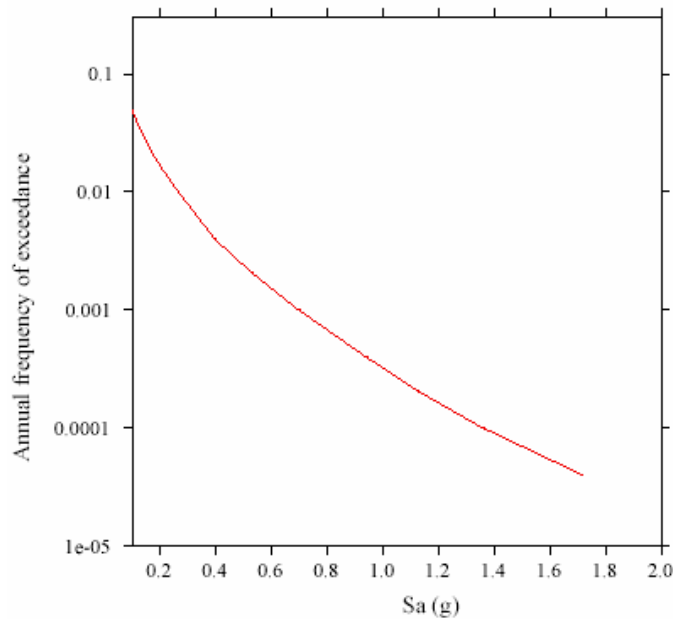


Fig. 3.2 Hazard curve for the 1.5 sec S_a for the Van Nuys Site, based on the USGS website results and modified for local site conditions

The disaggregation⁴ of the IM hazard shows that the hazard at the site is dominated by nearby earthquakes. Disaggregation is the process of decomposing the hazard (i.e., the annual probability of exceedance) into its various additive components. This can be done by faults, or it can be done by magnitude and distance. This latter disaggregation⁵ of the 0.0021 annual frequency is shown in Figure 3.3. This annual frequency corresponds to a 0.53g $S_d(T_1)$ (IM) value in Figure 3.2. Figure 3.3 confirms that the largest contributions to this hazard level arise from very close events of magnitude 6 to 7. This can be summarized by the mean (or modal) M and R values of this disaggregation distribution. These mean M and R values are provided by USGS and appear⁶ in Table 3.1. The mean magnitude is 6.75 and the mean distance becomes smaller for smaller probabilities (or larger ground motions). The disaggregation plot above can

⁴ Or alternatively, deaggregation.

⁵ This result was prepared, not from the USGS assessment, but from an independent hazard analysis of the site based on Norman Abrahamson's PSHA code. Details differ but the general conclusions are very similar. The latter results were more readily available for our use and presentation here.

⁶ The mean M and R results here are for 1 sec. at the probability levels specified. Note that the IM (or S_a) levels quoted in column 1 of Table 3.1 are given for the $T = 1.5$ sec values, not $T = 1$ sec. USGS does not report 1.5 sec results. There would be little difference in the mean M and R for periods this close to one another.

also be read to show that this low hazard is contributed primarily by comparatively unlikely amplitudes (given any particular M and R value); this is seen in the contributions by “epsilon” ranges which are primarily in the 1 to 2+ sigma range.

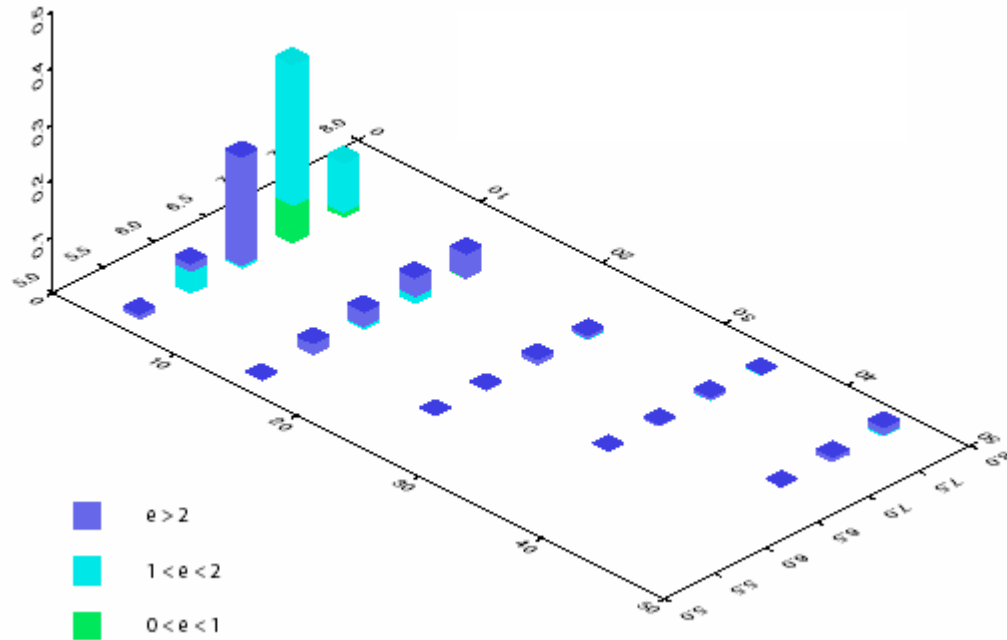


Fig. 3.3 Disaggregation of the hazard for $S_a(T = 1.5 \text{ s}) \geq 0.53\text{g}$ at the Van Nuys site. The vertical axis gives the fraction of the total hazard (which is approximately 0.002 per year) contributed by each magnitude-distance bin. The shading of the vertical bars gives the proportion of that hazard contributed by different values of “epsilon”, the number of standard deviations by which the level exceeds the median value for a particular magnitude and distance.

Table 3.1 Disaggregation of the mean annual frequency of exceedance of three levels of the IM (see footnote 6) at the Van Nuys building soil site

IM (S_a at 1.5 sec) level	Hazard level Per annum	Dominant Earthquake Faults	Mean M	Mean R
0.21g	0.014 (50% in 50 yrs)	Santa Susana, Northridge blind thrust	6.75	20 km
0.53g	0.0021 (10% in 50 yrs)	Northridge blind thrust, Santa Susana	6.75	10 km
0.97g	0.0004 (2% in 50 yrs)	Northridge blind thrust, Santa Susana	6.75	5 km

3.2.4 Ground Motion Accelerogram Sample Selection

The seismic threat to a multi-degree-of-freedom (MDOF) structure behaving in the nonlinear range is represented by more than simply the annual frequency curve of the IM, which captures the likelihood only of the amplitude of linear single-degree-of-freedom (SDOF) oscillator response, i.e., it is a measure of the strength of potential future records in a particular frequency range. While it is true that the IM has been chosen to capture the most important such range for the Van Nuys Testbed structure, because they may impact nonlinear MDOF behavior, other features of the threat are typically captured as well as possible in the next step of the process: record selection. In order to carry out the nonlinear dynamic analyses used to estimate the EDP distributions for specific levels of IM, it is necessary to provide a sample of representative accelerograms. At this site accelerograms recorded on Class D soil conditions are appropriate because soil conditions may affect frequency content. The PSHA disaggregation also reveals that nearby thrust faults are dominant; therefore it is prudent to use records from thrust fault events, if available, even if we do not understand fully as yet how, if at all, this factor may impact structural response.

Further, as discussed above, it is anticipated that directivity effects, such as pulse-like records, will not be experienced at this site from these dominant faults. Therefore records displaying such features are inappropriate. However, because they may affect the relative frequency content of — and hence response to — the future record, the expected magnitude and distance of the event causing the IM are also typically captured in the selection of the sample of accelerograms. Several (here three) levels of the IM are considered as in general these representative conditions may change with level. For each of three IM levels, the selected recordings were chosen to reflect the expected magnitude and distance as identified by the disaggregation of IM hazard (Table 3.1). In this application there is not a change in expected magnitude with level; as will be discussed further below, magnitude is generally believed to have a stronger effect on frequency content and peak displacement responses than distance.

A sample of size ten was selected for each level. The number of records is a trade-off between computational effort and accuracy in estimating EDP response statistics. In this PBEE study we are concerned with dispersion as well mean response; ten is therefore larger than the number used in current building practice. All of the recordings selected in this case by Somerville and Collins (2002) are from thrust earthquakes in the Los Angeles region, and

include the 1971 San Fernando, 1986 North Palm Springs, 1997 Whittier Narrows, and 1994 Northridge earthquakes. All of the selected recordings are free from strong directivity effects and are also from soil sites. In general different accelerograms were used for each level. The specific records selected for each of the three levels (with distances and magnitudes) are available in Somerville and Collins (2002).

The records as recorded reflect variability in magnitude, distance, source details and ground motion propagation. The PSHA, which provides the annual likelihood of a given S_a level, has already considered the randomness in magnitude, distance and propagation as they affect $S_a(T_I)$. Therefore this variability needs to be eliminated by scaling the recordings to each of a set of common $S_a(T_I)$ values for the purposes of estimating the variability of an EDP *given* the IM level, which is the second term in the PEER framing equation (Section 1.3). For each set of three-component recordings, a scaling factor⁷ was found by matching the east-west (the building's longitudinal direction) component of the accelerograms to the specific IM or $S_a(T_I)$ level. This scaling factor was then applied to all three components (east-west, north-south and vertical) of the recording⁸. This scaling procedure preserves the relative scaling and observed variability among the three components of the recording. It should be noted that the records have not been adjusted to make them "spectrum compatible" (Kramer, 1996), as is often done in practice, as this will reduce the variability and hence underestimate the likelihood of extreme responses to the records; one objective of the PEER methodology is to capture this variability faithfully.

⁷ These scale factors ranged in amplitude from 0.433 to 4.427. Concern has often been expressed when these scale factors become large, say 3 or more. Given the limited set of rare strong ground motions such scaling is necessary if recorded accelerograms are to be used. It is fair to say that it is not yet firmly established how much effect, if any, this scaling may have on the accurate prediction of structural response.

⁸ This approach implies that the longitudinal direction first period S_a is the scalar IM of choice here, which is consistent with the project's focus on building response in this direction. Had the interest been in a 3D study an alternative would have been to scale the records to the geometric mean of the two horizontal components. Only a few transverse frame or 3D studies were done in this project. As will be reported in ongoing PEER Year 8 work these options must be used with consistent hazard curves. While the record is not clear on this subject, here it is assumed that the USGS provided hazard curves for an arbitrary horizontal component (and not the geometric mean of the two).

3.3 VARIABILITY AND UNCERTAINTY IN THE GROUND MOTION HAZARD

Authors: C.A. Cornell, P. Somerville

3.3.1 Aleatory Uncertainty — IM Randomness and Record-to-Record Variability

By variability and uncertainty we refer here, respectively, to the aleatory and epistemic uncertainty. The future ground motion at the site is represented, first, by the IM (random variable) and second by the sample of accelerograms or time histories. The aleatory uncertainty (randomness) in the IM has been captured by the PSHA and is displayed in the “hazard curve” (Fig. 3.2). Each of the three sets of samples of ten longitudinal accelerograms has, by design, the exact same level of the IM, but they differ in their details. It is these details that cause the record-to-record (RTR) variability (aleatory uncertainty) in the structural EDP responses given IM. This variability would be zero if the structure were a linear 1.5 second SDOF system, and the variability is larger to the degree the structure is not well represented by such a simple model. One preliminary indication of how much the EDPs may vary from record-to-record is given by Figure 3.4. This shows the median and median +/- one (log) standard deviation of the response spectra of the samples of records. (Also shown for comparison is the UHS, but it is *not* to be expected that the sample will necessarily match these shapes because in the UHS different periods are typically driven by different magnitudes and distances.⁹) The scaling scheme used, of course, causes the variability to go to zero for the longitudinal component at 1.5 seconds. There is variability at all periods of the transverse component.

3.3.2 Epistemic Uncertainty

An important contributor to epistemic uncertainty in the prediction and probabilistic analysis of future structural behavior is that associated with the ground motions. The uncertainty in the IM is captured in modern site-specific PSHA studies (Kramer, 1996) by evaluating the degree of information available and hence the degree of confidence in alternative hypotheses and parameter values that are input into the seismological models within the PSHA. These are then

⁹ Current practice in the nuclear industry site characterization is to prepare different “target spectra” for different period ranges. In this case, as we have a specific structure in hand, we can tailor that process to a specific period, namely 1.5 sec, the one most critical to the Van Nuys Testbed structure.

Response Spectral Average of Scaled Horizontal Accelerations

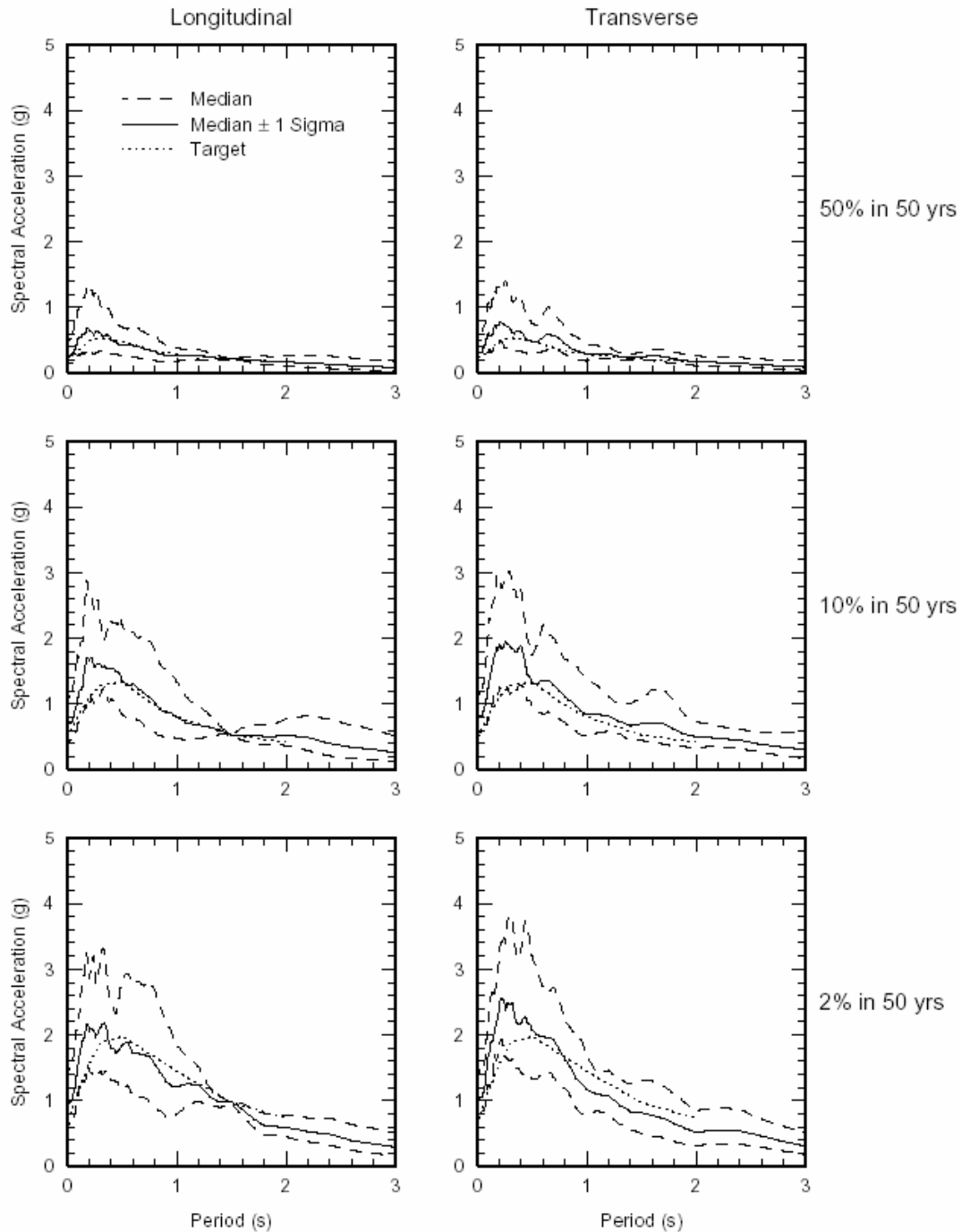


Fig. 3.4 Variability in the spectral accelerations of each set of ten scaled recordings for the longitudinal component for each of three ground-motion levels

propagated through the analysis to determine the resulting uncertainty in the annual frequency at each ground motion level. The result is a hazard curve and uncertainty bounds such as those

shown in Figure 3.5. As shown there the results are a median estimate, a mean estimate, and estimates with different likelihoods or “confidence levels” of non-exceedance. The 1996 USGS maps (used in the results displayed in Figures 3.1 and 3.2, and used as the primary basis for this study) are stated to be based on the mean estimates of the annual frequency of exceedance of any ground motion level, which is the appropriate estimate for determining mean estimates of structural limit state probabilities and mean annual losses. It should be recognized, however, that the 1996 USGS maps are based on an admittedly attenuated epistemic uncertainty analysis; more complete uncertainty analyses are promised for the subsequent maps.

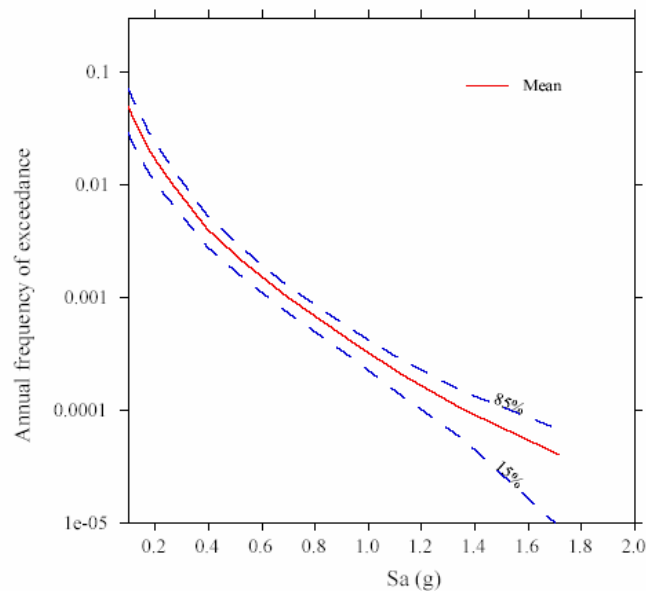


Fig. 3.5 Epistemic uncertainty in the 1.5 sec S_a hazard curve at the Van Nuys site. The mean and median estimates are virtually identical in this case.

The levels of uncertainty displayed in Figure 3.5 (e.g., the ratio between the 85-percentile and the median estimate) were taken from a parallel PSHA analysis¹⁰. These ratios can be interpreted to produce standard deviations of (natural) logs, which are useful for representing and comparing this source of epistemic uncertainty with others, as will be seen below. For example, at the three representative IM levels we have been focusing on, these “dispersions” are approximately 0.4⁻, 0.4⁺, and 0.7 for the 0.21, 0.53, and 0.97g levels respectively. It is often

¹⁰ Because of the limitations in the 1996 USGS uncertainty treatment these particular curves were produced by an application of Norman Abrahamson’s model and code. While the mean estimates differ from those developed above from the USGS website, the widths of the bands are representative and applicable. Therefore only the widths of the bands were used from the Abrahamson analysis.

heard that epistemic uncertainty in the PSHA is believed to dominate that due to other causes in the estimation of future seismic behavior of structures. The studies to follow will shed light on this conjecture (see, for example, Sec. 4.5.2 on collapse probability uncertainty).

There is clearly epistemic uncertainty, too, in how we represent the infinite array of possible accelerograms (time histories) that might occur in the future. As will be discussed in the next section, for example, the choice of the IM and the implicit assumption of independence of EDP from M , say, given IM, may introduce some unspecified degree of bias, and hence uncertainty. We proceed under the assumption that capturing the IM annual frequency epistemic uncertainty has been at least a first-order solution.

3.4 IM SELECTION FOR THE VAN NUYS BUILDING AND ITS IMPLICATIONS

Author: C.A. Cornell

3.4.1 IM Issues and Discussion

The variable selected for use as the Intensity Measure in the Van Nuys Testbed report is the spectral acceleration at a period near that of the first mode of the longitudinal direction of the building, $S_a(T_1)$. In application, this choice means, for example, that the hazard curve for S_a at $T = 1.5$ sec is used to capture the threat to this structure from the surrounding seismicity. Further the sample of records is scaled to a set of three common values of the spectral acceleration at $T = 1.5$ sec. in order to predict the statistics of the structural response (EDPs) at given ground motion threat levels. Therefore in the PEER methodology it is this IM that is used as the interface between the seismicity and the structural response.

Why and how was this choice made? What alternatives were considered and rejected? It is still not uncommon practice to use, for example, the peak ground acceleration in this same role. This observation raises questions such as what is the preferred measure of ground motion “strength” to use in that key role, how should one go about making that decision and what are the consequences of not making the “best” choice? These items are addressed next; the rest of this section will describe in more detail how the subject was addressed specifically for the Van Nuys Testbed.

An important first point is that we contend that the solution to these apparent “ground motion” questions should in fact be addressed, not purely as seismological questions, but rather primarily from the perspective of the larger PBEE analysis; in this context that means how does the choice of the IM affect the assessment of the EDPs and their likelihoods. What is the best IM from the perspective of its intended use? The EDPs are the place to focus because EDPs are the next step¹¹ in predicting the final PBEE objectives, namely DV likelihoods.

In brief a good IM does a good job of estimating the EDPs. For example, if we take a set of records from each of two different narrow ranges of magnitude (say, 5.0 to 5.5 versus 6.5 to 7.0), and scale them all first to the same $S_a(T_I)$ and then to the same PGA , and finally run the four scaled sets through dynamic analyses of a typical building, we will find that the average of, say, the third floor IDR will be more nearly the same for the two magnitude sets of records scaled to $S_a(T_I)$ than for the two sets scaled to PGA . This observation says that $S_a(T_I)$ is preferred to PGA as an IM because it is less likely to give the wrong answer if the choice of records used to predict the IDR is for any reason not consistent — with respect to magnitude, say — with those that threaten and ultimately shake the site. For this reason we say that $S_a(T_I)$ is more “sufficient” than PGA as a predictor of IDR. “Sufficient” because $S_a(T_I)$ is not typically aided by the additional knowledge of the event magnitude while PGA is. And the reason for this difference is that $S_a(T_I)$ already measures the strength of the ground motion in the frequency range that most affects the structural displacements, whereas PGA does not. Therefore knowing in addition the magnitude, in the latter case, helps one predict the correct spectral shape to which the PGA should be anchored so that the strength of the ground motion near the first-mode period can be better estimated. Further, for the same reasons, if we look at the scatter in $IDRs$ for a set of records scaled to the same $S_a(T_I)$ versus the same set scaled instead to the same PGA , the variability (as measured, typically, by the coefficient of variation or the standard deviation of the natural log — here called the “dispersion”) will be smaller in the former case. Again this outcome favors $S_a(T_I)$ over PGA . It implies that $S_a(T_I)$ is more “efficient” as a predictor of IDR , because one can predict IDR to the same degree of accuracy with a smaller set of records (hence

¹¹ Under the assumptions made in the PEER PBEE procedure (as exemplified by the framing Eq., Eq. (1.1) in Section 1.3), the likelihoods of different DM (and from there to likelihoods of different DV) levels are *conditionally independent of IM given a level of EDP*. In words, if I know the EDP level and wish to predict the DM value, it gives me no additional information about DM to also know the IM level that caused that EDP. The implication is that how we deal with IMs can be judged by the effects at the EDP level alone. Even if this conditional independence condition is not perfectly met in practice it is clear that the first-order effects will be at the EDP level. Any implications on DMs and DVs should be less sensitive to IM choice.

with fewer nonlinear analyses) with $S_a(T_I)$ as the IM than with PGA . Or, for the same number of records, one can predict IDR more confidently¹² with the former than with the latter as the ground motion measure or IM .

More precisely we can say that, all else being equal, we would like an IM which provides an accurate and high-confidence prediction of (to a first approximation) the mean value of the EDP for a given IM level. In more formal terms we would like that the IM provide an unbiased, minimum variance estimate of the mean EDP . A final practical requirement is that it is practically feasible to obtain the ground motion threat (the hazard analysis) in terms of the IM of choice. $S_a(T_I)$ and PGA are two cases for which a PSHA is always available, but this is not as yet true for many of the other more recently developed IM contenders. For example, we are only now developing the attenuation equations (ground motion prediction equations) necessary to produce a PSHA hazard curve for the inelastic spectral displacement of a simple elasto-plastic oscillator of given period and yield displacement, which is one of the proposals for the IM that we shall explore below.

3.4.2 The Process of Evaluation and Selection of IM for the Van Nuys Building

For the Van Nuys Testbed the team considered a list of contending IM s identified previously by the PEER IM working group (Bray, 2002) for building structures. These included the peak ground acceleration, PGA ; the spectral acceleration of a simple 5% damped elastic oscillator with a period in the 1.5 second (i.e., in the vicinity of the estimated first natural period of the longitudinal direction of the Van Nuys building¹³), $S_a(T_I)$; the inelastic spectral displacement of a simple bilinear inelastic oscillator with the same period and a specified yield displacement¹⁴, S_{di} ;

¹² Formally, the standard error of estimation of the mean IDR , which is proportional to the standard deviation of the IDR (divided by the square root of the sample size), is smaller if $S_a(T_I)$ is the IM than if PGA is put in that role.

¹³ Note it is not necessary that the period be precisely that of the structure, which is uncertain in any case, as it is only necessary to have a measure of the strength of the ground motion in the general period range in order for the S_a to be an effective IM . (Shome et al., 1998). The damping value is the standard value for which attenuation laws and hence hazard curves are available; it need not be the value that the structure itself might have. The $S_a(T_I)$ is being used only as a predictor not an estimator of the IDR and PFA responses. For this reason the (pseudo) spectral acceleration is equivalent to the spectral displacement because the two differ only by a constant.

¹⁴ This yield displacement should be representative of the actual structure and in principle should be obtained from a static pushover analysis of the building, if available (Luco and Cornell, 2004). The motivation for this IM is that, as a nonlinear oscillator response it is more representative of the anticipated behavior of the building than a linear oscillator, especially in the more severe, post-elastic, damaged regime. In addition a second version of the IM proposed by Luco that includes information about second-mode behavior and its potential impact on IDR s was

a measure proposed by Cordova et al. (2000) which is simply the square root of the product of the spectral acceleration at approximately the first-mode period and that at twice the first-mode period¹⁵, S_c ; and finally a set of vector IMs. These vector IMs include potentially, for example, simply $S_a(T_1)$ and the S_a at a second period (Shome, 1999), or as proposed by Conte (personal communication) $S_a(T_1)$ and any of a variety of second elements of the vector. These vector IMs have not as yet been well studied for any but SDOF systems and the hazard codes to make them practical are not as yet widely available (Bazzurro and Cornell, 2002); therefore these options were not considered further.

The study of alternative IMs for the Van Nuys testbed application consisted of tests of these IMs using three sources: the results of the OpenSees analyses of the longitudinal frame of the building, the assessment of more numerous results of other models of the Van Nuys building, and the review of other studies of MDOF structures. While sufficient for their intended purpose of PBEE response prediction, it was recognized that the OpenSees testbed analyses were quite limited for the purpose of IM studies. Therefore the OpenSees results were used more in a confirmatory basis. The general conclusion of prior studies (e.g., Shome, 1999) has been that $S_a(T_1)$ is generally an effective IM for first-mode dominated frame buildings with respect to displacement prediction, while PGA is a good candidate for peak floor acceleration estimation (Medina and Krawinkler, 2003, Taghavi and Aslani, 2003). (In particular each outperforms the other for the case cited.) These conclusions include considerations of practicality (e.g., availability of attenuation laws and PSHA results) as well as both efficiency and sufficiency. It has been shown that either S_{di} or S_c may well prove somewhat more efficient and sufficient than $S_a(T_1)$ for displacement prediction, especially for large ductility levels (Luco and Cornell, 2004, Cordova et al., 2000).

3.4.3 Results from Van Nuys IM Studies

The results of several Van Nuys building studies of IM efficiency are shown in Table 3.2. The entries in the table are the dispersions (standard deviations of the natural logs) or coefficients of

tested, but as anticipated it did not significantly outperform the simpler version for this seven-story structure so it will not be reported further here.

¹⁵ The motivation for this IM is that it “samples” the response spectrum of the input record both at the first mode period and at a longer period, which becomes a measure of the strength of the input in the period range to which the building is expected to become more sensitive while responding nonlinearly.

variation of the indicated EDP (maximum IDR or PFA) from three different sets of models and records and types of analyses of four alternative IMs. The lower this dispersion the more efficient the IM, i.e., the fewer the number of nonlinear analyses that must run in order to achieve any desired level of confidence band width. The general conclusions, given the first-digit accuracy of the estimates of the dispersions are (1) that *PGA* outperforms the other IMs listed as a predictor of PFA (Peak Floor Acceleration), and (2) that the other three IMs are all superior to *PGA* as predictors of IDR, while all provide levels of efficiency comparable to one another. The exception is perhaps at higher ductility levels, when $S_a(T_I)$ may not perform as well as S_c or S_{di} .

Table 3.2 Standard deviations of natural logs of EDPs for several IMs. Three models of the Van Nuys building and three sets of recordings, for two EDPs: max. IDR and max. PFA¹⁶.

	Jalayer Transverse Model and Baker Data				Lowes Long. OpenSees1 Model	Miranda Long. Model	
	Max. IDR (as recorded)	Max IDR (2x)	PFA (as recorded)	PFA (2x)	Max. IDR	PFA	PFA
$S_a(T = T_1; 0.8 \text{ or } 1.5)$	0.33	0.58	0.27	0.27	0.42	0.43	0.2 - 0.6
PGA (g)	0.49	0.76	0.18	0.17	0.60	0.28	0.1 - 0.25
Cordova IM	0.27	0.49	0.25	0.26	0.36	0.48	
S_{di}	0.30	0.53	0.26	0.29	0.40	0.37	
Luco q1I&2E	0.30	0.52	0.25	0.29	*	*	

The column headings in the table suggest that there are several significant differences among the three studies, in particular among the models used, the records analyzed and the treatment on the records and results. The last item in particular may have some affect on the conclusion that $S_a(T_I)$ is virtually as good as S_c and S_{di} as an IDR predictor. Let us briefly discuss these studies.

The Lowes OpenSees model will be discussed in Chapter 4; the records used and their scaling to three stripes of common $S_a(T_I)$ levels have been discussed above. As will be seen in

¹⁶ Note: given the limited sample sizes the estimates are accurate only to the first significant figure.

Chapter 4, at the higher two stripe levels most of the analyses (12 of 20) suggest very severe IDRs, (>10% drift ratios) interpreted here as predictions of collapse. Therefore the remaining 18 results have simply been treated as a “cloud” through which an EDP versus IM line has been fit¹⁷ with the dispersion being defined as the standard deviation of the residuals with respect to this line. One implication is that the dispersions cited are those of the non-collapse cases *only* and so do not reflect the large “collapse” displacements at higher ground motion levels; the dispersions are therefore in effect “too small” in absolute terms. While these non-collapse dispersions retain some comparative value (simply because they are all calculated in the same way for all IM candidates), it is nonetheless with respect to the larger, nonlinear displacements that S_c and S_{di} are expected to outperform $S_a(T_I)$ and these are not well reflected in this data set. (This set of runs was also used by T. Hutchinson (personal communication) to study several IMs, such as Arias intensity, preferred by geotechnical engineers because like PGA they are not “tuned” to any specific period. They proved less effective than either PGA as a predictor of PFA or $S_a(T_I)$ as a predictor of IDR.)

The E. Miranda model was designed to focus on less severe responses, prior to the onset of strength degradation in the members, where non-structural economic damages are typically dominant. Eighty records were scaled to eight different $S_a(T_I)$ levels, leading to eight unambiguous measures of the dispersion of the EDPs given the $S_a(T_I)$ as IM (Taghavi and Aslani, 2003). In the case of PGA as IM, however, the same 80 by 8 (640) EDP results were simply re-plotted versus PGA ; the dispersion was calculated for a sequence of PGA intervals giving dispersion versus PGA level. (This study compared only PGA and $S_a(T_I)$. The potential problem discussed in the previous footnote applies here as well.)

The F. Jalayer model (of the smaller, transverse frame) was used by J. Baker (unpublished) to study the testbed IMs with a set of seventy records selected to reflect primarily a range of magnitudes. They were first run simply as recorded and then again after scaling by a

¹⁷ The line is fit as a straight line on a log-log paper, i.e., the assumption is that the trend of EDP vs IM is a power law. Alternative ways to display and analyze such EDP vs IM data are discussed in Shome (1999) and Jalayer (2003). The notions of clouds, scaled clouds, stripes and IDAs (incremental dynamic analyses) are discussed. In this case the analyses were based on records initially “striped” with respect to $S_a(T_I)$ levels, and then the same EDP results were simply re-plotted versus the other IM choices, and treated as “cloud” data. There are some known potential interpretation difficulties when data that have first been “striped” based on one IM are then re-plotted versus another IM (Giovenale et al., 2004). For example, in the limit, if the results were all from a single $S_a(T_I)$ stripe, the dispersion when the EDP was plotted versus PGA would be strictly the dispersion of EDP given PGA and $S_a(T_I)$, which would be smaller than the dispersion given PGA alone. Therefore these results may somewhat underestimate the dispersion of the EDPs given IMs other than $S_a(T_I)$.

common factor of two. Therefore in each case the EDP results represent a “cloud” (or scattergram) of data no matter which IM they are plotted against. As with the OpenSees model the dispersions reported are based on the residuals from (curvilinear) lines fit to the data. The difficulties with this approach are that the results may depend on the functional form of the model fit and also on the range and distribution of the data because only a single value of the dispersion is obtained, whereas it is known that the IDR dispersion tends to increase as the degree of nonlinearity increases, while that in PGA may decrease. (Note that the single IDR dispersion increases when the record levels are doubled.) While the conclusions with respect to PGA versus the three other IMs are clear, these issues may cloud the more subtle distinctions among $S_a(T_I)$, S_c and S_{di} , especially because the first is insensitive to the degree of nonlinearity, the second reflects in effect a fixed degree of nonlinearity, while the last should mimic the degree of ductility. As mentioned the anticipated efficiency of the second two IMs with respect to $S_a(T_I)$ at higher ductility levels is displayed here only by comparing the as-recorded versus the scaled results, where the average ductility is higher. The anticipated inefficiency of S_c versus $S_a(T_I)$ in the linear and low ductility range is also not evident in these results.

In addition to these efficiency studies, which suggest that *PGA* would be the preferred IM for PFA prediction and that S_c or S_{di} might, on the whole, be somewhat preferable to $S_a(T_I)$ (especially for higher levels of nonlinearity), the choice of an IM depends on issues of practicality¹⁸. First, it is as yet uncommon and unfamiliar to use more than a scalar IM in either the hazard or response prediction phases. Therefore we cannot use one IM for PFA and another for IDR; given the lack of costly acceleration sensitive elements in the Van Nuys building, it is appropriate here to not select the *PGA* as the IM. With respect to the three other candidates, the current lack of an attenuation law for S_{di} makes it impossible to provide the IM hazard curve, λ_{IM} , needed for the full PBEE analysis. While (by design) it is straightforward to construct an attenuation law (and subsequently a hazard curve) for S_c , its only marginally greater efficiency

¹⁸ With respect to the question of sufficiency, a first-order check of the sufficiency of an IM is to do a regression analysis of EDP on IM and magnitude to assess whether, in the presence of the IM, magnitude adds new information. This can be checked by asking whether the estimated regression coefficient on magnitude significantly different from zero (i.e., the desired no dependence). It was not feasible to make such an assessment with the Van Nuys testbed records because they were all from virtually the same magnitude. The Jalayer Model/Baker Data Set was used for such a study and it was concluded, as expected from similar prior studies, that with respect to MIDR all the IMs here were sufficient with respect to magnitude except *PGA*, i.e., the magnitude coefficient was not significantly different from zero at the 5% significance level for all but *PGA*.

(at higher ductility levels only) with respect to the readily available $S_a(T_I)$, make it altogether less desirable in this case than $S_a(T_I)$ as the IM of choice.

It is worth stating what would have resulted if it had been concluded that another IM, e.g., S_{di} or S_c , was preferred. First a PSHA for that IM would be needed, with disaggregation analysis to suggest the most likely magnitude-distance scenarios causing the threat at several MAF levels. From these results record selection could proceed as before. It is likely at this site that in all IM cases, except perhaps PGA, the dominant scenarios would not change much. Further there is evidence that the conclusions of PBEE will not be very sensitive to the selection of records (at least provided, as at this site, that forward directivity is not an issue). Therefore the analysis would not differ significantly from that demonstrated in this report, except that either the uncertainty in the estimate of the EDPs (and subsequently the DVs) would improve to some degree, or alternatively the number of records selected at each MAF level might be somewhat reduced without loss of accuracy.

3.5 EFFECTS OF SITE SOIL PROFILE ON IMS AND GROUND MOTIONS

Author: S. Kramer

3.5.1 Introduction

The soil profile beneath the Van Nuys structure will influence the amplitude, frequency content, and duration of the motions that reach the structure. The extent of its influence will depend on the thicknesses, stiffnesses, and damping characteristics of the various soil layers that underlie the site. Because the site soil profile will affect performance of the structure, its characteristics and anticipated seismic response are described in the following paragraphs.

3.5.2 General

Intensity measures for the Van Nuys testbed site can be developed in different ways: (a) using target spectra developed from an attenuation relationship that allows specification of a broadly defined site category, (b) applying amplification factors to target spectra developed from a rock attenuation relationship, and (c) from site response analyses based on motions consistent with a

rock-level target spectrum. These approaches involve increasing levels of effort and information, but also provide increasing ability to consider detailed site conditions. Site response analyses can be one-, two-, or three-dimensional and can include basin and/or topographic effects when they are significant; it is most common, however, to perform one-dimensional site response analyses.

Stewart and Baturay (2002) studied these different approaches to ground motion prediction using suites of recorded motions. The ground motion records were divided into various site categories, and *IMs* from the recorded motions were compared with predictions from attenuation relationships, rock attenuation relationships with amplification factors, and ground response analyses. The results indicated that site-specific ground response analyses provided consistently improved estimates of surface motions (judged in terms of response spectral ordinates) only for soft soil sites (e.g. NEHRP Category E) at periods less than about 1 sec. For other conditions, the dispersion in spectral accelerations predicted by site-specific ground response analyses was not significantly lower than when predicted by attenuation relationships or attenuation relationships with amplification factors. Aleatory variabilities in soil properties were not considered in these studies.

Because the Van Nuys profile is moderately stiff (NEHRP Category D), predictions of ground surface response spectral ordinates by attenuation relationship and/or by attenuation relationship with amplification factors would be expected to be about as accurate as predictions based on site-specific ground response analyses. Somerville (2002) developed a set of ground surface motions based on the amplification factor approach — the rock spectra developed for the USGS ground motion maps were multiplied by amplification factors equal to the ratio of soil to rock spectral ordinates in the Abrahamson and Silva (1997) attenuation relationship to obtain corresponding soil spectra. Somerville then selected suites of ground motions that were consistent with the soil spectra. Using the results of Stewart and Baturay (2002), these spectra and ground motions should be as reasonable as spectra developed by performing site-specific ground response analyses. Nevertheless, a series of analyses were performed to investigate the influence of uncertainty in soil parameters on site response and structural performance.

3.5.3 Site Conditions

The Van Nuys site is located on the southeast corner of Roscoe Boulevard and Orion Avenue in San Fernando Valley. As part of a damage investigation following the 1994 Northridge Earthquake, Geosystems (1994) performed a geotechnical investigation for the Van Nuys building. Their report contains data from four borings up to 50 ft deep, one near each corner of the building. It also includes some density and moisture content data as well as direct shear test data and consolidation test data for the soils at the site. The soils are described as “mostly brown silty fine sand and sandy silts with some clay binder” and of a composition that “is fairly consistent” to depths of 30 – 35 ft. Fill materials were encountered to depths of 5 – 10 ft on the south side of the building. Logs of the four borings are summarized in Figure 3.6.

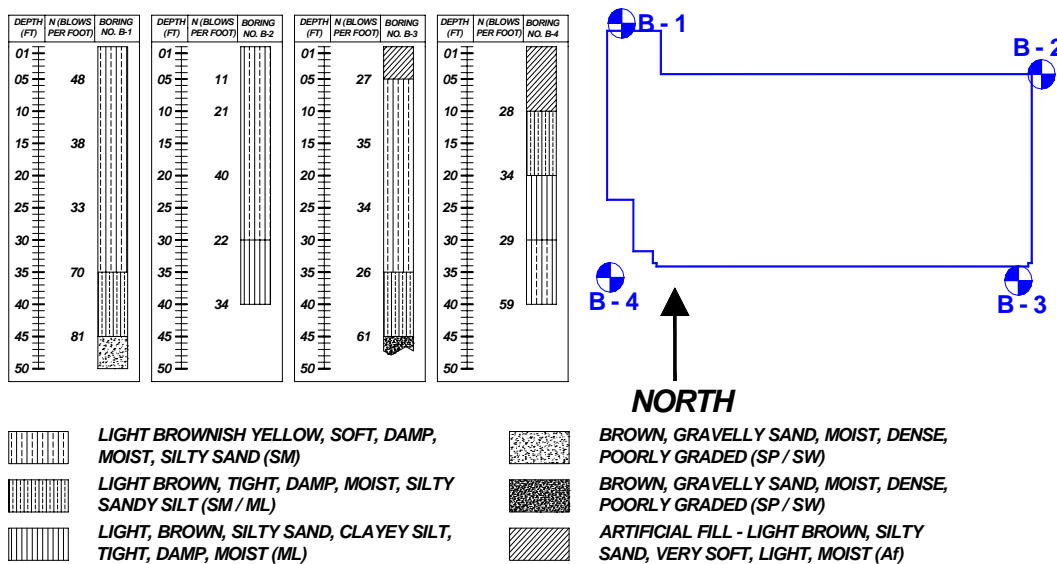


Fig. 3.6 Boring logs for Van Nuys testbed site

The results of penetration tests are presented in the boring logs, but detailed descriptions of the manner in which the penetration tests were performed were not presented. Various laboratory tests, including moisture-density, direct shear, and consolidation tests, were also performed. Assuming the penetration resistances are equivalent to Standard Penetration Test resistances, and using the available laboratory data, a generalized soil profile for the site was developed (Table 3.3). This profile represents a reasonable interpretation of the shallow

subsurface conditions given the available subsurface data. It should be noted that no deep subsurface information is available for this site.

Table 3.3 Interpreted soil profile for Van Nuys building site from available subsurface information

Depth (ft)	Description	Unit weight, γ (pcf)	Penetration Resistance, N_1
0 - 8	Fill	117	45
8 - 18	Silty sand	114	35
18 - 28	Silty sand	114	31
28 - 33	Silty sand	119	19
33 - 45	Sandy silt	122	11
>45	Gravelly sand	127	49

This profile was used to develop a best estimate stiffness profile for the purpose of performing site-specific response analyses. Because shear wave velocity measurements were not available, maximum shear modulus values were estimated by empirical correlation to SPT resistance. The SPT N -values listed in Table 3.3 were assumed to be equal to $(N_1)_{60}$ values (i.e., an energy ratio of 60% in the penetration tests, which corresponds to typical U.S. practice, was assumed) and then the empirical correlation by Ohta and Goto (1976) was used.

Since only shallow subsurface data was available, penetration resistances had to be extrapolated to greater depths in order to develop maximum shear moduli for those soils. Shear wave velocities were then computed from maximum shear moduli and soil densities. The best estimate shear wave velocity profile, which was used for the site-specific ground response analyses, is shown in Figure 3.7. This profile shows a relatively gradual increase in shear wave velocity with depth, i.e., a profile without strong impedance contrasts. While data to confirm this site characteristic is not available for the Van Nuys testbed site, shear wave velocity profiles from several sites in proximity to the Van Nuys testbed site measured as part of the ROSRINE program show similar velocity profiles. These profiles show a gradual increase in shear wave velocity as the range of velocities commonly assumed to represent “seismic bedrock,” i.e., material with a shear wave velocity greater than 2,500 ft/sec, are approached.

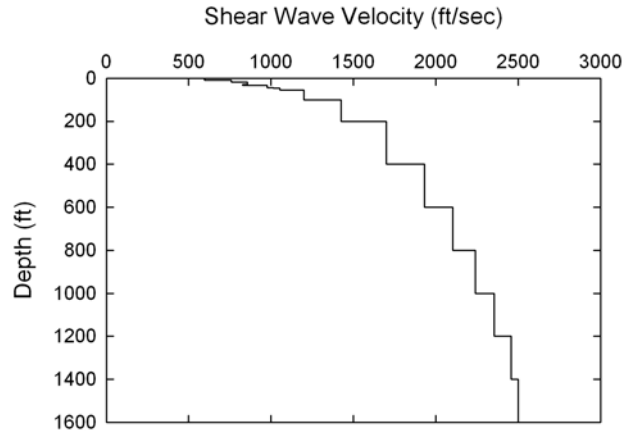


Fig. 3.7 Base case shear wave velocity profile

3.5.4 Site-Specific Ground Response Analyses

In order to evaluate the effects of aleatory uncertainties in soil properties on *EDPs*, a series of site-specific ground response analyses were undertaken. In order to maintain consistency with structural investigations, which used the Somerville soil motions as inputs to the base of the structure, an attempt at deconvolving the Somerville motions to bedrock level was made. Deconvolution of motions recorded at one site through generic soil profiles or soil profiles from other sites can lead to unreasonable results, particularly for deep soil profiles. In this case, suitable deconvolved motions could not be obtained for the Van Nuys testbed site. Local minima in the transfer function for surface/rock motion corresponded with significant high-frequency components of the Somerville motions to a degree that deconvolved rock motions with unreasonably high amplitudes were obtained.

3.5.4.1 Input Motions

To allow site-specific ground response analyses to be performed on the entire soil profile, a set of rock outcrop motions was developed. Development of this set of motions was done in a manner as consistent as possible with the manner in which Somerville obtained the soil motions. The procedure was intended to produce a suite of ground motions compatible, as an ensemble average, with the 475-year uniform hazard spectrum (rock). The PEER Strong Motion Database was queried to obtain motions that satisfied the following search criteria:

$V_s > 750$ m/sec site condition

$6.0 < M < 7.5$

$0 < R < 50$ km

This search returned a total of 42 strong motions records, each of which was examined for compatibility with the 475-year rock spectrum. Each motion was scaled by a constant value until the least squares error w/r/t the target spectrum was minimized. A ranked list of the scaled motions, from smallest least squares error to largest, was created. The error magnitudes and the scaling factors required to produce those error magnitudes were examined for selection of a suite of 20 motions. Selection of the 20 motions used in the initial analyses was based on consideration of both the error magnitudes and the magnitudes of the scaling factor. The motions were then all scaled by a factor that caused their mean value to match the target (rock) spectrum at a period of 1.5 sec. Response spectra for the resulting 20 motions are shown in Figure 3.8.

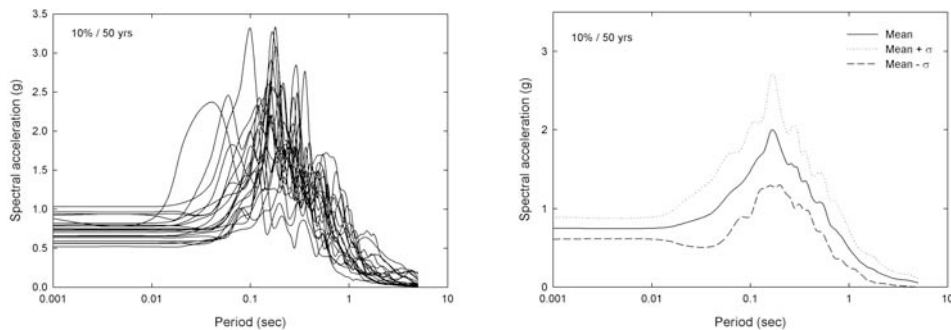


Fig. 3.8 Rock outcrop response spectra for 10%/50 yr hazard level (a) spectra for individual motions, and (b) mean and mean $\pm \sigma$ spectra

The issue of intensity measure definition can be examined by considering examples of site response analyses. Structural engineering research has established spectral acceleration at the fundamental period, $S_a(T_1)$, as an efficient and sufficient intensity measure for structures like the Van Nuys testbed structure (Section 3.4). The effect of the Van Nuys soil profile on the definition of an optimum intensity measure was illustrated with a series of analyses. A suite of 60 motions covering a range of magnitudes and distances was applied to the Van Nuys profile, with the resulting surface motions applied to a bilinear SDOF structure (using the computer program, SNAP). The correlation between the resulting *EDPs* and bedrock-level spectral acceleration were computed for 150 spectral accelerations at periods ranging from 0.001 sec to

20 sec (assuming a power law relationship between S_a and EDP). Using the cyclic ductility, d_{cyc} , as the EDP , the computed correlation was highest (Figure 3.9(a)) for $S_a(T = 1.70 \text{ sec})$, indicating that the compliance of the soil deposit caused the period of maximum EDP efficiency to be increased from 1.5 sec (the fundamental period of the structure) to 1.7 sec. A scatterplot of the $EDP-IM$ relationship at that period is shown in Figure 3.9(b). All subsequent analyses were performed with the motions scaled to the target (bedrock-level) spectral acceleration at $T = 1.7$ sec.

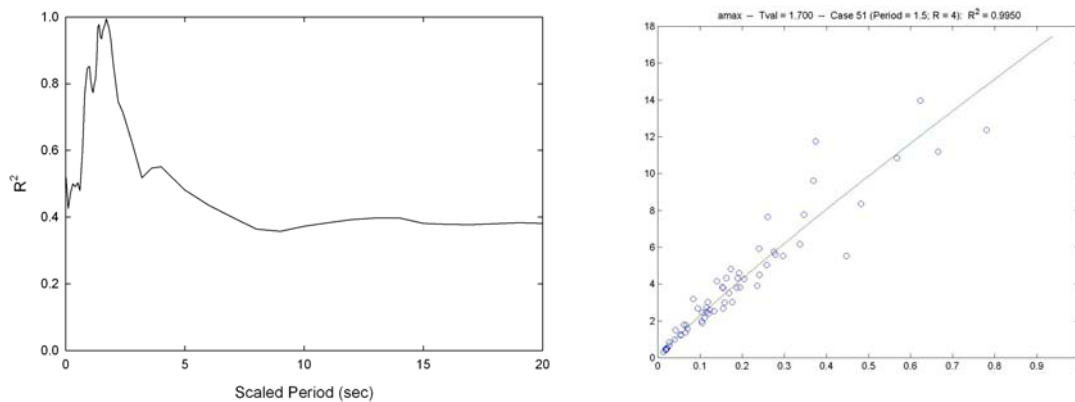


Fig. 3.9 Response of SDOF structure with $T_l = 1.5 \text{ sec}$, $R = 4$, and $\alpha = 0.05$: (a) correlation between spectral accelerations at various structural periods and EDP (d_{cyc}), and (b) d_{cyc} vs. $S_a(T = 1.70 \text{ sec})$

3.5.4.2 Soil Properties

The effects of uncertainties in soil properties on $EDPs$ were examined by a series of site and structural response analyses. The Van Nuys structure was modeled as a bilinear SDOF system with a natural period of 1.5 sec, an R -factor of 4, and an α parameter (strain hardening ratio) of 0.05. The results presented in the following sections relate to equivalent linear site response and the EDP d_{cyc} , although similar conclusions were obtained for other $EDPs$.

In equivalent linear analyses, soils are characterized in terms of their unit weights, low-strain stiffnesses (using either low-strain shear modulus, G_{max} , or shear wave velocity, V_s), their modulus reduction behavior and their damping behavior. Near-surface (depth < 50 ft) unit weight information was available and deeper unit weights could be estimated with good accuracy. Modulus reduction and damping behavior, which describe the degree of nonlinear

behavior of the soil, are related, and were described using the model of Darendeli (2001). Low-strain stiffness is ideally obtained by in-situ shear wave velocity measurements; because such measurements were not available for the Van Nuys structure, low-strain stiffnesses had to be estimated by empirical correlation to SPT resistance. Because significant uncertainty exists in the empirical correlations between SPT resistance and low-strain shear modulus (Ohta and Goto, 1976) as well as in the SPT measurements themselves, a high degree of uncertainty was assigned to the low-strain stiffness, particularly in the deeper soils where the presence of gravel-sized particles increases the uncertainty in both SPT resistance and the SPT- G_{\max} correlation. This uncertainty would have been lower if in-situ shear wave velocity measurements had been made. Assumed soil property uncertainties are described in Table 3.4.

Table 3.4 Assumed coefficients of variation for rock, soil, and structural properties

Property	Coefficient of Variation	
Structural		
Yield strength, η	0.12	
Damping ratio, ξ	0.40	
Post-yield stiffness, α	0.40	
Soil	Unit 1 (Depth < 33 ft)	Unit 2 (Depth > 33 ft)
Unit weight, γ	0.10	0.10
$(N_1)_{60}$	0.40	0.60
G/G_{\max}	Darendeli	Darendeli
Damping	Darendeli	Darendeli
Friction angle, ϕ	0.10	0.20
$G_{\max} (N_1)_{60}$ correlation	0.65	0.65
Rock		
Unit weight, γ	0.10	
Shear wave velocity, V_{sr}	0.30	

Friction angle, unit weight, and SPT resistance were assumed to be correlated at a given depth. All soil properties were assumed to be spatially correlated with an exponential autocorrelation function in the vertical direction.

3.5.5 Uncertainty in $EDP|IM$

The conditional uncertainty in EDP given IM was evaluated for each of the 20 input motions using both simplified and more rigorous techniques. The simplified analyses were performed using first-order second-moment (FOSM) analyses, and the more rigorous analyses using Monte Carlo simulations. Recognizing that the uncertainty in specification of the IM is likely to dominate that involved in $EDP|IM$ and that only COV-level information is available for the majority of the soil/structural properties involved in the $EDP|IM$ calculation (Cornell, personal communication, 2003), characterization of the uncertainty in $EDP|IM$ using the simplified approach is likely to be appropriate for PBEE analyses.

The FOSM and Monte Carlo analyses were observed to produce results with consistencies that depended strongly on the level of nonlinearity induced in the soil deposit. Because this level of nonlinearity varied significantly from one ground motion to another, the following sections compare and contrast the uncertainties in $EDPs$ produced by the two methods of analysis for two ground motions — one which induced strong nonlinearity in the soil and one which did not.

3.5.5.1 FOSM Analyses

FOSM analyses showed that the mean EDP values (i.e., first moments) were generally well behaved from one rock input motion to another. However, the analyses frequently showed significant differences in computed variances (second moments) — one group of motions produced low variances and the other produced substantially higher variances. For example, two motions, referred to as Motion 6 and Motion 13, produced mean d_{cyc} values of 5.51 and 6.51, respectively. The two motions produced very different second moments, however — variances of 2.6 and 20.7, respectively. Examination of the FOSM calculations showed that motions producing high variances generally did so because of a high gradient produced by strongly nonlinear behavior in the Unit 1 (depth < 33 ft) soils when the modulus reduction curve was

permuted in the “soft” direction. This high gradient produced a contribution to FOSM variance that was not present in other motions.

3.5.5.2 Monte Carlo Analyses

Monte Carlo analyses allowed estimation of the entire distribution of computed *EDPs*. The Monte Carlo analyses, however, were also affected by the tendency of some motions to induce large strains in the shallow soils for realizations that had low G_{\max} values and/or low modulus reduction curves.

The results of Monte Carlo analyses for Motion 6 are shown in the form of a histogram in Figure 3.10(a). Motion 6 produced first and second moments of 5.06 and 2.84, respectively, and very few values of $d_{\text{cyc}} < 1$ (linear structural response); these moments correspond reasonably to those (5.51 and 2.60) produced by the FOSM analyses for that motion. The simulated Monte Carlo results are most reasonably fit by a normal distribution — a normal distribution with moments equal to those of the Monte Carlo simulations are shown in Figure 3.10(b). The normal distribution with moments equal to those obtained from the FOSM analyses is also shown; that distribution is seen to be offset from the Monte Carlo distributions by the difference in mean values (approximately 0.5 d_{cyc} units) obtained from the two analyses.

The results of Monte Carlo simulations for Motion 13 are shown in the form of a histogram in Figure 3.11(a). The difference between the histogram of Motion 6 d_{cyc} results is striking, particularly the large fraction of the simulations that produced $d_{\text{cyc}} < 1$ (linear structural response). Examination of the results of the Motion 13 simulations showed that the low d_{cyc} values were associated with simulations that produced large strains within the soil profile. A period ratio, T/T_s , can be defined as the ratio of the fundamental period of the soil deposit based on strain-compatible stiffnesses to the original fundamental period of the soil deposit (based on low-strain stiffnesses); this quantity increases with increasing “damage,” as reflected by plastic strains, to the soil profile. The plot of Figure 3.11(b) shows that the majority of the simulations that produced low (less than unity) values of d_{cyc} produced high values of the period ratio. In these cases, large soil strains caused the ground surface motions to be diminished, at least in the range of periods that most strongly influence d_{cyc} — the highly nonlinear behavior of the soil deposit “shields” the structure from damage due to ground shaking, at least as reflected in d_{cyc} .

Similar behavior was observed for other *EDPs*. It is important to recognize, however, that strong degradation of soil stiffness may produce irregular permanent soil deformations that could cause structural damage that would not be reflected by the *EDPs* considered here.

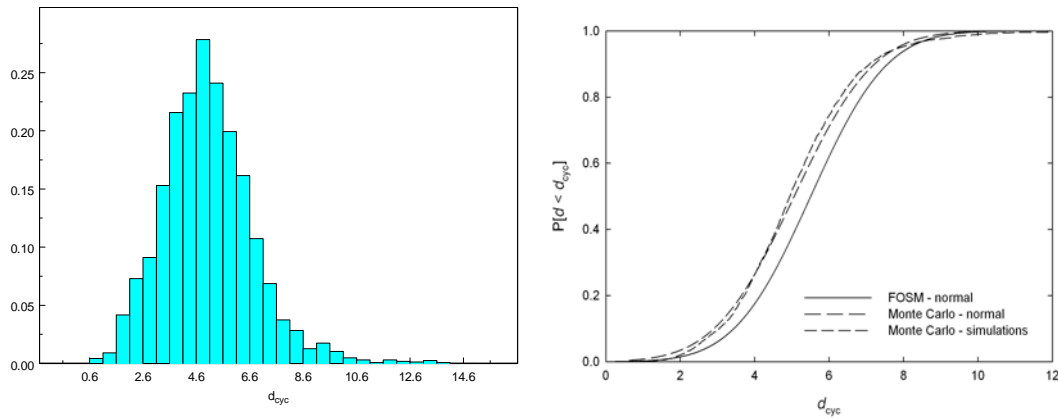


Fig. 3.10 Results of Monte Carlo simulations for Motion 6: (a) histogram of d_{cyc} values, and (b) comparison of distribution obtained from simulations with normal distributions based on FOSM and Monte Carlo moments

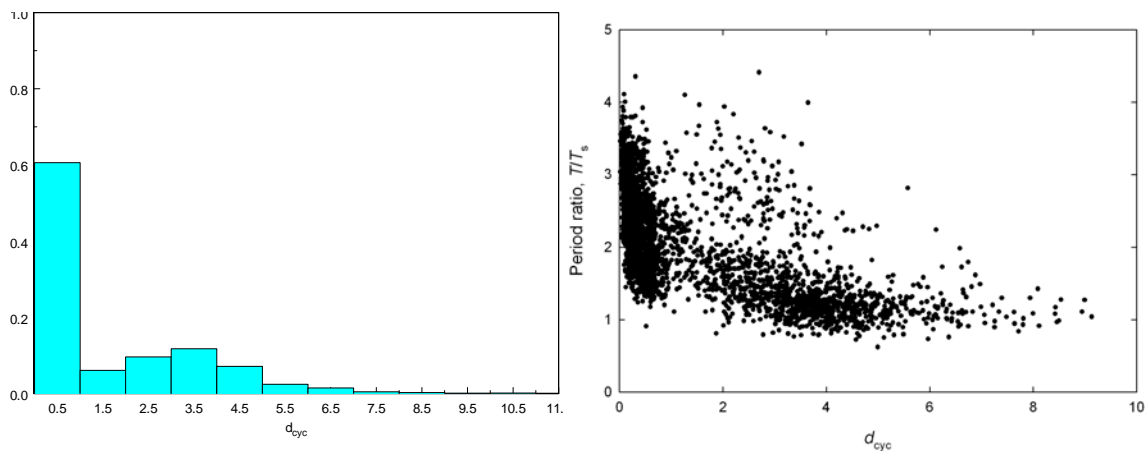


Fig. 3.11 Results of Monte Carlo simulations for Motion 13: (a) histogram of d_{cyc} values, and (b) scatterplot of d_{cyc} and period ratio values

3.5.5.3 Discussion

The results of the FOSM and Monte Carlo analyses indicate that, at least for equivalent linear site response analyses, FOSM analyses can produce reasonable estimates of *EDP*|*IM* when significant nonlinearity is not induced in the soil. The Monte Carlo analyses showed, however,

that certain motions produced substantial nonlinearity in soil response for some realizations of low-strain soil modulus and/or modulus reduction behavior; for those cases the FOSM analyses indicate high variances, but the Monte Carlo analyses allow a more complete visualization of the relationship between soil response and structural response. The analyses performed for the Van Nuys testbed lead to several important conclusions:

Selection of intensity measures must consider both the soil and the structure. For the Van Nuys structure, which had a fundamental period of 1.5 sec, compliance of the soil profile indicated that lower dispersion in *EDPs* would be expected when bedrock-level ground motions were scaled to spectral accelerations at a period of 1.7 sec.

Ground motion selection for performance-based evaluations must be performed with particular care when the fundamental period of the soil deposit differs significantly from the fundamental period of the structure. Ground motions scaled to spectral acceleration at a period expected to minimize dispersion in a structural *EDP* (a period of 1.7 sec for the Van Nuys case) may have substantially different amplitudes at the fundamental period of the soil deposit (approximately 3.3 sec for the Van Nuys case); these differences can lead to significant differences in the response of the soil profile, particularly at lower hazard levels (i.e., stronger levels of shaking). At the 10%/50 yr hazard level, some motions induced strongly nonlinear soil response and others did not, leading to substantial record-to-record variability.

Both geotechnical and structural aspects of response must be considered in a performance-based evaluation, particularly in cases where uncertainties are high. The high uncertainties in soil stiffness, which resulted from the fact that the low-strain stiffness had to be estimated using empirical correlations to SPT blowcounts, led to significant probabilities of highly nonlinear site response for some ground motions. This behavior indicates the need for definition and tracking of geotechnical *EDPs*, and for corresponding *DMs* and *DVs* that will allow the effects of geotechnical performance to be properly considered within the PEER PBEE framework.

4 Prediction of EDPs

4.1 CONNECTING HAZARD ANALYSIS WITH STRUCTURAL ANALYSIS

Given the ground motion hazard, a vector of Engineering Demand Parameters, *EDPs*, needs to be computed, which defines the response of the building in terms of parameters that can be related to *DMs* and *DVs*. The *EDP* vector should include all parameters of relevance for damage and losses to the soil/foundation/structure system as well as the nonstructural and content systems. The tool used here for the computation of *EDPs* is nonlinear response history analysis (NRHA), which requires seismic hazard information and ground motion records as well as development of an analytical model that incorporates all important characteristics of the soil-foundation-structure system.

The preceding chapter has provided pertinent information on the ground shaking hazard, with the following main results and observations:

- The spectral acceleration at the first mode period of the structure, $S_a(T_1)$, has been selected as the primary *IM*. For this relatively simple building, which is located at a site that is not significantly affected by near-fault effects, this *IM*, for which hazard data are readily available, is believed to be sufficient. Other scalar *IMs*, such as *PGA*, S_{di} , and S_c , deserve consideration but are not pursued further in this study.
- Hazard curves for $S_a(T_1)$ have been developed, with T_1 being the first mode period of the structure. Since the structure was damaged in several previous earthquakes, the first mode period was estimated as $T_1 = 1.5$ seconds.
- Three sets of ten ground motions each have been generated, representing the ground shaking at the 50/50, 10/50, and 2/50 hazard levels.
- The hazard curves and ground motions have been generated for “generic” soil profile type D, without consideration to the local site soil conditions. A sensitivity study on the

effects of variations in soil properties on the response of SDOF systems has indicated that local site conditions may have an important effect on the response if the ground motion causes significant soil nonlinearity. This effect is not pursued further in this study.

- The hazard curves and ground motions are for the free-field, i.e., they ignore potential soil-foundation-structure effects. This issue is pursued further in Section 4.2.

The IM hazard curve, together with the three sets of ground motion, can be utilized in different ways to predict EDPs by means of nonlinear response history analysis (NRHA). As provided in Somerville and Collins (2002), the three sets are scaled to the 50/50, 10/50, and 2/50 values of the $S_a(T_l = 1.5 \text{ sec})$ hazard curve. With this scaling, NRHA will produce 10 values each of EDPs at these three hazard levels, generating statistical information at three discrete values of $S_a(T_l)$. This type of analysis, referred to as stripe analysis (Jalayer, 2003), provides information that may or may not be sufficient to carry out the integration involved in Eq. (1.1), particularly if the relationship between the IM and the EDP is highly nonlinear. More comprehensive statistical data on IM-EDP relationships are generated through an Incremental Dynamic Analysis (IDA) in which the IM is increased in small increments, providing a large number of statistical data points on EDPs that permit numerical integration of the two rightmost terms of Eq. (1.1), see Figure 4.1. The outcome of this explicit integration over the full IM hazard curve is an EDP hazard curve of the type shown in Figure 4.2. The integration process, defined by the following equation, is straightforward but presumes that the ground motions used to determine EDPs are representative for the full range of IMs contributing significantly to the integral (Krawinkler et al., 2003).

$$\lambda_{\text{EDP}}(y) = \int \text{P}[\text{EDP} \geq y \mid \text{IM} = x] \, d\lambda_{\text{IM}}(x) \quad (4.1)$$

where $\lambda_{\text{EDP}}(y)$ = mean annual frequency of EDP exceeding the value y
 $\text{P}[\text{EDP} \geq y \mid \text{IM} = x]$ = probability of EDP exceeding y given that IM equals x
 $\lambda_{\text{IM}}(x)$ = mean annual frequency of IM exceeding x (ground motion hazard)

Both the stripe option and the IDA option have been exercised in this testbed study. The problem with the stripe option is that the model of the structure exhibits dynamic instability (collapse) for several of the 10/50 and most of the 2/50 ground motions, resulting in incomplete

data sets at two of the three stripes. Thus, more emphasis is placed on the IDA option, which also permits an assessment of the collapse probability of the structure (Section 4.5).

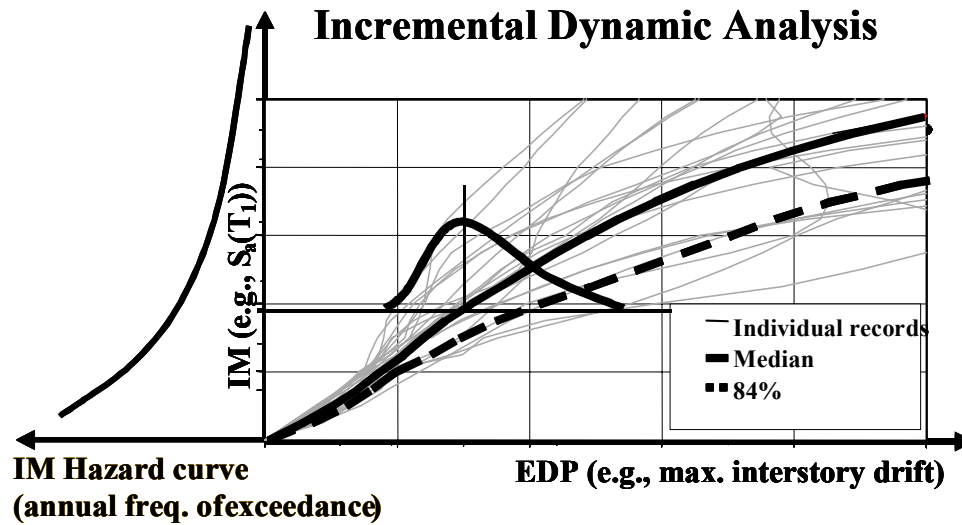


Fig. 4.1 Illustration of probabilistic seismic demand analysis (Krawinkler and Miranda, 2004)

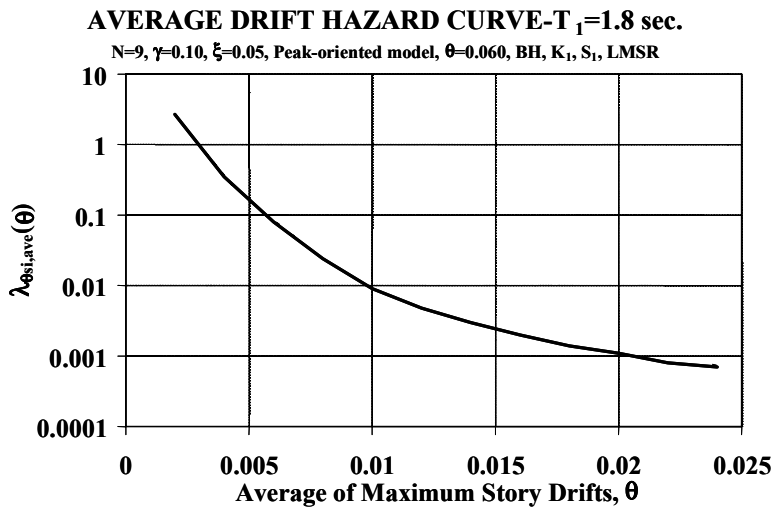


Fig. 4.2 Example of drift hazard curve (Krawinkler et al., 2003)

The validity of the predicted EDPs may depend strongly on the type of analytical model used in the NRHA. In this study only two-dimensional models were employed, but much attention has been paid to replication of all important phenomena that may significantly affect the EDPs at all levels of deformations. This generated large modeling challenges, which are addressed in Section 4.3. The question whether soil-foundation-structure interaction effects have

a significant effect on the EDP predictions is addressed in Section 4.2. Results for EDPs are presented in Section 4.4. Considering that most of the potential losses are from structural components and nonstructural drift sensitive components and subsystems, the primary EDP of interest is the interstory drift ratio, IDR. The issue of collapse is addressed in Section 4.5, with a relatively straightforward procedure proposed for the prediction of the collapse probability. The process was not carried forward explicitly to an estimation of fatalities. A study that provides data on fatalities given that collapse occurs, is summarized in Appendix D. Even though this study does not relate directly to the Van Nuys building, it is important because it provides a fatality model for non-ductile concrete frame structures that could be applied to the Van Nuys building as it existed before being strengthened after the Northridge earthquake.

4.2 FOUNDATION MODELING AND EFFECTS OF SFSI ON EDPS

Authors: B. Kutter, S. Kramer, G. Martin, T. Nagae, T. Hutchinson, J. Stewart

4.2.1 Introduction

There are at least two aspects to soil-structure interaction (SFSI) that should be evaluated in performance based design of buildings.

1. Dynamic SFSI — the influence of soil and foundation on the vibrations of the structure. Dynamic SFSI may affect resonant frequencies and damping of structure vibrations. The dynamic SFSI may be due to inertial interaction and kinematic interaction, including base area averaging and interaction over the height of deep foundations.
2. Static SFSI — the loads applied to the structure associated with permanent or gradual deformations of the soil and/or foundation. Differential displacements and rotations of different portions of the building foundations put stress on the building. These effects can be significant if the dynamic and static loads approach or exceed the capacity of the foundations.

The foundation conditions at the testbed site were studied and the effects of SFSI on the building response were evaluated. The effect of SFSI on building response, due to compliance of the pile foundations, was evaluated by comparing calculated building response with SFSI to

fixed-base building response. Two methods are used to account for pile foundation compliance: discrete uncoupled “soil springs” using ground surface motions as input and explicit inclusion of piles with p-y springs attached to the free field ground motions.

4.2.2 Foundation Conditions at the Van Nuys Testbed

The foundation below the Van Nuys building is a series of friction piles integrated with pile caps as shown in Figure 4.3. There are approximately four different types of pile-pile-cap arrangements, ranging from single piles at select perimeter locations to 4-pile groups. Pile and pile-groups are nominally integrated with 24" deep grade-beams at the perimeter of the building and 12" deep tie beams in the interior. A geotechnical report prepared by GeoSystems (1994) indicates primarily medium dense silty sands at the site as shown in the four boring logs reproduced in Figure 3.6.

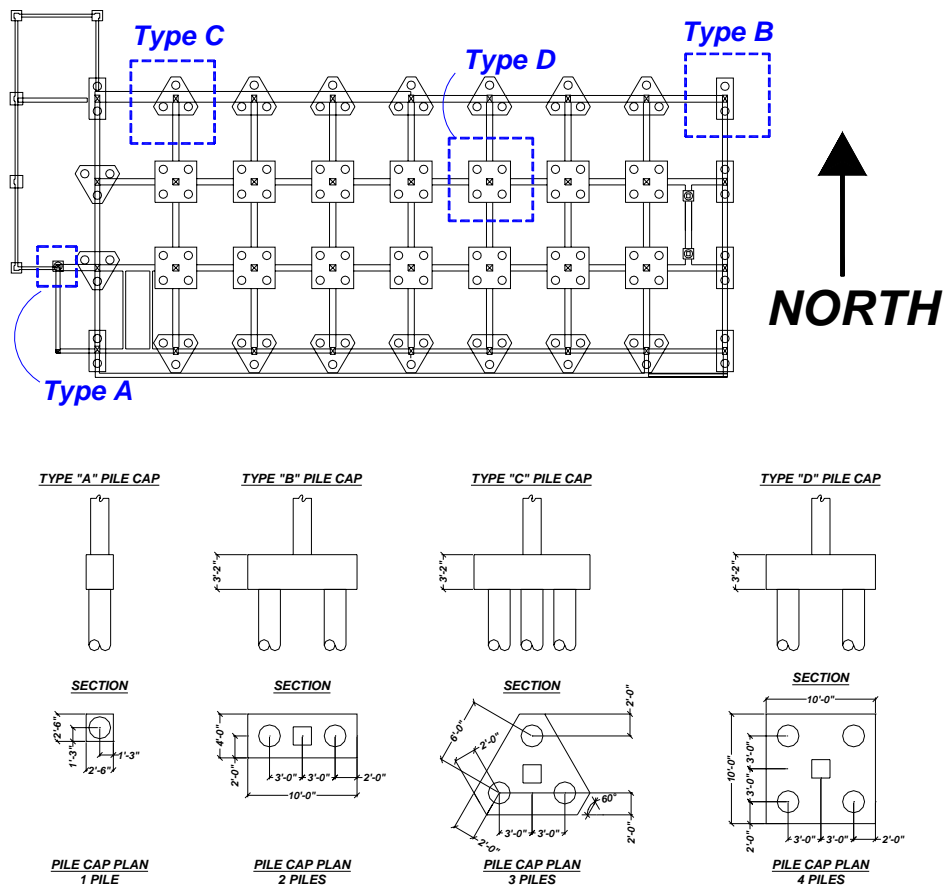


Fig. 4.3 Foundation plan and primary types of pile-pile-cap combinations

The soil condition at the Van Nuys testbed site is classified as NEHRP Category D. The soils are fairly consistent and competent, and the ground water table is deep. Bore hole data was summarized in Section 3.5. The capacities of the pile foundations well exceed the combined static and dynamic loads applied to the foundations; therefore, for the Van Nuys testbed, static SFSI (permanent deformations) of the foundations is not considered important.

Various options for accounting for inertial interaction, in order of increasing sophistication are:

1. Apply ground surface motions directly from attenuation relationships as specified motions of a fixed-base model of the building (neglecting SFSI).
2. Apply ground surface motions directly from attenuation relationships as specified motions to foundation “springs” attached to the footings. The complexity of the “springs” may vary; for this report, an uncoupled set of horizontal, vertical and rotational springs was applied at each footing (3 springs for 2-D analysis, or 6 springs for a 3-D analyses). The springs include flexibility of the foundation elements and soil supporting the foundation elements. Viscous damping can be applied with the foundation springs to represent the radiation damping, and to a first approximation, the hysteretic damping if the strains are small.
3. Include explicit representation of foundation elements (footings, slabs, and/or piles) in the model of the building and use subgrade reaction springs, or p-y springs, to represent the connection of the foundation elements to the soil. Ground motions (varying with location) may be applied to these subgrade reaction or p-y springs.
4. Include building and foundation elements, and represent soil elements as 3-D solid elements with contacts elements between the soil and foundation in the model. The model could conceivably be extended to include the fault source and propagation of motions to the building site. At present, this process is time consuming and hence it is more applicable to research than to design; thus this approach was not used in this study.

As a general rule, the effects of foundation/soil flexibility and damping (i.e., inertial soil-structure interaction effects) can be neglected when the structure is relatively flexible in comparison to the foundation and soil. Based upon structural analysis presented later, the upper structure is expected to yield at a base shear ratio of about $V/W=0.2$, where V is base shear and W is total weight. For the Van Nuys testbed, the lateral load capacity of the pile groups is much

greater than the lateral load capacity of the superstructure. The associated deflections of the pile caps are on the order of a few millimeters.

Using a linear procedure, the relative structure/soil stiffness is often quantified by the dimensionless parameter $\bar{h}/(v_s \cdot T)$, where \bar{h} = effective height of structure and T = fixed-base first mode period of the building (Stewart et al., 1999). On the basis of theoretical analyses and analyses of building case histories, the value of $\bar{h}/(v_s \cdot T)$ for the testbed is small and hence it is associated with minimal period lengthening (values near unity) and foundation damping (values near zero).

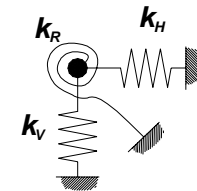
Simple techniques for accounting for the kinematic interaction effects of base-slab averaging and foundation embedment are presented in FEMA (2003). These kinematic interaction effects are generally most important at periods significantly lower than the first-mode period of the Van Nuys building, and hence would only have a significant impact on design spectral ordinates for higher mode responses.

4.2.3 Accounting for Foundation Compliance Using Foundation Springs and p - y Springs

For preliminary assessment of effects of SSI in seismic demand assessment, the foundation actions may be approximated by uncoupled elastic spring components representing vertical, horizontal and rotational resistances. Using the methodology suggested in FEMA 273/274 (1997) elastic spring resistances have been estimated.

For preliminary assessment of effects of SSI in seismic demand assessment, the foundation actions may be approximated by uncoupled elastic spring components representing vertical, horizontal and rotational resistances. Using the methodology suggested in FEMA 273/274 (1997) and an estimated friction angle of $\phi' = 35^\circ$, elastic spring resistances have been estimated and are provided in Table 4.1. Such estimations are based on the assumption that the pile-pile-cap connection provides no rotational restraint (i.e., pinned) and that base contact at the pile-cap is negligible; thus all lateral restraint is provided by the passive resistance against the piles. In addition, rotational resistance was estimated assuming that only the axial stiffness of the individual piles contributes.

Table 4.1 Preliminary recommendations for elastic vertical, horizontal and rotational spring stiffnesses

Description	k_V (kip/in)	k_H (kip/in)	k_R (kip in/rad)	
4 pile group (Type C)	12000	300	16×10^6	
3 pile group (Type D)	9000	290	8×10^6 (N-S axis) 12×10^6 (E-W axis)	

For the p - y representation, the piles were modeled as line elements with flexural stiffness EI_e defined as $\alpha\beta EI_g$ ($\alpha = 0.7$, $\beta = 0.54$). The backbone of the p - y curve for sand was defined based on American Petroleum Institute recommendations (API 1993). The radiation damping was modeled by a dashpot with the coefficient c determined by the elastic theory solution. A variety of conditions were assumed for the p - y analysis including variations in the depth of embedment, friction angle varying between 30° and 35° , fixed and pinned pile head conditions, and variations in pile flexural stiffness by a factor of about 2.

The results of pushover analysis of two p - y models for a 3-pile group and a 4-pile group are compared in Figure 4.4 with the uncoupled linear k_H springs of Table 4.1. The uncoupled elastic spring stiffness compares to the lower end of the range of stiffnesses considered by the p - y analysis, which corresponds to using a stiffness of the p - y springs equal to $1/8^{\text{th}}$ of the best estimate value. These results show the large variation in spring stiffnesses that can be obtained from various methods. However, as shown in the next section, the effects of these large variations on the response of the structure are very small.

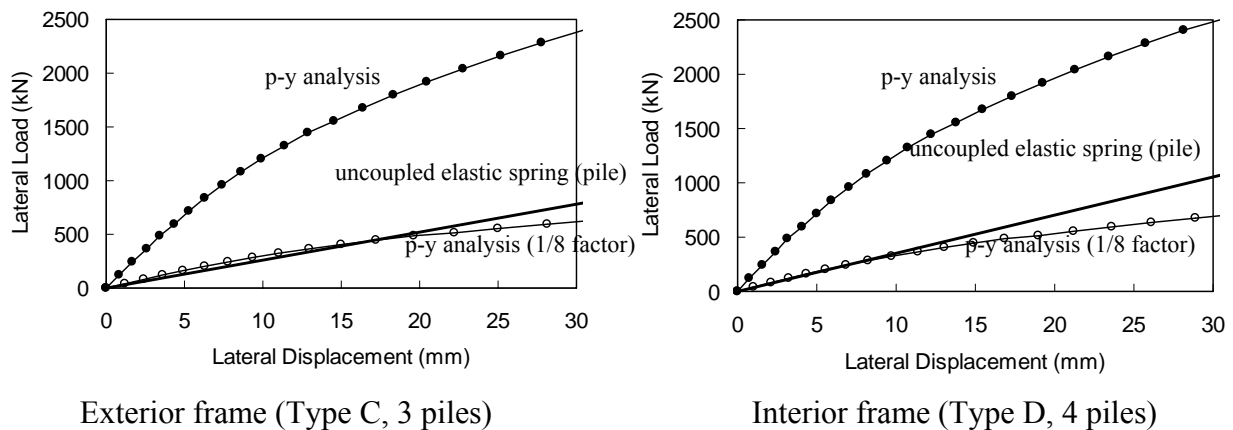


Fig. 4.4 Results of p - y pushover analysis compared to stiffness of uncoupled elastic spring

4.2.4 Dynamic 2-D Frame Model of Building Coupled with p - y Analysis

Analyses of the Van Nuys building and foundation to evaluate the effect of soil-pile-structure interaction on the interstory drift and natural period of the structure are summarized here. The sensitivity of the building response to variations in the building stiffness and sensitivity to different representations of the foundation were investigated. Figure 4.5 shows the elevation of the building supported on piles with p - y springs.

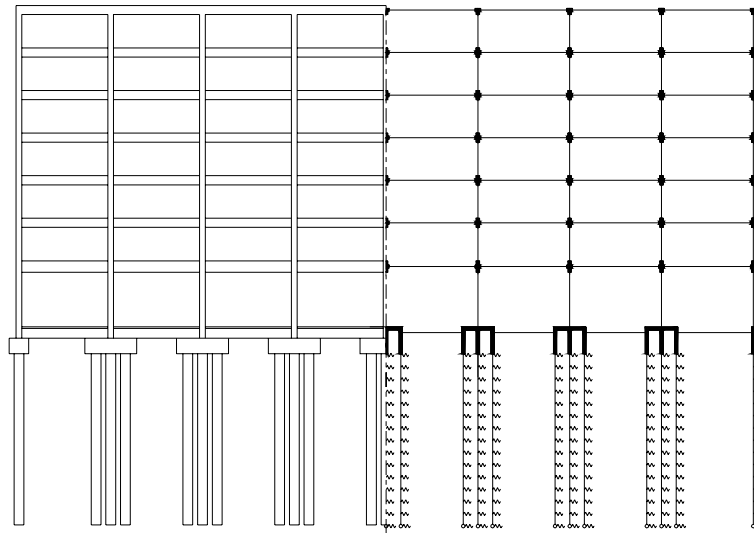


Fig. 4.5 Elevation of Van Nuys building exterior frame with piles and p - y springs (right half shows analytical model)

The numerical procedure employed includes the calculations of ground response, soil-pile interaction, pile-building interaction, and building response all in one process. The soil was represented by a one-dimensional soil column that was assigned a very large mass so that the mass of the building and piles had negligible effect on the soil column response. The soil column was connected to the piles by p - y springs, the piles were rigidly connected to the bases of the building columns, and the building was modeled as a nonlinear 2-D frame structure. The soil column was represented by a Ramberg-Osgood type model with Masing hysteretic damping. The maximum shear modulus was taken from Ohta and Goto (1976) correlations between the SPT N value and the shear wave velocity. The depth of the soil considered in the analysis was 13 m (just below the depth of the pile tips).

The ground motion was applied to the base of the nonlinear soil column. The input motion at a depth of 13 m was determined based upon ground surface motions used in this testbed study. The computer program SHAKE, was used to deconvolve the ground surface motions to calculate the ground motion at a depth of 13 m. To perform the deconvolution, rock was assumed at 54 m depth of soil. The shear wave velocities used in the analysis gradually increased from 200 to 350 m/s over the top 13 m of the soil deposit.

The motions calculated from SHAKE at a depth of 13 m were used as input to the nonlinear soil column analysis. The surface motions calculated as output of the nonlinear analysis produced ground surface motion spectra that accurately reproduced the spectra of the original surface motion, with some exceptions for periods between about 0.3 and 0.5 seconds. Figure 4.6 shows a comparison between surface motion input, the motion deconvolved to a depth of 13 m, and surface motion calculated by the nonlinear soil-column analysis. Since the Van Nuys building natural period is about 1.5 s, the errors at 0.5 s. and less are not considered important.

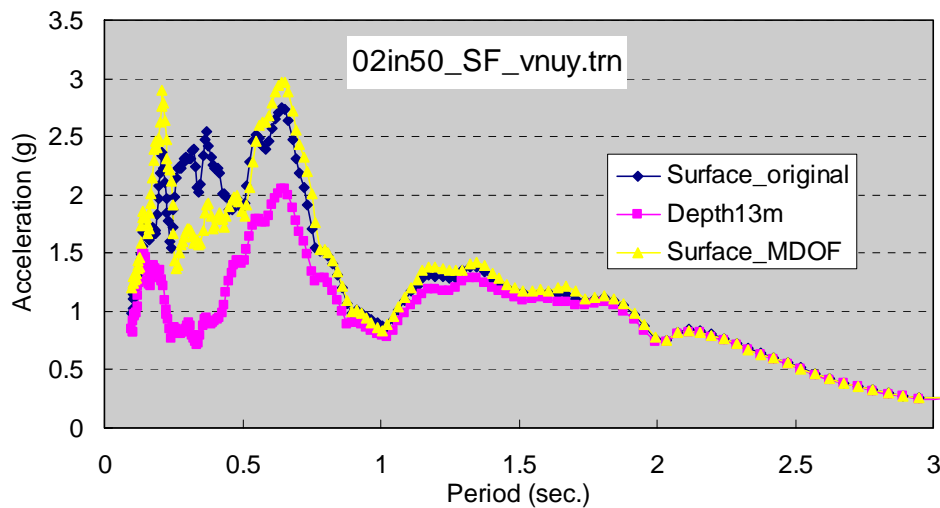


Fig. 4.6 Comparison of spectra of original surface motions, deconvolved motion at 13 m, and surface motion output from nonlinear soil column analysis

The building has a natural period is 1.5 sec. for the fixed base condition. It is found that the natural period increases only between 0.9% and 2.7% for different representations of foundation compliance, even when the p - y spring stiffness and strength are decreased to $1/8^{\text{th}}$ of their base case value. When the building is stiffened by a factor of 2, the fixed-base natural period is 1.06 s, and increases by 1.6% to 5.4% for the range of foundation representations

considered. These comparisons confirm that the natural period of the building is not sensitive to the soil-foundation parameters.

Story drifts obtained from NRHA for various soil-foundation conditions were also compared. The 3rd story drift was chosen because either the 3rd or the 4th story had the largest drift of any stories. The effect of SFSI on the maximum third story drift was at most 17%, and that occurred for the case of very soft and weak p - y springs. For the 10 ground motions the drift varied 1% to 4% for different foundation representations. The conclusion is that SFSI is not important for this structure, and therefore, the models discussed in the subsequent sections did ignore SFSI and are based on the assumption of fixed base conditions of all columns.

4.3 ANALYTICAL MODELS OF STRUCTURAL SYSTEM

Authors: L. Lowes, F. Zareian, H. Krawinkler

4.3.1 Modeling Objectives — OpenSees

The objectives of this phase of the effort were the use of the OpenSees analysis platform to predict EDPs for the testbed building, as it existed prior to the Northridge earthquake, for three levels of earthquake hazard and to assess the impact of modeling uncertainty on the predicted EDPs. To accomplish this objective, two two-dimensional models of the structure were developed. The first model, identified as OpenSees1, was developed early in the project using the OpenSees modeling tools and the understanding of the building as it existed at that time. This model was used to predict EDPs for a suite of 30 ground motions representing three hazard levels and to investigate the impact of modeling uncertainty on prediction of EDPs. The second model, identified as OpenSees2, was developed later in the project timeline to utilize the improved modeling capabilities available in OpenSees; this model was intended to provide improved prediction of response. Both models were evaluated through comparison between simulated and observed response to the Northridge earthquake ground motion. Details of the OpenSees1 model are documented in “Seismic Analysis of Older Reinforced Concrete Structures” (Paspuleti 2002); details of the OpenSees2 model are documented in “The Impact of

Beam-Column Joint Damage on the Response of an Older Reinforced Concrete Frame Building” (Theiss 2005).

4.3.2 Modeling Assumptions and Decisions — OpenSees Models

A number of assumptions and modeling decisions were required to develop the OpenSees1 and OpenSees2 models of the structure. The most critical ones are discussed in the following sections.

Two-Dimensional Simulation of Building Response. To reduce the computational intensity of the simulation effort, response was simulated only in the longitudinal (east-west) direction of the building. Preliminary analyses using three-dimensional models comprising only beam-column elements indicated that three-dimensional modeling would not be feasible for creation of a comprehensive EDP dataset for the suite of ground motion records representing three earthquake hazard levels. In making this modeling decision, it was recognized that two-dimensional modeling (1) would neglect the fact that the building is not structurally symmetric, but includes masonry in-fill in the first story on the south side of the building and (2) would not be sufficient to enable simulation of the structural damage observed after the Northridge earthquake, which was concentrated on the south side of the building.

The two-dimensional model of the structure comprised one interior and one exterior frame. At each floor the lateral (EW) displacements of the exterior and interior frames are constrained to be equal. The response of the exterior slab-beam-column and the interior slab-column framing system was simulated by assuming that an effective width of the two-way slab, centered at the column-line, contributes strength and stiffness to the longitudinal frame. For both the external and internal frames, this effective slab width was assumed equal to the column-strip width. For the interior frame, this is approximately consistent with the recommendations of FEMA 356 (ASCE 2000) and ACI Committee 318 (2002). For the external frames, this is approximately consistent with the recommendations of FEMA 356 but exceeds the recommendations of ACI Committee 318 (2002).

Initial Fundamental Period of the Structure. The objective of the modeling effort was to develop a model of the building as it existed prior to the 1994 Northridge earthquake. As discussed in Section 2.5, analyses by others of the building acceleration records from the

Northridge earthquake indicate that the fundamental period of the structure at the beginning of the earthquake was approximately 1.5 sec. Using effective elastic component stiffnesses, as defined in FEMA 356 and ACI 318-02, the effective elastic period of the structure in the longitudinal direction was between 1.1 and 1.2 seconds. However, as the Van Nuys building underwent several earthquakes in the past, which caused damage and therefore period elongation, a fundamental period of 1.5 at the beginning of the Northridge earthquake is reasonable. To enable evaluation of the current models on the basis of simulated and observed response under the Northridge earthquake ground motion, 1.5 sec. was taken as the target initial period of the baseline nonlinear models, and component stiffnesses were adjusted to achieve this initial fundamental period.

Simulation of Material Response. In both of the OpenSees models, the behavior of beams and columns is defined, ultimately, by the one-dimensional material response of the concrete and steel that compose the structure. Concrete material response was simulated using the OpenSees Concrete01 material model that characterizes zero tensile strength and a parabolic stress-strain response in compression up to the point of maximum strength with a linear deterioration in the post-peak regime. Because the transverse reinforcement ratio for beams and columns in the Van Nuys building is relatively low and detailing does not meet modern code requirements, concrete was modeled as “unconfined” with peak strength achieved at a strain of -0.002 and minimum post-peak strength achieved at a strain of -0.004. The results of previous research indicate that the compressive strength of in-situ concrete exceeds the design strength due to increased strength at the time of casting as well as age; this was included in the model by increasing the concrete peak compressive strength by a factor of 1.5 as recommended in FEMA 356. Concrete design strength is provided on the original building drawings as listed in Appendix A. Minimum post-peak strength was defined to be 80% of the maximum strength; it was found that values less than 80% resulted in softening of the section moment-curvature response and instability in simulation of member response.

Longitudinal reinforcing steel response was simulated using the OpenSees Steel02 material. This model simulates a bilinear stress-strain envelope with curvilinear unload-reload response; this is representative of observed stress-strain histories under cyclic loading. As with plain concrete, the results of previous research indicate that the observed yield strength of reinforcing steel exceeds the nominal strength. Again, the recommendations in FEMA 356 were

used to define an expected yield strength for Grade 40 of 50 ksi and an expected yield strength for Grade 60 reinforcement of 75 ksi. Both Grade 40 and Grade 60 reinforcement were assumed to have a post-yield modulus equal to 2% of the elastic modulus, which was assumed to be 29,000 ksi. Additional parameters required to define the Steel02 material model were taken equal to those recommended in the OpenSees User's Manual (<http://opensees.berkeley.edu>).

Simulation of Slab, Beam and Column Response. Simulation of slab, beam and column response was accomplished using fiber-hinge beam-column line elements. In OpenSees1, the Beam-With-Hinges (BWH) element formulation was used; in OpenSees2, the BWH2 element formulation was used. Both the BWH and BWH2 elements are force-based elements in which a linear moment distribution is assumed along the length of the member and an internal-element solution is required to determine member deformations that satisfy system compatibility. Member force-deformation response is computed assuming that inelastic action occurs at the member ends and that the middle of the member remains elastic. Inelastic action at member ends is defined by response of the fiber-sections. For the BWH element, two fiber sections, one each located in the middle of each of the element hinge regions, are used to compute element response. For the BWH2 element, a total of four sections are used, with one section located at each end of the element and one section located at the mid-point of the plastic-hinge region located at each end of the element. These differences in the element formulations result in the OpenSees1 model, which uses the BWH element formulation, predicting higher strength, since for the BWH element member end moments are extrapolated linearly beyond that which is defined at the section.

Member force-deformation response is defined by (1) the force-deformation response (moment-curvature and axial load-deformation response) histories of the fiber sections located within the plastic-hinge regions at the ends of the member, (2) the lengths of the member plastic hinge regions, and (3) the elastic member properties. For both the OpenSees1 (BWH) and OpenSees2 (BWH2) models, fiber sections were created with maximum fiber dimensions of 0.5 inches, section geometries defined by gross section properties as the assumed effective slab width, and material response characterized using the models discussed above. For the OpenSees1 model, member plastic hinge lengths are defined equal to the member depth. For the OpenSees2 model, member plastic hinge lengths are defined using the model developed by Corley (1966) in which hinge length, l_p , is defined:

$$l_p = 0.5D + 0.05L \quad (4.2)$$

where D is the member depth and L is the length from the point of maximum moment to the point of zero moment. Results of a study by Lehman (1994) indicate that this relatively simple model can be used to predict observed drift for bridge columns of variable designs. For both models, the elastic section properties were defined by the elastic concrete modulus, taken equal to $57,000\sqrt{f_c}$ psi where f_c is the concrete compressive strength in psi, per the recommendations of ACI Committee 318 (2002), an assumed concrete Poisson ratio of 0.175, gross section dimensions, assumed effective slab width, and a stiffness reduction factor, α , that was applied to all members. This stiffness reduction factor was used to adjust the model so that the initial period of the structure was 1.5 seconds, the observed period of the building at the beginning of the Northridge earthquake (see Section 2.5).

Simulation of Column Splice Failure. The OpenSees models simulate two brittle column failure mechanisms: failure of column longitudinal steel splices and column shear failure. Failure of column splices is simulated by modifying the stress-strain response model for the reinforcing steel at the location of the splice. Following the recommendations of FEMA 356, the predicted steel yield strength is defined as the true yield strength multiplied by the ratio of the provided splice length to the required splice length, with the required splice length computed following the recommendations of ACI Committee 318 (2002) with the exception that the 1.3 factor required when all bars are spliced at the same location was neglected. A bilinear stress-strain relationship (OpenSees material model Steel01) is used to simulate the material response of the steel, and the post-yield stiffness is defined to be negative and equal to -0.5% of the elastic modulus.

Simulation of Column Shear Failure. The OpenSees models also simulate brittle shear failure, with a unique column shear response defined for each column. In the OpenSees1 model, shear response is defined by a shear force versus shear distortion model that is independent of load history and drift demand. Initial shear strength is computed using the recommendations of Kowalsky and Priestley (2000) and assuming that concrete in the flexural hinge zone contributes only the minimum residual capacity defined by Kowalsky and Priestley. The impact of column shear strength and the use of other column shear strength models on prediction of EDPs are investigated using the OpenSees1 model. For the OpenSees2 model, the column shear failure

model developed and implemented by Elwood and Moehle (2003) is used. This model defines shear strength to be a function of inter-story drift, as well as geometric, material and design parameters.

Simulation of Joint Response. For both the OpenSees1 and 2 models, beam-column joints are assumed to be rigid, with joint rigidity enforced through the use of rigid-end offsets for beams and columns.

Simulation of Foundation Response. For the OpenSees1 model, the building foundation was assumed to be rigid. For the OpenSees2, foundation flexibility is simulated using the foundation spring stiffnesses discussed in Section 4.2.

Simulation of System Response. The only system variable defined for the OpenSees models was the level of viscous damping developed in the 1st and 2nd response modes. For both models this was defined to be 5% of critical.

Simulation of Gravity Loading. At the time the OpenSees1 model was developed, it was not possible to simulate distributed gravity loading using the OpenSees platform. Thus, gravity loading was not included in the model. At the time the OpenSees2 model was developed, distributed gravity loading was fully functional within the platform, and gravity loading equivalent to self-weight plus 10 psf for partitions was applied.

4.3.3 Model Evaluation — OpenSees Models

The OpenSees models were evaluated using the results of pushover analyses and dynamic analysis using the Northridge earthquake ground motion, as recorded at the site. In both cases the simulated damage mechanisms were compared with the damage patterns observed following the Northridge earthquake.

Pushover Results. The results of nonlinear static analyses were used to identify the mechanisms that could be expected to determine the response of the structure under earthquake loading. Lateral loads were applied using the load distribution recommended in FEMA 356 (2000) for static linear analysis (FEMA 356 Section 3.3.1.3.2); this vertical distribution of lateral loads is recommended also for nonlinear static analysis if a uniform load distribution is considered also (FEMA 356 Section 3.3.3.2.3). Roof displacement, as predicted at the center column line, was used to control the analysis demand. Figures 4.7 and 4.8 show total base shear

(for one external and one internal longitudinal frame) versus roof displacement (at the center column) as predicted using the OpenSees1 (Fig. 4.7) and OpenSees2 (Figure 4.8) models. Beam and column section moment-curvature response data and shear force versus shear distortion data were evaluated to identify the initiation of the inelastic mechanism identified in the figures.

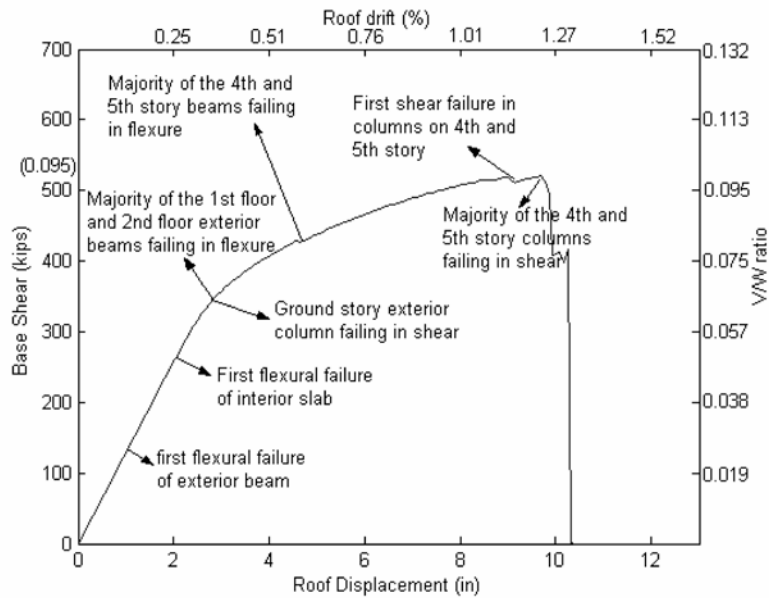


Fig. 4.7 Base shear versus roof displacement for baseline OpenSees1 model

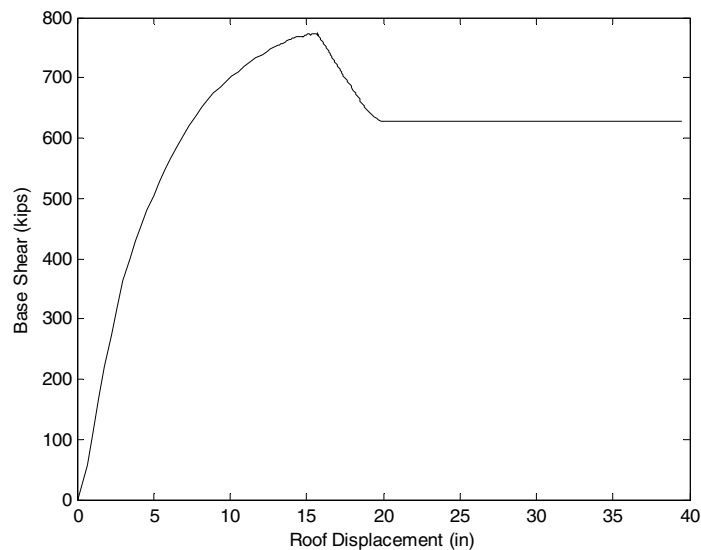


Fig. 4.8 Base shear versus roof displacement for baseline OpenSees2 model

The data in Figures 4.7 and 4.8 show that the OpenSees1 model predicts substantially smaller base-shear and roof displacement capacities for the building than does the OpenSees2 model. These differences are due to the application of distributed gravity load in the OpenSees2 model and the different column shear response models used in the OpenSees1 and OpenSees2 models. The application of gravity load in the OpenSees2 model increases column flexural strength due to axial load and delays positive moment yielding in beams and slabs. Both of these factors result in increased strength in the OpenSees2 model. For the OpenSees1 model, column shear strength is defined assuming a minimal concrete contribution, and post-peak response is assumed to be highly brittle. Using this model, the 1st story exterior and 4th and 5th story columns do not develop nominal flexural strength, but fail in shear prior to flexural yielding. For OpenSees2, column shear strength is defined using the Elwood and Moehle (2003) model in which the concrete contribution to column shear capacity does not diminish until flexural yielding occurs. Using this model, columns exhibit increased strength and drift capacity than is predicted by the brittle shear-failure model used in the OpenSees1 model.

Comparison of the predicted response mechanisms identified in Figure 4.7 and 4.8 with damage observed following the Northridge earthquake provides a basis for evaluating the models. The results shown in Figure 4.7 for the OpenSees1 model indicate that inelastic response of the building is due initially to flexural yielding of 1st and 2nd story beams and shear failure of 1st story exterior columns. Eventually, inelastic action includes also flexural yielding of 4th and 5th story beams. Finally, the structure collapses due to shear failure of the 4th and 5th story columns. Similar yield mechanisms are observed for the OpenSees2 model (Fig. 4.8), with loss in lateral strength due to flexure-shear failure of 4th story columns. Following the Northridge earthquake, damage was concentrated primarily in the exterior columns between the 4th and 5th floors. Both of the OpenSees models predict this failure mode.

Prediction of Dynamic Response to the Northridge Ground Motion Record. The results of nonlinear dynamic analyses were also used to evaluate the accuracy of the models. Here again, the predicted failure mechanisms were compared with the observed damage patterns. Additionally, the predicted roof displacement history was compared with the roof displacement history computed using roof acceleration histories measured during the Northridge earthquake. Beam and column section moment-curvature response data and shear force versus shear distortion data were evaluated to identify the initiation of the inelastic mechanism identified in

the figures. Figures 4.9 and 4.11 show the predicted and “observed” roof displacement history. Figures 4.10 and 4.12 show the predicted response mechanisms for the exterior and interior frames.

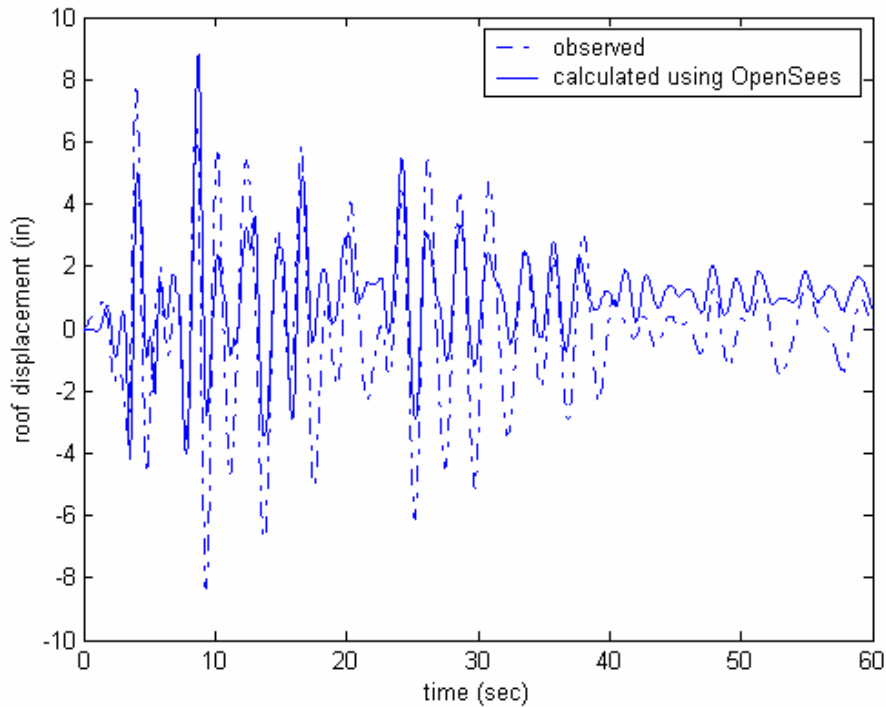


Fig. 4.9 Roof displacement during the Northridge earthquake (1994), as computed from sensor data (“observed”) and as predicted using the OpenSees1 model

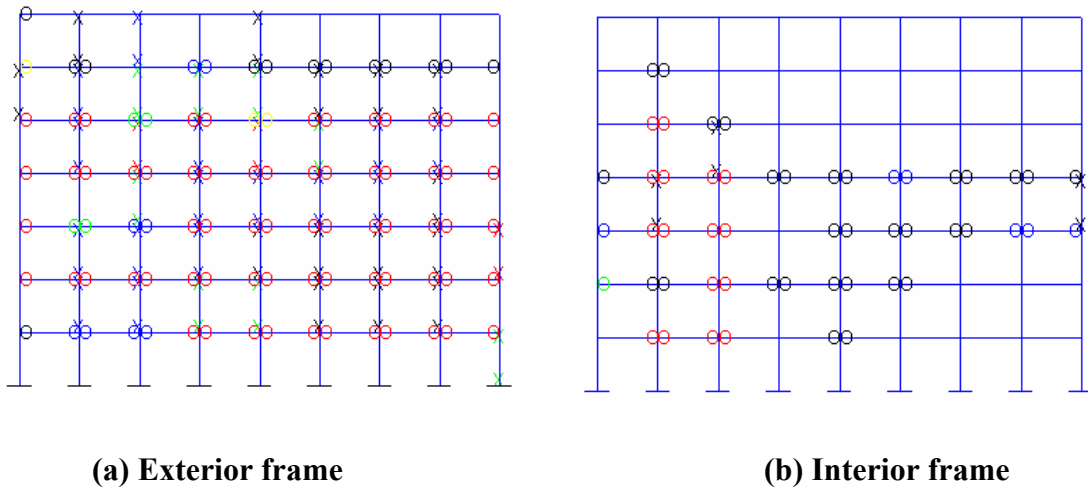


Fig. 4.10 Frame member curvature ductility demands under Northridge earthquake ground motion as predicted using the OpenSees1 model (O’s indicate flexural response and X’s indicate shear failure)

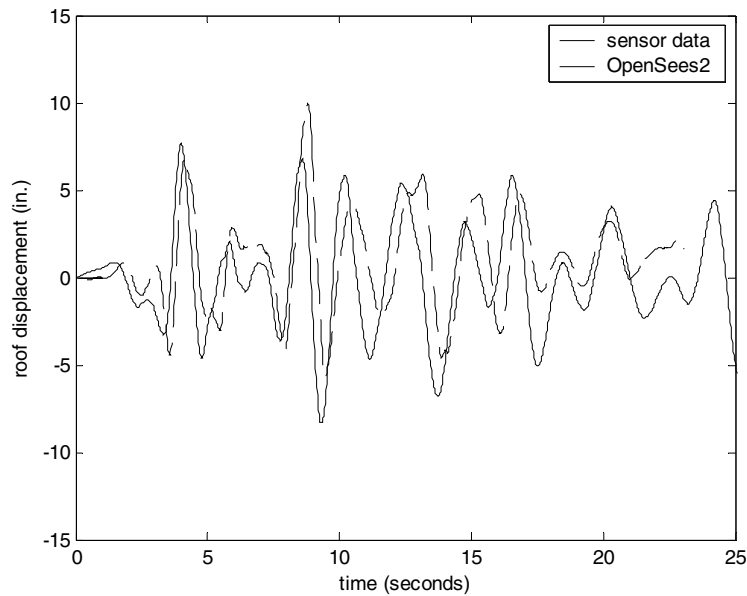


Fig. 4.11 Roof displacement during the Northridge earthquake (1994), as computed from sensor data (observed) and as predicted using the OpenSees2 model

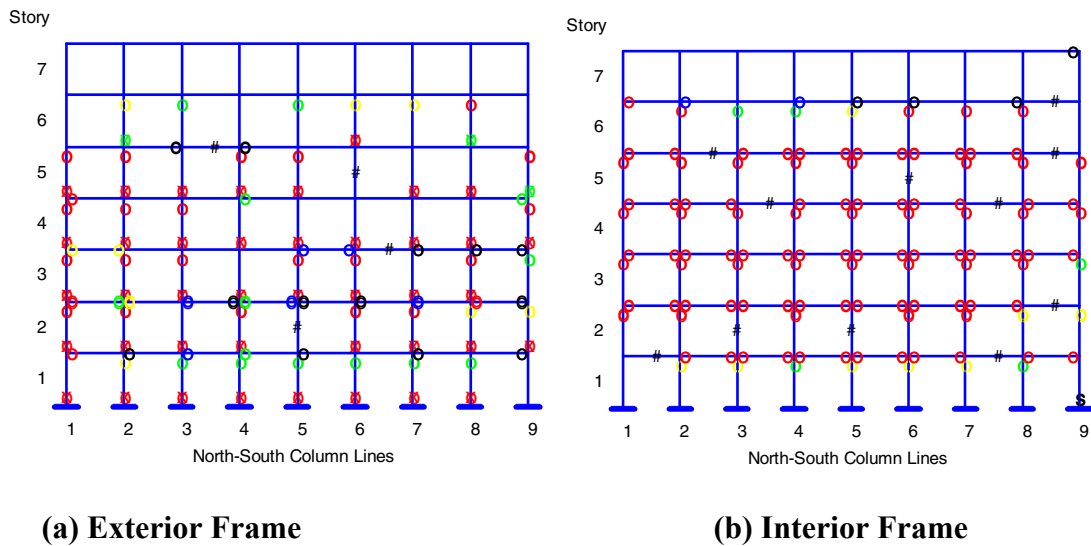


Fig. 4.12 Frame member curvature ductility demands under Northridge earthquake ground motion as predicted using the OpenSees2 model (O's indicate flexural response, XO's indicate shear-flexure failure, S's indicate splice failure, and #'s indicate unknown failure mode)

Comparison of the predicted response mechanisms identified in Figures 4.10 and 4.12 with damage observed following the Northridge earthquake provides the easiest approach to evaluating the accuracy of the models. The results shown in these figures suggest that inelastic

response of the building is due to flexural yielding of exterior and interior frame beams, shear failure of exterior columns and shear failure of a very few columns in the interior frame. Thus, both models appear to over-predict damage induced by the Northridge earthquake.

4.3.4 Validation of OpenSees Models

The numerical models of the Van Nuys building include a series of atypical structural component models that simulate the non-ductile response of reinforced concrete components with design details that are typical of pre-1970s construction, but are considered inadequate by today's standards. These models simulate (1) the loss of column lateral load capacity due to inadequate shear capacity and (2) the non-ductile response of spliced column longitudinal reinforcement. The validation of these component models is discussed in the following subsections.

4.3.4.1 Validation of Column Shear Failure Models

Experimental investigation of the earthquake response of reinforced concrete columns with low transverse steel ratios and poor transverse steel detailing (i.e., 90-degree rather than 135-degree hooks) indicates that shear capacity is a function of column drift demand (e.g., Lynn et al. 1996, Kowalsky and Priestley 2000). However, at the time the OpenSees1 model was developed, models were not available to enable simulation of shear capacity as a function of column drift demand. Thus, the OpenSees1 model describes shear response using a shear force versus shear deformation model. The OpenSees2 model employs a shear failure model in which column shear strength is defined to be a function of column drift demand.

A total of four shear response models are employed to simulate column shear failure. As discussed in Section 4.3.2, for the OpenSees1 baseline model, shear capacity is defined as the residual shear capacity proposed by Kowalsky and Priestley (USCD model). The Kowalsky and Priestley model defines shear strength assuming that the concrete contribution diminishes with inelastic flexural action; in the current study the residual concrete capacity that is achieved at large flexural curvature demand is used to define column shear capacity. In evaluating the impact of shear capacity on prediction of EDP's, two additional shear-strength models are employed. As discussed in Section 4.3.2, one of these follows the recommendations of ACI Committee 318 with the assumption that concrete in the plastic-hinge zone contributes fully to

shear strength (ACI model) and the second follows the recommendations of the FEMA 356 document (FEMA 2000) (FEMA model) in which it is assumed that concrete does not contribute to column shear strength. The OpenSees2 model employs the shear-failure model developed by Elwood and Moehle (2003) (Limit State model) in which the concrete contribution to column shear strength diminishes with drift demand.

These four shear-failure models were evaluated through comparison of predicted and observed response. The results of a study by Camarillo (2003) evaluated column shear strength models using experimental data provided in the PEER structural performance database (<http://nisee.berkeley.edu/spd/>). The results of the Camarillo study indicate that the ACI model used in the current study provides a conservative estimate for the shear strength of columns that exhibit pure shear failure but is somewhat non-conservative for columns that exhibit flexure-shear failure. From the Camarillo study it can be concluded that the UCSD model, as defined in the current study, and the FEMA 356 model are very conservative for columns that exhibit shear failure. The reader is referred to Elwood and Moehle (2003) for discussion of validation of the Limit State model.

4.3.4.2 Validation of Column Splice Failure Models

Both the OpenSees1 and OpenSees2 models employ the approach recommended in FEMA 356 to define the strength of spliced column longitudinal steel with inadequate spliced detailing. The yield strength of the spliced column reinforcement is defined equal to the actual yield strength multiplied by a ratio of provided to required splice length. FEMA 356 recommends that splice strength be defined using the ACI 318 building code and commentary (ACI 2002). In the current model, this is done with the exception that the 1.3 factor that the Code applies to the splice length for members in which all bars are spliced at the same location is ignored. This less conservative modeling approach is justified on the basis of bond strength data and spliced steel strain data presented by two groups (Lynn et al. 1996, and Melek and Wallace 2004) who conducted experimental testing of spliced columns with detailing similar to that present in the Van Nuys building. The results of these two test programs suggest that the proposed modeling approach represents a conservative estimation of the yield strength of spliced reinforcing steel in older columns.

4.3.5 Drain-2DX Models

Two other models of the Van Nuys building, identified as “Drain $T_1=1.5\text{sec.}$ ” and “MCB,” were developed and analyzed with the Drain2DX program (Powell 1992). The “Drain $T_1=1.5\text{sec.}$ ” model has been developed with assumptions and decisions similar to those made for the “OpenSees1” model. Notable differences were in modeling of the external frame slab, columns shear failure, and inclusion of P-Delta effects (which was not included in the OpenSees models). For the “Drain $T_1=1.5\text{sec.}$ ” model it was assumed that an effective width of the two-way slab equal to the external frame’s column strip width contributes to strength and stiffness. Also for this model, column shear strengths were obtained from the recommendations made by Kowalsky and Priestley (2000), and assuming that the concrete contribution to shear strength is related to the hinge zone flexural ductility demand. In order to consider the shear transfer limitation in the interior flat slab to column joints, the maximum plastic rotation of the slab in the internal frame was limited to 0.04. The “Drain $T_1=1.5\text{sec.}$ ” model incorporated the P-Delta effects in all the nonlinear response history analyses.

The “MCB” model consists of an exterior frame linked to an interior frame of the structure. Strength and stiffness of all elements present in this model were calculated using bilinear moment-curvature relationships with 3% strain hardening and no deterioration. The effects of gravity loads and of P-Delta were also considered in this model. Details of the “MCB” model can be found in Miranda & Aslani (2003).

Pushover curves of the two Drain2DX models and the “OpenSees1” and “OpenSees2” models are compared in Figure 4.13. The figure shows that the “OpenSees1” model has the least strength. The additional strength of the “Drain $T_1=1.5\text{sec.}$ ” model with respect to the “OpenSees1” model is due to the fact that in the former the exterior frame has more strength as a result of incorporating the contribution of a slab width equal to column strip width in the flexural strength of beams. The “OpenSees2” model uses the same assumption for the exterior frame, which results in the two models having very similar pushover curves. The “MCB” model has the largest strength and the least reduction in stiffness due to the assumptions on equivalent slab widths of exterior and interior frames made in the development of this model and the fact that the strain hardening in all beam and column elements was set to 3%, which is higher than in all other models. Also, no deterioration or failure mechanisms have been considered in modeling the beams and columns of this model.

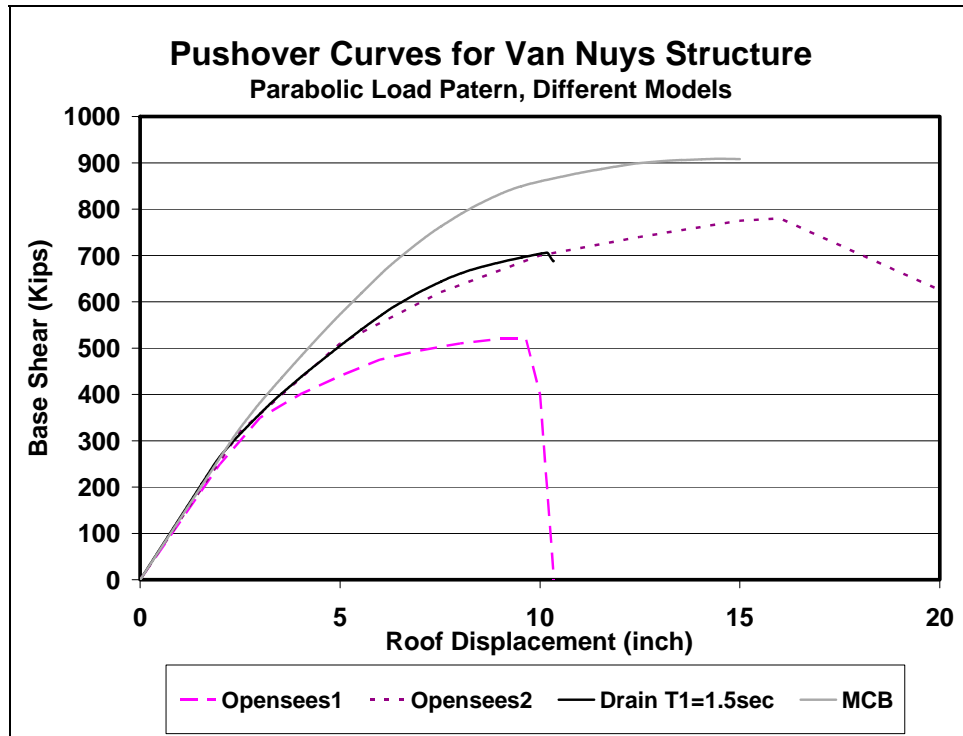


Fig. 4.13 Base shear versus roof displacement pushover curves for different models

4.4 PREDICTION OF EDPS FOR DAMAGE ASSESSMENT

Authors: L. Lowes, F. Zareian, H. Krawinkler

4.4.1 Prediction of Engineering Demand Parameters — OpenSees1 Model

The OpenSees1 model was used to predict engineering demand parameters for the 30 ground motion records selected to represent three earthquake hazard levels (50%, 10% and 2% probability of exceedance in 50 years). Review of experimental data characterizing the response of reinforced concrete components with design details typical of pre-1970s construction (PEER Structural Performance Database, <http://nisee.berkeley.edu/spd/>) indicates that interstory drift may be an adequate demand parameter for use in predicting structural damage. It also serves as a good parameter to estimate damage in deformation-sensitive nonstructural components. In addition to peak interstory drifts at all stories, peak floor velocities and peak floor accelerations were recorded for use in estimating damage to acceleration-sensitive nonstructural components

and to contents. Figures 4.14, 4.15, and 4.16 show predicted peak interstory drift demands at each story computed using the three sets of 10 ground motion records representing the three hazard levels. Drift values in excess of 10% are considered to represent collapse and are not shown in the figures. The number of collapses is 0, 4, and 6 at the 50/50, 10/50, and 2/50 hazard levels, respectively.

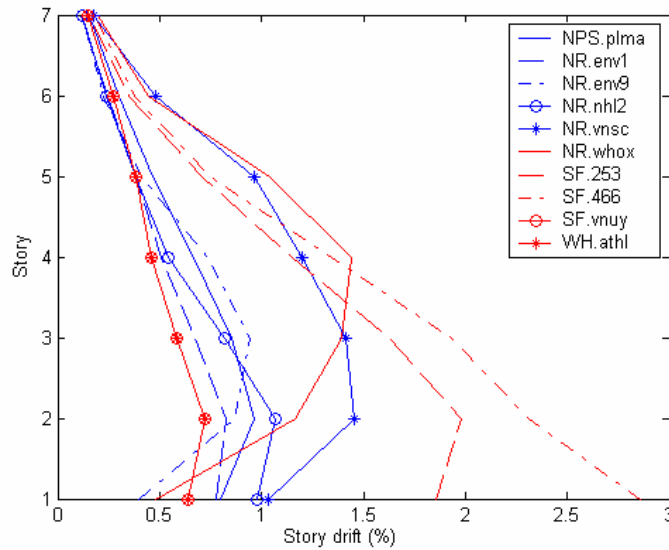


Fig. 4.14 Maximum interstory drifts for 50/50 ground motion records

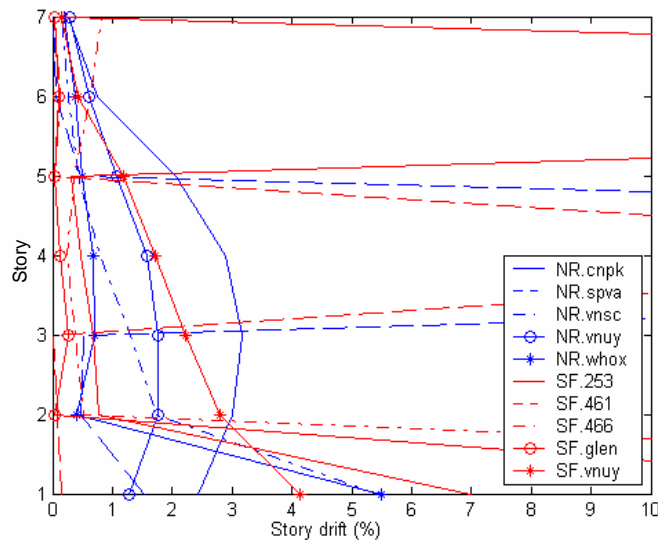


Fig. 4.15 Maximum interstory drifts for 10/50 ground motion records

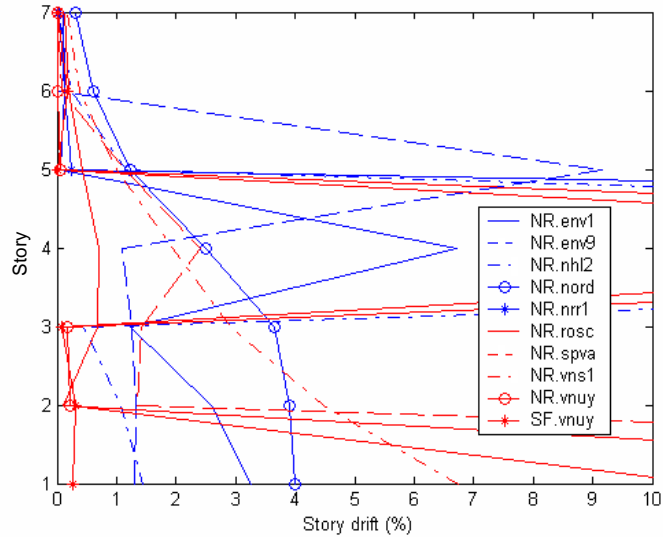


Fig. 4.16 Maximum interstory drifts for 2/50 ground motion records

4.4.2 Effect of Modeling Uncertainties on Prediction of EDPs — OpenSees1 Model

In developing the model of the Van Nuys building, the capabilities of the OpenSees platform, with its scripting language input format, were used to develop a family of models to facilitate investigation of the impact of modeling uncertainties on prediction of EDPs (Paspuleti 2002). The OpenSees1 model, including the modeling assumptions and decisions discussed previously, was defined as the baseline model for this investigation. Starting with the OpenSees1 model, multiple models of the building were created by changing a single modeling decision or varying a single model parameter. Modeling decisions and modeling parameters that were varied included those defining the following aspects:

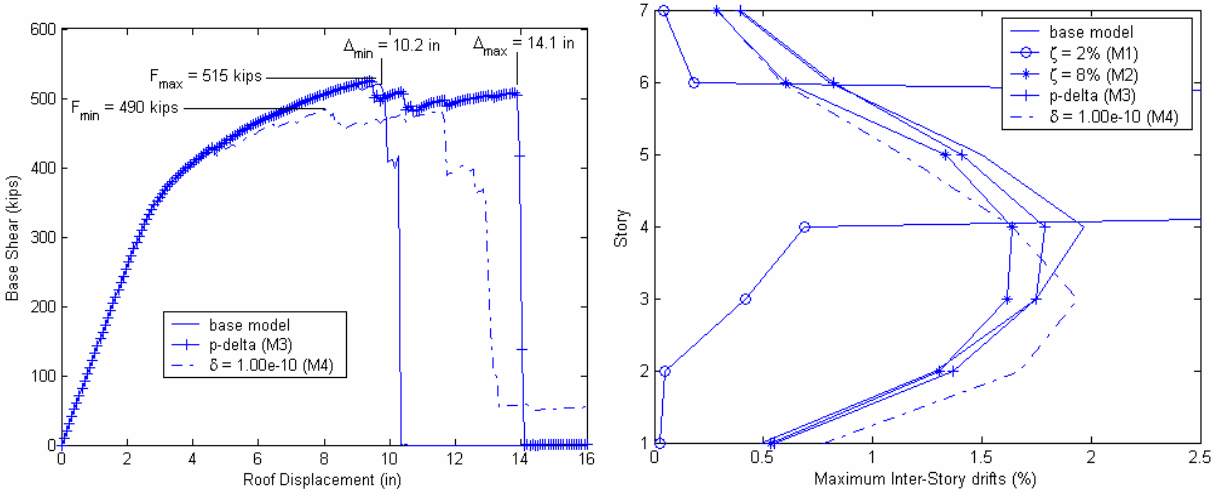
- Global system/simulation parameters, including the level of viscous damping and the global solution tolerance.
- Element models, including the element formulation, the length of the inelastic region at the ends of the element, the width of the slab considered to be effective in resisting lateral loads, the assumption of flexible beam-column joints through the use of centerline dimensions.
- Failure mechanism models, including assuming that column splices do not affect response, defining column shear strength on the basis of the recommendations of ACI

Committee 318 and FEMA 356, rather than Kowalsky and Priestley (2000), and varying the shear strengths defined by Kowalsky and Priestley by 20%.

- Material models, including the use of a bilinear hysteretic model to simulate steel response, defining concrete compressive strength to be the design strength rather than increasing the strength to account for age and variability at the time of casting, defining concrete post-peak strength to be 20% of the maximum strength rather than 80%.

The multiple models described above were analyzed under static and dynamic loading. For static (pushover) loading the load distribution recommended by FEMA 356, as discussed in Section 4.3.3 was utilized. Dynamic analyses were conducted using either the Northridge ground motion record or the 30 ground motion records discussed in Section 3.2.4.

Impact of Global System Parameters on EDPs. Figure 4.17 shows the results of static pushover analysis and dynamic analysis using the Northridge ground motion record as input. Results are shown for the baseline model as well as four additional models that represent the baseline model with viscous damping in the first mode adjusted to 2% of critical (M1) and 8% of critical (M2), with the impact of P-delta (p-delta M3), and with the global solution tolerance adjusted from the $1e-6$ value used in the baseline model to $1e-10$ (M4).



(a) Pushover analysis results

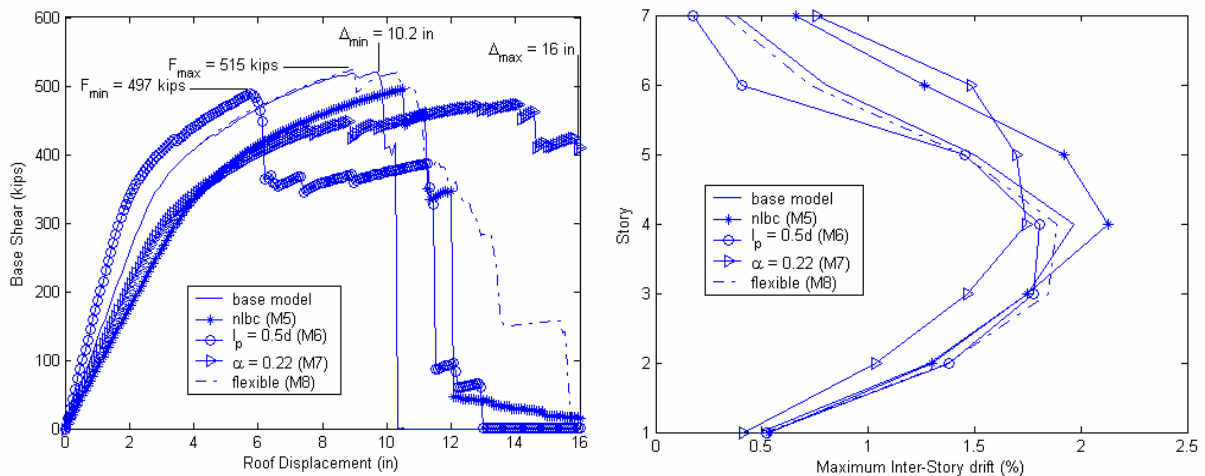
(b) Max. drifts for Northridge ground motion

Fig. 4.17 Impact of global system modeling parameters on EDP prediction

The results in Figure 4.17a show that reducing the tolerance used to define convergence has an impact on the predicted base shear and drift capacity of the building, indicating the

reduced solution time for the baseline model comes at the cost of not finding a fully converged solution state. The data in Figures 4.17a and 4.17b indicate also that accounting for P-delta effects results in increased displacement capacity for static loading and somewhat reduced interstory drift demands for dynamic loading. Since gravity loads are not applied to the structure in the OpenSees1 model, it is not obvious why simulation of P-delta effects should have a measurable impact on predicted response. The results in Figure 4.17b show that the level of assumed first mode viscous damping can have a significant impact on predicted response. As shown in the figure, if damping is reduced from 5% to 2% of critical, the building experiences extremely large interstory drift demands in the fifth story that could be expected to result in collapse, while the interstory drift demands in other stories are reduced.

Impact of Element Model Parameters on EDPs. Figure 4.18 shows the results of static pushover analysis and dynamic analysis using the Northridge ground motion record as input, again in the longitudinal direction. Data are shown for the baseline model as well as four additional models that represent the baseline model with the element formulation changed from a lumped-plasticity element to a spread-plasticity element (nlbc M5), with the length of the plastic hinge adjusted to 50% of the member depth ($l_p = 0.5d$ M6), with the effective slab width taken as 22% of the column strip width ($\alpha = 0.22$ M7), and with beam-column joint flexibility simulated by the use of centerline dimensions to define member lengths (flexible M8).



(a) Pushover analysis results

(b) Max. drifts for Northridge ground motion

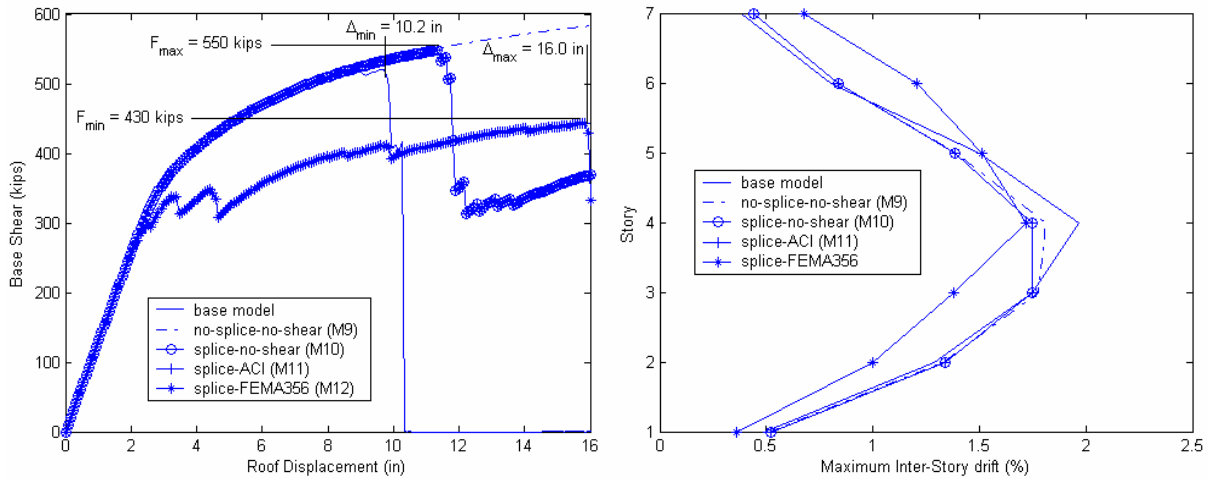
Fig. 4.18 Impact of element model parameters on EDP prediction

The results in Figure 4.18a indicate that reducing the plastic hinge length for the lumped-plasticity element formulation from the full member depth to half the member depth substantially increases stiffness and reduces displacement capacity. The data indicate also that using a spread-plasticity element or assuming a substantially smaller effective slab width reduces the lateral stiffness of the building and increases, albeit slightly for the spread-plasticity element, the displacement capacity. The increase in flexibility resulting from use of the spread plasticity element follows from the use of a concrete material model that has zero tensile strength; using the material model, each section along the length of the spread-plasticity element has a maximum flexural stiffness equivalent to the cracked section stiffness. The results in Figure 4.18b suggest that despite the differences in stiffness resulting from the element modeling decisions, maximum interstory drift under the Northridge ground motion record is not affected substantially. This is attributed to the element modeling decisions not changing substantially the yield and failure mechanism that develop under the Northridge ground motion and the Northridge ground motion not being sufficiently intense to produce story collapse.

Impact of Column Failure Model Parameters on EDPs. Figure 4.19 shows the results of static pushover analysis and dynamic analysis using the Northridge ground motion record as input. Data are shown for the baseline model as well as four additional models that represent the baseline model with variation in the column shear strength and the strength of spliced column reinforcing steel. The first model (no-splice-no-shear M9) removes simulation of column shear and splice failure. The second model (splice-no-shear M10) removes simulation of column splice failure. In the third model (splice-ACI), column shear strength is defined on the basis of the recommendations of ACI Committee 318 (2002) and the assumption that plain concrete contributes to column shear strength within the zone of flexural yielding. This model predicts column shear strengths that are substantially larger than predicted by the baseline model. In the fourth model (splice-FEMA356), column shear strength is defined on the basis of the recommendations of the FEMA 356 document (2002).

The data in Figure 4.19a indicate that, as expected, neglecting to simulate column shear and splice failure results in increased strength and displacement capacity. The results indicate also that, as expected, building base shear strength and displacement capacity is reduced if column shear strength is reduced. The data in Figure 4.19b suggest that for the Northridge ground motion the choice of a failure model is not particularly significant. This is attributed to

the column failure modeling decisions not substantially changing the failure mechanism that develops under the Northridge ground motion and the Northridge ground motion not being sufficiently intense to produce story collapse.



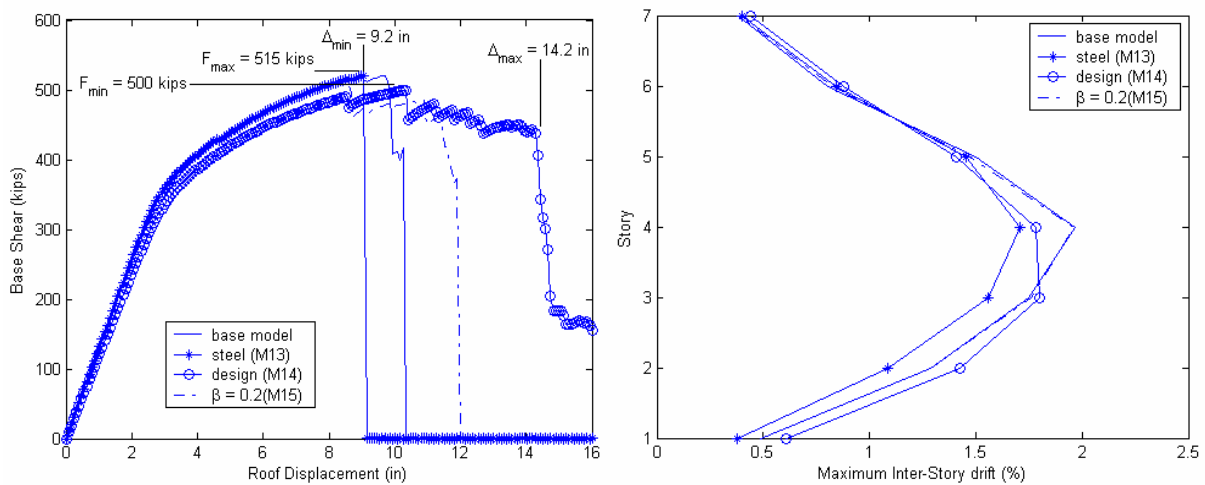
(a) Pushover analysis results (b) Max. drifts for Northridge ground motion

Fig. 4.19 Impact of column failure model parameters on EDP prediction

Impact of Material Model Parameters on EDPs. Figure 4.20 shows the results of static pushover analysis and dynamic analysis using the Northridge ground motion record as input. Data are shown for the baseline model as well as three additional models that represent variation in material model parameters. In the model identified as *steel* (M13), the steel material model is changed from the OpenSees Steel02 model, which simulates the Bauschinger effect using curvilinear unload-reload paths, to the OpenSees Steel01 model, which is a basic plasticity model with isotropic hardening. In the model identified as *design* (M14), concrete compressive strength is defined to be the design strength identified on the original building drawings rather than the adjusted strength used in the baseline model which accounts for overstrength due to variability in strength at time of casting and age. The model identified as β (M15), defines the residual post peak concrete compressive strength to be 20% of the maximum strength rather than the 80% used in the baseline model.

The results in Figure 4.20a indicate that the material model parameters considered have a minimal impact on building shear strength, but do affect displacement capacity. In particular, the data in Figure 4.20a show that defining concrete compressive strength equal to the design

strength rather than an increased value associated with age results in a substantially increased roof displacement capacity, and that reducing the concrete residual strength results in an increase in roof displacement capacity. These effects are attributed to a change in concrete strength and stress-strain response resulting in a change in the failure mechanism that is developed. The data in Figure 4.20b indicate that variation in the chosen material parameters does not have a significant impact on predicted response under dynamic loading, for the Northridge ground motion record. Again, this is attributed to the fact that the material model decisions do not affect substantially the yield and failure mechanisms that develop under the Northridge ground motion.



(a) Pushover analysis results (b) Max. drifts for Northridge ground motion
Fig. 4.20 Impact of material model parameters on EDP prediction

4.4.3 Statistics of the Preliminary Parameter Study

Table 4.2 shows data and statistics of the parameter study conducted using the OpenSees1 model and pushover analysis. It was found that, for all the parameter models considered, the mean base shear was 505 kips and the mean roof displacement at collapse was 12.56 in. For the OpenSees1 model there was very little variation observed in the maximum base shear across different parameter models but the roof displacement at collapse had a variation of around 19%. Table 4.3 shows data and statistics of the parameter study for the dynamic analyses using the OpenSees1 model and the Northridge earthquake ground motion record.

Table 4.2 Data and statistics of modeling parameter study — pushover analyses

Model Type		Base Shear (kips)	Roof Displacement at Collapse (inches)
Base model		515	10.2
Global Model Parameters	Pdelta, M3	515	14.1
	$\delta = 10^{-10}$, M4	490	13.0
Element Model Parameters	nlbc, M5	497	12.1
	$l_p = 0.5d$, M6	490	11.7
	$\alpha = 0.11$, M7	497	16.0
	Flexible, M8	515	15.8
Column Failure Models	No-splice-no-shear, M9	660	39.0
	splicenoshear, M10	550	11.9
	splice-ACI, M11	550	11.9
	splice-FEMA356, M12	430	18.5
Material Model Parameters	steel, M13	515	9.2
	Design, M14	500	14.2
	$\beta = 0.2$, M15	500	12.1
Mean¹⁹		505	13.13
C.O.V*		0.06	0.19

Table 4.3 Data and statistics of modeling parameter study — dynamic analyses using Northridge earthquake ground motion

Model Type	T _A sec	S _A (g)	Maximum inter-story drifts (%)							Roof disp.(in)
			1	2	3	4	5	6	7	
Baseline	1.56	0.41	0.48	1.28	1.75	1.97	1.50	0.81	0.38	8.82
$\xi = 2\%$, M1	1.56	0.41	0.03	0.05	0.42	0.69	20.7	0.18	0.04	22.66
$\xi = 10\%$, M2	1.56	0.41	0.54	1.30	1.61	1.64	1.33	0.60	0.28	7.95
pdelta, M3	1.56	0.41	0.55	1.37	1.75	1.78	1.41	0.82	0.39	8.75
$\delta = 10^{-10}$, M4	1.56	0.41	0.77	1.67	1.94	1.64	1.14	0.58	0.29	8.85
nlbc, M5	1.94	0.25	0.53	1.30	1.75	2.13	1.92	1.26	0.66	10.29
$l_p = 0.5d$, M6	1.30	0.41	0.52	1.38	1.78	1.80	1.45	0.41	0.17	8.16
$\alpha = 0.11$, M7	1.62	0.38	0.41	1.03	1.46	1.74	1.69	1.48	0.76	9.20
flexible, M8	1.56	0.41	0.51	1.37	1.85	1.89	1.45	0.73	0.32	8.78
nosplicenoshear, M9	1.56	0.41	0.51	1.33	1.78	1.81	1.39	0.84	0.44	8.76
splicenoshear, M10	1.56	0.41	0.52	1.34	1.75	1.75	1.39	0.84	0.44	8.69
splice-ACI, M11	1.56	0.41	0.52	1.34	1.75	1.75	1.39	0.84	0.44	8.69
splice-FEMA356, M12	1.56	0.41	0.36	0.99	1.38	1.72	1.51	1.21	0.68	8.41
steel, M13	1.56	0.41	0.37	1.09	1.56	1.71	1.45	0.84	0.40	7.98
design, M14	1.63	0.38	0.61	1.43	1.80	1.78	1.41	0.88	0.44	9.07
$\beta = 0.22$, M15	1.56	0.41	0.49	1.28	1.76	1.96	1.47	0.83	0.39	8.83
Mean²⁰			0.51	1.30	1.71	1.81	1.46	0.86	0.43	8.75
C.O.V*			0.19	0.13	0.09	0.07	0.12	0.22	0.37	0.064
Mean²¹			0.51	1.30	1.71	1.78	1.40	0.81	0.40	8.59
C.O.V[†]			0.21	0.13	0.09	0.06	0.073	0.20	0.27	0.04

¹⁹ The outlier, model M9 was not taken into account in calculation of the mean and C.O.V.

²⁰ The outlier for these analyses was the model with $\xi = 2\%$ which is not taken into account in the calculation of the mean and C.O.V.

²¹ These are the means and the C.O.V's for the models with T_A = 1.56 sec.

The outlier for these analyses was the model that had a damping of 2%, which is not taken into account in the calculation of the mean and the coefficient of variation for the maximum inter-story drifts and maximum roof displacement. It was found that variation of some model parameters resulted in shifting of the fundamental period of the structure. Since the ground motion record was not re-scaled for any of the shifts in period, the demands on the building were altered, causing some of the variation in predicted interstory drifts.

4.4.4 Prediction of Engineering Demand Parameters — Drain2DX Models

The “Drain $T_1=1.5\text{sec.}$ ” was also used to predict engineering demand parameters for the 30 ground motion records that represent the 50/50, 10/50, and 2/50 hazard levels. Eight of the ten ground motions selected for the 10/50 hazard level caused collapse at the 10/50 level, and nine of ten of the ground motions representing the 2/50 hazard level caused collapse at the 2/50 level, which prevents us from providing a meaningful probabilistic assessment of the structural response at these two hazard levels. Figure 4.21 shows the maximum interstory drift at the 50/50 hazard level for different models. It is seen that there is good agreement in the median of results, especially between the MCB model and the “Drain $T_1=1.5\text{sec.}$,” which is due to the fact that at this hazard level the response is only slightly nonlinear. The median and dispersion are higher for the drifts obtained from the OpenSees1 model, which indicates that this model is experiencing more nonlinear behavior. This is expected given the pushover curves provided in Figure 4.13, which show that the strength and the ductility capacity of the OpenSees1 structure are smaller than those of other models.

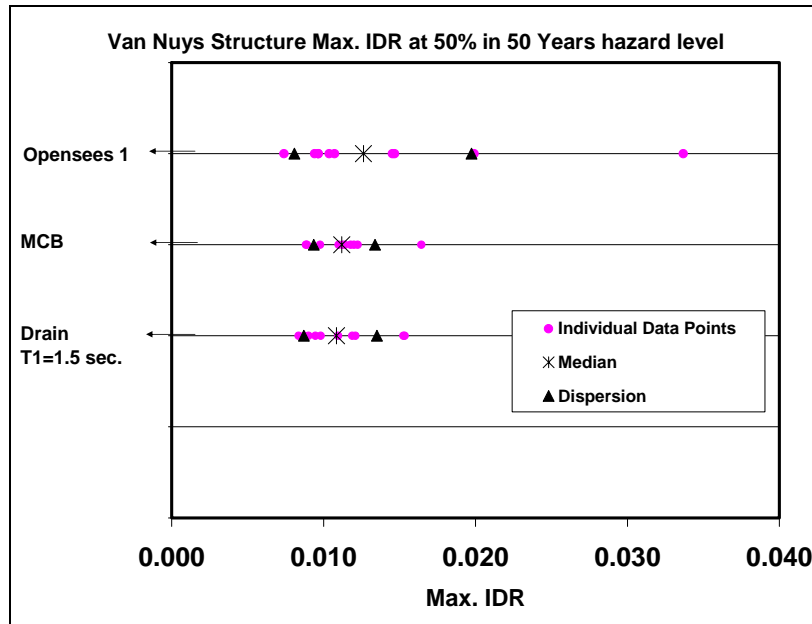


Fig. 4.21 Maximum interstory drift at the 50/50 hazard level for different models

The “Drain $T_1=1.5\text{sec.}$ ” model was used also to derive IM-EDP relationships using incremental dynamic analysis (IDA). For this purpose a suite of 17 ground motions was utilized, which represent all the records in the 10/50 and 2/50 sets (three of the records were in both sets). Figures 4.22 and 4.23 show maximum interstory and roof drift ratios, respectively, from the IDAs for this model using these 17 ground motions. In both figures, the IM is the ground motion 5%-damped spectral acceleration at the first mode period ($S_a(T_1)$) normalized by “g”. The light gray lines are individual IDA curves, the solid bold black line shows the median, and the dashed bold black lines are the 16th and 84th percentiles of the response, representing the dispersion of EDP as function of $S_a(T_1)$. The point at the end of each gray line represents the collapse point for the particular ground motion (for any further increase in $S_a(T_1)$ the increase in EDP approaches infinite (see Krawinkler and Ibarra, 2004). The 50/50, 10/50, and 2/50 hazard levels are marked in each figure with gray bold dashed dot lines. The intersection of the 50/50 line with median and 84th and 16th percentile IDA curves leads to results that are close to those shown in Figure 4.21 for the “Drain $T_1=1.5\text{sec.}$ ” model (the results are not identical because different records are used). For the same hazard level, the median value of maximum roof drift ratio is clearly smaller than the median of maximum interstory drift ratio, which shows that even at this hazard level there is a concentration of drifts in one or two stories. The issue of collapse is discussed in the next section.

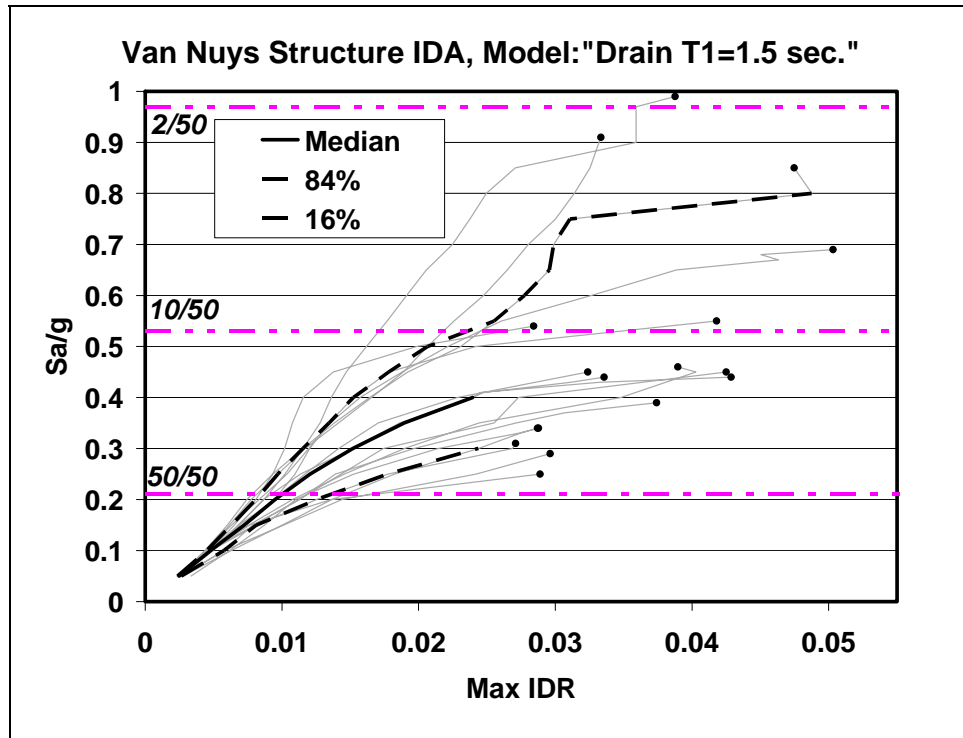


Fig. 4.22 Maximum interstory drift ratio from IDAs, "Drain T1=1.5sec." model

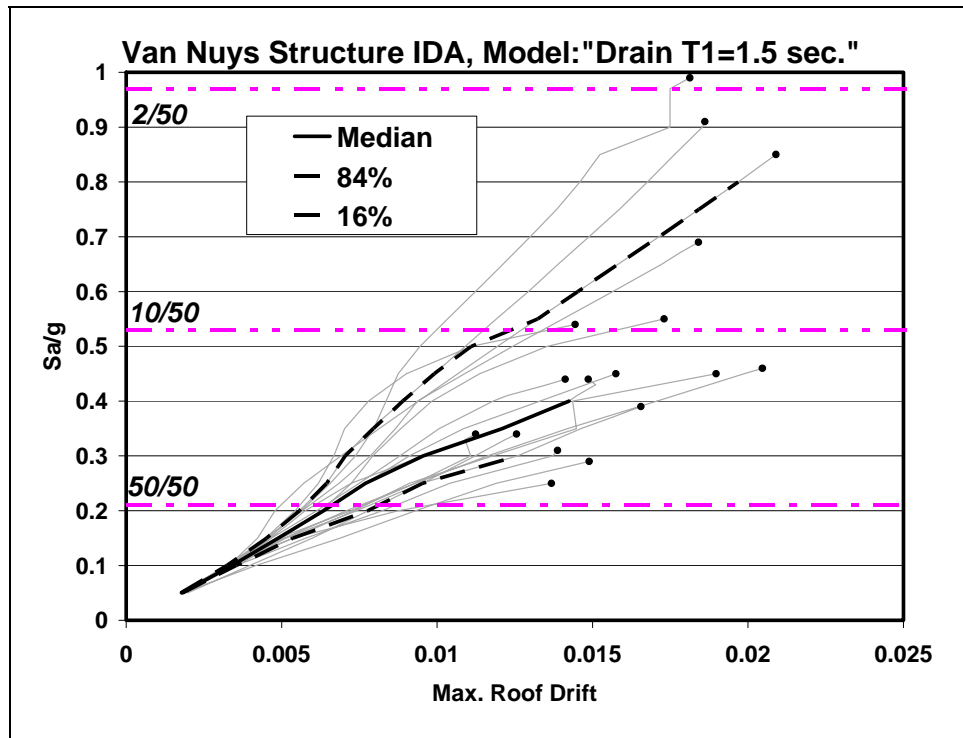


Fig. 4.23 Maximum roof drift ratio from IDAs, "Drain T1=1.5sec." model

4.5 PREDICTION OF PROBABILITY OF COLLAPSE

Authors: C.A. Cornell, F. Zareian, H. Krawinkler, E. Miranda

4.5.1 Calculating the Mean Annual Frequency of Collapse

The mean annual frequency of collapse, λ_{Coll} , is found from the following version of the framing equation:

$$\lambda_{Coll} = \int_{S_a} F_{C|S_a}(s_a) |d\lambda_{S_a}(s_a)| = \int_{S_a} f_{C|S_a}(s_a) \lambda_{S_a}(s_a) \quad (4.3)$$

in which $F_{C|S_a}(s_a) = P[C < s_a | IM = s_a]$ and $f_{C|S_a}(s_a)$ are the cumulative distribution function (CDF) and the probability density function (PDF) of the collapse capacity (measured in spectral acceleration terms) treated as a random variable²², C . The collapse capacity, defined as the IM ($S_a(T_I)$ is used as IM) causing collapse of the structure for a given ground motion record (see Figure 4.22), will vary from record to record and may depend strongly on modeling assumptions.

Three examples of estimates of the CDF of the collapse capacity, which is denoted from here on as the collapse fragility curve, are shown in Figures 4.25 to 4.27. The first estimate has been obtained from the nonlinear analyses of the Van Nuys building described in Section 4.3 as the “OpenSees1” model. At each of the three hazard levels (50/50, 10/50, and 2/50) there is a certain fraction of the 10 analyses that display very large IDRs implying effectively building collapse. These fractions are shown as points on Figure 4.25. The second estimate has been obtained from a set of Incremental Dynamic Analyses (IDAs) of an alternative model of the Van Nuys building described in Section 4.3 as the “Drain T=1.5sec.” model. Each of the 17 distinct records in the 10/50 and 2/50 sets was incremented and run until an S_a level was reached at which the IDR grew rapidly implying dynamic instability, see points at end of IDAs in Figure 4.22. The 17 points in Figure 4.26 are a cumulative histogram, displaying the fraction of records with a S_a capacity less than any value, s_a . Finally the third estimate was obtained by running IDA’s of a simpler model of the building (with bilinear nondegrading moment-rotation hinges

²² The PDF is the derivative of the CDF. Strictly these distributions are conditioned on the value of the ground motion demand (IM) level, S_a , but we assume here that the capacity is independent of the input level, so $F_{C|S_a}(s_a) = F_C(s_a)$ and the PDF becomes simply $f_C(c)$. That the first and second versions of these equations are equivalent as can be shown by an application of integration by parts.

and called MCB in Section 4.3) until any structural element (e.g. a column or a slab-column connection) attains a deformation limit that is associated with complete loss of vertical load carrying capacity of this element, see Figure 4.27. A discussion of drift capacities of structural elements associated with loss of vertical carrying capacity is presented in Section 5.2.

In all three cases the smooth lines are a lognormal model CDF fit through the data points. (Recognize that these points are only small sample estimates of what the fraction might be in a very large sample). The estimated medians and log standard deviations of the three lognormal models of the collapse capacity are $\eta_C = 0.60g$ and $\beta_{RC} = 0.72$ in the first case, $\eta_C = 0.45g$ and $\beta_{RC} = 0.37$ in the second case, and $\eta_C = 0.62g$ and $\beta_{RC} = 0.49$ in the third case.

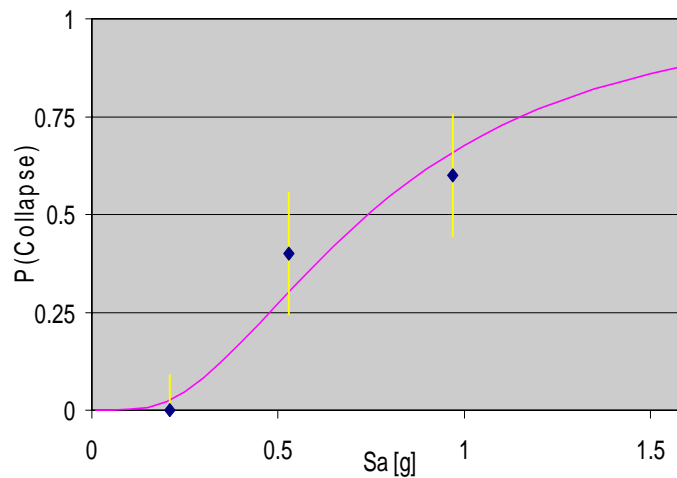


Fig. 4.25 Collapse fragility curve based on “OpenSees1” model

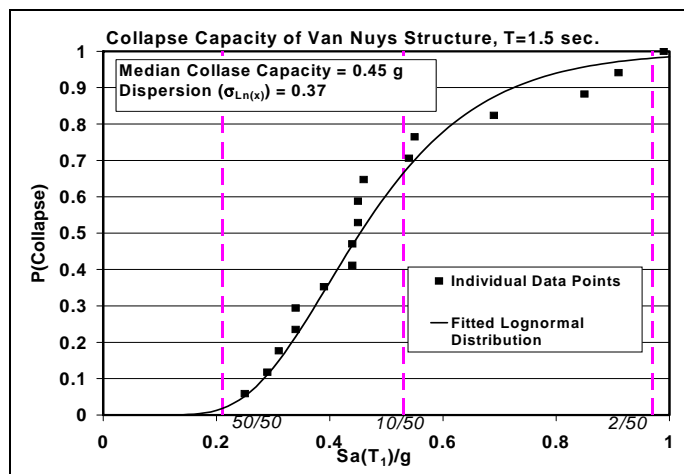


Fig. 4.26 Collapse fragility curve based on “Drain T=1.5sec.” model

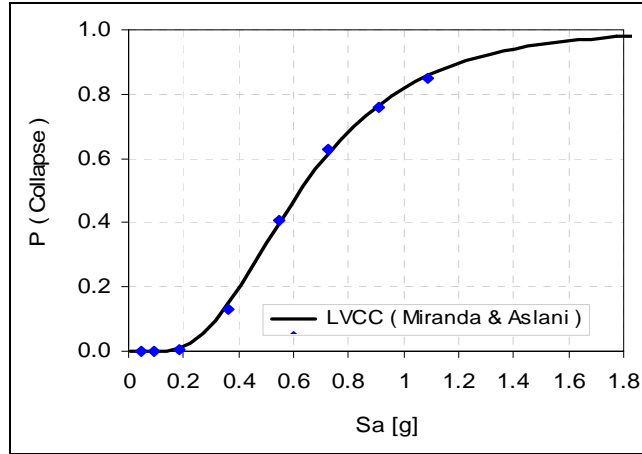


Fig. 4.27 Collapse fragility curve based on a bilinear nondegrading hinge model, MCB

The first two analyses capture the possibility of sideways collapse in the structure due to dynamic instability caused by large lateral displacements but do not take into account the possibility of collapse triggered by the loss of vertical load carrying capacity of individual structural members (e.g., the axial load failure of a column). Meanwhile the third analysis captures the loss of vertical carrying capacity of individual members but does not capture the possibility of a global sideways collapse.

Differences among collapse capacity results can be explained by the characteristics of each model. One of the main differences between the “Drain T=1.5sec.” model and the “OpenSees1” model is that the former considers P-delta in the analysis whereas the latter does not. The P-delta effect has been found to be a dominant factor as a structure approaches collapse [Ibarra 2003]. The “MCB” model does not have deteriorating properties but captures the loss of vertical carrying capacity, LVCC, by assigning deformation capacities to individual components. Because of the nondeteriorating bilinear properties of elements and by not considering the shear failure potential of columns, the median value of collapse capacity is higher than for the “Drain T=1.5sec.” model.

If one postulates that sideways and LVCC modes of collapse are mutually exclusive and their capacities are independent, then the probability of collapse considering the possibility of both collapse modes can be computed as follows:

$$F_{C|S_a}(s_a) = F_{C_1|S_a}(s_a) + F_{C_2|NC_1, S_a}(s_a) \cdot F_{NC_1|S_a}(s_a) \quad (4.4)$$

where $F_{C_1|S_a}(s_a)$ is the probability of occurrence of sideways collapse conditioned on IM, $F_{C_2|NC_1,S_a}(s_a)$ is the probability of occurrence of collapse triggered by the loss of vertical carrying capacity (LVCC) given that sideways collapse has not occurred at the intensity level s_a , and $F_{NC_1|S_a}(s_a)$ is the probability of not experiencing a sideways collapse at a given intensity level s_a . The latter cumulative probability is one minus $F_{C_1|S_a}(s_a)$, hence Eq. (4.4) can also be written as

$$F_{C|S_a}(s_a) = F_{C_2|NC_1,S_a}(s_a) + F_{C_1|S_a}(s_a)[1 - F_{C_2|NC_1,S_a}(s_a)] \quad (4.5)$$

Figure 4.28 compares the collapse fragility curves for the Van Nuys structure for the cases of sidesway collapse (from Figure 4.26) without (dashed line) and with (solid line) consideration of collapse triggered by the loss of vertical carrying capacity. From Eq. (4.4) or this figure it can be seen that neglecting the possibility of having a collapse triggered by the loss of vertical carrying capacity of individual elements leads to underestimation of the probability of collapse. For the testbed structure the estimated median and log standard deviation now become $\eta_C = 0.40g$ and $\beta_{RC} = 0.34$ rather than $\eta_C = 0.45g$ and $\beta_{RC} = 0.37$ for sidesway collapse alone.

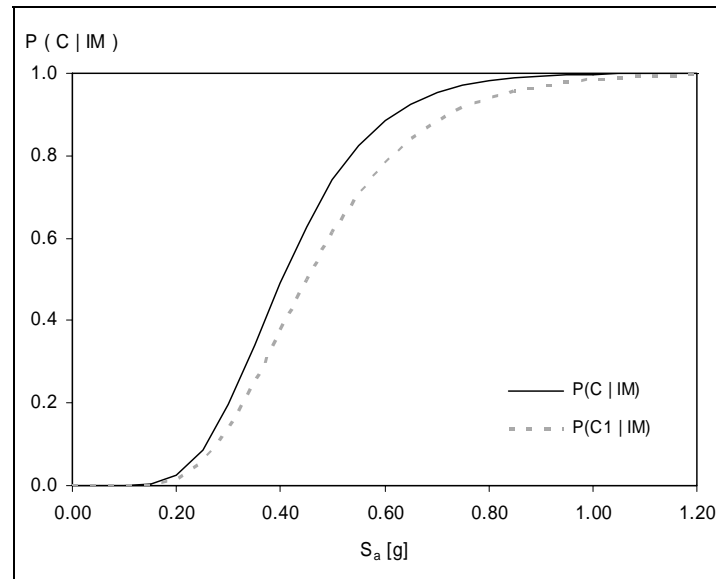


Fig. 4.28 Comparison of collapse fragility curves for the testbed structure with and without considering the possibility of having a collapse triggered by the loss of vertical carrying capacity in structural elements

Having obtained a collapse fragility curve, the mean annual frequency of collapse can be computed from the collapse fragility curve and an appropriate hazard curve, by either numerical

integration of Eq. (4.3) or using the following simplification proposed in Cornell 1996 and Cornell 2002:

$$\lambda_{Coll} = \int_{S_a} F_{C|S_a}(s_a) |d\lambda_{S_a}(s_a)| = \lambda_{S_a}(\eta_C) \exp\left(\frac{1}{2} k^2 \beta_{RC}^2\right) \quad (4.6)$$

The simplified expression on the right-hand side contains the MAF of the spectral acceleration associated with the median collapse capacity, $\lambda_{S_a}(\eta_C)$, and a term that accounts, in an approximate manner, for the uncertainties inherent in the computation of the collapse capacity. This term contains the slope of the hazard curve at the referenced spectral acceleration value, k , and the dispersion(s) in the collapse fragility curve, β (the σ of the log of the data if a log-normal distribution is assumed for the probability of collapse given the spectral acceleration). In the expression given by Eq. (4.6) only record-to-record (*RTR*) variability if considered, i.e., $\beta = \beta_{RC}$, which is explicitly contained in the collapse fragility curve. Using the example fragility curve of Figure 4.26, η_C is 0.45g and β_{RC} is equal to 0.37, and using the hazard curve of Figure 3.5 ($\lambda(0.45g) = 0.0026$, $k = 2.3$), the MAF of collapse is computed as

$$\lambda_C \approx \lambda(0.45) \exp[(0.5)(2.3)^2(0.37)^2] = 0.0026 \times 1.44 = 0.0037 \text{ /yr} \quad (4.7)$$

This value is large, indeed, demonstrating a large potential for collapse (equivalent to a 17% probability of collapse in 50 years). In fact, for this building the collapse potential is so large that it greatly affects the predicted direct losses (see Chapter 5), which for buildings with conforming (ductile) structural systems usually are dominated by smaller more frequent earthquakes that do not cause collapse.

In order to explore the sensitivity of collapse fragility and the probability of collapse of the Van Nuys building to period variation, the collapse fragility curve was also computed for the “Drain T=1.1 sec.” model, with the result shown in Figure 4.29. It is seen that the estimated median collapse capacity and the standard deviation of log of the collapse capacity have changed to $\eta_C = 0.54g$ and $\beta_{RC} = 0.32$. Although there is an increase in the median estimate of the collapse capacity compared to the case with the fundamental period equal to 1.5 sec., by comparing the probability of collapse for the same hazard levels (10% in 50 years) in Figures 4.26 and 4.29 it is seen that the probability of collapse for T_l equal to 1.1 seconds is higher than for the structure with T_l equal to 1.5 seconds. The mean annual frequency of collapse can be estimated by numerically integrating Eq. (4.3). The resulting λ_{coll} for the $T_l = 1.5$ sec. and $T_l =$

1.1 sec. models, together with the appropriate hazard curves, are shown in Figure 4.30. The λ_{coll} has increased from 0.0037 to 0.0043. Considering all the uncertainties involved in this process, this increase is insignificant, i.e., the $T_1 = 1.1$ sec. model predicts about the same probability of collapse as the $T_1 = 1.5$ sec. model. This indicates that for this range of fundamental periods the collapse probability is not sensitive to the decision on component stiffnesses.

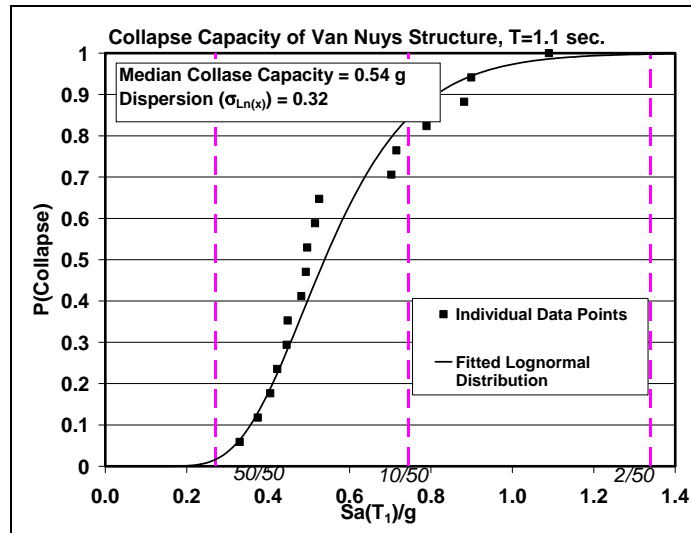


Fig. 4.29 Collapse fragility curve based on “Drain T=1.1sec.” model

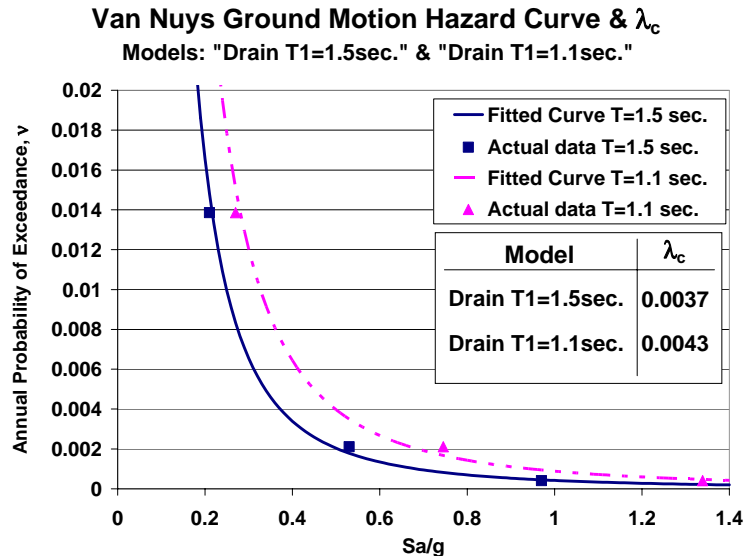


Fig. 4.30 Mean annual S_a hazard curves and annual probability of collapse for “Drain $T_1=1.5$ sec.” and “Drain $T_1=1.1$ sec.” models

4.5.2 Effect of Epistemic Uncertainty on the MAF of Collapse

Epistemic uncertainty exists both in the hazard curve and in the collapse fragility. First-order treatment of this uncertainty can be conducted as follows (Cornell et al., 2002; Ibarra, 2003). A model for the collapse capacity random variable that includes both aleatory randomness and epistemic uncertainty is:

$$C = \hat{\eta}_C \cdot \varepsilon_{UC} \cdot \varepsilon_{RC} \quad (4.8)$$

where $\hat{\eta}_C$ is the best (median) estimate of the median capacity, and ε_{UC} and ε_{RC} represent the epistemic uncertainty and the aleatory randomness in the capacity, respectively. Consistent with the (aleatory) model discussed before, we represent ε_{RC} by a lognormal model with median 1 and dispersion (log standard deviation) β_{RC} . We model the epistemic uncertainty in the capacity²³ also by a lognormal variable with median 1 and β_{UC} . The two variables are assumed to be independent lognormals. A representative value for β_{UC} for the Van Nuys structure and this degree of analysis might be 0.4 to 0.5 (Baker and Cornell, 2003; Ibarra, 2003).

The epistemic uncertainty in the S_a hazard curve is represented in this simplified approach by assuming that the actual curve, $\lambda_{S_a}(s)$, can be represented as a product of its “best” (here, central or median) estimate, $\hat{\lambda}_{S_a}(s)$, and a lognormal uncertain variable²⁴, ε_{UH} , with median 1 and dispersion $\beta_{UH}(s)$. Then the mean estimate of the hazard curve²⁵ is

²³ This is “first-order” representation of the epistemic uncertainty in the capacity in that it is formally treating only the median of C as uncertain, i.e., as if we were “sliding” the CDF shown in Fig. 4.29 left or right an uncertain amount (but not allowing for the fact that the slope of curve might be less or more and the shape different. (The latter two elements of uncertainty can be incorporated approximately by inflating β_{UC} . This uncertainty representation is practiced commonly in the nuclear industry seismic probabilistic risk assessments (Ref, Kennedy et al., 1980)

²⁴ As the hazard curve is a function of s, we must really specify fully a random function, including for example, the correlation between the values of $\lambda_{S_a}(s)$ at all pairs of values s_1 and s_2 . Here we are in effect assuming these values are all perfectly correlated; this assumption is conservative (Baker and Cornell, 2003)

²⁵ Note that this result implies that the ratio between the mean and median estimate is an indirect measure of the uncertainty in the estimation of the curve. For cases, such as coastal California, where the uncertainty is comparatively narrow, this is too fine an interpretation of this model. Instead β_{UH} should be estimated from the ratio of approximately the 85% estimate and the median estimate, because the “mean plus one sigma” (in log terms) is the 86th percentile, and hence, $\beta_{UH} = \ln(S_a^{86} / S_a^{50})$. Note from Fig. 3.5 that the value of β_{UH} will vary as a function of S_a level. In the current application one should use a value for S_a equal to roughly the estimate of the median capacity, $\hat{\eta}_C$. We shall see below that the ratio of mean to median hazard at about 0.45g is, in fact, in this case, very close to that obtained indirectly from the estimate of β_{UH} .

$\bar{\lambda}_{s_a}(s) = \hat{\lambda}_{s_a}(s) \exp\left(\frac{1}{2} \beta_{UH}^2(s)\right)$. In the vicinity of 0.45g, i.e., near the median capacity, the value of $\beta_{UH}(0.45g)$ is about 0.35, see Figure 3.5.

Given these two representations of the epistemic uncertainty in the collapse capacity and in the seismic hazard curve, it is possible to derive analytically the probability distribution describing the epistemic uncertainty in the estimate of the MAF of collapse (e.g., Cornell et al., 2002, Jalayer and Cornell, 2003). The result is that the *mean* estimate of the MAF of collapse is:

$$\bar{\lambda}_{Coll} = \int_{S_a} \bar{F}_{C|S_a}(s_a) |d\bar{\lambda}_{S_a}(s_a)| = \bar{\lambda}(\eta_C) \exp\left[\frac{1}{2} k^2 (\beta_{RC}^2 + \beta_{UC}^2)\right] \quad (4.9)$$

where the overbars stand for mean estimates. Note that this is just the estimate (0.0037 numerically) found before (without epistemic uncertainty, Eq. 4.6) times a factor representing capacity (epistemic) uncertainty, $\exp(1/2 k^2 \beta_{UC}^2)$, if the estimate above is in fact based on the mean (rather than the median) estimate of the hazard curve. For $\beta_{UC} = 0.4$ and $k = 2.3$, this is a factor of about 1.5, yielding a mean estimate of λ_{Coll} of about 0.0056 (or 24% in 50 years). The effect of hazard epistemic uncertainty is contained in the fact that we are using the mean estimate. Recall, from above, that $\bar{\lambda}_{s_a}(s) = \hat{\lambda}_{s_a}(s) \exp\left(\frac{1}{2} \beta_{UH}^2(s)\right)$, which is larger than the median by a factor here²⁶ of 1.07.

The analysis concludes further that the MAF has a lognormal distribution with

$$\beta_{\lambda_{Coll}} = \sqrt{\beta_{UH}^2 + k^2 \beta_{UC}^2} \quad (4.10)$$

This information can be used to determine confidence statements about collapse MAF estimates. For the values suggested above $\beta_{\lambda_{Coll}}$ equals the square root of $(0.35)^2 + (2.3)^2(0.4)^2$ or about 0.98. Note that this number is dominated by the second, structural capacity uncertainty term and not by the hazard term, in contrast to much conventional wisdom. (Note that this does not mean that the *aleatory* uncertainty is not dominated by the ground motion hazard. It seems to be but is

²⁶ This ratio is that according to the model with the estimate of β_{UH} found as described above; the ratio is 1.07 as calculated by the PSHA; this 7% difference is hardly visible in Fig. 3.5.

harder to quantify.) The factor k^2 has a lot to do with this conclusion²⁷. This value of $\beta_{\lambda_{coll}}$ implies that, for example, the 86% upper confidence bound (or “mean plus one sigma” (in log terms) bound) on the collapse MAF is the *median* estimate times $\exp(\beta_{\lambda_{coll}})$ or times 2.7. The median estimate of the collapse MAF is the mean estimate times $\exp(-1/2 \beta_{\lambda_{coll}}^2)$, which here equals 0.62, implying that the median collapse estimate is $(0.0056)(0.62) = 0.0035$. The 86% upper confidence bound is thus $(0.0035)(2.7) = 0.0095$ per annum, which is about 70% larger than the mean estimate. One can find other confidence bounds in the same way by using appropriate multipliers²⁸ on $\beta_{\lambda_{coll}}$ in the factor $\exp(\beta_{\lambda_{coll}})$. Note that the mean collapse MAF estimate lies at a confidence level between 50% and 86%.

²⁷ The factor k (slope of the log-log hazard curve) enters because the capacity uncertainty is being measured in the S_a dimension while seismic hazard and collapse MAF are both measured on the mean frequency (“probability”) axis. In different words, a factor of 2 change in capacity affects the MAF by a factor of about 2^k or about 4 here.

²⁸ The multipliers and their associated probabilities (confidence levels) come from a standard Gaussian table.

5 Prediction of Losses

5.1 CONNECTING STRUCTURAL ANALYSIS WITH DAMAGE AND LOSS ANALYSIS

In the context of performance assessment, structural analysis serves to predict, in a probabilistic format, a vector of EDPs from which all relevant decision variables (DVs) such as dollar losses, downtime, and deaths (the three D's) can be computed. In most (but not all) cases an intermittent variable, called a *Damage Measure*, DM , has to be inserted between the EDP and the DV , simply to facilitate the computation of DVs from $EDPs$. A DM describes the damage and consequences of damage to the structure or to a component of the structural, nonstructural, or content system, and the term $P(DM|EDP)$ can be viewed as a fragility function for a specific damage (failure) state. If the fragility functions for all relevant damage states of all relevant components are known, the DVs of interest can be evaluated either directly or by means of cost functions that relate the damage states to repair/replacement costs.

The Van Nuys testbed studies focused on the prediction of direct dollar losses. They did not address in depth the issues of downtime and casualties. If collapse is considered as surrogate DV for casualties, then the material discussed in Section 4.5 provides comprehensive information on this DV. The focus from here on is on providing methods, data, and results for the prediction of dollar losses for the Van Nuys building. As such, this focus incorporates collapse as a major contributor to direct financial losses.

In the context of dollar losses, the EDPs of primary interest are interstory drifts (for losses in the structural system (SS) and the nonstructural drift sensitive system ($NSDSS$)) and floor accelerations (for losses in the nonstructural and content systems that are sensitive to floor accelerations ($NSASS$)). The emphasis in the previous chapter was on interstory drift prediction, but complementary information is available on floor accelerations (Aslani and Miranda, 2003). It is understood that EDPs also include force quantities, particularly in cases of components in

which a certain action (e.g., axial force in a column) may be associated with non-ductile behavior. The effects of such force-based EDPs may be incorporated in the component force-deformation models or they may be evaluated in the $EDP \rightarrow DM$ phase through appropriate fragility functions.

In the context of loss estimation, the following summary observations are made on EDP prediction:

- For the testbed structure, the effect of soil-foundation-structure interaction effects on EDPs is found to be negligible.
- The results obtained from nonlinear response history analysis (NRHA) are sensitive to the analytical model of the structure, particularly in the range in which the properties of structural components are expected to deteriorate.
- OpenSees has advanced tools that permit the development of refined structural models that can replicate most of the common failure modes occurring in RC frame structures. At this time, the effort involved in developing such a refined structural model and in executing the large number of NRHAs needed for a comprehensive statistical description of EDPs is very large.
- To carry out the integration required in the framework equation (1.1) it is necessary to compute statistical measures of EDPs for the full range of IMs of interest. Stripe analysis (e.g., NRHA analysis with ground motions scaled to IMs for specific hazard values, such as 50/50, 10/50, and 2/50) may or may not provide sufficient response data for this purpose. IDAs deliver all the information needed, provided the ground motions are representative for the full IM range of interest.
- The dispersion in EDPs due to record-to-record variability (aleatory uncertainty) is large if $S_d(T_1)$ is selected as the IM, but it can be well predicted by means of IDAs. Pilot studies performed to explore the sensitivity of EDPs to epistemic (modeling) uncertainty disclosed the importance of this type of uncertainty, but were insufficient to provide comprehensive data. More work is needed to quantify the effects of epistemic uncertainty on EDPs and their dispersion.
- IDAs with deteriorating models of the Van Nuys structure led to dynamic instability (sidesway collapse) at relatively low IMs, indicating that the structure has a low threshold to collapse. Collapse fragility curves, which define the probability of collapse given IM,

and which are needed to predict the mean annual frequency of collapse, are very sensitive to the deterioration characteristics of the structural model used in the analysis.

The upshot is that statistical values (central value and measure of dispersion) of all EDPs needed for loss estimation can be predicted with various degrees of certainty. Both aleatory and epistemic uncertainties contribute significantly to variations in EDPs, which points out the importance of best-effort analytical modeling for improving the reliability of response prediction and performance assessment.

Once all relevant EDPs are described probabilistically for the full range of IMs affecting the integral given by Eq. (1.1), the process of damage modeling and loss estimation can be carried out. It requires an inventory of all structural, nonstructural, and content components that may contribute significantly to losses, the identification of damage measures, DMs, the availability of fragility functions that relate these DMs to EDPs, and the availability of cost functions that express the consequences of being in a damage state (e.g., repair costs) in terms of dollars. In this chapter the emphasis is on a summary of fragility functions, with more details presented in Appendix B, and on examples of options and results of the loss estimation methodology. The mathematical formulations of the implemented loss estimation methodology are presented in Appendix C.

5.2 DAMAGE ESTIMATION

Authors: E. Miranda, H. Aslani (Sections 5.2 to 5.4)

Once the response of the structure is known, damage states (damage measures, DM) in individual components can be obtained through the use of fragility functions. Fragility functions are functions that permit the estimation of the probability that a structural or non-structural component will be in a certain damage state when it is subjected to an engineering demand parameter EDP with intensity equal to edp . This section summarizes some of the fragility functions that were developed for estimating the physical damage in structural and non-structural components in the Van Nuys building.

5.2.1 Fragility of Structural Components

Four different groups of structural components were identified for Van Nuys testbed; slab-column connections, columns, interior beam-column connections and exterior beam-column connections. For each group, damage states associated with different repair actions were identified. Fragility functions for each damage state were then developed using the results of experimental results available in the literature. Table 5.1 summarizes the damage states that were used for each group of components.

Analysis of the result of various damage states indicates that fragility functions could be assumed to have a lognormal distribution (Aslani and Miranda, 2003). Therefore, only two parameters, namely the median and logarithmic standard deviation of the *EDP*, were required to define the fragility function corresponding to a certain damage state. The engineering demand parameter used in the fragility functions of structural components is interstory drift ratio. Figure 5.1 shows an example of fragility functions fitted to the experimental results for the first two damage states of slab-column connections. More details are presented in Appendix B.

Interstory drift ratios corresponding to certain damage states of structural components exhibit a very large scatter. For example, interstory drift ratios reported to produce punching shear failures in slab-column connections vary from 0.6% to 6.3%. In order to reduce the uncertainty in damage estimation for these damage states, fragility surfaces were developed (Aslani and Miranda 2003). In a fragility surface the mean and standard deviation of *EDP* corresponding to a damage state are evaluated as a function of a new parameter, α , which allows the incorporation of additional information. The parameter α can incorporate information on the element (e.g., geometry, detailing, etc.), the loading and or a combination of the two. The probability of exceeding the damage state is then estimated as a function of the level of *EDP* in the component but also as a function of the parameter α . Figure 5.2 presents an example of the fragility surface developed for punching shear failure in slab-column connections. In this case the probability of punching shear failures is computed as a function of the level of interstory drift ratio in the connection and as a function of a normalized gravity shear force. The last column in Table 5.1 presents the damage states of different structural elements for which fragility surfaces were developed for the Van Nuys testbed. The reader is referred to Appendix B for more details on fragility surfaces of certain damage states of structural components.

Table 5.1 Definition of damage measures, DM , in structural components

Damage Measures	Damage State	Repair Action	Fragility Surface
<i>Slab-column connections</i>			
DM_1	Initial cracking	Patching and/or painting of the cracks	No
DM_2	Significant cracking	Epoxy injection	No
DM_3	Punching shear failure	Spall repair	Yes
DM_4	LVCC*	Partial or total collapse	Yes
<i>Columns</i>			
DM_1	Significant cracking	Epoxy injection	No
DM_2	Shear failure	Crack stitching and spall repair	Yes
DM_3	Axial failure (LVCC)	Partial or total collapse	Yes
<i>Interior beam-column connections</i>			
DM_1	Beam or column cracking	Epoxy injection	No
DM_2	Joint cracking	Epoxy injection	No
DM_3	Spalling	Spall repair	No
DM_4	LVCC	Partial or total collapse	No
<i>Exterior beam-column connections</i>			
DM_1	Beam or column cracking	Epoxy injection	No
DM_2	Joint cracking	Epoxy injection	No
DM_3	Spalling	Spall repair	No
DM_4	LVCC	Partial or total collapse	No

* Loss of vertical carrying capacity

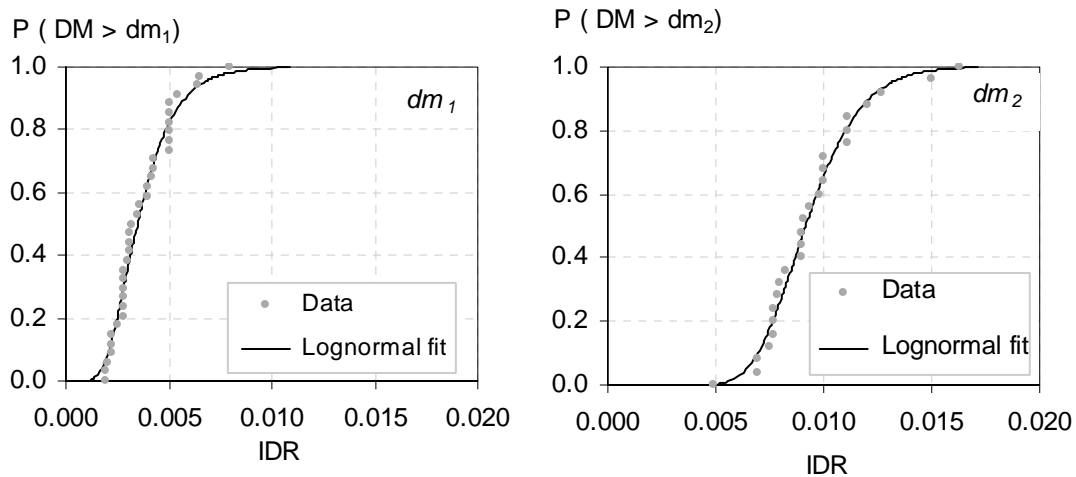


Fig. 5.1 Fragility functions corresponding to damage measures dm_1 and dm_2 in slab-column connections

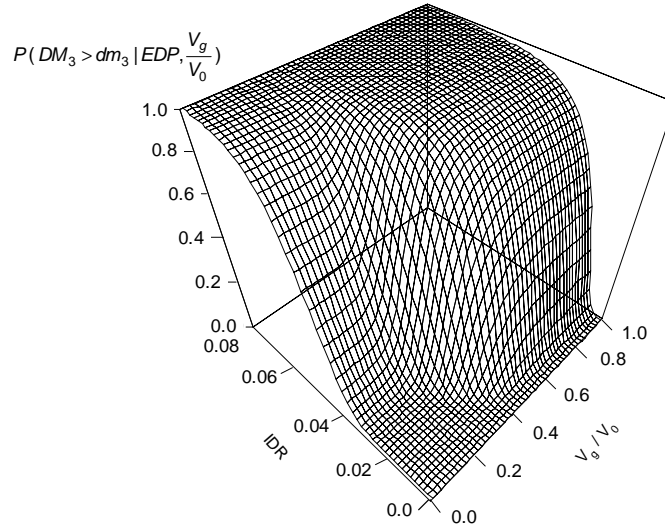


Fig. 5.2 Fragility surface for punching shear failure in slab-column connection as a function of the interstory drift ratio and normalized gravity shear force

5.2.2 Fragility of Non-structural Components

Nonstructural components installed on each floor were identified from the original architectural drawings of the building. The total estimated cost of non-structural components in the building is \$6,500,000 in 2002 dollars. Figure 5.3 presents a breakdown of the cost of the non-structural components. As shown in this figure, 42% this cost corresponds to mechanical equipment, while interior construction takes about 30%. More information on classification of non-structural components, their performance and cost can be found in the PEER report by Taghavi and Miranda (2003).

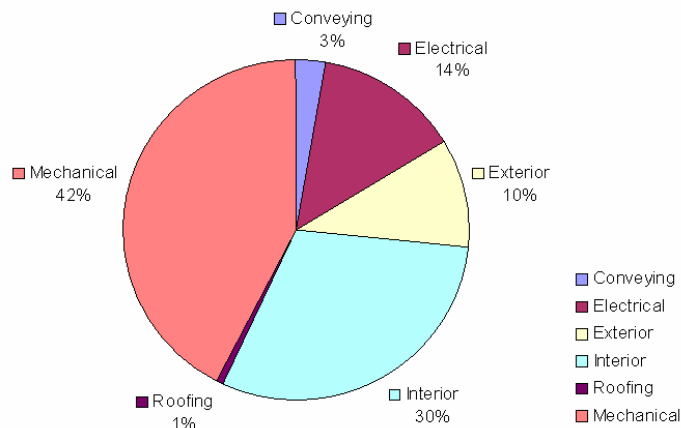


Fig. 5.3 Distribution of cost of nonstructural components in the building

Whenever possible, fragility functions were based on results of experimental studies available in the literature. Similar to the structural components, damage states of each component were defined based on distinctive tasks required to repair or replace a component. Our studies show that fragility functions for non-structural elements can also be modeled with a cumulative lognormal distribution. Therefore, only two parameters, median and the logarithmic standard deviation of the data, are required to develop each of the fragility functions. Two *EDPs*, namely interstory drift ratio and peak floor acceleration are used to define fragility functions for non-structural elements.

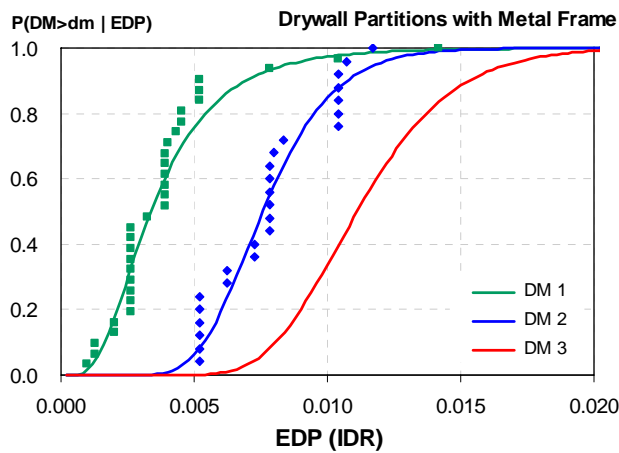


Fig. 5.4 Fragility functions of metal stud gypsum board partitions

Figure 5.4 presents an example of fragility functions developed for gypsum board partitions as a function of the level of the interstory drift ratio in the component. As can be seen in the figure, three damage states are identified for this element. Each of the damage states corresponds to a different course of action required to repair or replace the partition. For some non-structural elements for which no experimental data were available fragility functions recommended in HAZUS (1999) were used. A description of the fragility functions used in the study is presented in Appendix B, Section B.1.

5.3 LOSS ESTIMATION

Once the probability of experiencing various damage states has been determined in a component, loss functions are used to estimate the consequences of such damage. Consequences can include

economic losses, repair/replacement times (times required to bring the component back to its pre-damage conditions), possible injuries or other types of losses. A loss function provides the probability that a loss will occur or will be exceeded, conditioned on the component being in a particular damage state. Here emphasis is given to economic losses resulting from repair and/or replacement actions required to bring the component to its original condition. An example of loss functions for drywall partitions is shown in Figure 5.5. Ordinates provide the probability that a cost, normalized to the cost of installing a new partition, is reached or exceeded, conditioned on the partition being in a particular damage state. In general, there is no information available on the probability distribution of repair costs of either structural or nonstructural components. In this figure, for illustration purposes, the distribution has been assumed as lognormal. However, it should be noted that only the median and dispersion (first and second moments of the probability distribution) are used in estimation of economic losses in the building. If there was no variability in the cost to repair a particular damage state, these fragility functions would be perfectly vertical lines varying from zero to one at a normalized cost equal to the deterministic value of repairing the partition. However, as shown in the figure, considerable dispersion exists in these repair/replacement costs. For example, the cost of replacing a gypsum partitions can vary anywhere from about 65% to 200% of the average cost of a new partition.

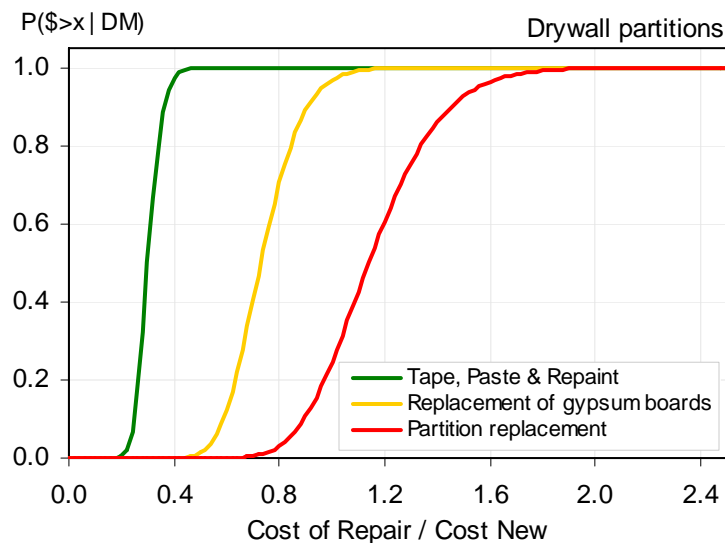


Fig. 5.5 Loss functions of metal stud gypsum board partitions

5.4 APPLICATION OF LOSS ESTIMATION METHODOLOGY

The aim of PEER's loss estimation efforts is to describe the seismic performance of structures quantitatively by continuous variables rather than discrete performance levels such as those used in the FEMA 273 or FEMA 356 documents. In this section the seismic performance of the Van Nuys testbed structure is measured in terms of economic losses and downtime.

5.4.1 Measures of Economic Losses

There are many possible measures of economic loss that can be used to describe seismic performance. A recent workshop organized in the context of the ATC-58 project concluded that while some stakeholders find it more useful to work with simple measures of economic losses in order to make their decisions, others prefer more complex measures of economic losses (ATC, 2003). In this work, different measures of economic loss were computed in order to demonstrate how the PEER loss estimation methodology can satisfy the needs of a wide range of stakeholders. Ordered by increasing level of complexity, the measures of performance computed for the Van Nuys testbed are:

- (a) Average economic loss for a given earthquake scenario.* This measure of seismic performance is the expected value of the total loss in the building in a given earthquake scenario, where the scenario is defined by a given ground motion intensity, IM . Hence, this measure of seismic performance corresponds to the expected value of the total loss conditioned on the ground motion having an intensity im , $E[L_T | IM=im]$.
- (b) Average economic loss for a family of earthquake scenarios.* This measure of seismic performance provides the average loss in the building for a family of earthquake scenarios, and describes the variation of the loss as a function of increasing ground motion intensities. At the expense of more simulations, this measure of seismic performance describes average losses in a continuum of earthquake scenarios.
- (c) Average annual loss.* By combining the expected loss in a family of scenarios with the annual frequency of occurrence of each scenario, this measure of seismic performance

provides the average economic loss that is produced in the structure every year. Owners, lending institutions, insurers, and other stakeholders can then quantitatively compare, for example, annual revenues versus expected annual losses. Similarly, they can compare annual earthquake insurance premiums to expected annual losses, etc.

While measures of seismic performance previously described provide information of expected values of economic losses (i.e., average losses) that can occur in a given scenario, in a family of scenarios, or that occur every year, they do not provide information on how large these losses can become in a given scenario or in a given year. In other words, they do not provide information on the dispersion around those average losses. In order to provide improved measures of seismic performance for the testbed structure, the following measures of performance were also computed:

(d) Probability of exceeding a certain dollar loss in a given earthquake scenario. This measure of seismic performance provides the probability of facing an economic loss larger than a certain dollar amount in an earthquake with intensity im , $P(L_T > l_i | IM = im)$. This measure of seismic performance can also provide dollar losses associated with certain probabilities of being exceeded in a given earthquake scenario. For example, it can provide the dollar loss that has a 10% probability of being exceeded in a given earthquake scenario.

(e) Probability of exceeding a certain dollar loss in a family of earthquake scenarios. This measure of seismic performance is similar to the previous one, but for a family of scenarios. Hence, it can provide variations of the probability of facing a loss larger than a certain amount, with increasing ground motion intensity, or variations of the dollar loss associated with a probability of exceedance in a given scenario with changes in the severity of the earthquake scenario.

(f) Probability of having a loss equal to or larger than a certain amount. This measure of performance combines the probability of losing more than a certain dollar amount in a given earthquake scenario (i.e., for a given value of IM) with the annual probability of experiencing a ground motion of an intensity equal or larger than im . It provides information on the annual probability of experiencing an economic loss larger than a certain dollar amount (e.g., the probability of losing more than one million dollars due to earthquake damage in the

structure). It can also provide dollar amounts associated with particular probabilities of being exceeded (e.g., the total dollar loss that has 1% probability of being exceeded in 50 years).

5.4.2 Dollar Loss Estimation

Using the total probability theorem, the *expected loss in a building for a scenario* that has a level of intensity of im , $E[L_T | IM=im]$, can be computed as

$$E[L_T | IM = im] = E[L_T | NC, IM = im] \cdot P(NC | IM = im) + E[L_T | C] \cdot P(C | IM = im) \quad (5.1)$$

where $E[L_T | NC, IM=im]$ is the expected loss in the building provided that collapse does not occur at the level of intensity of im , $P(NC | IM = im)$ is the probability of non-collapse conditioned on IM , $E[L_T | C]$ is expected loss in the building when a global collapse occurs in the building and $P(C | IM = im)$ is the probability that the structure will collapse under a ground motion with a level of intensity, im . The first expression on the right-hand side of this equation corresponds to the expected losses when there is no collapse, while the second expression on the right-hand side corresponds to the expected losses when collapse occurs.

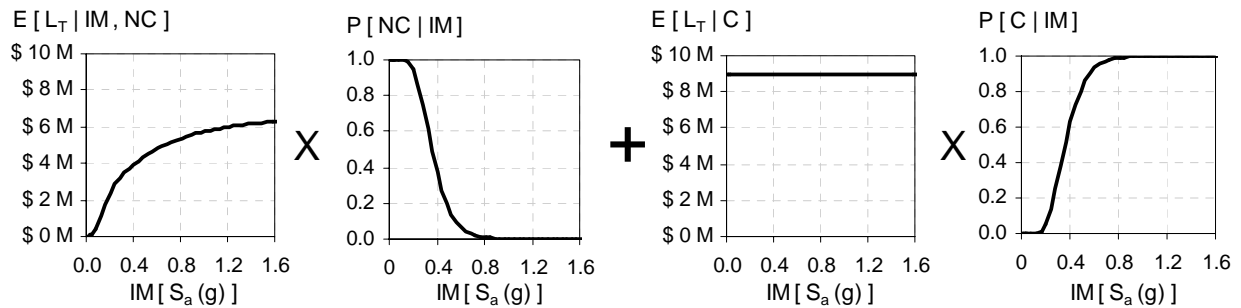
The expected total loss in the building provided that collapse does not occur at the level of intensity of im , $E[L_T | NC, IM = im]$, is computed as the sum of the losses in individual components of the building as

$$E[L_T | NC, IM = im] = E \left[\sum_{i=1}^N (a_i \cdot L_i | NC, IM = im) \right] = \sum_{i=1}^N a_i \cdot E[L_i | NC, IM = im] \quad (5.2)$$

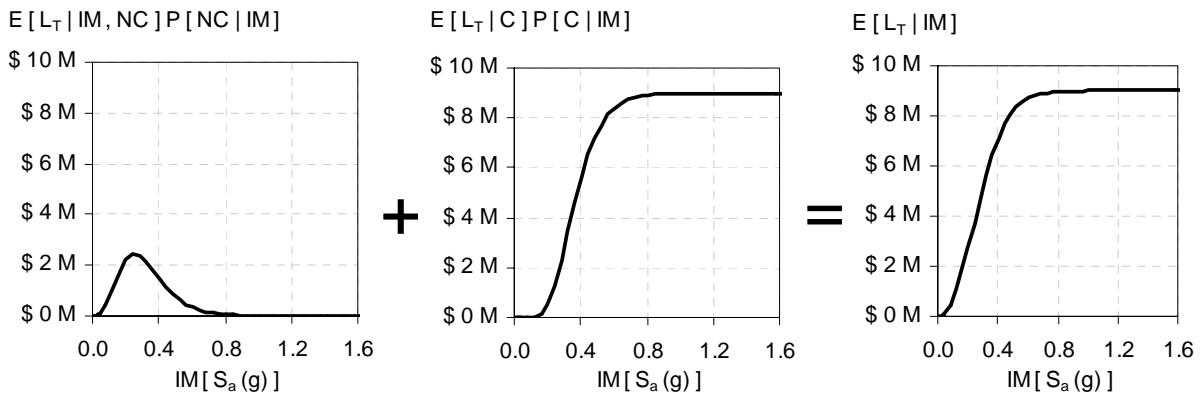
where $E[L_i | NC, IM = im]$ is the expected normalized loss in the i th component given that global collapse has not occurred at the intensity level im , a_i is the expected value of the cost for the new component i , and L_i is the normalized loss in the i th component defined as the cost of repair or replacement in the component normalized by a_i . Details on the computation of $E[L_T | NC, IM = im]$ and $E[L_T | IM = im]$ are given in Miranda and Aslani (2003) and in Appendix C.

Figure 5.6a shows a graphic representation of the four terms in Eq. (5.1). It can be seen that $E[L_T | NC, IM=im]$ gradually increases as the ground motion intensity increases. However, these losses are then multiplied by the probability of non-collapse, which for this building decreases rapidly as the ground motion intensity increases; hence, as shown in Figure 5.6b, this

first term reaches a maximum of about \$2.4 million for a spectral acceleration of about 0.3g and reduces to zero for ground motions with a spectral acceleration of 0.9g. On the other hand, the expected value of the loss conditioned on collapse is multiplied by a rapidly increasing function. Figure 5.6b shows that, with the exception of intensities smaller than about 0.3g (which corresponds to a frequent event, see Figure 3.5), for this testbed building the losses due to collapse are more important than losses associated with non-collapse.



(a) Each term on right-hand side of Eq. (5.1)



(b) Non-collapse loss + collapse loss = total loss

Fig. 5.6 Graphic representation of the computation of expected losses (in millions of dollars) as a function of the ground motion intensity

The *expected annual loss* in the building, $E[L_T]$, is computed by integrating $E[L_T | IM = im]$ over all possible levels of intensity as follows (Rosenblueth 1976, Wen et al. 2001):

$$E[L_T] = \int_0^t \int_0^\infty e^{-\lambda\tau} E[L_T | IM = im] \cdot \left| \frac{d\nu(IM)}{dIM} \right| dIM d\tau \quad (5.3)$$

where $e^{-\lambda\tau}$ is the discounted factor of the loss over a reference time t , λ is the discount rate per year, and $d\nu(IM)/dIM$ is the derivative of the seismic hazard curve at the site. The time period t can correspond to the design life of a new structure, the remaining life of an existing structure or another reference time period. For a long reference time, where the effect of the finite life span of the facility becomes negligible, the expected annual loss (in 2002 dollars) computed for the Van Nuys testbed structure is \$198,000. Despite losses associated with non-collapse being relatively small in this structure, 65% of the average annual losses are produced by non-collapse cases. This is because, even though these losses are smaller, they occur far more often than those associated with earthquakes that produce the collapse of the structure. It should be noted that for structures in which collapse is delayed due to a larger deformation capacity, expected annual losses will typically be dominated even more by non-collapse cases.

Expected annual losses can be disaggregated to find out the ground motion intensities that contribute more to annual losses in a structure. For the Van Nuys testbed structure it is interesting to note that about 70% of the expected annual losses are produced in earthquakes with intensities between 0.09g and 0.8g. Furthermore, 87.8% of the expected annual loss is associated with nonstructural components and only 12.5% with structural components.

Two different approaches are used to compute the ***probability of losing a certain dollar amount in a given scenario***, $P(L_T > l_T | IM = im)$. In the first approach, $P(L_T > l_T | IM = im)$ can be written as

$$P(L_T > l_T | IM = im) = P(L_T > l_T | NC, IM = im) \cdot P(NC | IM = im) + P(L_T > l_T | C) \cdot P(C | IM = im) \quad (5.4)$$

where $P(L_T > l_T | NC, IM = im)$ is the probability of having a loss in the building greater than a certain dollar amount, l_T , provided that collapse does not occur at the level of intensity of im , and $P(L_T > l_T | C)$ is the probability of experiencing a loss greater than l_T given that collapse has occurred in the building. If the probability distribution of the total loss in collapse and non-collapse cases is known, then Eq. (5.4) permits computing the probability of exceedance of the total loss conditioned on a ground motion intensity level im . When using this approach it was assumed that $P(L_T > l_T | NC, IM = im)$ is normally distributed and that $P(L_T > l_T | C)$ is lognormally

distributed. In the second approach, the first two moments of $P(L_T > l_T | IM = im)$ are first computed as described in Appendix C and then this probability is computed by assuming that it is lognormally distributed.

An example of using the first approach to compute the *loss that has a 20% chance of being exceeded* for an earthquake scenario corresponding to a ground motion intensity of 0.32g is shown on the left-hand side of Figure 5.7. The right-hand side of this figure shows the probability of having a loss larger than 4 million dollars, also at an intensity level of 0.32g.

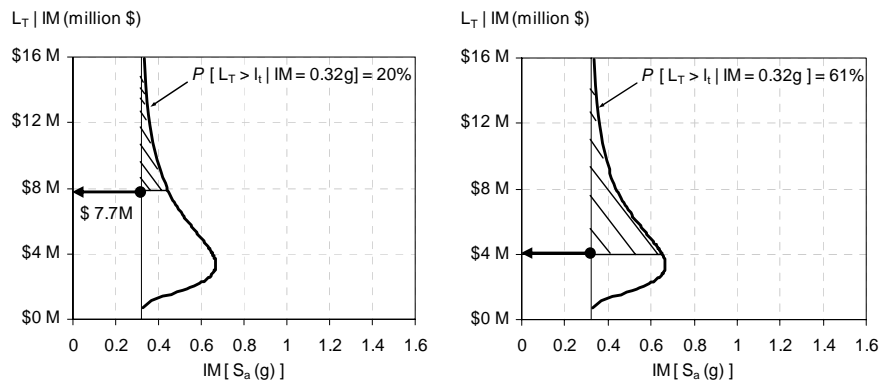


Fig. 5.7 (a) Dollar loss in the testbed structure associated with a 20% probability of exceedance in ground motion with an intensity of 0.32g; (b) Probability of experiencing a loss larger than 4 million dollars in an event with a ground motion intensity of 0.32g.

Losses that have a 10% probability of exceedance for two ground motion intensity levels are shown in Figure 5.8. Similarly to expected losses, these losses sharply increase from ground motion intensities of about 0.1g to about 0.6g.

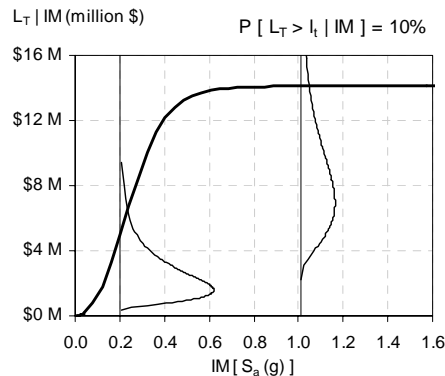


Fig. 5.8 Dollar losses in the testbed structure associated with a 10% probability of being exceeded for two levels of ground motion intensity

The mean annual frequency (MAF) of a certain dollar loss can be computed by integrating $P[L_T > l_T | IM = im]$, (Eq. 5.4), over all possible levels of intensity, as follows

$$v[L_T > l_T] = \int_0^{\infty} P[L_T > l_T | IM = im] \cdot \left| \frac{dv(IM)}{dIM} \right| dIM \quad (5.5)$$

For values smaller than 0.01, the mean annual frequency of exceedance of a loss l_T is approximately equal to the probability of losing more than a certain dollar amount l_T in any given year, $P[L_T > l_T]$, hence Eq. (5.5) can be rewritten as

$$P[L_T > l_T] \approx \int_0^{\infty} P[L_T > l_T | IM = im] \cdot \left| \frac{dv(IM)}{dIM} \right| dIM \quad (5.6)$$

The loss curve for the Van Nuys testbed structure is shown in Figure 5.9, where it can be seen that losses smaller than \$1,000,000 have relatively high mean annual frequencies of exceedance. It can also be observed that a large increase in loss is produced with changes in mean annual frequency from 0.008 and 0.005. This large increase is associated with the large increase in losses that is produced between intensity measures of 0.1g and 0.5g.

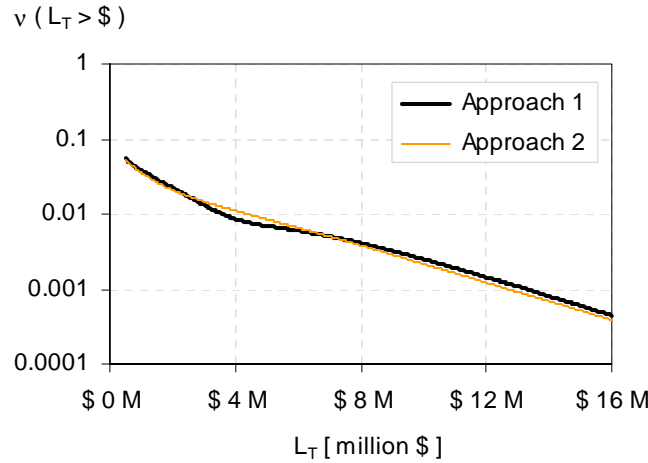


Fig. 5.9 Loss curve computed for the Van Nuys testbed structure

Also shown on Figure 5.9 is a comparison of the effects of the two approaches for estimating $P[L_T > l_T | IM = im]$, on the loss curve. As shown in the figure, results from both approaches are very close.

5.4.3 Downtime Estimation

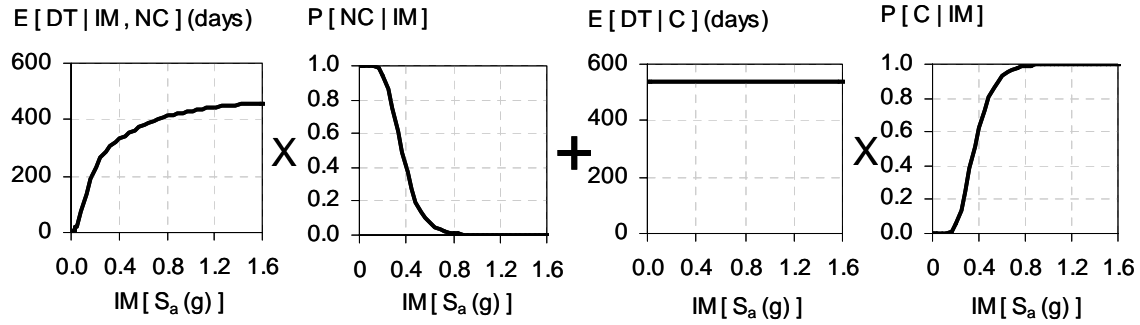
Besides direct economic losses associated with repairs, the time required to repair or replace the building, commonly referred to as “downtime,” is also a very important decision variable. Downtime can be computed in a similar fashion as economic losses; for instance, the expected value of the downtime (e.g., average number of days of downtime) conditioned on a ground motion intensity is given by

$$E[DT | IM = im] = E[DT | NC, IM = im] \cdot P(NC | IM = im) + E[DT | C] \cdot P(C | IM = im) \quad (5.7)$$

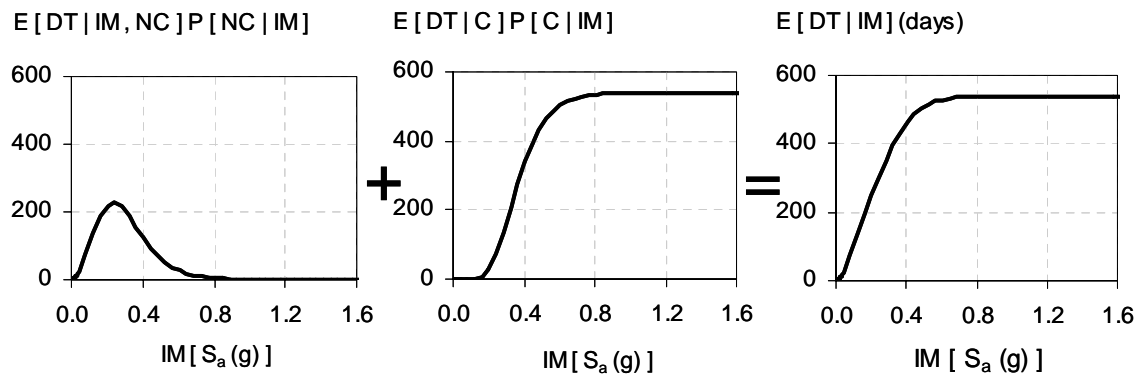
where $E[DT | NC, IM = im]$ is the expected value of the downtime in the building provided that collapse does not occur at the level of intensity of im , $P(NC | IM = im)$ is the probability of non-collapse conditioned on IM , $E[DT | C]$ is expected downtime in the building when a global collapse occurs in the building (i.e., the average time from the time in which the collapse occurs to the time the structure would be fully rebuilt), and $P(C | IM = im)$ is the probability of collapse conditioned on IM .

Estimation of downtime is complicated by the fact that it may have significant variations depending on the resources that are allocated to the repair process. It is well known that additional economic resources can result in shorter construction times. Furthermore, downtime is greatly affected by variables that are based on external socio-economic conditions, such as the time it takes to mobilize a large enough skilled labor force and to make the site accessible to large equipment. Other issues involve design time, time for permit approvals, time for securing repair/reconstruction financing, etc. Estimation of downtime is a complex problem that needs to be researched in much more depth. In this study a rough estimation of downtime was obtained by assuming that $E[DT | NC, IM = im]$ is a linear function of $E[L_r | NC, IM = im]$. Implicit in this simplifying assumption is that labor costs represent a major portion of the repair costs, such that as economic losses due to repair/replacement of structural and non-structural components in no-collapse cases increases, the time required to bring those damaged components to their pre-damage condition will also increase. Although this assumption is probably too simplistic, it permits a rough estimation of the downtime. Figures 5.10 show the graphical presentation of Eq. 5.7. Comparison of Figures 5.6 and 5.10 indicates that, congruent with the simplifying assumption previously described, the variation of $E[DT | NC, IM = im]$ with ground motion

intensity has the same shape as $E[L_T | NC, IM = im]$. Furthermore, it can be seen that for ground motion intensities larger than 0.4g, the downtime is dominated by the probability of collapse, and the role of the simplifying assumption is very small.



(a) Each term on right-hand side of Eq. (5.7)



(b) Non-collapse downtime + collapse downtime = total downtime

Fig. 5.10 Graphic representation of the computation of expected downtime (in days) as a function of the ground motion intensity

The expected annual downtime in the building, $E[DT]$, can be computed by integrating $E[DT | IM = im]$, Eq. (5.7), over all possible levels of intensity, using the total probability theorem

$$E[DT] = \int_0^{\infty} E[DT | IM = im] \cdot \left| \frac{dv(IM)}{dIM} \right| \cdot dIM \quad (5.8)$$

where $dv(IM)/dIM$ is the derivative of the seismic hazard curve at the site. The expected annual downtime estimated for the Van Nuys testbed structure is 32 days.

6 Propagation of Uncertainties from *IM* to *DV*

Authors: K. Porter, A. Cornell, J. Baker

6.1 SOURCES OF UNCERTAINTIES

Every stage of a PBEE analysis involves uncertainty. A PEER working group identified the following incomplete list of main sources of uncertainty that should be quantified and propagated in the performance assessment process:

- Uncertainties associated with Intensity Measures (IMs)
 - Random occurrence of earthquakes in space and time (distance and rate of occurrence)
 - Earthquake magnitude
 - Attenuation from source to site
 - Inherent randomness of ground motion time histories
- Uncertainties associated with geotechnical aspects (IM-EDP)
 - Geotechnical geometric and material properties and their effects on ground motion time histories (site soil modification)
 - Geotechnical geometric and material properties and their effects on SFSI
- Uncertainties associated with Engineering Demand Parameters (EDPs)
 - Structural geometric and material properties
 - Modeling uncertainties at component and system levels
 - Statistical uncertainty (mainly arising from limited sample size)
 - Measurement uncertainty (arising from errors made during measurements and observations).
 - Prediction method (bias introduced by analysis method)
 - Construction uncertainties
- Uncertainties associated with Damage Measures (DMs) (at component level)
 - Characterization of damage states (e.g., damage observation and repair action)
 - Inadequate fragility data
 - Construction uncertainties
- Uncertainties associated with Decision Variables (DVs)
 - Consequences of limit state exceedance (collapse, life safety, \$ losses, downtime)
 - Economic assumptions (discount rate and other assumptions in cost modeling)

- Economic consequence modeling
- Recovery rates (availability of finances, business/construction capability, state of economy in region)

Table 6-1 lists specific examples of sources of uncertainty (referred to here as basic random variables) in a PBEE analysis, as well as references to quantify that uncertainty. Most of the variables in Table 6-1 are multidimensional or vector-valued, and there is typically correlation among the elements of such a vector (e.g., floor-to-floor EDP correlations) and between the different variables (e.g., the DMs given the EDPs). The latter are captured explicitly in the PEER Framework Equation, e.g., in the form of conditional distributions such as $G_{DM|IM}$. The former are only implicit in that equation.

Table 6.1 Examples of sources of uncertainty in PBEE analysis

	Relationship	Basic variables	References
Hazard analysis	$\lambda(IM_r)$	Seismicity model, attenuation relationship(s). IM_r refers to IM on reference site class	Frankel and Leyendecker (2001)
	$p[IM IM_r]$	Soil G - ξ relationship, shearwave velocity v_s , depth to bedrock (DTB), and soil density γ .	Jones et al. (2002), see also Section 3.5
	$p[GM IM]$	Record selection or simulation parameters; GM refers to ground motion	Silva (2000), Atkinson and Silva (2000)
Struct'l analysis	$p[EDP GM]$	Mass, M	Ellingwood et al. (1980)
		Damping, β	McVerry (1979), Beck (1982), Camelo et al. (2001)
Damage analysis	$p[EDP GM]$	Force-deformation behavior, FD	Ellingwood et al. (1980), Ibarra (2003)
		$p[DM EDP]$	Component capacity, X (i.e., EDP at which components are damaged)
Loss analysis	$p[DV_s DM]$ (repair costs)	Unit repair cost, C (cost to restore a damaged component);	Porter et al. (2001, 2002a), Beck et al. (2002), Miranda et al. (2003)
		Contractor overhead & profit, C_{OP} (factor added to total direct costs)	
	$p[DV_f DM]$ (deaths)	Fraction of occupants killed given collapse, K Number of occupants, O	Appendix D; Seligson et al. (2002)
Loss analysis	$p[DV_t DM]$ (downtime)	Unit repair time, U (crew-hours to restore a damaged component)	Porter and Kiremidjian (2001)
		Crews available, E	
		Change-of-trade delay, R_T (time from one trade completing work to next arriving) Mobilization time, T_0 (time between earthquake and arrival of repair crews)	

Several methods are available to propagate uncertainty through a PBEE analysis, each suiting different objectives. The total analysis may involve only one method, e.g., Monte Carlo analysis, or a mix of methods selected to match the accuracy and/or computational aspects of each step in the Framework Equation. Consider four objectives, addressed hereafter: (1) feature selection; (2) studying the body of a DV distribution; (3) estimation of the first two moments of a $DV|IM$; and (4) estimating the probability of low-probability events.

6.2 TORNADO DIAGRAM ANALYSIS

For feature selection, the question is which basic variable(s) appear to contribute most strongly to overall uncertainty in DV . This information can be used to select the variables that should be treated as uncertain, allowing the rest to be fixed at a single mean value. Feature selection can also be used to target important features for additional study to reduce uncertainty. In the case of PBEE, the model being assessed is one that estimates quantities such as $p[DV | IM]$ or $p[DV]$ where DV is a decision variable such as future economic loss and IM represents a shaking intensity level. As discussed elsewhere (Chapters 5 and 8) the DV may be in annual terms or in terms of a planning period such as 50 years.

In an approach taken from decision analysis by Porter et al. (2002a), one begins by estimating three values of each basic variable: lower bound (e.g., 10th percentile), upper bound (e.g., 90th percentile) and best estimate (e.g., median). One also needs a model to relate the basic variables to DV , i.e., producing a deterministic value of DV given specific values of each basic variable. The model includes four stages:

1. *Hazard analysis.* Select IM value of interest and select a ground-motion time history GM and scale it to IM . Currently there is no probability distribution associated with recorded ground-motion time history, so one must sample a number of ground-motion time histories to account for record-to-record variability.
2. *Structural analysis.* Calculate M , β , and FD (see Table 6.1 for definitions) of the facility and perform a nonlinear response-history structural analysis to determine EDP .
3. *Damage analysis.* Determine the capacities (fragilities) $X_{i,dm}$ of each damageable component of the facility, i.e., the EDP at which a component of each type $i = 1, 2, \dots, n_{CT}$ reaches

exceeds each of damage states $DM = 1, 2, \dots, n_{DM}$, where n_{CT} is the number of damageable component types in the facility and n_{DM} denotes the number of possible damage states of the component. Then for each component, calculate

$$DM = \max(dm): X_{i,dm} < EDP \quad (6.1)$$

where EDP is the engineering demand parameter to which that component is sensitive. Calculate each $N_{i,dm}$, the number of damaged components of type i and damage state, dm .

4. *Loss analysis (repair cost)*. Determine the unit costs $C_{i,dm}$ to restore a component of type i from each of its possible damage states dm . Determine the contractor's overhead and profit factor, C_{OP} . Calculate the total repair cost as

$$DV = (1 + C_{OP}) \sum_{i=1}^{n_{CT}} \sum_{dm=1}^{n_{DM}} N_{i,dm} C_{i,dm} \quad (6.2)$$

In the tornado-diagram analysis (Fig. 6-1), one does not need a full probability distribution for each basic variable. The next step is to take all basic variables at their best-estimate values, and calculate the resulting DV , thus establishing a baseline. One then varies a single basic variable, setting it first to a lower-bound value and calculating DV , and then setting it to its upper-bound value and again calculating DV . The difference between these two values is referred to here as the DV swing associated with that variable. The process is repeated for each basic variable to find the DV swing associated with each basic variable. A larger DV swing suggests a more-important basic variable.

The variables can be sorted in decreasing order of DV swing, and a bar chart created showing DV on the x -axis and the basic variables on the y -axis. Bars are horizontal, one for each basic variable. The variable with the largest swing is shown on the top of the chart; the variable with the smallest swing at the bottom. The effect of each basic variable is shown by one bar whose ends are at the DV values produced by setting that variable to its lower and upper bounds. The resulting graph resembles the profile of a tornado, hence the name "tornado diagram."

Porter et al. (2002a) present such an analysis of the Van Nuys testbed, studying the DV of the maximum single-event repair cost during a planning period $t = 50$ yr. Variables examined are listed in Table 6-2. Ground motions associated with bounds and median are those among 20 sampled that produced the 10th, 50th, and 90th percentile values of DV ; they were selected from 100 offered by Somerville et al. (1997). For the chosen bounds (10th and 90th percentile) the

authors found that the top contributors to uncertainty in DV appear to be component capacity (X) and the maximum value of IM to which the facility is subjected during t . Secondary contributors include the ground-motion time history (GM), unit costs (C), and damping (β). For the pre-selected bounds, uncertainty in DV associated with FD , M , and C_{OP} are small, suggesting that these might reasonably be treated deterministically. No attempt was made to address fatalities or repair duration, or to account for geotechnical uncertainties. Kramer (2003), however, has studied the sensitivity of ductility demand at the Van Nuys site to IM and various geotechnical uncertainties, finding that the top contributors are IM , v_s , and $G-\xi$ (see also Section 3.5).

Table 6.2 Parameters of the sensitivity study

Parameter	10 th pctile	Median	90 th pctile	Comment
S_a (g)	0.11 (LA50, 0.52)	0.27 (LA50, 1.28)	0.58 (LA50, 2.74)	Spectral acceleration (Record, scaling factor)
Ground motion	LA45, 1.10	LA50, 1.28	LA49, 1.26	Record, scaling factor
Mass, M	$0.872M_n$	M_n	$1.128M_n$	M_n : nominal mass
Damping, β	2.4%	5.0%	7.6%	Percent of critical
Force-deformation multiplier ε_{FD}	0.90	1.00	1.10	Factor applied to F & D in FD relationships
Assembly capacity X	$e^{\ln x_m - 1.28\zeta}$	x_m	$e^{\ln x_m + 1.28\zeta}$	x_m and ζ : see Beck et al. (2002)
Costs: unit costs C	$e^{\ln x_m - 1.28\zeta}$	x_m	$e^{\ln x_m + 1.28\zeta}$	x_m and ζ : see Beck et al. (2002)
C_{OP}	0.15	0.175	0.20	Overhead and profit (O&P)

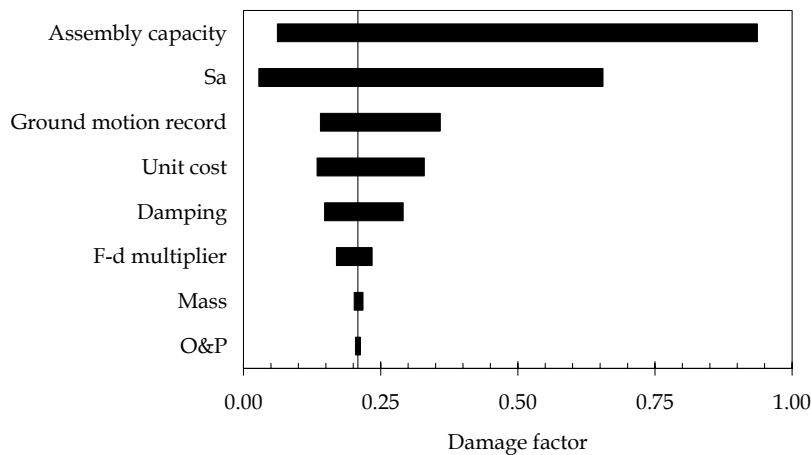


Fig. 6.1 Tornado diagram analysis of Van Nuys testbed by Porter et al. (2002a)

6.3 MONTE CARLO SIMULATION FOR STUDYING THE BODY OF A DV DISTRIBUTION

In this case, the objective is to examine the body of the DV distribution without making assumptions about its shape. Monte Carlo simulation (MCS) has been used to estimate $p[DV | IM]$ and $p[DV | t]$ by creating a number of samples of DV . One needs a deterministic model relating the basic variables to DV . One begins by assuming the form and parameters of the distributions of the basic uncertain variables. There are several approaches to Monte Carlo simulation; we describe here the simplest as it applies to the study of $p[DV | IM]$. Let X denote the vector of N basic uncertain variables, which are denoted individually by $X_i : i \in \{1, 2, \dots, N\}$. Let $f(X)$ denote the deterministic model that relates X to DV , i.e., $DV = f(X)$. One can model $f(x)$ as discussed in Section 6.2.

Now let $F_{X_i}(x_i)$ denote the cumulative distribution function (CDF) of X_i evaluated at x_i . For further simplicity, let us assume that DV is a scalar such as repair cost and that the model has been defined so that $X_i \perp X_j$ for $i \neq j$ and $i, j \in \{1, 2, \dots, N\}$, i.e., the components of X are independent. Let M denote the number of sample values of DV to be created. One draws samples of X consistent with their distribution; let x denote a sample of X , and let x_i denote the i^{th} component of x . One convenient way to create sample x vectors is by the inverse method, in which one first draws a sample vector U with N components U_1, U_2, \dots, U_N , where each U_i is uniformly distributed between 0 and 1, and $U_i \perp U_j$ for $i \neq j$ and $i, j \in \{1, 2, \dots, N\}$. Let u_i denote the sample value of U_i . One inverts the CDF of each X_i at u_i , i.e.,

$$x_i = F_{X_i}^{-1}(u_i) \quad (6.3)$$

For example, if X_i is normally distributed with mean value μ_i and standard deviation σ_i , then

$$x_i = \Phi^{-1}(u_i)\sigma_i + \mu_i \quad (6.4)$$

where $\Phi^{-1}(p)$ represents the inverse standard normal distribution evaluated at p . One then calculates the sample value $dv = f(x)$ for x , repeating the process M times. One compiles the M samples and sorts the dv values in increasing order. Let dv_1 represent the smallest sample value of DV , dv_2 represent the next larger, etc., up to dv_M . The CDF of DV is then approximated by

$$\begin{aligned}
F_{DV}(dv) &= 0 & dv < dv_1 \\
&= \frac{m}{M} & dv_m \leq dv < dv_{m+1}, \quad 1 \leq m < M \\
&= 1 & dv_M < dv
\end{aligned} \tag{6.5}$$

The larger the number of samples M , the more closely $F_{DV}(dv)$ will resemble the “true” CDF of DV . For models of reasonable complexity (such as a 2-D analysis of the Van Nuys testbed represented by a simple non-deteriorating model), it is currently practical to perform hundreds of simulations overnight on a common desktop computer. (See, e.g., Beck et al., 2002 and Porter et al., 2002b; in these studies, the Van Nuys testbed building and 19 others were each analyzed from ground motion to DV in 400 simulations.) The most computationally expensive stage of the analysis is the structural analyses; damage and loss calculations do not add substantially to the computational effort. One can increase the efficiency of the process through Latin Hypercube simulation of X or by a moment-matching approach (neither described here).

Beck et al. (2002) performed such a study of the Van Nuys testbed, using the model described in Porter et al. (2002b), and produced the seismic vulnerability function ($DV|IM$) shown in Figure 6-2(a). The study found that $DV|IM$ is approximately lognormally distributed as shown in Figure 6-2(b), that the coefficient of variation of repair cost decreases with increasing IM as shown in Figure 6-2(c), and in a companion study (Porter et al., 2004) as shown in Figure 6-2(d), that IM values associated with recurrence periods of 40 to 300 years dominate expected annualized repair cost (denoted by EAL , for expected annualized loss). The study required 7 hours of computer time to perform the 400 nonlinear response-history structural analyses, and less than 1 hour to perform the damage and loss calculations. Thus, using simple non-deteriorating component models for structures of moderate size and complexity, such as the Van Nuys testbed, MCS is not computationally expensive — with the assumptions made in the analysis.

However, there is a caveat to the aforementioned argument of computational efficiency and the associated results. The MCS was performed on a simple non-deteriorating model of the Van Nuys structure. As discussed in Chapters 4 and 5, the Van Nuys structure has many non-conforming structural elements that exhibit early deterioration in strength and stiffness, which leads to amplification of story drifts and to potential collapse at relatively low spectral accelerations. For instance, Figure 4.26 indicated a 50% probability of collapse at $S_a(T_1) =$

0.46g. Thus, the damage factors for large spectral accelerations are expected to be much larger than those shown in Figure 6.2(a) once deterioration in strength and stiffness is incorporated in the analytical model. Clearly, this will render the structural analysis effort more complex and much more computationally expensive.

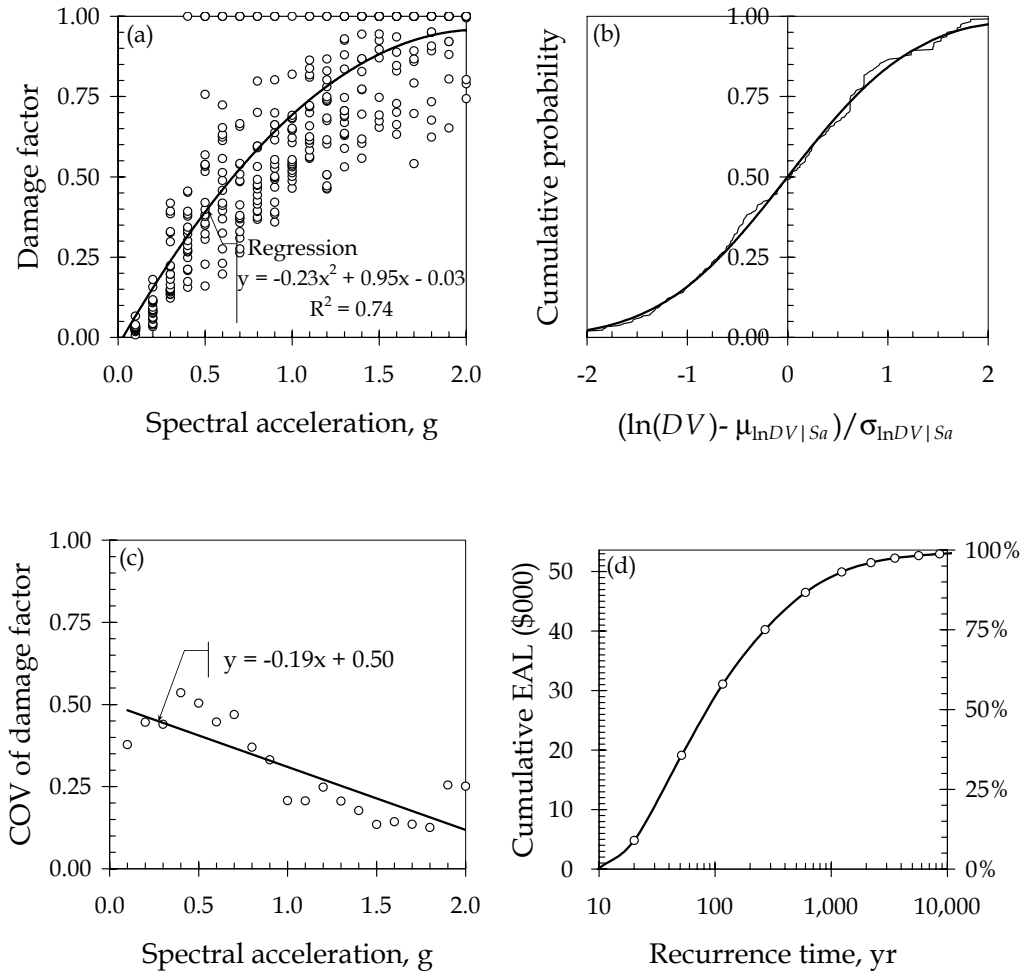


Fig. 6.2 Results of MCS analysis: (a) seismic vulnerability for the Van Nuys testbed building, (b) lognormal distribution of damage factor (repair cost as a fraction of replacement cost), (c) trend of decreasing coefficient of variation of damage factor with increasing *IM*, and (d) apparent dominance of low to moderate *IM* on economic risk. (Beck et al. 2002a, Porter et al., 2004.)

6.4 FOSM FOR ESTIMATING THE FIRST TWO MOMENTS OF DV

Another method for propagation of uncertainty is proposed by Baker and Cornell (2003), using a combination of First-Order Second-Moment (FOSM) methods and numerical integration. This method attempts to lower the computational expense relative to direct Monte Carlo simulation, especially when multiple runs are required to calculate sensitivities and/or when low probabilities are needed. The FOSM approximation (e.g., Melchers 1999) is used to obtain estimates of the conditional moments of $DV|IM$ (i.e., the mean and variance *given* the value of the IM) from the conditional moments of EDP , DM and DV . Then $DV|IM$ is numerically integrated with the ground motion hazard curve, $\lambda(IM)$.

The motivation for this hybrid method is the assumption that the uncertainty in the IM hazard curve is the most significant contributor to variance of the total loss. Therefore, the full distribution for IM itself (the ground motion hazard curve) is retained, but FOSM approximations are used for the first and second moments of the other random variables, conditioned on IM . In addition, data on the full distributions of some variables (e.g., repair costs) are very limited and so using only the first two moments of these distributions should not result in a significant loss of information.

In the structural dynamic analysis stage of this procedure, a deterministic structural model is repeatedly subjected to each of a number of ground-motion time histories that are scaled to several values of IM as described in Chapter 4. This simulation accounts for record-to-record variability in structural response. To account for uncertainty in structural parameters (i.e., several of the variables from Table 6.1) it is necessary to vary the parameters in accordance with the estimated distribution of possible values, and evaluate the resulting uncertainty in the structural response. This can be performed using Monte Carlo simulation during the repeated dynamic analyses, or using a finite difference method outlined by Baker and Cornell (2003). From the output of this analysis, one easily obtains the mean value of each EDP and also the full covariance matrix of the EDP vector, both conditioned on the IM level. These outputs are fit by simple functions of IM allowing the uncertainty to be propagated using analytical equations.

To illustrate, suppose that, the repair cost DV_k of the k^{th} component can be modeled²⁹ as some function of EDP_i , $g(EDP_i)$, plus a zero-mean random variable, ε_k , with variance = $h(EDP_i)$, and that for a given level of the IM EDP_i has mean $\mu_{EDP|IM}$ and variance $\sigma_{EDP|IM}^2$. Then the FOSM procedure approximates $g(EDP_i)$ by a first-order expansion or linear approximation, $g(\mu_{EDP_i}) + (dg/dEDP)(EDP_i - \mu_{EDP_i}) + \varepsilon_k$, where the derivative is evaluated at the mean value of the EDP . If the mean and variance of this linear function of EDP are computed one finds simply:

$$E[DV_k | IM] \cong g(\mu_{EDP|IM}) \quad (6.6)$$

$$Var[DV_k | IM] \cong \left(\frac{dg}{dEDP}\right)^2 \sigma_{EDP|IM}^2 + h(\mu_{EDP|IM}) \quad (6.7)$$

The total repair cost must be obtained from the sum of such component repair costs; this requires assumptions about the correlation among them, as is discussed below.

FOSM results can also be used to examine sensitivities to each random variable, allowing identification of those sources of uncertainty providing the greatest contribution to total uncertainty in repair costs.

In addition, using this framework and making several functional form assumptions, there is a simple closed form solution available for calculating the annual rate of exceeding a given level of repair costs. The assumptions needed are:

1. The conditional expected value of Total repair Cost (TC) given IM , $E[TC|IM=im]$, is approximated in the region of interest by a function of the form $a(im)^b$, where a' and b are constants.
2. The uncertainty in $TC|IM$ is represented by a lognormal distribution (note that for the example this assumption appears to be justified by Figure 6.2b above). The logarithmic standard deviations in $TC|IM$ due to aleatory and epistemic uncertainty are assumed constant for all IM in the region of interest and denoted β_R and β_U , respectively.
3. An approximate function of the form $\hat{\lambda}_{IM}(x) = k_0 x^{-k}$ is fit to the mean IM hazard curve, again in the region of interest. This form for the hazard curve has been proposed previously by Kennedy and Short (1984) and Luco and Cornell (1998). The epistemic

²⁹ This may come after “collapsing out” the intermediate DM variable, as described in Baker and Cornell (2003).

uncertainty in this hazard curve is represented by a lognormal random variable with logarithmic standard deviation β_{UIM} .

Under these assumptions, the mean estimate of $\lambda_{TC}(z)$, the mean annual of exceeding a given TC level z , is given by:

$$E[\lambda_{TC}(z)] = k_0 \left(\frac{z}{a'} \right)^{-k/b} \exp \left(\frac{1}{2} \frac{k}{b} \left(\frac{k}{b} - 1 \right) (\beta_R^2 + \beta_U^2) \right) \quad (6.8)$$

and the standard error of estimation or epistemic uncertainty in this estimate is given by:

$$\sigma_{\ln \lambda_{TC}(z)} = \sqrt{\beta_{UIM}^2 + \frac{k^2}{b^2} \beta_U^2} \quad (6.9)$$

These results are derived from related problems that are used in the SAC methodology (Cornell et al., 2002 and FEMA-355F, 2000). The applicability of this special closed form solution will depend on the accuracy of the required analytic assumptions. Nonetheless, this analytical formulation provides simple equations that may be useful. In cases where fewer analytic assumptions are desired, the hybrid FOSM method also provides a more general solution that is solvable using numerical integration.

It can be shown from Eq. (6-8) above that even for relatively large uncertainties in repair costs given IM (i.e., large values of β_R and β_U), the mean estimate of $\lambda_{TC}(z)$ is typically dominated by the first factor which is simply the hazard curve evaluated at the value of the IM found from the mean cost z versus IM equation.. This is one reason it is believed that FOSM approximations of $DV|IM$ are sufficient to provide an adequate result.

6.5 CONSIDERATION OF CORRELATIONS

Correlations among uncertain properties (e.g., among structural properties or among repair costs of assemblies) must be considered carefully in propagation of uncertainty, as they may have a large effect on the variance of total repair costs. Unfortunately data on correlations, especially correlations of repair costs, are lacking in the literature. Baker and Cornell (2003) address this topic and provide several models that may be useful.

In the absence of additional information, it may be helpful to use the following characterization scheme. To illustrate, let the logarithmic component repair cost for a given

damage state, $\ln DV_k | DM_i$, be represented by the summation of a deterministic mean and three random variables: $\ln DV_k | DM_i = g(DM_i) + \ln \varepsilon_{Struc} + \ln \varepsilon_{ElClass_m} + \ln \varepsilon_{El_k}$, where ε_{Struc} represents uncertainty common to all elements in the entire structure (e.g., general labor rates), $\varepsilon_{ElClass_m}$ represents uncertainty common only to elements of class “ m ” (e.g., drywall partitions, moment connections, etc.) and ε_{El_k} represents uncertainty unique to element k . All of these ε random variables are assumed to be mutually uncorrelated. We then define $Var[\ln \varepsilon_{Struc} | DM_i] = \beta_{Struc}^2$, $Var[\ln \varepsilon_{ElClass_m} | DM_i] = \beta_{ElClass}^2$ for all m , and $Var[\ln \varepsilon_{El_k} | DM_i] = \beta_{El}^2$ for all k . The variance of $\ln DV_k | DM_i$ is the sum of these variances. For this special case, a simple closed-form solution exists for the correlation coefficient between repair costs of two components. If two elements are in the same class (e.g. drywall partitions), then the correlation in their repair costs, DV_j and DV_k , is:

$$\rho_{\ln DV_k, \ln DV_j | DM_i} = \frac{\beta_{Struc}^2 + \beta_{ElClass}^2}{\beta_{Struc}^2 + \beta_{ElClass}^2 + \beta_{El}^2} \quad (6.10)$$

If two elements are in the different classes (e.g. a drywall partition and a moment connection), then the correlation in their repair costs, DV_j and DV_k , is:

$$\rho_{\ln DV_k, \ln DV_j | DM_i} = \frac{\beta_{Struc}^2}{\beta_{Struc}^2 + \beta_{ElClass}^2 + \beta_{El}^2} \quad (6.11)$$

Loosely speaking, the correlation coefficient between two DV 's can be said to be the ratio of their shared variances to their total variance.

Consideration of correlations is necessary no matter what method used to propagate uncertainty and thus the model above is applicable for all methods of propagation. It has been incorporated in the FOSM work of Baker and Cornell (2003). Correlations can also be modeled with the Monte Carlo method, although simulation of a vector of correlated random variables requires methods beyond the simple inverse method described in Section 6.3. Correlations can also be explicitly incorporated into the reliability methods described in Section 6.6 below.

6.6 RELIABILITY METHODS FOR MODELING LOW-PROBABILITY EVENTS

Reliability methods such as the First Order Reliability Method (FORM, e.g., Melchers, 1999) can be used for PBEE analysis in cases where interest is in the probability of low-probability events, such as structural collapse or the probability that repair cost, number of fatalities, or downtime will exceed some unacceptable threshold. In a reliability approach, the same basic information as in MCS is required: the distribution of the basic variables, X , as well as a deterministic model of performance. The probability of structural collapse is sometime approximated using a displacement or deformation proxy, e.g., if interstory drift exceeds some threshold, then collapse is assumed to occur. In this case, X need only include those listed in Table 6-1 under hazard and structural analyses. Reliability analysis for $P[EDP > x]$ has been well treated elsewhere; we will not recap such approaches here. The interested reader is referred to Au et al. (2004) for an application of subset simulation to a reliability assessment of the Van Nuys testbed building. Au and Beck (2001) present the basic theory. See also Der Kiureghian (2003) for PEER's development of OpenSees tools to perform first-order-reliability-method (FORM) analysis.

7 Relation to Presently Accepted Engineering Approaches

Authors: J. Heintz, R.G. Pekelnicky

The purpose of this chapter is to summarize the current state of engineering practice with regard to assessing the seismic performance of existing buildings. It is intended to illustrate how an engineering office might evaluate the performance of the Van Nuys Testbed building, and communicate the expected performance to a client. Since actual practices can vary significantly from one office to another, this section includes a discussion on several methodologies currently available for use by practitioners. An evaluation using one of these methodologies is conducted on the Van Nuys Testbed building for comparison to the PEER methodology.

7.1 CURRENT PRACTICE OF SEISMIC EVALUATION AND STRENGTHENING

Seismic evaluation of existing buildings has evolved as a specialized practice in structural engineering over the last 60 years. Since it has existed over most of that time period without any codified or standardized procedures, current engineering practice can vary significantly from one office to another. The methodologies employed by a given engineer can be function of personal biases and engineering opinion, as well as the practical needs of the client.

The overriding principle for an engineering consultant is that the practice of engineering is a business. The goal is to provide the client with what is requested, while spending no more than the fee negotiated for the work. Implicit in getting the work in a competitive market is to charge fees consistent with what the market will bear, whether that is based on fees charged by competitors for similar services, or fees based on what the client expects to pay. In the case of seismic evaluation, the needs of the client dictate the level of effort and schedule. The focus is

on getting practical answers to questions about building performance as quickly as possible. Conservatism, simplicity, and speed are regularly chosen over improved accuracy, increased level of effort, and additional time.

Public reaction to the damaging effects of recent urban earthquakes has shown that there is a disconnect between what the general population perceives to be acceptable earthquake performance and what the building codes provide as minimum performance. This has led to the development of performance-based engineering concepts in which practitioners seek to better quantify the expected performance of a building and communicate that performance to an owner.

A real consideration in practice is the complexity of new and emerging technologies. As we learn more about the performance of buildings in earthquakes, and recognize more about the limitations of our past analytical techniques, new methodologies have become increasingly complex. Skill levels vary between offices, and successful application of advanced nonlinear analyses can be a challenge even in the most skilled engineering offices. The willingness of an engineer to accept advancements in engineering practice is a function of comfort with historic practice, bias towards new and emerging technologies, and ability to charge clients for new, more expensive services. Clearly, the latter can only be accomplished if the client sees a benefit in spending more money up front.

7.1.1 Methodologies and Tools Currently in Use

Historic practice of seismic evaluation and strengthening has been to apply code provisions for new buildings to the analysis of existing structures. This practice still exists today in many situations. Local jurisdictions with an interest in promoting long-term seismic safety will trigger a mandatory seismic upgrade when a certain amount of work is proposed for an existing building. Current code, or some fraction of it, is often the specified criterion in these situations.

Methodologies developed specifically for existing buildings were not available until the late 1980's. One of the first such documents was ATC-14, *Evaluating the Seismic Performance of Existing Buildings*, published in 1987. This landmark document incorporated the collective observations of damaging earthquakes and used them to identify building characteristics that demonstrated poor performance in past earthquakes.

Since that time structural engineers and researchers have developed a number of guidelines and standards for seismic evaluation and rehabilitation, many with a specific focus or intent. Some address specific building types, such as steel moment frames or unreinforced brick bearing walls, and others address specific subsets of the building inventory, such as hospitals or federally owned buildings. Table 7.1 provides a list of many of the most common references for seismic evaluation and strengthening used in practice, along with a brief summary of the content of each document.

Table 7.1 Summary of reference codes, standards, and guidelines used in practice

Document	Use
Uniform Building Code (<i>UBC</i>); (similarly for other model codes such as <i>SBC</i> , <i>NBC</i> , <i>IBC</i> , and <i>NFPA 5000</i> .)	Provisions for new buildings and legal requirements for additions, alterations, and repairs to existing buildings. Specified as criteria for mandatory triggered seismic upgrades in some jurisdictions.
State Historic Building Code	Sets minimum seismic standards and criteria for use of archaic materials for buildings with designated historic status.
California Building Code, Title 24, Chapter 16, Division VI-R	Code-based static equivalent lateral force procedure with beta factors to adjust for element ductility. Includes allowance for alternative performance-based analysis. Applies to existing state-owned buildings.
Uniform Code for Building Conservation, (<i>UCBC</i>)	Allowable stress design procedures for prescriptive correction of selected building deficiencies that have exhibited significant damage in past earthquakes.
UCBC, Appendix Chapter 1	Special procedure for retrofit of unreinforced masonry buildings with flexible diaphragms.
Guidelines for the Seismic Retrofit of Existing Buildings (<i>GSREB</i>)	Latest edition of the UCBC with strength-based provisions. Addresses the following specific building types: concrete tilt-up, URM, unbraced wood cripple walls, multi-story residential with open front garages, non-ductile concrete frames.
Standards of Seismic Safety for Existing Federally Owned and Leased Buildings - ISCCC RP6	Sets minimum standards for seismic safety of existing federally owned or leased buildings. Originally based on FEMA 178, seismic evaluation criteria have been updated to ASCE 31.
California Senate Bill 1953 (<i>SB 1953</i>)	Sets minimum standards for seismic safety of existing California hospital facilities. Includes timeline for mandatory upgrade and extensive requirements for nonstructural systems. Seismic evaluation criteria based on FEMA 178.
Tri-Service/Navfac P335.2 Seismic Design Guidelines for Upgrading Existing Buildings	One of the first comprehensive guides for evaluation and upgrade of existing buildings. Includes nonstructural upgrades. Uses the Capacity Spectrum method and IDR analysis.

Document	Use
ASCE 31 Seismic Evaluation of Existing Buildings	Performance-based evaluation of existing buildings based on historic observations of damage in past earthquakes. Utilizes displacement-based analytical procedures and individual component ductility factors. <i>(Formerly FEMA 310, FEMA 178, ATC-14).</i>
ATC-40 Recommended Method for Seismic Evaluation and Retrofit of Concrete Buildings	Performance-based analysis and design recommendations for existing concrete buildings. Includes the Capacity Spectrum Method and provisions for foundation modeling.
FEMA 156 Typical Costs for Seismic Rehabilitation of Buildings	Methodology for estimating costs of seismic rehabilitation based on historic data. Includes coefficients for adjusting basic costs data to account for building type, location, year of construction. Addresses structural and nonstructural costs.
FEMA 351 Recommended Seismic Evaluation and Upgrade Criteria for Existing Welded Moment Resisting Steel Structures	Product of SAC Joint Venture research, provides a reliability-based methodology for evaluating the performance of steel moment resisting frames.
FEMA 356 Prestandard and Commentary for the Seismic Rehabilitation of Buildings	General performance-based analytical procedures and detailed deformation-based acceptance criteria, applicable to all building types, for design of seismic strengthening. Includes the Coefficient Method for estimation of target displacement <i>(Formerly FEMA 273, ATC-33).</i>
International Existing Building Code <i>(IEBC)</i>	Developed by ICC as a companion document to the IBC, but specifically intended for existing buildings. Specifies seismic criteria based on 75% of IBC, GSREB or FEMA 356

Reference: *SEAOC Existing Buildings Committee Green Book*

7.1.2 Seismic Evaluation versus Strengthening

Historic practice of seismic evaluation has been to evaluate existing buildings for somewhat lesser criteria than used to design new buildings or to design seismic strengthening. While not unanimously accepted by all, this concept has met with general consensus within the engineering community. Detractors note that this practice leads to two defined levels of acceptable performance, one for existing buildings and one for new or strengthened buildings. While this could be difficult to explain on the surface, it is more closely in tune with the underlying needs of a client in evaluation and rehabilitation efforts. Giving existing buildings a “break” lowers the threshold of acceptable performance and requires strengthening only in those cases that really need it. This preserves the capital of the building owner and is consistent with the desire to spend money where it is most useful. On the other hand, once a building is strengthened, the

owner's perception is that the building is "fixed" for good, so strengthening to a higher criterion helps ensure that the building performs to the expectations of the client.

7.1.3 Communicating Performance to An Owner

Many factors contribute to the decision of a building owner to consider seismic risk and rehabilitation. These include the type of ownership (public, private, non-profit), type of structure, level of risk, perception of liability and risk, market and economic considerations, regulatory requirements, costs, perceived benefits, financial aid, and insurance (EERI, 1998).

In managing seismic risk, a building owner can consider one of four options: retaining the risk (or self-insuring); mitigating through seismic strengthening; purchasing insurance; or passing on the risk in the form of dependence on federal disaster assistance (EERI, 1998). The most sophisticated clients are able to make a present value cost-benefit analyses to decide which course of action yields the best financial result for their situation.

Often the key decision variables that prompt an owner to begin looking at seismic issues are, first and foremost, a perceived risk on the part of an owner, and then a desire to provide life safety protection for building occupants or to protect building contents. The next obvious consideration then becomes cost, and a corresponding measure of the benefits of the dollar investment made in seismic strengthening.

Once a building owner has determined that there is some exposure to seismic risk, the key decision variable is building performance. Building performance is communicated to clients through an education process that explains potential post-earthquake damage states in understandable terms and graphical images of actual earthquake damage. Some discussions regarding probabilities and recurrence intervals can occur, but these discussions are often less successful. Most clients want to know performance levels on a deterministic basis — either the building is "safe" or not, for a given magnitude earthquake (scenario event). More sophisticated clients are interested in considering a range of options from various commonly defined performance levels: collapse prevention, life-safety, and immediate occupancy. Some will listen to probabilistic based assessments such as a 90% confidence level that the building will meet the intended performance criteria. It is often difficult to provide a client with a defined earthquake

magnitude. Unfortunately, discussions of earthquakes with a 10% chance of exceedance in 50 years, or an event with a 500 or 2000 year return period are almost never successful.

Successful discussions on building performance with owners require a consistent standardized definition of performance levels with a proven track record in observations following major earthquakes. For that reason, the performance-based methodology of the ASCE 31 (updated FEMA 310) and FEMA 356 documents is attractive to practitioners.

Normal practice on an individual building project consists of engineering evaluation, development of conceptual strengthening, and cost estimation. Cost estimation can be performed by a contractor or cost-estimating professional, or using empirical data in the FEMA 156 *Typical Costs for Seismic Rehabilitation of Existing Buildings*. The owner then makes a financial decision based on the affordability of the strengthening work, and the real or perceived benefits of safety of building occupants, protection of property, savings in repair costs or losses due to down-time, or savings in insurance premiums.

On large building inventories, as in the case of insurance and financial lending industries, loss estimation on the portfolio is the key decision variable. This can be losses due to building structure and contents damage, or losses due to downtime. Practitioners perform loss estimation on buildings and contents using any one of several proprietary or commercially available loss estimation software. There are several PML methodologies available and a lack of consensus standards on how loss estimation should be performed, but a popular reference on loss estimation is *Earthquakes, Volcanoes and Tsunamis, An Anatomy of Hazards*, by Karl Steinbrugge. Estimation of downtime is performed using engineering judgment and professional experience. Much of the expertise in this area comes from interpretation of data from ATC-13, *Earthquake Damage Evaluation Data for California*.

7.2 ENGINEERING EVALUATION OF THE VAN NUYS TESTBED BUILDING

The methodology selected for the engineering assessment of the Van Nuys Testbed building consists of the latest standards for seismic evaluation and rehabilitation developed by the American Society of Civil Engineers for the Federal Emergency Management Agency. ASCE 31 *Seismic Evaluation of Existing Buildings* (formerly FEMA 310), and FEMA 356 *Prestandard and Commentary for the Seismic Rehabilitation of Buildings* form a set of documents

representing state of the art procedures that might be used in high-end engineering offices for clients interested in quantifying the potential seismic performance of existing buildings.

7.2.1 The FEMA Methodology for Seismic Evaluation and Rehabilitation

ASCE 31 and FEMA 356 are comprehensive documents that cover the seismic issue in general, dealing with all building types, all seismic hazard levels, multiple performance goals, and structural as well as nonstructural systems. They were developed by the American Society of Civil Engineers for the Federal Emergency Management Agency with the expressed purpose of creating nationally applicable consensus standards for addressing seismic performance of existing buildings. The FEMA methodology consists of displacement-based analytical procedures, which are the state of the art for investigation of performance of existing components. It explicitly includes the historic practice of evaluating existing buildings to lesser criteria than that used for rehabilitation design.

ASCE 31, is the fourth in a series of evaluation documents that began with ATC-14. It is a three-tiered procedure that includes both the simplified checklist methodology for identifying potential seismic deficiencies that was first developed in ATC-14, and a more advanced analytical process for evaluating and predicting building performance. This document has gained widespread acceptance because of its relative simplicity and foundation in observations from past earthquakes. ASCE 31 utilizes the Pseudo-Lateral Force procedure, which is a force-based calculation procedure used to evaluate displacement-based acceptance criteria. This simplified procedure substitutes conservatism for accuracy, and satisfies the practitioner's need to provide clients with quick and inexpensive answers. ASCE 31 also includes provisions for performing more detailed nonlinear analyses by referencing the procedures in FEMA 356.

FEMA 356 is the successor to the landmark FEMA 273 *NEHRP Guidelines for the Seismic Rehabilitation of Buildings*. It contains comprehensive procedures for designing the rehabilitation of building using linear static (LSP), nonlinear static (NSP), linear dynamic (LDP), and nonlinear dynamic (NDP) analyses. It provides the practitioner with comprehensive generalized information on a variety of systems, components and material types. It also contains tables of explicit displacement-based acceptance criteria for evaluating individual components of various lateral-force-resisting systems. Because of the magnitude of the scope and generality of

the document, the procedures apply well to the majority of buildings and situations, but there are some limitations. FEMA 356 may need to be supplemented by more specific information from other references that have been specifically developed for certain building types or structural systems, or from recent advances in analytical procedures.

7.2.2 The FEMA Methodology and the PEER PBEE Framework

Many of the variables considered in the PEER framework are implicit within the ASCE 31 and 356 methodologies. The basic intensity measure (IM) is the spectral acceleration at the fundamental period of the building, except for NDP analyses, which use ground motion time-history records.

Engineering demand parameters (EDP) and damage measures (DM) vary with the analytical procedure selected. If linear procedures are used, then bending moments, shear, and axial loads serve as EDP's, and local element ductility factors (*m*-factors) serve as DM's. If nonlinear procedures are used, EDP's consist of plastic deformations (rotations, shear or axial deformations) in each of the ductile hinge elements, and forces in non-ductile elements. DM's consist of tabulated values of permissible nonlinear deformations for each element and material type, adjusted for the local ductility characteristics of the element under consideration. Tabulated DM's in ASCE 31 and FEMA 356 have been developed over the years based on research, material and component testing when available, and judgment and expert opinion of researchers and engineering professionals.

The primary decision variable (DV) contained within the FEMA methodology is the Building Performance Level. DM's (*m*-factors for linear procedures and plastic deformations for nonlinear procedures) vary based on the target building performance level. The maximum ratio of the EDP to the DM serves as the measure by which the performance of the building is judged.

Quantitative estimates of dollar loss, strengthening, or repair costs are outside the scope of the ASCE 31 and FEMA 356 documents. For loss estimation, practitioners turn to any one of a number of proprietary or commercially available PML loss estimation software or procedures. Cost estimation is often done using contractors or qualified cost estimating professionals. Alternatively, approximate costs averaged over large building inventories can be obtained using the FEMA 156, *Typical Costs for Seismic Rehabilitation of Existing Buildings*.

7.2.3 Building Description

The Van Nuys Testbed building is a seven-story reinforced concrete frame structure. It is rectangular in plan measuring approximately 150 feet long by 61 feet wide by 66 feet tall. It is described in detail in Chapter 2 and Appendix A. This section highlights key features of the building that are pertinent to the modeling assumptions used in the FEMA analysis.

The primary lateral force resisting system was intended to be perimeter spandrel beam-column moment frames around the exterior of the building. However, the interior flat slab-column moment frames were found to provide a significant portion of the lateral stiffness of the building, so both interior and exterior frames were considered in the analysis. Designed and constructed in the 1960's, the concrete frame elements lack detailing needed for ductile performance. Column bars are lapped just above the floor levels with inadequate lap splices and poor confinement. Elements were modeled considering potential lap splice, embedment or shear failures. The building is founded on piles, so column bases were considered fixed.

Along the north elevation of the building, a portion of the frame is infilled with masonry in the first story. Drawings show a 1-inch expansion gap around the infill. Parametric analyses both with and without the infill were conducted to investigate the potential torsional response of the structure.

7.2.4 Seismic Hazard (IM)

The building is located on soil classified as site class S_D . Spectral accelerations were taken from site-specific response spectra provided for seismic hazards with a probability of exceedance of 2%, 10%, and 50% in 50 years. The spectra, along with the 1994 Northridge Earthquake data are shown in Figure 7.1.

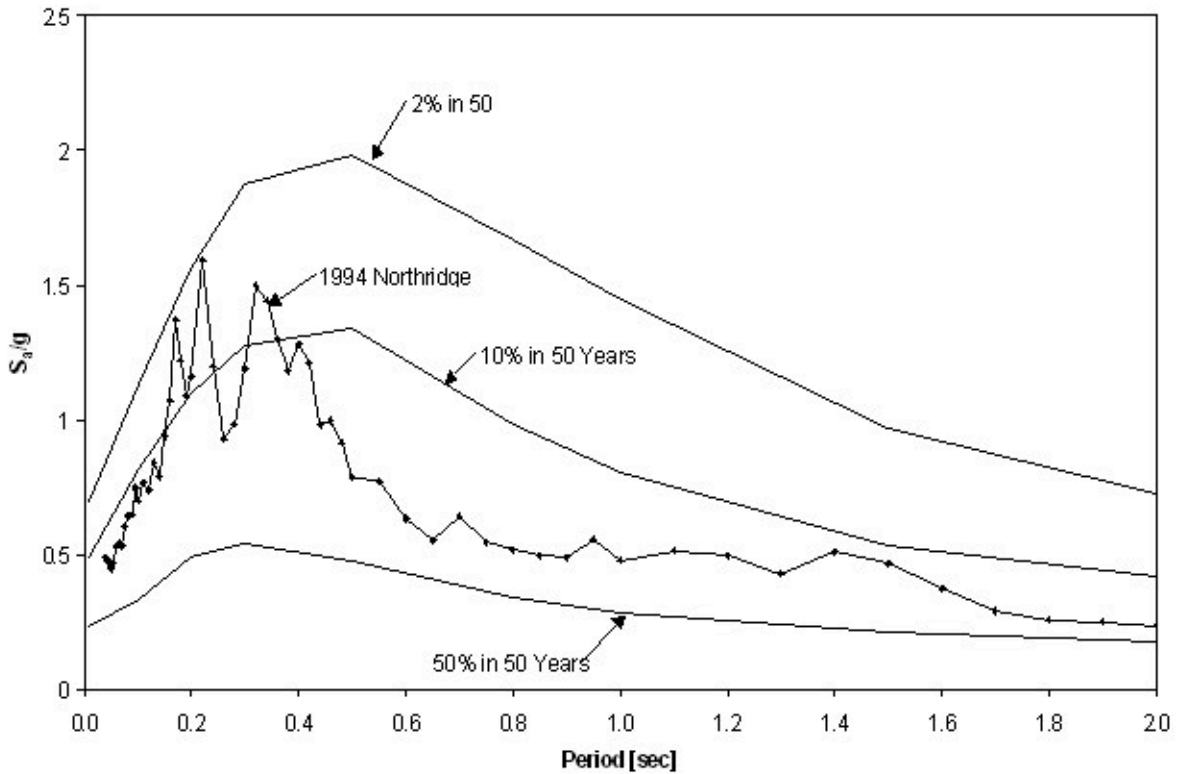


Fig. 7.1 Site-specific response spectra

7.2.5 Preliminary Evaluation (Preliminary DV/DM/EDP/IM)

A preliminary evaluation was performed using the Tier 1 checklist screening procedure of ASCE 31. The Tier 1 procedure is a convenient tool regularly used in engineering practice to quickly assess the performance of one building, or an inventory of buildings, and provide an owner with a key DV in the form of building performance with minimal investment. The Van Nuys building is classified as type C1: *Concrete Moment Frame*. The Basic and Supplemental Structural checklists from ASCE 31 were completed and the results summarized below. Quick check calculations were performed using a pseudo lateral base shear of $V=1.13W$. This is based on a seismic hazard of two-thirds of the MCE, short period and 1-second spectral response accelerations of 1.1g and 0.71g respectively, site class S_D , fundamental period of approximately 0.69 seconds, and modification factor $C=1.1$.

The Tier 1 screening process identified the following potential deficiencies based on the configuration of the building:

- Soft Story: The first story can be classified as a soft story.
- Torsional Irregularity: The presence of the infill frames on only one side of the building creates a potential torsional irregularity in plan.
- Interfering Walls: The infill walls will impact the performance of the concrete moment frame.
- Column Shear Stress: The shear stress in the columns based on the “Quick Check” procedure is greater than acceptable values of 100 psi or $2\sqrt{f'_c}$.
- Shear Failures: The shear capacity of the members is less than the shear corresponding to the flexural capacity of the members.
- Weak Column / Strong Beam: The flexural capacity of the columns is less than that of the beams framing into them.
- Column Bar Splices: Column lap splices are not confined by closely spaced hoops and are located within a region of potential plastic demand.
- Beam Bar Splices: Beam lap splices occur over the columns in regions of plastic demand.
- Column Tie Spacing: Ties are not spaced at $8d_b$ at locations of potential plastic hinging and are not spaced at $d/4$ over the entire member.
- Stirrup Spacing: Some beams do not have stirrups spaced at $8d_b$ at locations of potential plastic hinges.
- Joint Reinforcing: Only one tie is provided within joint region.
- Stirrup and Tie Hooks: Some stirrups are not closed and do not have seismic hooks.
- Deflection Compatibility: Secondary components are not detailed for ductile behavior.
- Flat Slabs Over Columns: There is no continuous bottom reinforcement passing through the columns.
- Uplift at Pile Caps: There is no negative moment reinforcement within the pile caps.

Based on this list of significant potential deficiencies, the Van Nuys Testbed building fails the criteria of the Tier 1 procedure, and would not be expected to provide life safe performance in a major earthquake. In this methodology, an owner can stop here, and make a decision based on building performance with little initial investment. These potential deficiencies are further evaluated in more detailed analyses using FEMA 356.

7.2.6 Analytical Procedures and Goals (Prediction of EDP's)

A detailed evaluation was performed using the analytical procedures contained in FEMA 356. Three-dimensional linear static (LSP) and linear dynamic (LDP) analyses were performed to evaluate the elastic properties of the system, mode shapes, modal participation factors, distribution of forces between the interior and exterior frames, and to study the potential torsional response of the building. A two-dimensional nonlinear static (NSP) analysis was performed to evaluate the force-displacement behavior of the building, potential failure modes,

and to evaluate the overall performance of the building after selected members have yielded and degraded.

7.2.7 Model Development

All models were developed using SAP 2000, common office production software. Primary and secondary members in the structure that contribute to lateral resistance were modeled, including interior and exterior columns, exterior frame beams, floor slabs, and stair tower beams and columns. For beams cast monolithically with floor slabs, an effective width of slab was included in the member properties based on FEMA 356 (same as ACI-318). For the interior slab-column frames, floor slabs were modeled as effective beams as recommended by Luo et. al., 1994. Gravity loads and seismic masses were determined based on a review of the values used in the original structural calculations.

7.2.7.1 Linear Model Development

Cracked section properties were approximated using Table 6-5 in FEMA 356. $0.5 \cdot I_g$ was used for the effective moment of inertia for the beams and columns and $0.33 \cdot I_g$ was used for the slabs as suggested by Vanderbilt and Corley (1983).

Lumped mass was assigned to each node in the three dimensional model, based on the assumed gravity load tributary to the node. Accidental torsion was included considering 5% of the dimension of the building perpendicular to the direction of loading. In the dynamic models a lumped mass moment of inertia was assigned to the center of mass. In the static models, forces were applied to a node offset from the center of mass.

Models with and without infill were developed for both the linear static and dynamic analyses. For simplicity, infill was modeled as a compression strut per FEMA 356. The models were developed to bound the response of the building and identify the significance of the torsional response.

7.2.7.2 Nonlinear Model Development

A two-dimensional arrangement of one interior frame and one exterior frame were modeled in SAP2000, and hinges were assigned at all the locations where inelastic deformation could occur. A two-dimensional idealization was used to simplify the model and reduce computational time. Because the linear analyses did not show a significant enough torsional response to require amplified consideration of torsion, the two-dimensional idealization was considered adequate.

Two lateral force distributions were applied, one proportional to the story shear distribution calculated by combining modal responses from a response spectrum analysis (required when the fundamental period is greater than 1 second) and one representing a uniform distribution of load based on the mass per floor. Figures 7.2 and 7.3 show the load patterns used to displace the frame.

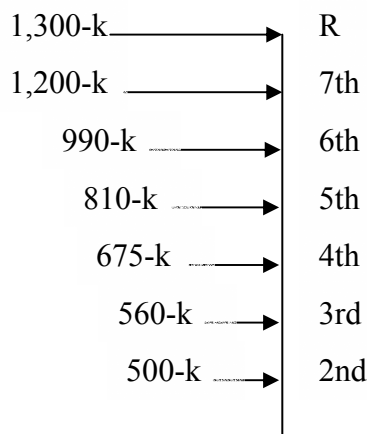


Fig. 7.2 Modal load pattern

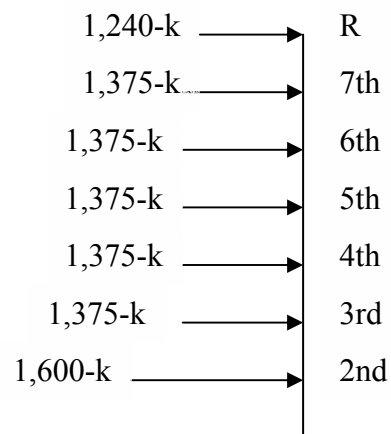


Fig. 7.3 Uniform load pattern

7.2.7.3 Nonlinear Member Properties

Nonlinear member properties were in the form of $M-\theta$ curves, defined by the yield moment, corresponding rotation, and other points representing strain hardening and strength degradation. The typical backbone curve is shown in Figure 7.4. Flexural hinges were applied at member ends. Shear hinges were applied at midspan of the members to monitor potential shear failures in case the yielding pattern resulted in increased shear demands on the elements.

In order to determine the hinge properties, $M-\phi$ curves were generated using RcSection v1.1. Based on FEMA 356 recommendations, expected material properties were taken as 150% of the specified f'_c for concrete and 125% of the nominal yield strength for reinforcing steel. From bi-linear approximations of the $M-\phi$ curves flexural yield and ultimate moments were taken. These values were compared against other failure modes such as flexure-shear interaction, shear failure, lap splice failure, and embedment failure.

Based on the controlling failure mode, one of several backbone curves was used. For beams and columns controlled by flexure, FEMA 356 tabulated values are used in conjunction with the typical backbone curve shown in Figure 7.4. Similarly, beams controlled by shear followed the typical backbone curve.

Since the columns do not possess adequately spaced ties, the curve for the shear controlled hinges is linear from zero to the moment at which the shear failure occurs, then falls off, giving no post yield stiffness or residual strength, as shown in Figure 7.5.

For lap splice or embedment controlled hinges, the curve is elastic up to the moment at which lap splice or embedment failure occurs. This point is taken as the yield moment multiplied by the ratio f_s/f_y , where f_s is the stress that can be developed in the bars due to the reduced lap splice or embedment. If the splice is not confined by transverse reinforcement then the splice capacity is assumed to degrade from $f_s = f_y * l_{avail}/l_{req'd}$ to $0.2 * f_s$ at a ductility demand or DCR equal to 2.0. After the point of maximum moment, the strength degrades to 20% of capacity, and maintains that strength up to a rotation of 0.01 radians. A sketch of this curve is shown in Figure 7.6. Lap splice strength and ductility limitations are key parameters in the analysis of the Van Nuys Testbed building.

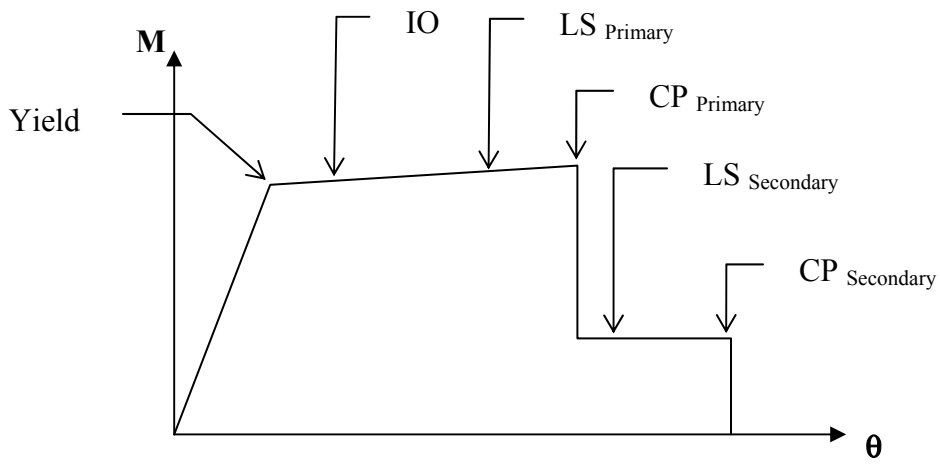


Fig. 7.4 Typical FEMA 356 backbone curve

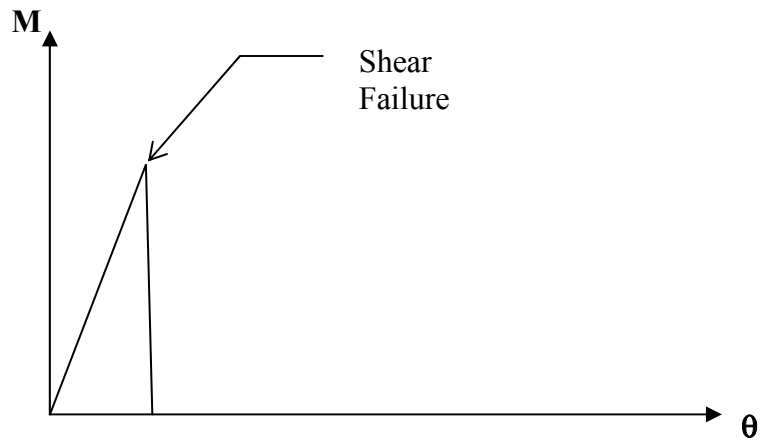


Fig. 7.5 Shear controlled backbone curve

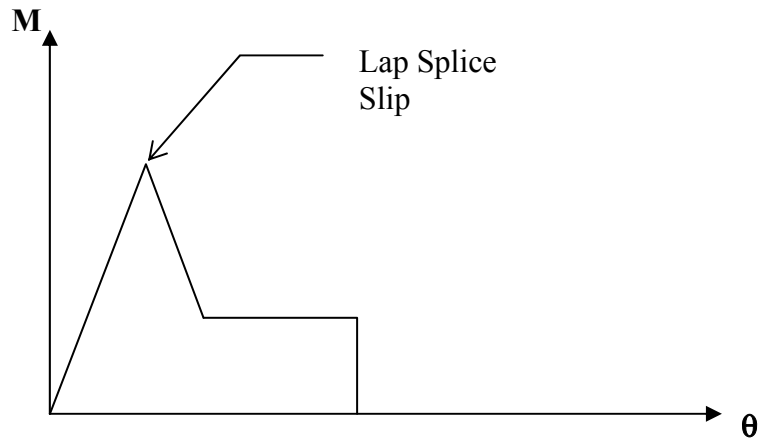


Fig. 7.6 Column splice hinge backbone curve

7.2.8 Engineering Demand Parameters (EDP's)

The following engineering demand parameters (EDP's) are used to evaluate the performance of the structure. For the linear analyses, the building is loaded with pseudo elastic forces intended to displace the roof to the maximum expected roof displacement. The following forces are investigated as force-controlled actions: column shear, beam shear, slab punching shear. The following forces are investigated as deformation controlled actions: column flexure, beam flexure, and slab flexure.

In the nonlinear analyses, the building is displaced to the estimated target displacement, and the forces and deformations are calculated. The following forces are investigated as force-controlled actions: beam shear outside of hinge region. The following forces or deformations are investigated as deformation-controlled actions: beam-column joint shear, beam plastic hinge rotation, column plastic hinge rotation.

7.2.9 Linear Model Results (EDP/IM)

Table 2 shows calculated periods and participating mass ratios for the first two modes in each direction, and the empirical estimate of period used in the preliminary evaluation. The table shows the building is more flexible than would be predicted by empirical equations.

Table 7.2 Modal periods and participating mass ratios

		Without Infill		With Infill	
	Transverse	Longitudinal	Torsional	Longitudinal	Torsional
Empirical Eq.	T = 0.63 sec.	T = 0.63 sec.	N/A	T = 0.63 sec.	N/A
Mode 1	T = 1.27 sec. PMR = 85%	T = 1.20 sec. PMR = 89%	T = 1.03 sec. PMR _{Long} = 0%	T = 1.12 sec. PMR = 77%	T = 1.00 sec. PMR _{Long} = 8%
Mode 2	T = 0.42 sec. PMR = 11%	T = 0.43 sec. PMR = 9%	T = 0.35 sec. PMR _{Long} = 0%	T = 0.38 sec. PMR = 10%	T = 0.34 sec. PMR _{Long} = 1%

By inspection of the modal participating mass ratios, it appears that while the infill walls do increase the torsional response of the structure, the effect is not significant. The change in mass participation in the longitudinal direction is only 12% between the two cases.

Displacements from the linear static analysis, which are not large enough to trigger FEMA 356 provisions for amplified torsion, confirm this conclusion.

The LSP analysis also identified the importance of the interior slab-column frames in the total lateral resistance and overall response of the building. In the longitudinal direction, 60% of the lateral stiffness comes from the two interior slab-column frames. In the transverse direction only 16% of the lateral stiffness comes from the two exterior moment frames, while the seven interior slab-column frames account for the other 84%.

7.2.10 Nonlinear Model Results (EDP/IM)

The results of the pushover analyses are shown in Figure 7.7, which overlays the pushover curves for both the modal and uniform load patterns. Both curves are similar in shape, indicating that the overall response of the structure is not significantly different for the different load patterns. The structure is nearly elastic until the yield base shear is reached, followed by a significant negative post-yield stiffness and rapid degradation and loss of strength. The individual curves are annotated with significant events in Figures 7.8 and 7.9.

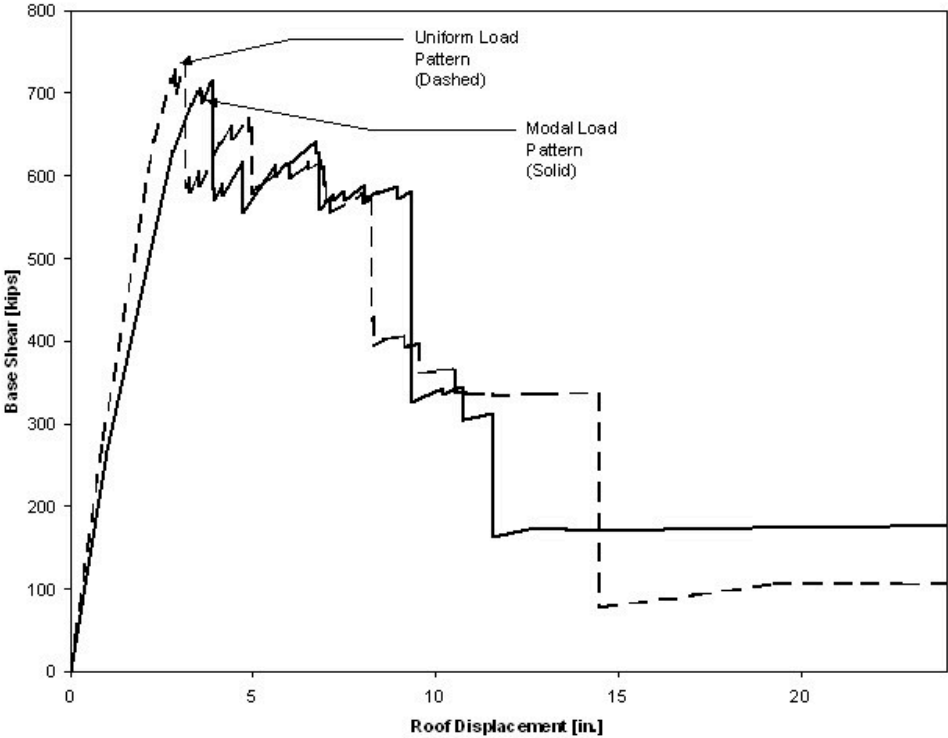


Fig. 7.7 Nonlinear pushover curves for two load patterns

First yield occurs in the slab positive moment hinges in the first floor at 1-inch. This is followed closely by interior column lap splice yielding at the first floor and slab positive moment yielding in the upper floors at a little more than 2 inches. For the modal load pattern, first degradation occurs when the interior slab negative moment hinges yield in the 2nd through the 4th floors at 3.5 inches. Negative post-yield stiffness begins when exterior column lap splice hinges yield and the exterior beams and interior slab negative moment hinges yield at 3.9 inches.

Between 3.9 inches and 9.4 inches, the strength degrades, and then remains somewhat constant. During this period, column lap splices hinge at the second floor and there are some isolated shear failures in exterior columns at the second floor. By 9.4 inches the exterior columns have formed a two-story mechanism and by 11.5 inches the interior frames have completed the mechanism resulting in a soft-story response between the second floor and the base.

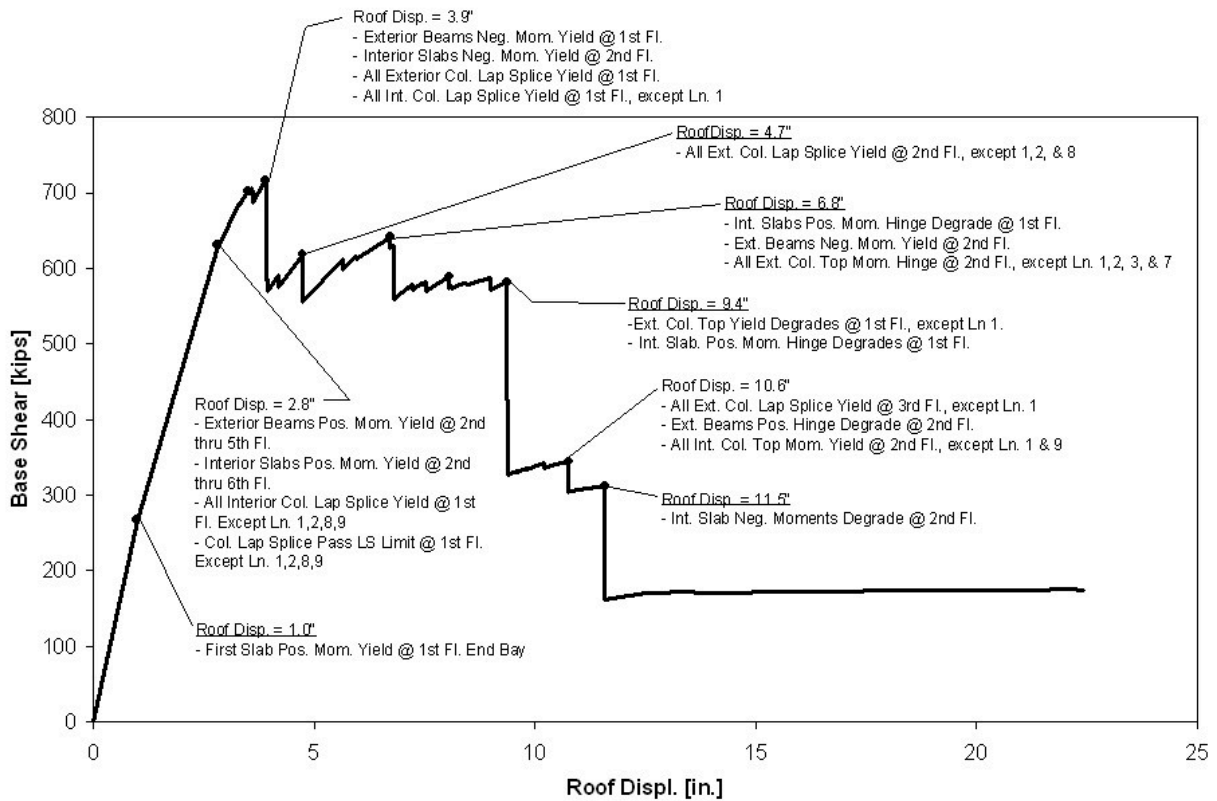


Fig. 7.8 Annotated modal pattern pushover curve

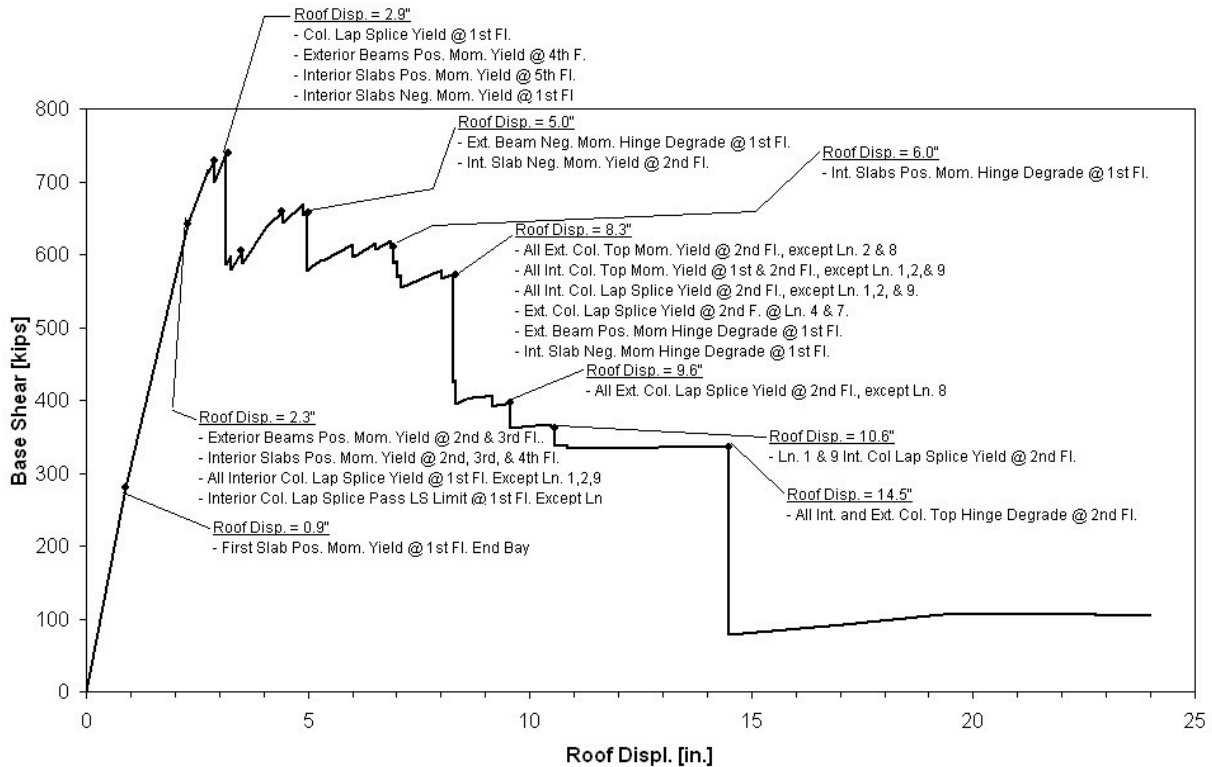


Fig. 7.9 Annotated uniform pattern pushover curve

7.2.11 Performance Assessment (DV/DM/EDP)

To assess building performance, the plastic rotations of the deformation-controlled hinges (EDP's) were checked against FEMA 356 tabulated values (DM's), and the forces in the force-controlled elements were checked to see if they were less than lower-bound capacities. Because the pushover model included explicit modeling of element degradation, FEMA 356 permits the use of secondary performance limits in evaluating degrading components.

Based on this, the first performance limit to be reached occurs at the interior column lap splices at the first floor. Immediately after yielding, redistribution of forces in the model causes the lap splice rotations to instantaneously pass their LS and CP limits within the same load step. Thus the displacement limit for this building is 2.8 inches based on the modal load pattern and 2.3 inches based on the uniform load pattern. Any target displacement beyond these limits will place the building beyond the Collapse Prevention performance level. Also, pushover results at larger displacements are in question because the hinge rotations are beyond what FEMA 356

specifies as ultimate rotation limits. Theoretically, these elements should not be counted on to resist load beyond these limits.

The target displacement was calculated using the coefficient method of FEMA 356 using a bilinear representation of the pushover curves. Because both curves have steep negative post-yield stiffnesses, the displacement is amplified due to dynamic P-Delta effects. Table 7.3 shows the target displacements calculated for the structure at various seismic hazard levels.

Table 7.3 Target displacements for various hazard levels

Seismic Hazard Recurrence	Uniform Load Pattern	Modal Load Pattern
50% in 50 years	4.8 inches	6.9 inches
10% in 50 years	20 inches	24 inches
2% in 50 years	96 inches	94 inches

As can be seen from the table, calculated target displacements are much greater than can be accommodated by the building based on the pushover curves generated. Also, at these deformation levels, the forces generated in force-controlled elements would have exceeded their capacities.

Based on these results, the Van Nuys Testbed building does not meet the FEMA 356 Collapse Prevention performance level, even for the smallest of the three scenario earthquakes considered. The DV provided to the building owner based on this analysis would be that the Van Nuys Testbed building is a collapse hazard.

7.2.12 FEMA 356 Assessment versus Northridge Performance

The Van Nuys Testbed building has been the subject of many correlation studies available in the literature (Islam, 1994 and ATC-40, 1996). Some have had success tuning analytical models to produce EDP results that matched strong motion records. Others have demonstrated weaknesses in the ability of a variety of simplified analytical methods to predict observed behavior. None have been able to match observed behavior satisfactorily.

From Figure 7.1 showing relative magnitude of response spectra, the Northridge Earthquake falls between the 50%/50 and 10%/50 earthquake hazard levels. Given the many features identified as potential deficiencies in the preliminary evaluation, it is not surprising that

the building was found to perform poorly. The FEMA 356 model, however, did not match up well in predicting the actual mode of failure or the exact location of damage that occurred in the Van Nuys Testbed building as a result of the Northridge Earthquake. The FEMA 356 methodology correctly identified the building as a collapse hazard for design level (10%/50) and higher (2%/50) earthquakes, which was also shown to occur in the OpenSees modeling studies. The methodology, however, predicted lap splice failures rather than shear failures. Analytically the model predicted hinging between the 1st and 3rd levels when column damage occurred in the 4th to 5th levels. Had the shaking in Northridge been more intense or of longer duration, the building could very possibly have collapsed.

Since the FEMA 356 model takes into account component strength degradation, and most of the components have very non-ductile moment-rotation properties, it is not surprising that the resulting pushover curves show a rapid loss in strength. Limiting the capacity of the members after degradation to the residual strength also adds to the rapid degradation of the building's pushover curve.

This lack of correlation between calculated and observed results suggests that some aspects of the FEMA 356 methodology are overly conservative with regard to the Van Nuys Testbed building. Specifically, it can be seen from the above discussion that the lap splice limitations are very restrictive. Given the limited strength and ductility allowed for this aspect of the column construction, higher shear forces could not be developed in the columns to generate the shear failures observed in the Northridge Earthquake. This failure mode had the biggest impact on the results of this FEMA 356 analysis and was the biggest source of difference between calculated and observed performance in this evaluation.

7.2.13 FEMA 356 Assessment versus PEER PBEE Assessment

In comparing the FEMA 356 to PEER OpenSees modeling, there are differences that contribute significantly to dissimilarities in predicted response. The FEMA 356 model has features that are present in both OpenSees1 and OpenSees2, so direct comparison with one specific set of OpenSees results is not possible.

The OpenSees pushover results, as shown in Figures 4.7 and 4.8, could be characterized as a gradual yield with positive strain-hardening slope to a base shear ranging from 500k to

800k. Yielding was distributed throughout the building, and column shear failures develop at approximately the locations observed in Northridge. Major degradation of the model is shown to occur in the range of 10–15 inches. Local element deformation criteria are not evaluated.

In comparison, the FEMA 356 model results, presented in Figures 7.7 through 7.9, showed a steep initial slope, with an early yield at a high base shear of approximately 700k, followed by negative post-yield slope. Yielding was concentrated at lap splice locations in the first two stories, and major degradation occurs at about 9 inches. Many elements fail local deformation criteria along the curve, including lap splice failures in the range of 2-3 inches, and would not be judged acceptable at these deformation levels.

The key parameters in tuning the models to match Northridge performance relate to initial stiffness, building period, and post yield ductility. The initial stiffness in the OpenSees models was partially determined by slab-column moment frames that had smaller effective slab widths than were used in the FEMA 356 model. In addition, member properties were adjusted to match the measured period of 1.5 seconds. The FEMA 356 model was not tuned to match period, and parameters used in the model resulted in a fundamental period of 1.2 seconds.

OpenSees used fiber elements with post-yield properties from material stress-strain curves, while the FEMA 356 model used degrading hinges with step function backbone curves. In OpenSees, the post-peak concrete strength was set at 80% of f'_c , while the FEMA 356 model elements were developed using 20% of f'_c . For lap splice considerations, the OpenSees models approximately used FEMA 356 estimates of strength, but differed significantly regarding post-yield behavior. OpenSees assumed a gradual negative slope based on the material response of the reinforcing steel, while the FEMA 356 model used a limited ductile response with a severe negative slope and degradation to residual strength at a ductility demand of 2. This difference is probably the single biggest contributor to differences between modeling results.

Given the additional modeling effort required to develop the OpenSees models and conduct the parametric studies, one would expect to see better correlation with observed Northridge behavior to justify the effort. In general, this was the case. As the OpenSees models were tuned, Northridge column shear failures appear to have been predicted in general consistency with observed damage locations. OpenSees, which has the ability to develop element post-yield behavior based on material properties, offers the advantage of a refined modeling platform that can be used to adjust these parameters to obtain a desired response.

However, in an actual engineering evaluation the response is not known, and one must still make assumptions regarding what parameters to choose.

Additional OpenSees parametric studies showed the building was unstable, and that collapse would be expected at the 10%/50 and 2%/50 earthquake hazard levels. Although the FEMA 356 model did not explicitly match failure mode and location, the end result in terms of a key decision variable (DV), building performance, at these hazard levels was the same. While in performance-based engineering there is always a desire to know exactly what happens and where, there are significant uncertainties in the entire process that make this a very difficult goal to achieve. From an engineering standpoint, given the difference in level of effort between OpenSees and FEMA356, uncertainty in specific results, and appropriate conservatism, either can be an acceptable approach to seismic performance assessment. A practitioner and client must weigh the benefit of more detailed and accurate information versus the additional time and expense needed to develop the information. This is particularly true in the case of global and discrete decision variables such as building performance. For the Van Nuys Testbed building, both methodologies predicted collapse at design level and higher earthquake hazards. The capability to predict collapse in a probabilistic format, with due consideration given to ground motion and structural modeling uncertainties, may prove valuable in the future. At this time it appears that much improvement is needed in modeling the behavior of structural components as they lose strength and the structure approaches collapse.

In the case of Northridge level shaking, OpenSees offered the advantage of being a better predictor of damage extent and location. In terms of decision variables based on loss estimation, this improved response prediction together with a consistent loss estimation procedure such as the one discussed in Chapter 5, can be a valuable improvement in engineering procedures and our ability to provide information to a building owner or client.

7.3 FEMA 356 REHABILITATION DESIGN

7.3.1 Summary of Deficiencies

The FEMA 356 analysis indicates that the building is vulnerable to a soft story failure and ultimate collapse due to weaknesses in the columns resulting from short lap splices, lack of confinement or inadequate shear strength. The building does not have the displacement capacity to reach the target displacement, which is very large due to the flexibility and rapid degradation in strength of the concrete frame system.

7.3.2 Rehabilitation Objective

The selected rehabilitation objective for this study consists of the life safety structural performance level at the 10%/50 year earthquake hazard level. Nonstructural components are not addressed. The design is developed in detail in the longitudinal direction, and similar strength and stiffness will be added in the transverse direction. The design follows the FEMA 356 methodology and acceptance criteria.

7.3.3 Rehabilitation Approach

The goal of the rehabilitation design is to protect brittle elements from premature failure by controlling the target displacement. The most effective way to do this in concrete structures is to add stiffness to decrease the period and decrease the resulting building displacements. In addition, the deformations need to be distributed over the entire height of the structure to avoid concentration of inelastic action in a story mechanism. The controlling condition is the limitation on column deformations due to short lap splices. To protect unstrengthened columns, the target roof displacement would have to be reduced to approximately 2 inches. This is difficult to achieve, so some column strengthening is considered. To protect strengthened columns, the target would need to be reduced to approximately 6 inches.

7.3.4 Rehabilitation Considerations (DV's)

In most cases, decision to perform a seismic rehabilitation is subject to other considerations such as cost, disruption of the occupants, operations of the facility, and the architectural fabric of the building. The strengthening measures must be designed to minimize impacts on these considerations. The architectural layout of the first floor and hotel rooms were considered in development of a rehabilitation scheme. On the first floor, lobby, dining, banquet and laundry services limited possible locations for new shear walls.

In the upper levels, the layout of the existing hotel rooms and arrangement of core and restroom spaces made interior shear walls impractical without significant rearrangement of those spaces. In addition the layout of the hotel rooms does not coincide with the column lines. Since it was considered important that at least one window be maintained in each room, this places a strict geometry constraint on the size of any new exterior walls.

7.3.5 Rehabilitation Alternatives

The rehabilitation design was based on an iterative process guided by interim results. Three schemes were considered in order to decide on the most cost-effective and best performing solution.

7.3.5.1 Scheme 1 — Shear Walls

The first scheme investigated consisted of large new shear walls intended to provide the necessary stiffness to limit the target displacement at the 10/50 hazard level to 2 inches to protect the unstrengthened columns. The walls, with window openings, were located on the building perimeter, and centered on each of the longitudinal elevations of the building. The new wall would be doveled into the existing columns and beams. Because of the stringent drift requirements and limitations due to window geometry, a 112 feet long by 18-inch thick wall would be required, as shown in Figure 7.10. This scheme was judged not architecturally desirable or economically feasible.

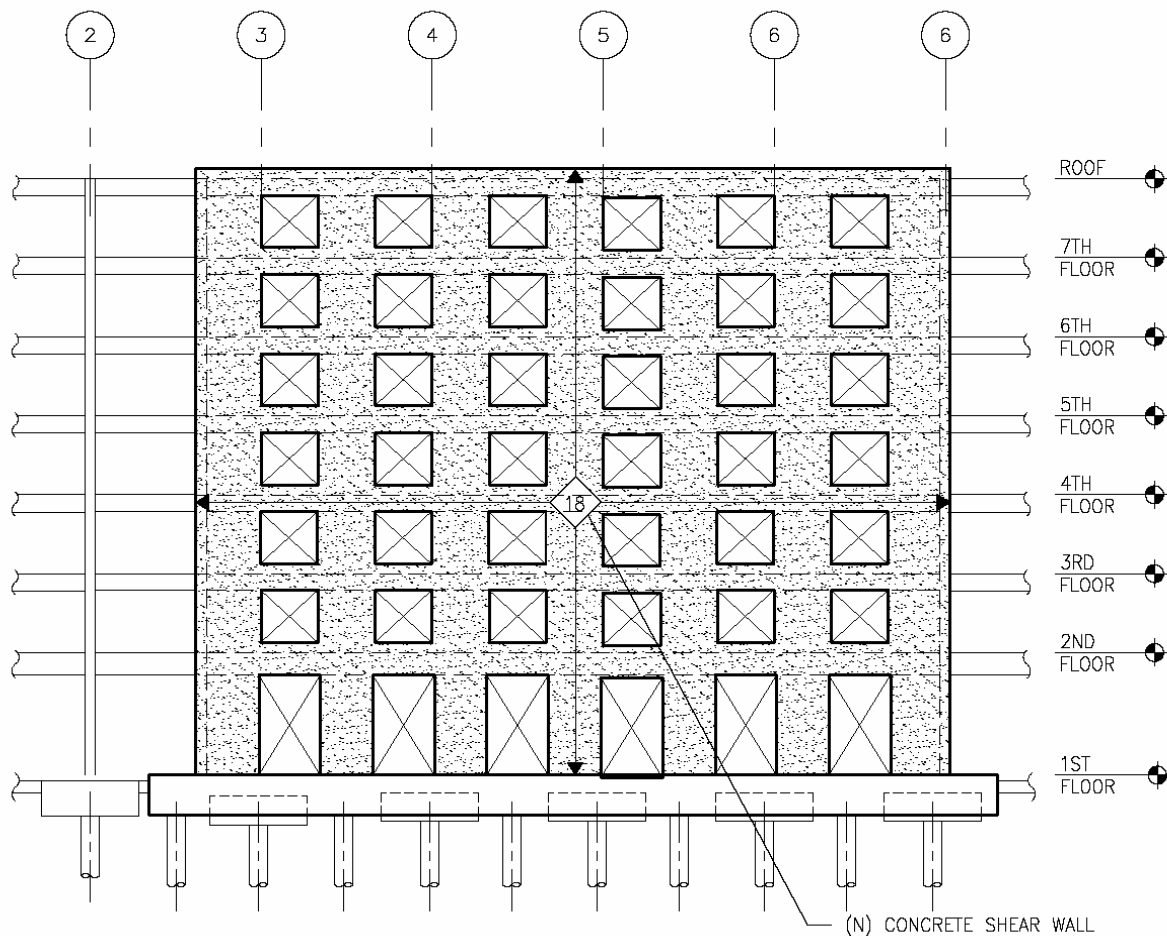


Fig. 7.10 Scheme 1 — Shear wall elevation

7.3.5.2 Scheme 2 — Shear Walls and Concrete Frames

In order to minimize the amount of new shear wall required, an option to encase the existing columns in reinforced concrete and build a new supplemental concrete moment resisting frame was considered. This scheme had the potential benefit of protecting the existing columns and adding additional stiffness. This resulted in a pair of 20 foot long by 12-inch thick walls at each end of the longitudinal wall lines, shown in Figure 7.11, in conjunction with new concrete column encasement and concrete beams along the existing spandrel beams as shown in Figure 7.12. Because of the labor and expense of encasing the existing concrete frame elements, this scheme was judged not economically feasible.

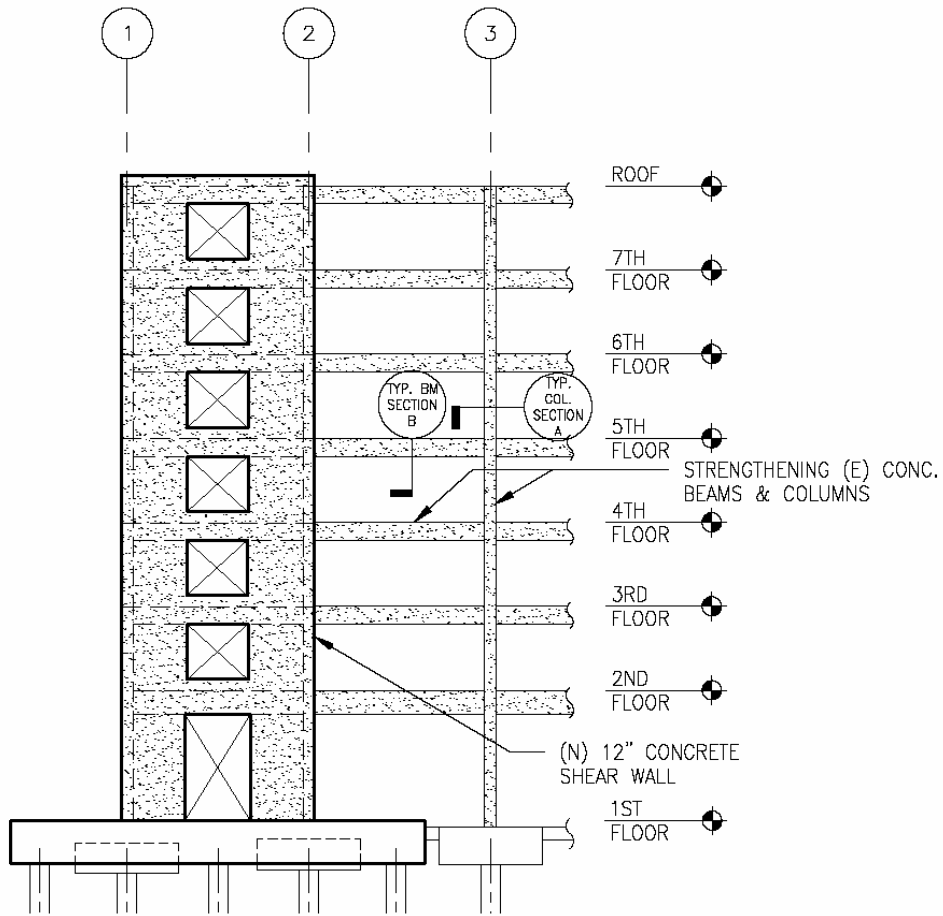


Fig. 7.11 Scheme 2 — Shear wall elevation

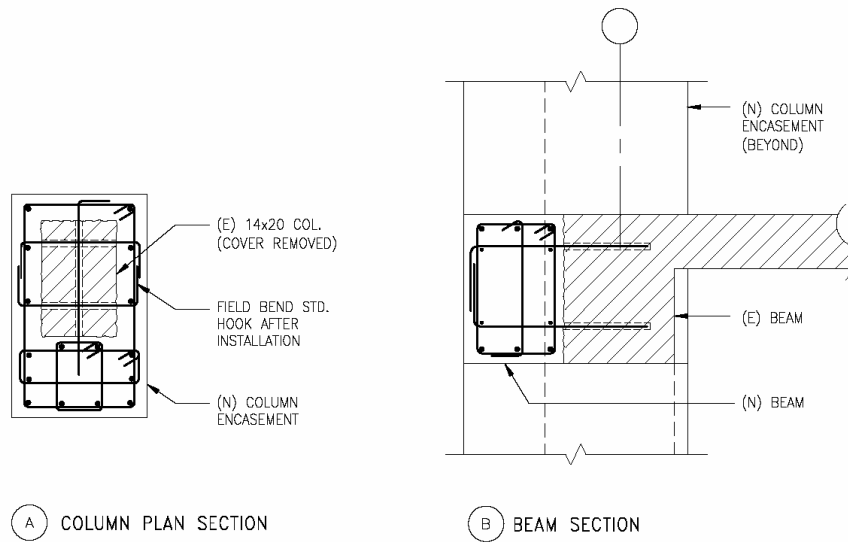


Fig. 7.12 Scheme 2 — Concrete frame upgrade details

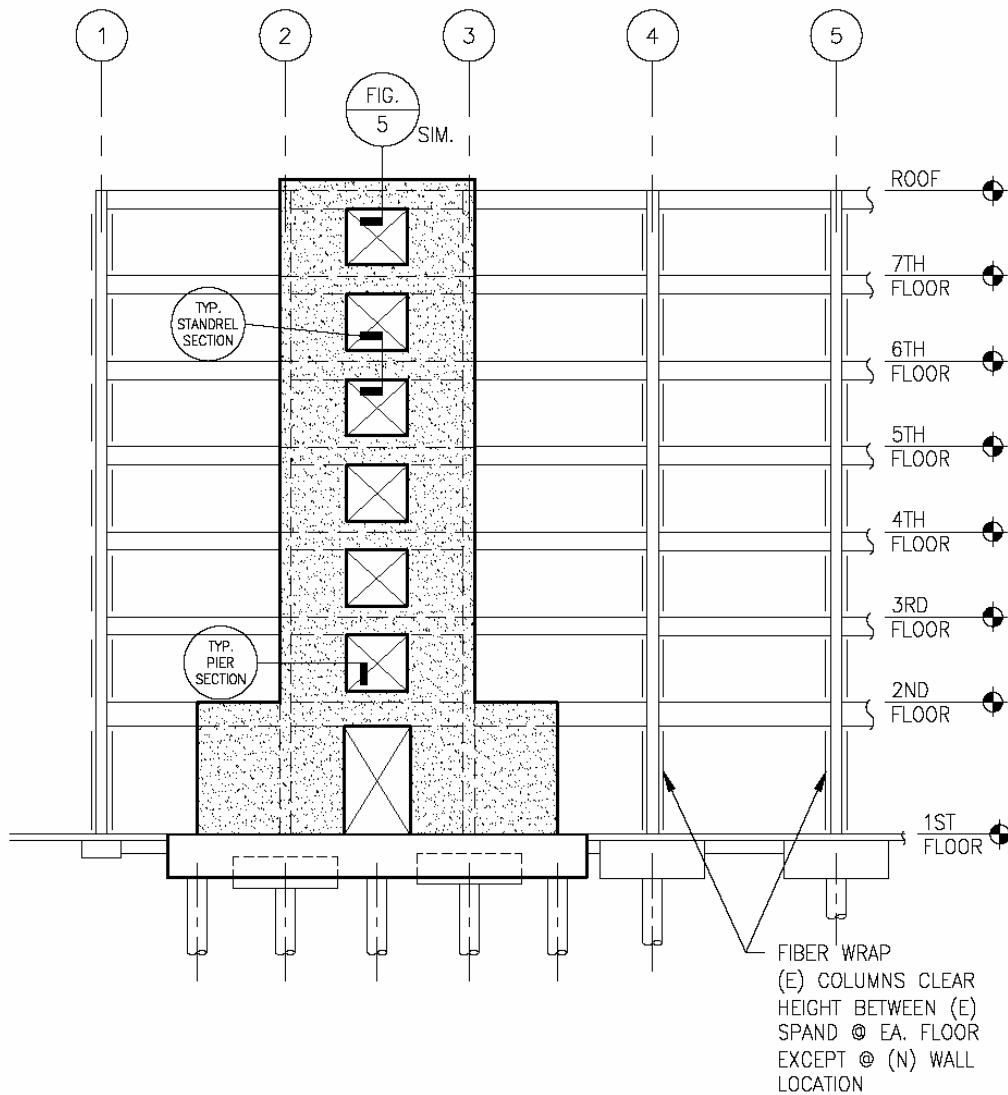


Fig. 7.14 Scheme 3 — Shear wall and fiber-wrap elevation

7.3.6 Retrofit Design

With the scheme chosen, the walls were first designed and detailed to have enough stiffness to accommodate the required target displacement. Utilizing two walls, each 20-feet long and 12 inches thick, consisting of 7-foot wide pier and 3-foot deep spandrel beams, would provide enough stiffness to keep the drifts down to below the required target displacement. The reinforcement was then proportioned so that the wall assemblies would have enough strength to maintain positive post yield stiffness and to meet the deformation limits in FEMA 356 for walls

and coupling beams. The new elements were detailed in accordance with the requirements for special reinforced concrete walls in Chapter 21 of ACI 318. Spandrels were sized to prevent the need for diagonal reinforcing. The piers have been detailed to include confined boundary elements, as shown in Figures 7.15 and 7.16.

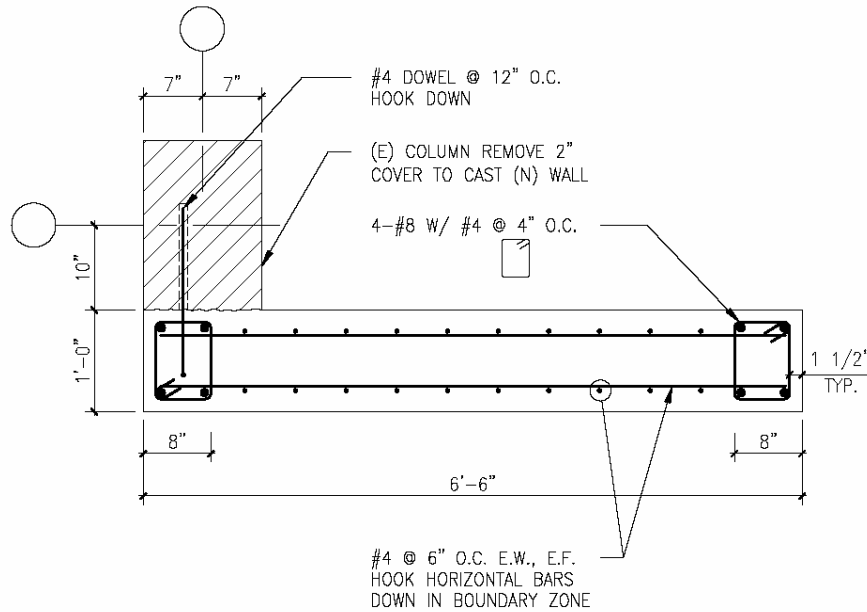


Fig. 7.15 Scheme 3 — New shear wall pier detail

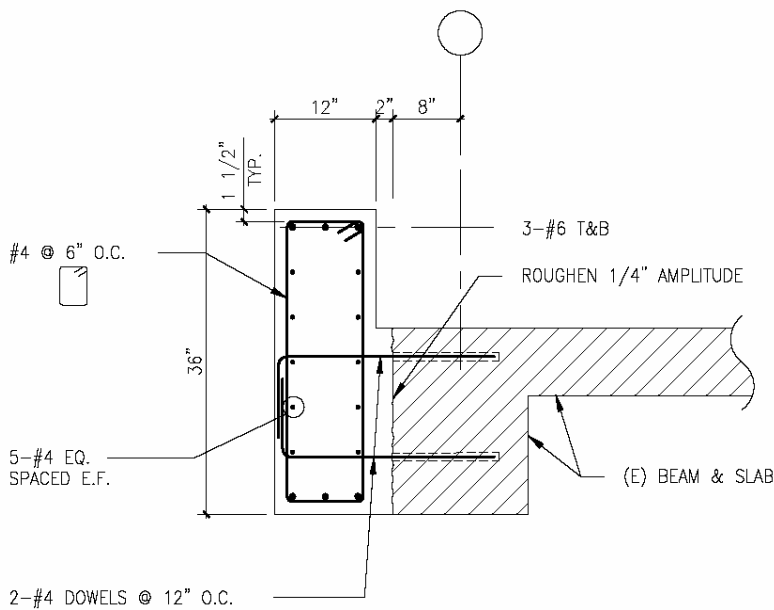


Fig. 7.16 Scheme 3 — New shear wall spandrel beam detail

Design of the fiber-wrap is normally done in a design-build arrangement with a fiber-wrap supplier. One or several manufacturers would be consulted to help determine the best type of material and method of application to be used to meet the performance criteria of the project.

7.3.6.1 Foundation Design

Because the existing components are sensitive to the total building displacements, foundation flexibility had to be considered in the design. With strict controls on the target displacement it was important to provide a foundation capable of developing the capacity of the walls without uplift and rocking. To achieve this, pile foundations were chosen, however new pile locations were limited by the placement of existing piles. In addition, the installation of new pile caps was complicated by the location and configuration of existing pile caps, which had to be considered in the overall placement of new foundation elements. Capacities of the new pile elements were calculated using the procedures in FEMA 356.

In order to make the piles work, the base of the 20-foot-long walls needed to be spread out to generate additional overturning resistance. In total, six new piles are added below each new wall — two at each end for overturning and two in the middle to support the additional gravity load added by the new walls. A 4-foot-deep pile cap was required. The new pile caps were carefully configured to prevent disruption of the existing pile caps, maintain existing gravity support for the building, and avoid costly shoring. A plan of the new wall foundations can be seen in Figure 7.17 and a detail can be seen in Figure 7.18.

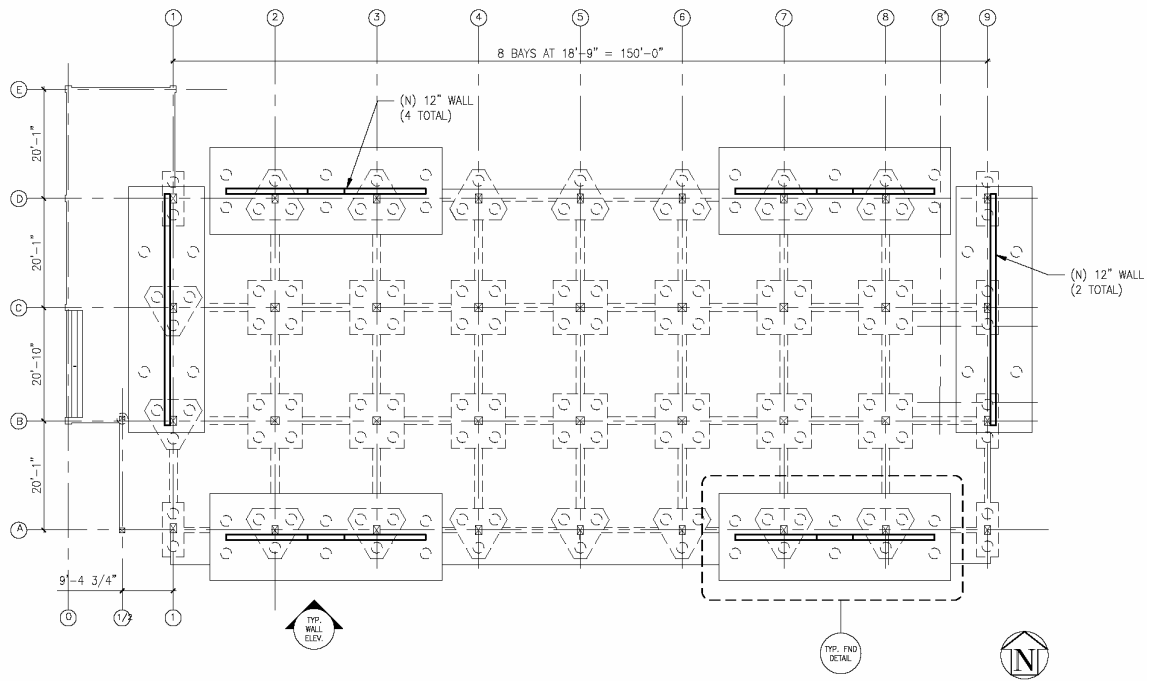


Fig. 7.17 Scheme 3 — Foundation plan

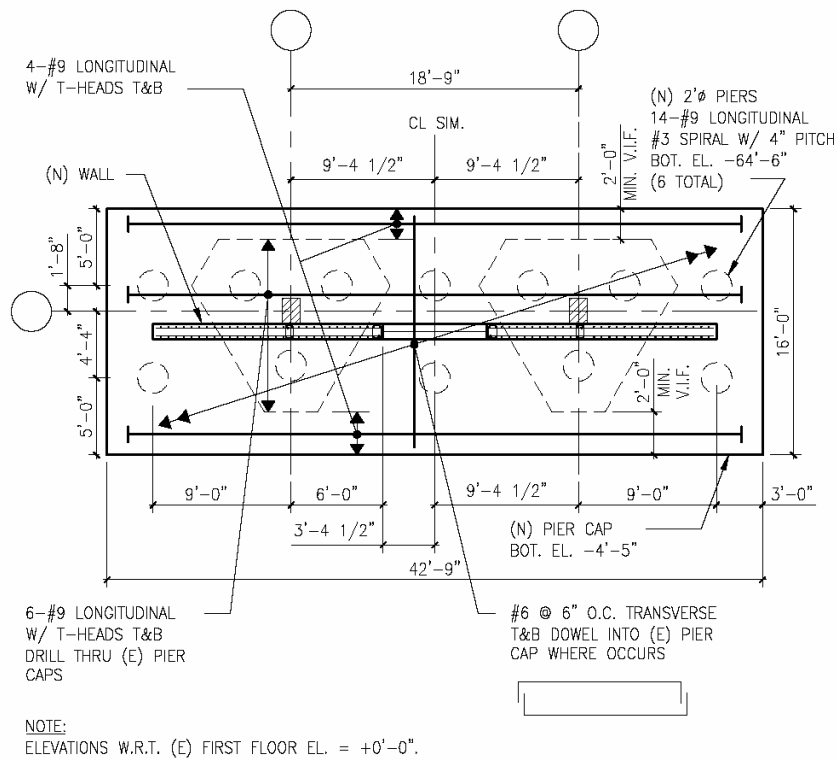


Fig. 7.18 Scheme 3 — Typical new wall foundation

7.3.6.2 Strengthened Building Analysis and Results (Strengthened DV/DM/EDP/IM)

To verify that the strengthened building meets the selected rehabilitation objective, the previous nonlinear static pushover analysis was revised to incorporate the new wall piers, spandrels, foundation elements, and revised column ductilities. New wall elements were assigned nonlinear properties similar in the same manner as the existing elements were.

The period of the strengthened building is 0.5 seconds, reduced from 1.2 seconds, based on an effective moment of inertia of the new walls equal to $0.50 \cdot I_g$. The target displacement for this period was found to be 5.2 inches. As before, two load patterns consisting of a modal pattern and a uniform pattern were applied. The modal load pattern was found to control, since the walls were flexurally controlled and the modal load pattern produces a larger moment for the same shear as the uniform pattern. The pushover curve for the modal load pattern is shown in Figure 7.19, overlaid on the original pushover curve to illustrate the change in performance.

The confirming analysis demonstrates that given the spectral accelerations from the 10%/50 Earthquake Hazard Level (IM), no forces or plastic deformations (EDP's) exceed FEMA 356 tabulated acceptance criteria (DM's), and that the design meets the selected performance level (DV).

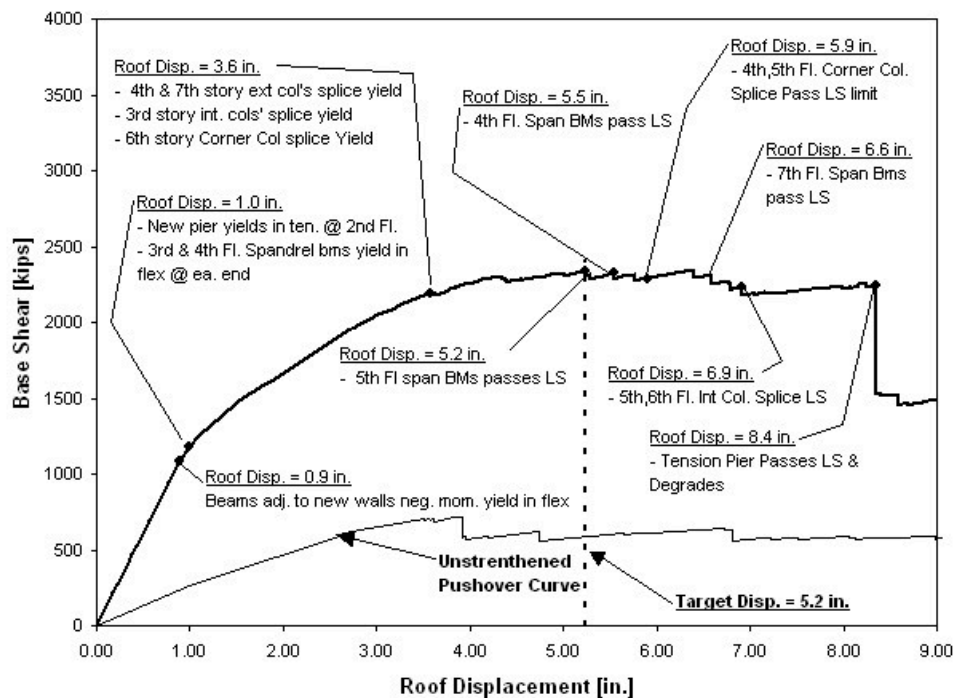


Fig. 7.19 Strengthened building pushover curve

7.4 ENGINEERING ASSESSMENT OF THE PEER PBEE METHODOLOGY

The goals of the PEER PBEE methodology contain many advancements of interest to the engineering profession. The plan to develop a performance-based, probabilistic loss estimation methodology founded in rigorous scientific research would fill gaps in the knowledge base of engineering practice currently filled by engineering judgment, and would be very desirable to many practitioners.

Intensity Measures: Engineers practicing performance-based earthquake engineering understand the lack of direct correlation between traditional IM's, such as spectral acceleration, and the ultimate damage state of a structure. Research on improved IM's that result in better correlation with damage is highly desirable. However, the improved IM's must be as straightforward and easy to comprehend as spectral acceleration has been to engineers.

Engineering Demand Parameters: Recent advancements in performance-based engineering have included new and often complex analytical procedures intended to produce better results. As the body of knowledge increases, we are finding out that even these new procedures have significant limitations on reliable prediction of EDP's. Developing algorithms to improve calculation of EDP's, identifying EDP's that can most accurately be predicted, and selecting the EDP's that best correlate with damage, is much needed.

Damage Measures: Once EDP's are predicted, the potential damage must be measured and translated into some kind of performance assessment such as loss or damage state (collapse). Current performance based methodologies contain DM's based on some research and materials testing, but for the most part have relied on expert opinion and engineering judgment. Research and testing to develop quantitative damage measures on specific components or assemblies would be highly beneficial in filling holes in current body of knowledge of performance based engineering.

Decision Variables: One of the biggest challenges in practice is communicating decision variables to building owners in a manner that is understandable, and helps them make sound financial decisions. Developing a rigorous, reproducible method of loss estimation, with a variety of DV's (performance, dollar loss, lives lost, repair costs), as an alternative to the current PML environment, would be a substantial improvement to the loss estimation industry.

Nonstructural Losses: Although the value of nonstructural losses can exceed structural losses in a given building, current practice for estimation of nonstructural losses does not have a

rigorous methodology. Often based on judgment or simple percentage ratios applied to value, we lack the data on nonstructural damage measures and analytical tools to systematically evaluate nonstructural losses. This is one of the biggest gaps that can be filled with the PEER PBEE methodology.

Uncertainty: As the profession educates the public in performance based engineering, attempts to predict building performance, and communicates that performance to building owners, our ability to reliably predict EDP's and quantify any of the DV's under consideration becomes a paramount concern. Given known limitations in our ability to correlate various aspects of the DV/DM/EDP/IM chain, developing a way of quantifying the uncertainty into a confidence level for consideration along with a DV could be the single most important contribution of the PEER methodology to the current practice of performance based engineering.

7.4.1 Implementation of the PEER Methodology in Engineering Practice

The fundamental consideration for implementation of the PEER PBEE methodology into engineering practice must be the economies of a consulting engineering business. If it provides an identifiable benefit that can be sold to building owners, it will be willingly adopted by engineering professionals.

The potential benefits have been outlined above. The PEER methodology offers to fill holes or make improvements over current performance assessment methodologies. These benefits make the methodology, or pieces of it, at least initially attractive to high-end engineering firms practicing performance based engineering. Potential impediments to implementation of the methodology in practice would be the comfort level of engineers with historic practice, biases against acceptance of new procedures, lack of understanding of new procedures, the complexity of the procedures, the time it may take to perform the work, and the ability to charge that time to the client.

Another issue regarding the PEER methodology is the translation of the rigorous probabilistic definitions and mathematics into simpler terms that engineers several years removed from the classroom can understand. For the typical engineer, even in the high-end offices, opening a book or report, seeing a triple integral equation, and reading probabilistic

terms they have never heard of could be intimidating and lead to dismissal of the idea as being “too academic.”

In order to help overcome potential impediments to implementation of the methodology into practice, the following is needed:

Education — The methodology must be clearly laid out and explained in a manner that can be understood by practitioners. Engineers must be taught how to use the procedures.

Demonstration of benefits – The advances in technology and improvements over current procedures must be clearly demonstrated.

Validation — The methodology must be shown to correlate with observed damage and losses for earthquakes where data is available.

Simplification — The procedures will be most useful if there are ways of abbreviating the process (perhaps sacrificing accuracy) and performing the work in a tiered level of effort to adjust schedule and budget to suit the needs of the client.

The software must be comparable to current office production software in terms of graphical interfaces for input and output as well as ease of use.

8 PBEE Adoption and Decision Making

Authors: J. Meszaros, U. Ince

8.1 INTRODUCTION

Performance-based approaches to regulation offer several potential advantages over prescriptive approaches. Ideally, they can reduce “rigidity and compliance burdens while promoting innovation and lower compliance costs” [May, 2003]. Assuming effective implementation and enforcement, performance-based earthquake engineering (PBEE) has potential to yield better building performance at lower total cost than code-based engineering by allowing engineers to design customized solutions for specific conditions. If this intent were achieved, PBEE could yield a number of private and public benefits, including better performance in terms of safety, disruption and damage at similar or lower cost (see Table 8.1). Improved ability to predict levels of loss, injury and disruption alone — which should be possible if PBEE analyses were widely conducted — should reduce costs for insurance and promote more efficient and effective public planning for earthquake contingencies.

Table 8.1 Potential private and public benefits from PBEE in case of major earthquakes

Fewer lives lost and injuries
Lower direct economic loss
Less disruption
More predictable levels of injury, loss and disruption

Though PBEE holds promise for significant advantages, widespread adoption is not likely if the PBEE analyses do not fit well with the social and economic context in which earthquake engineering investment decisions are made. At this time, engineering clients are accustomed to a code-based decision environment that shields them from the complexity of and

responsibility for choices about preparing their structures for earthquakes. PBEE demands far more involvement by clients and, at least in these early days of its development, greater initial expense. The question of how to interest clients in authorizing PBEE assessments is nontrivial.

The Van Nuys testbed sheds some interesting light on how building owners currently tend to think about earthquake upgrades. Testbed interviews revealed that this building's owners never wanted to consider upgrades other than those mandated by building codes. We examine their reasoning with an eye toward lessons about what might increase building owners' interest in PBEE upgrades. Section 8.2 describes what we learned in Van Nuys about owners' decision processes and criteria. Section 8.3 explores the implications of these findings for potential widespread adoption of PBEE, drawing an analogy to medical practice.

Resistance to PBEE may decline if clients are exposed to potential advantages over code that resonate with their own priorities. With this in mind, the testbed team developed an analysis tool tailored to client investment criteria related to capital investments in general and retrofit investments in particular. Section 8.4 describes this multiple-objective decision tool. It is building specific, includes the major decision criteria PBEE clients express concern with, and employs the financial metrics preferred by most corporate and financial investment analysts.

Finally, Section 8.5 summarizes the testbed's lessons for PBEE decision making, including conclusions about likely patterns of early adoption and longer term potential for widespread adoption. Continued development of site-specific tools for estimating performance in terms of injuries and downtime as well as direct losses should be the keys to potential future adoption.

8.2 PAST INVESTMENT DECISIONS

Since the Van Nuys building was damaged in the 1971 San Fernando and 1994 Northridge earthquakes, its owners are aware that earthquake risks in this location are real and can significantly affect the value of the property. Damage from the Northridge earthquake was such that the facility could not reopen as a full-service hotel. None of the economically viable repair and retrofit options included a full-service kitchen. Without a full-service kitchen, the earning potential of the hotel was reduced by more than \$1 million a year.

Van Nuys has had two types of owners with different economic goals and different levels of business sophistication in the years since Northridge: an investment consortium and an individual owner. As previously mentioned, neither owner type has been interested to make physical seismic improvements other than those required by code. Both, however, were concerned enough about earthquake risks to secure earthquake insurance. We explore both owners' thoughts on earthquake preparation in some detail below. Their financial sophistication, asset bases and business goals were quite different but there were striking similarities in their concern (or lack of concern) about mitigating the property's earthquake risks.

8.2.1 Investment Consortium

An investment consortium specialized in hotel ownership owned the Van Nuys building at the time of the Northridge earthquake. They oversaw the repair and renovation of the building after it was damaged in that quake. We interviewed the architects who worked on the renovation. The architects shared their recollections of the owners' decision criteria.

The owners were initially interested to return the building to operability for minimum investment. They were not concerned with future earthquake risks beyond meeting the requirements of code. They were not interested in even discussing such options.

City codes were the most important influence on the design of the retrofit and repair. At one point, the building insurer became an important constraint on the owners' options because the insurer would not accept a shoring solution that was acceptable under older city building codes. In the end, though, damage was so extensive that it was determined the building would have to meet newer codes which, like the insurer, excluded the initially proposed shoring solution.

To repair the hotel after Northridge, the architects devised a new structural system that met the owners' financial goals and city codes. This is the design that was, unfortunately, not compatible with returning the hotel to function as a full-service hotel. The hotel was closed for three years for design, repair and re-sale.

Table 8.2 summarizes the consortium's repair and retrofit decision criteria. They sought to minimize investment subject to regulatory constraints.

Table 8.2 Consortium owners' repair and retrofit considerations

Minimum cost
Minimum time to re-open and sell
Meet code requirements
Meet insurer requirements
Resell at good price

We examined the consortium's approach to potential upgrades in terms of three investment-decision variables: the probability of a loss, the magnitude of a potential loss and the likelihood of recouping an investment in improvements. The first two of these relate to expected losses in future earthquakes, the third to expected returns on a retrofit investment.

Loss probability: Since the consortium was expected to hold this asset for only a short period of time they could have presumed that the chances of another earthquake during the short period of their ownership were quite low. Their expected loss from a quake would therefore not be large enough to justify investment in an earthquake engineering upgrade.

Loss severity: Since the consortium owned hotels in a number of locations, their financial vulnerability to a disaster in any single location was limited. A total loss of the Van Nuys hotel would not have been financially devastating. Research in other domains suggests that risk of ruin may often precipitate investments to mitigate the effects of low-probability threats. In this case, geographic diversification ensures that this firm does not face a risk of ruin from an earthquake in this location.

Direct Return on Investment: The resale value of the Van Nuys hotel had to be a crucial consideration for this set of financially sophisticated owners. If they anticipated that potential buyers would fully value an earthquake upgrade, they should have at least explored possible upgrades with their architects. Their lack of interest in exploring improvements beyond code implies that these sophisticated hotel owners believed that other potential owners would not value earthquake improvements.

8.2.2 Individual Owner

The hotel's current owner purchased the building in 1998, after its repair and retrofit. He is an individual approaching retirement. The hotel is the major asset in his retirement portfolio. He

apparently relies heavily on his general manager to ensure the business viability of the property as he himself has no experience working in the hotel industry.

Unlike the previous owners, the current owner's investment portfolio is not well diversified. A disaster in this location would be a financial disaster for him, yet he lives quite comfortably with this risk. The hotel's General Manager indicated that the owner is not worried about earthquakes because he has lived with earthquake risks in Southern California his entire life. This familiar hazard does not worry him.

The General Manager has several decades of experience in hotel management, including a number of years in the Los Angeles area. He is familiar with common attitudes and practices in this industry in Southern California. According to the General Manager, while visitors ask hotel employees about earthquake risks nearly every day, quakes have never been a source of worry to him or his colleagues. He is not aware of hotels investing in earthquake mitigation except insofar as required by building codes. This suggests that even though customers ask about this risk, the industry is not convinced they could recoup an investment in greater safety by marketing this advantage to customers.

The manager assumes the Van Nuys building is earthquake safe because it has performed well in recent small quakes. "We've had a couple of shakers, no cracks," he noted. He said that the hotel does carry earthquake insurance, though he was not sure whether the insurance policy includes business interruption coverage.

Even though the hotel is instrumented for quake and we presented ourselves as a team of experts knowledgeable about both earthquake risks and structural performance for this particular location, the manager asked no questions about what earthquake risks they faced, whether the building might be made safer or whether we had any advice or concerns about the building. His complete lack of curiosity about the risks to his building actually seemed a bit odd to us at the time; it seemed as if he may have preferred not to have more specific information about these risks. The manager agreed to meet with us as a courtesy, to help us with our work, not in order to learn about the building or the risks.

Thus, the owner, who relies on the property for his future financial security, and his manager, who is safeguarding the value of the business, showed no concern for earthquake risks beyond adhering to codes and purchasing earthquake insurance (see Table 8.3). Yet, unlike the

previous owners, this owner is not diversified and expects to own the property for a relatively long period of time.

Table 8.3 Current owner’s EQ preparation considerations

Meet code Maintain earthquake insurance
--

8.2.3 Summary

Van Nuys allowed us to study the investment priorities and decisions of two quite different owners. Neither considered an investment in earthquake mitigation to be of interest. They sought to meet code and secure insurance. Beyond these measures, they showed no concern for the effects of earthquakes on the future operation or value of the business.

Both owner types offered clues to the beliefs and attitudes of a larger marketplace. The consortium implicitly bet that potential buyers would not fully value earthquake improvements other than meeting code. The current manager believes that hotel customers may ask about earthquakes but that they would not pay more to stay in an exceptionally earthquake-safe building. It seems that asset markets may not currently value earthquake performance and may not provide incentives for mitigation.

8.3 ENABLING A PBEE MIND-SET

Code-based structures render design and retrofit decisions relatively simple, particularly from a client’s perspective. They remove responsibility for deciding which risks to worry about. They eliminate the need to consider trade-offs between costs and risk reduction. They conceal most of the uncertainties inherent in risk assessments. Most clients presume code compliance takes care of their legal and moral responsibility for earthquake risks. It seems that most also presume that code compliance means that no one will be killed in their building in an earthquake.

For building owners to become involved in PBEE decisions, they must be willing and able to think about earthquake risks in a different way. This means, in part, grappling with somewhat complex analytic assessments of risks and potential benefits. It also means they must be willing to face earthquake risks and to share responsibility for choices about risk reduction.

Also significant is the fact that, in the current environment, PBEE analyses cost clients more in time and money than code-based analyses. With little PBEE experience behind the profession, engineers would be hard pressed to estimate the likelihood that a particular PBEE analysis would be likely to yield designs with significant cost-benefit advantages.

8.3.1 Code-Based vs. PBEE Mind-Sets

To appreciate the change in mind-set necessary for PBEE adoption, consider an analogy to medical practice. In the middle part of the 20th century, the practice of medicine was largely paternalistic. Patients asked few questions and ceded the dominant role for treatment to their physicians. It was presumed that “best” treatments existed, that these had been scientifically established, that doctors knew which were most current and valid, and that doctors (rather than patients) were in the best position to evaluate trade-offs and make treatment choices [Charles et al., 1999]. As Parsons [1951] described this paternalistic model, patients were essentially passive and fully dependent on their physician experts. Physicians were seldom questioned; second opinions were rare; good patient relations had more to do with reassurance than with information sharing.

The code-based decision environment that currently characterizes most earthquake engineering resembles paternalistic medical practice. Clients leave it to their engineers to ensure code compliance. They presume there are “best” design solutions, that these are based on scientific study and are captured in building codes, and that their engineers are best positioned to make design trade-offs and decisions. Clients need not be concerned with frightening or complicated information about earthquake risks and building performance. They are also shielded from cost-risk trade-offs and from grappling with the reality that “built to code” does not mean absolute life safety. Engineers in turn face few client questions or challenges and are left to essentially practice and make decisions on their own.

A continuum of alternatives to paternalistic medical practices — from “informed consent” to “professional-as-agent” and “shared decision making” models — has evolved during the latter half of the 20th century [Charles et al., 1997]. All involve greater information sharing, more patient responsibility, less presumption of physician omnipotence and recognition that diagnoses and treatment options are based on values and judgment, not just on facts or formulas.

Patients are now commonly apprised of likely (but not certain) prospects and the risks and benefits associated with treatment options. Patients share responsibility for choices and introduce decision criteria related to their own lifestyles and life objectives. Doctors have to communicate better and to work *with* client decision makers rather than on behalf of them.

Fully implemented, PBEE would transform engineering practice from paternalism to shared decision making. Clients would accept more responsibility for decisions about protections. Engineers would cede some autonomy and control and develop greater skills in collaborating with clients on decisions involving complex, probabilistic and sometimes frightening information.

At least two other issues associated with PBEE and engineer-client relations will matter to adoption. First, liability issues are potentially simpler for clients and engineers in a regulated situation than in a performance-based one. Though the argument that regulations (e.g., building codes) were followed is not a fail-safe liability shield [Huber, 1990], it can mitigate charges of negligence in at least some professional domains. PBEE weakens this shield. To the extent that the advantages of PBEE methods derive because structures are less “over engineered” than code-based designs, liability issues could be quite serious.

Second, PBEE analyses take more time and therefore cost more than analyses associated with code-based design. Before clients can even consider potential superiority of a PBEE solution over a traditional one, they must agree to pay for a PBEE analysis. They will also have to be willing to allow the design phase to take more time. These cost factors alone will discourage adoption. It is also worth noting that clients may suspect that engineers prefer more costly, time-consuming analyses not because they are in the client’s interest but because they may yield higher fees and greater profits for engineers.

Table 8.4 contrasts some important differences in client mind-set required under PBEE versus under code-based regulation. These sorts of “soft” factors will make it challenging to get clients to adopt PBEE. The experiences of the medical profession suggest these need not be insurmountable barriers but that they are major and will take time and significant changes in attitudes. This process took nearly half a century in medicine. Notably, medical practice evolved because patients clamored for change. As yet, the public is not clamoring for more involvement in or responsibility for their earthquake exposures.

Table 8.4 Contrasts in “mind-sets” associated with code- vs. performance-based earthquake engineering practice

Mind-set	Code-based	Performance-based
Client aware of specific earthquake risks	Not necessary	Necessary
Client aware of residual risk after code compliance	Not necessary	Necessary
Client given options for risks borne	Not necessary	Necessary
Client faces cost-risk trade-offs	Not necessary	Necessary
Engineering analysis costs	Less Costly	More Costly
Time for engineering analysis	Shorter	Longer
Liability risk	Lesser	Greater
Concern about engineers’ profit motives	Lesser	Greater

8.3.2 The Role of Emotion in Earthquake Investment Decisions: Working with Worry

Our research team was struck by the description of Van Nuys’ current owner as being “not worried” about earthquake risks. That description resonated with research into risk preparation from a number of different contexts. It seems that the best predictor of voluntary preventive investments is an emotional-cognitive factor: worry. Individuals with identical rational estimates of the probability and severity of, for example, an earthquake will take radically different decisions about investing to prepare for quakes depending on whether quakes worry them or not [Baron et al., 2000]. This is true for business owners as well as homeowners [Palm, Carroll, 1998; Meszaros, Fiegenger, 2003]. We do not yet understand well what worry is and what creates it, but it has become clear that prevention decisions include an emotional side that must be addressed.

Providing scenario-type information that vividly portrays the potential effects of a bad event may be the best means to ensure that a decision maker has engaged their emotions as well as their cognition before making a decision [Kunreuther, Schade 2001]. The PBEE methodology offers significant opportunities to develop scenarios that are meaningful to particular structures and, therefore, to help decision makers integrate the emotional and rational components of their decision preferences. The Investment-Decision Support System described below is designed to engage both emotion and rationality by being site specific and event specific. It also enables trade-offs among noncommensurable, multidimensional objectives for outcomes from potential earthquakes.

8.4 A PBEE-ENABLED SEISMIC INVESTMENT DECISION SUPPORT SYSTEM

As with many investment decisions, seismic upgrade decisions will hinge on a single or a limited set of performance variables that are of high priority by key decision makers. If only a single variable matters, optimization is relatively straightforward. When multiple decision variables (DVs) are to be considered, the decision maker's task is more complicated. The optimization process will involve subjective trade-offs and joint optimization.

In the Van Nuys testbed we pursued four essential steps for making PBEE analyses maximally appealing and useful to potential decision makers (Fig. 8.1):

- A. Determine the set of DVs that are important to stakeholders.
- B. Generate structure-specific exceedance probabilities for these DVs.
- C. Communicate the decision analyses involving multiple DVs in terms of decision metrics that are familiar to and preferred by building owners of many types.
- D. Validate the resulting decision tool via surveys and case applications.

In this section, we describe the current status of the PBEE methodology with respect to each of these steps. Step A requires identification of what the ultimate end users of the system see as relevant consequences. Step B requires determination of expected losses and costs. Step C involves creating a format for presentation and communication of analyses. The format is designed to be consistent with established industry practices in order to minimize resistance to adoption. Step D will ensure the generalizability and reliability of the decision support system are solidly established.

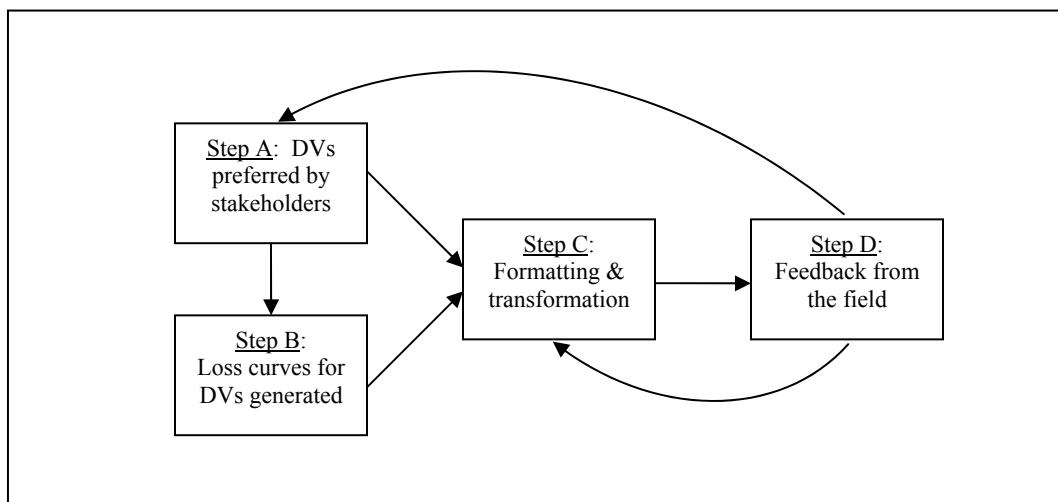


Fig. 8.1 The process of creating a PBEE decision support system

8.4.1 Step A: Decision Variables That Are Important to Stakeholders

Over the last several years, researchers have used several different venues and methods in order to understand which DVs are of critical importance for various stakeholders. A general pattern has emerged that we call the “3-D model,” with the three “Ds” being “deaths” (i.e., preventing harm to occupants), “downtime” (i.e., preventing business disruption) and “dollars” (i.e., preventing direct losses and repair costs). According to a survey of practicing engineers, these three factors, in this order of importance, are what most concern clients when they undertake PBEE projects [Meszaros, et al. 2003]. Table 8.5 outlines several engineering-based discussion forums that have drawn similar conclusions about what matters most to clients in terms of decision variables.

The order of importance of the 3Ds may vary for different stakeholder groups. For example, owners with an exclusively financial interest in a property may focus almost exclusively on dollar exposures. By contrast, businesses with significant operational exposures (e.g., manufacturing plants that might be shut down or retail businesses that might not be able to receive customers) may focus more heavily on downtime as a threat to their survival. In any case, the ability to provide information about the 3Ds should help meet the decision needs of a large swath of stakeholders.

Deaths. Historically, life safety has been the prime motivator for seismic mitigation [Mileti, 1999]. However, recent earthquakes in the U.S. have yielded huge economic losses and relatively few fatalities or serious injuries. Lack of significant human consequences in the U.S. in recent decades may have created a false sense of security and thereby discouraged seismic investments. PEER discussions and ATC-58 notes as reflected in Table 8.5 suggest that life safety is still a big decision criterion. To the extent that PBEE-based designs can make building occupants safer, they should interest a number of building owners.

Downtime. Downtime looms as a frightening prospect for many types of building owner. For small business owners, particularly those with tight cash flows, relatively brief closures can threaten business survival [Webb, et al. 2000; Meszaros, Fiegenger 2003]. Large businesses may suffer losses in revenue when a manufacturing line stops or a reservation system is not available for even a short period. Both small and large businesses worry that closures and disruptions will lead customers to switch to other sources for goods and services. Market share may never fully recover [Chang 2003]. Finally, downtime losses are harder to insure than direct losses.

Downtime may be a priority for physical mitigation to the extent that adequate financial mitigation for downtime is not readily available.

Table 8.5 Summaries of engineering-based, interdisciplinary discussions of client needs and PEER-PBEE capabilities

	PEER-funded projects	Prior test-bed meetings	ATC 58 Project workshop	Van Nuys Testbed
Methodology	"Investor-based" decision making explicitly addressing costs and benefits at different levels of seismic safety		Rigorous cost-benefit analysis	The framework output is compatible with well known investment decision tools such as NPV, IRR and PP
	Tradeoffs between investing in seismic resistance or alternative forms of risk management			Securitized risk transfer is not included. At the retail client level not feasible. Insurance is a viable alternative. Not yet incorporated.
	Consequences and tradeoffs among different levels of safety		Range of potential outcomes may be desirable.	Financial and Non-financial consequences at different safety levels presented to facilitate trade-off
Relative vs. absolute	Consequences expressed in relative terms rather than absolute	Relative risk considerations		Consequences expressed in relative terms
Probability		Move from scenario analysis to more refined probabilistic statements	Probabilistic statements are not favorably received. Scenario analysis preferred. 90% confidence level.	The output is % probability of annual loss for three DVs under various mitigation levels. Possible to pare down to scenario based presentation
Decision Variables	Public safety: saving lives/avoiding injuries	Life-safety	Life losses (not the focus of discussion, though)	Life safety may be possible to incorporate in the future
	Cost of damage repair	Repair costs	Direct economic losses (especially down-time)	Loss curves available for the structure as is. Loss curves under different retrofit scenarios still needed
	Cost of down-time	Down-time		It is a significant variable for Van Nuys. Currently work ongoing. Likely to be available in the near future
Time Horizon		Relevant time horizon needs to be considered	<i>Annual</i> probability is not desirable	Reduction in <i>annual</i> expected losses at different levels of mitigation investments is obtained.
Externality	Consider externalities		Indirect economic losses	No. These are location/structure specific and hard to incorporate in a general framework. For Van Nuys externality data not available

Table based in part on material provided by Peter May

Dollars. Significant and rising economic losses may make PBEE interesting to many owners. The 1989 Loma Prieta quake yielded an unprecedented \$8.6 billion in monetary losses. In Northridge, the insurance industry sustained losses beyond anyone's expectation (\$20.8B). Even relatively moderate quakes now yield large losses because large asset bases are located in seismically active areas. The moderate 2001 Nisqually earthquake was the most costly natural disaster in Washington State's history (\$2B in total losses). Private building owners may be

willing to invest in preparation and mitigation beyond the requirement of building codes if such investments are cost effective. Exposures for relatively common earthquakes may, in some cases, justify PBEE upgrades that coincidentally also provide better performance in less frequent, more serious quakes.

8.4.2 Step B: Methodology to Generate Structure-Specific Exceedance Probabilities

Having ascertained that potential PBEE clients favor the 3D variables, we employed the PEER methodology to estimate the desired DVs for the testbed structure. The effort has so far been most successful in generating information relevant to the “dollar” variable (i.e., building repair cost estimates given a particular structure). Exceedance probability curves for the testbed were developed by Miranda, et al. (see Chapter 5 of this report).

Depending on the specific needs and sophistication of the end-user, PBEE decision-support analyses can be expressed in terms of a scenario-based, probable maximum loss (PML) point estimate or other suitable presentation format, including probabilistic distributions of PMLs. Figure 8.2 shows how this information can be applied to an investment decision problem for the Van Nuys building. Expected repair costs for the building in case of the most likely severe earthquake given two potential levels of retrofit are graphed in this figure.

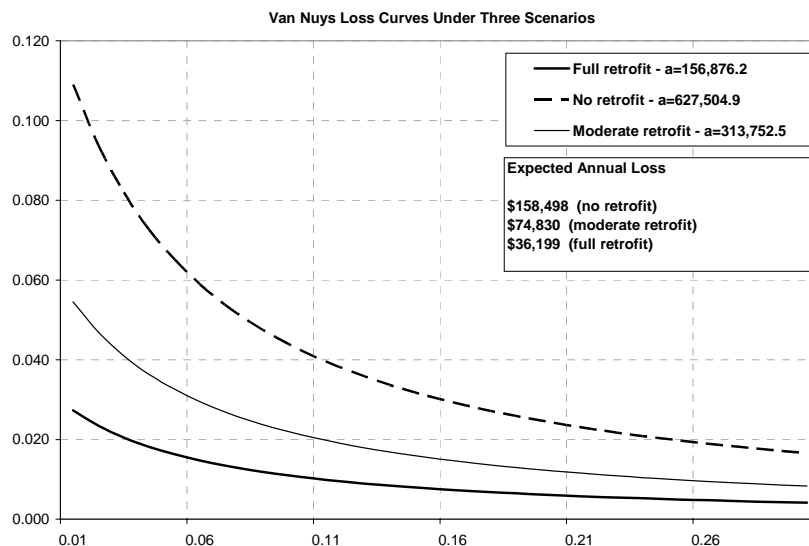


Fig. 8.2 Repair cost loss curve and its variations under two retrofit assumptions

There is further research under way to generate similar output for the downtime and life-safety DVs [Krawinkler and Miranda, 2004]. The ideal output for these two DVs would be exceedance probability curves expressed in number of days and number of fatalities, similar to the exceedance curves for losses in Figure 8.2. At this time, only probability distributions for deaths and downtime are available. Even this incomplete information can be useful to an owner, however. A multi-attribute presentation of expected outcomes can allow an owner to compare and impute priorities among these several objectives. Note also that an owner can readily translate downtime into dollar losses given their operational cash flows. Miranda and Aslani [2003] have found that in the case of Van Nuys there is a close relationship between repair costs and downtime.

It would also be desirable to include contents losses when developing a complete analysis of PBEE options. These can be significant. For example, we know that non-structural damage in the Van Nuys building is expected to be approximately 70% expected structural losses [Miranda and Aslani, 2003].

8.4.3 Step C: Communication of Decision Alternatives

As mentioned previously, in order for PBEE to achieve widespread adoption, the presentation and communication of PBEE analyses should fit well with the decision tools that are widely used by potential end-users. The PEER-PBEE methodology can generate relatively rich, building-specific information about expected repair costs DV in the form of annual exceedance probability curves. Although this is an extremely valuable output, it is certainly not the end of the story.

A user-friendly “shell” that will enable end-users to make informed assessments of the financial and non-financial consequences of varied levels of mitigation investments is desired. Using such information, end-users can make well-informed decisions about how much (if at all) to invest in structural mitigation. The DV output generated via the PEER-PBEE methodology can be transformed into all the decision metrics that the business end-user community is familiar and comfortable with.

In for-profit business settings, large-scale capital investment decisions are typically made using relatively straightforward capital-budgeting metrics, including net present value (NPV),

internal rate of return (IRR), and payback period (PP). All these metrics are similar to the output of cost-benefit or cost-risk analysis, which are quite familiar to the engineering community. However, depending on the nature of the investment and the industry, some companies will tend to prefer some metrics over others. Additionally, while these metrics are most commonly expressed in terms of point estimates, they can also be expressed in more advanced and/or specialized forms such as value at risk (VAR) and probabilistic distributions such as those generated via Monte-Carlo (MC) simulation.

A recent survey of Chief Financial Officers of Fortune 500 companies found that 75% of the respondents report that they always or almost always use IRR or NPV when evaluating capital investment alternatives [Graham, Harvey, 2001]. Currently, the most sophisticated and sound corporate investment decisions in probabilistic settings are made using NPV methods.

PP is also relatively popular, used always or almost always by 56% of respondents. PP is essentially an inferior tool because it is biased against long-term investments, ignores cost of capital, and it lacks a clear criterion for acceptance and rejection. Nevertheless, its relatively wide use among a relatively sophisticated community indicates that a simpler method may have some advantages over more complicated but sounder decision-making tools.

Using building-specific loss-exceedance probability curves for Van Nuys, an NPV/MC simulation-based procedure was developed that would meet the needs of the more sophisticated corporate decision maker [Ince and Meszaros, 2003]. This procedure requires repair-cost exceedance curves for three different levels of structural mitigation investment levels: zero; moderate; and full retrofit. The analysis also demands: a time-horizon for the useful life of the proposed retrofit investments; a cost of capital (i.e., discount rate) based on the riskiness of the project and the funding costs of the investing company; and the initial cost of retrofit investments at the three levels. Once design options have been generated, engineers and clients can presumably generate all of these parameters relatively easily. At this point, expected NPVs, IRRs, and PPs for the three investment levels can be generated and used to inform decisions made on a strictly financial basis.

The three financial metrics for two retrofit options for Van Nuys are presented in Figure 8.3.³⁰ The full retrofit is financially undesirable insofar as it has a negative NPV and an IRR lower than the owner's cost of capital (13%).

	Moderate retrofit	Full retrofit
Payback period	→ 3.0 years	4.1 years
Net Present Value	\$ → 142,178	\$ (61,319)
Internal Rate of Return	→ 16.7%	12.2%

Fig. 8.3 Financial decision metrics for two different mitigation levels

Financial metrics are next presented together with estimates for other relevant DVs so that a decision maker can directly compare options across all relevant decisions considerations. Figure 8.4 presents point estimate comparisons of deaths, downtime and dollar losses for Van Nuys.

	Expected NPV (Structural)	Downtime	Deaths
Do nothing	\$0	16 days	0.13
Moderate retrofit	\$142,178	7.6 days	0.06
Extensive retrofit	-\$61,319	3.2 days	0.02

Fig. 8.4 Decision/trade-off table presenting financial and non-financial DVs

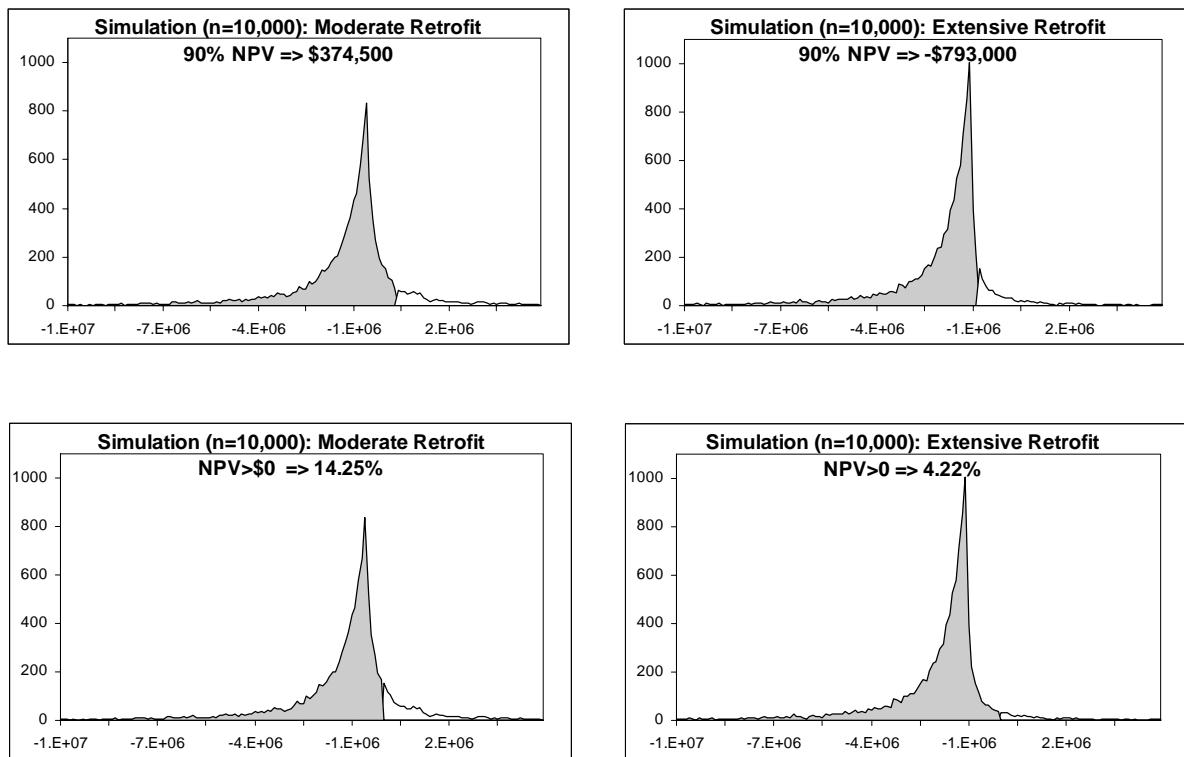
If Van Nuys owners had had access to the decision platform described above following the Northridge quake, they would have been able to compare multiple retrofit options based on cost-effectiveness criteria, downtime and safety consequences of their potential choices. By explicitly trading off financial and non-financial DVs, they would have considered a more complete picture of costs and consequences. They may (or may not) have chosen the financially unattractive full retrofit option because of the additional days of downtime and fatalities avoided.

³⁰The calculations assume a 50-year life span for the building, 13% annualized cost of capital, \$500,000 cost for moderate and \$1,000,000 cost for extensive retrofit. The loss curves for the three decision variables for the existing structure were modified using an ad-hoc procedure to produce the loss curve for the two design levels.

8.4.4 Step D: Presenting Distributions of Potential Outcomes

By taking advantage of the probabilistic output of PEER-PBEE methodology we are able to generate distributions of NPVs in addition to point estimates. This form of presentation allows end-users to consider the extremely skewed nature of cash flows associated with high-loss, low-probability events.

The top two panels in Figure 8.5 present the 90% probability NPV for the moderate and full retrofit options for Van Nuys. That is, they show the NPV levels that would almost surely be exceeded by these two specific mitigation investments. The bottom two panels portray the probabilities that these two investments would yield positive NPVs.



a. Moderate retrofit

b. Extensive retrofit

Fig. 8.5 Simulated structural loss net present value distributions

To the degree that loss curves or expected losses for downtime and life-safety DVs can be obtained from the PBEE methodology, the non-financial dimensions of mitigation decisions could also be presented to the decision maker in a manner similar to Figure 8.5. The decision

maker would then be able to consider the expected annual reductions in downtime and in number of fatalities that would be achieved at each level of investment and at what financial consequence.

It is relatively easy to communicate point-estimate expected NPV values to a manager with basic finance training. The effectiveness of using simulated NPV probability distributions is an entirely open question. When one moves into simulated probability distributions of NPV, the benefits of conveying a more complete picture of future outcomes that are highly skewed should be weighed against the difficulty encountered by many laymen to relate to and interpret NPV probability distributions. In fact, one engineering-focused interdisciplinary discussion outlined in Table 8.5, the ATC 58 Project workshop in 2002, concluded that probabilistic information is generally not well received at this time. Some participants deemed annual exceedance probabilities not desirable, and expressed a preference for scenario-based presentation. However, some in the same group were receptive to expressions in terms of 90% confidence level of exceeding a particular value, which is a metric derived from a probability distribution.

With time and exposure, stakeholders may become more comfortable with probability-based expressions. Sophisticated statistical techniques are used with regularity in certain segments of the corporate world; particularly in financial sectors. Insurance companies simply cannot exist without a strong in-house expertise in probability. Many risk-consulting firms have been using PBEE-like methods for a while now. We should expect more acceptance and enthusiasm for the PEER-PBEE methodology among decision makers in financial, insurance and trading companies.

8.5 LESSONS FOR PBEE IMPLEMENTATION AND DIFFUSION

The Van Nuys testbed has highlighted both challenges to and opportunities for PBEE acceptance. In addition to answering several questions about how best to proceed in developing PBEE as a decision technology, the testbed exercise suggests which open questions ought to be addressed next:

- *Clients currently focus on building to code and insuring for earthquake damage.*

Convincing analyses will be those that compare PBEE options to code-based design options and to insurance.

- *Clients not worried about earthquake risks will not invest in PBEE assessment.*

PBEE-based decision models can create highly specific descriptions or “scenarios” of expected outcomes from expected earthquakes. Specific and vivid descriptions of risks are thought to be the best available means to ensure that decision makers have engaged their emotions (i.e., worry) as well as their rationality (i.e., expected value) in consideration of potential earthquake risks.

- *Clients may prefer not to address cost-risk trade-offs (and potential associated liabilities) so long as building codes and engineering practices allow them to do so (i.e., paternalism is comfortable).*

PBEE-based design can enable clients and engineers to customize solutions to particular structures and particular shake risks. In return for accepting responsibility for earthquake exposure decisions, they may find opportunities to achieve better earthquake performance for similar or lesser investments.

- *Clients do not make earthquake investment decisions on financial grounds alone. They are concerned with human well-being and operational disruptions.*

PBEE-based analyses can enable clients to directly examine trade-offs among multiple performance objectives, particularly among the 3Ds of deaths, downtime and dollars.

- *Sophisticated clients make investment decisions based on measures such as IRR and NPV.*

PBEE enables multiple outcome measures to be converted to multiple investment-return measures.

- *The Van Nuys testbed illustrates that a performance-based retrofit can have positive financial returns.*

This sort of result should be of interest to a variety of owner types.

- *PBEE techniques for better estimating human impacts and downtime are needed.*

Retrofit options with negative NPV might still be of interest to clients if they present opportunities for greater human safety or lesser anticipated downtime.

- *PBEE demands changes in engineering practice, including significant changes in client relations as well as greater sophistication in technical practice.*

The client-relations problem is in some ways a chicken-and-egg problem. When clients recognize the value of participating in earthquake design trade-offs, they will demand that their engineers engage them. Until engineers make the value of participation apparent, clients will not make this demand.

Appendix A: Past Earthquake Damage in Van Nuys Building

Author: K. Porter

A.1 DAMAGE IN 1971 SAN FERNANDO EARTHQUAKE

The building was strongly shaken by the M6.6 1971 San Fernando event, approximately 20 km to the northeast. Earth Sciences AR-240 strong-motion accelerometers were located at the southeast corner of the ground floor, middle of the 4th floor, and southwest corner of the roof (Figure A.1). The instruments recorded peak accelerations at the ground floor of 240 cm/sec² in the transverse direction, 130 cm/sec² longitudinally, and 170 cm/sec² in the vertical direction. Peak roof accelerations were 384 cm/sec² transverse and 315 cm/sec² longitudinally at the southwest corner of the building (Trifunac et al., 1999). The 5%-damped acceleration response spectra for the ground-floor instruments are shown in Figure A.2 (calculated using Bispec [Hachem, 2000]).

Islam (1996) reports building periods of 0.70 sec in the early part of the 1971 earthquake, and 1.5 sec during peak response (Table A.1). Hart and Vasdevan (1975) performed system identification analysis of the accelerometer records to estimate equivalent viscous damping ratios of 16.4% of critical in the longitudinal direction and 9.7% transverse. McVerry (1979) estimated 17.3% in the longitudinal direction and 19.2% transversely.

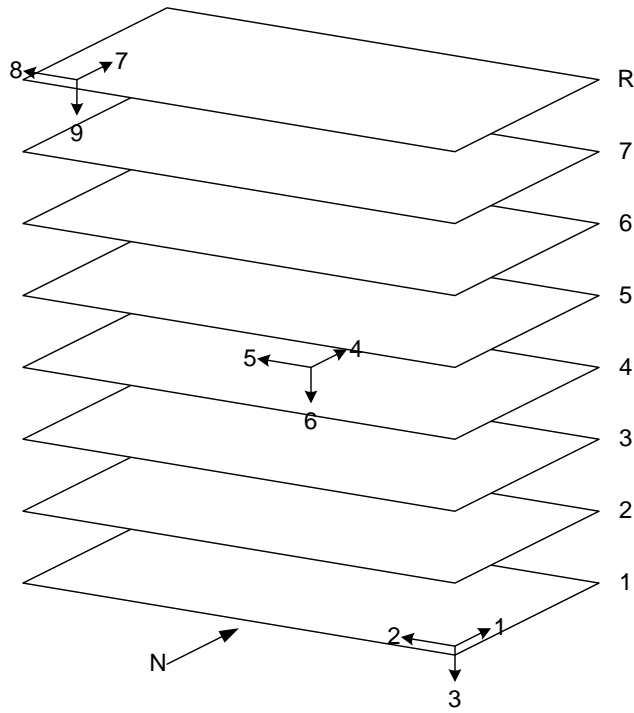


Fig. A.1 Instrument locations in 1971 San Fernando earthquake

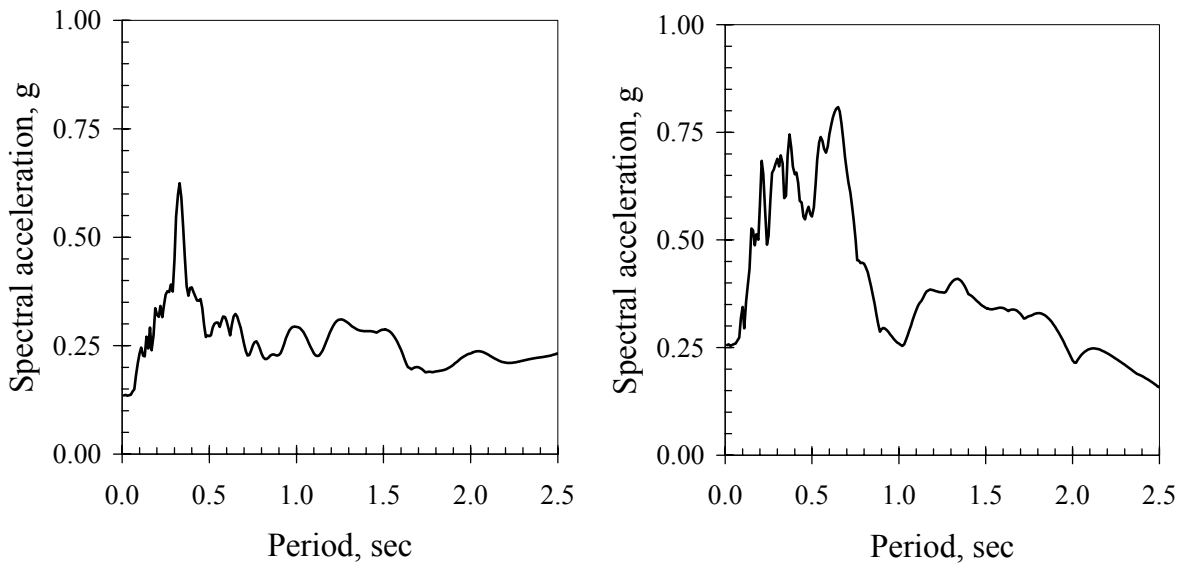


Fig. A.2 Spectral acceleration, 1971 ground-floor motions, longitudinal (left) and transverse (right)

Table A.1 Approximate fundamental building periods (Islam, 1996)

	Longitudinal	Transverse	Torsional
Pre-1971 San Fernando, ambient vibration	0.52 sec	0.40 sec	
1971 San Fernando earthquake			
Early part of earthquake	0.70	0.70	
During peak response	1.5	1.6	
1994 Northridge earthquake			
Early part (0-10 sec)	1.5	2.2	1.4
Middle part (10-20 sec)	2.1	2.2	
Toward the end (>25 sec)	2.4	2.0	

The damage in 1971 mostly required architectural repairs. Jennings (1971) describes “extensive damage to the interior plaster walls, to the plumbing fixtures, etc., on the second, third, and fourth floors. The upper three floors were not damaged severely.... The structural frame received some cracks, indicating strains beyond the elastic limit; the cracks were repaired with epoxy cement.” John A. Blume & Associates (1973) report:

The structural repair consisted of patching the second-floor beam-column joint on the north side (east end) of the structure.... Some structural distress appeared at some column pour joints located near the exterior beam soffits.... Epoxy repaired the spalled concrete [sic]. Paint was applied to areas where only flaking of paint occurred.

Nonstructural damage was extensive. Almost every guest room suffered some damage. About 80 percent of the repair cost was spent on drywall partitions, bathroom tile, and plumbing fixtures. The damage was most severe on the second and third floors and least severe at the sixth and seventh floors.

Some gypsum wallboard had to be replaced. Interior partitions required paint and new vinyl wall covering.... Forty-five bathtubs ... and 12 water closets had to be replaced. Bathroom tile had to be patched, grouted, or replaced in over half the bathrooms.... Spalling occurred at architectural concrete attached to structural concrete columns at the ground floor.... Exterior cement plaster spalled and cracked. Windows in every room required some alignment and caulking, although none needed replacing. Doors needed adjustment.

John A. Blume & Associates (1973) report the repair cost as “approximately \$145,000,” of which \$2,000 was for structural repair. Trifunac et al. (1999) report the cost of repair as \$143,000, while Jennings (1971) estimated repair costs as approximately \$250,000.

In 1980, additional accelerometers were installed; their locations are shown in Figure A.3 (California Strong Motion Instrumentation Program, 2001). As of this writing, they have been triggered in 11 subsequent events, whose magnitudes, epicentral distances, intensities are shown in Table A.2. According to the available literature, and judging by construction permits on file in the Los Angeles Department of Building and Safety, none of these subsequent events other than Northridge series caused significant damage.

Van Nuys - 7-story Hotel
(CSMIP Station No. 24386)

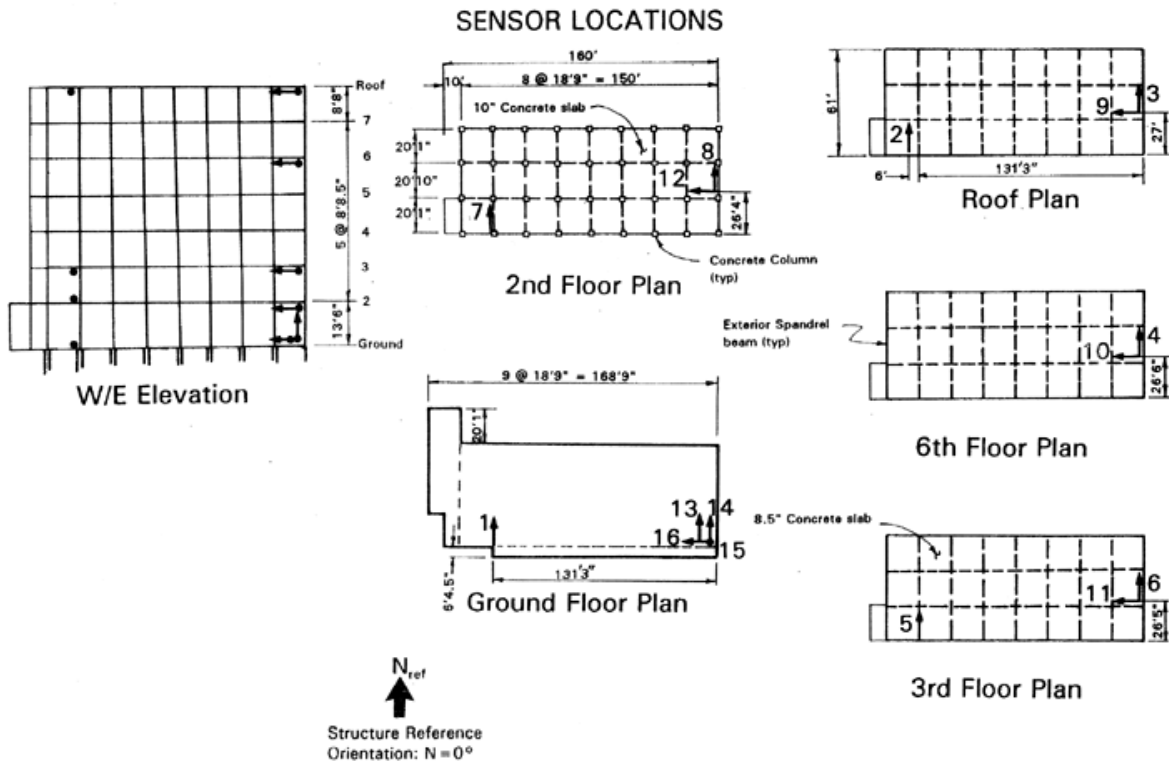


Fig. A.3 Instrument locations after 1980

Table A.2 Events causing strong motion (Trifunac et al., 1999; CSMIP, 1994)

Earthquake	Date	<i>M</i>	<i>R</i> (km)	<i>PGA</i> (cm/sec ²)		<i>PGV</i> (cm/sec)		<i>PGD</i> (cm)	
				Trans	Long	Trans	Long	Trans	Long
1. San Fernando	9 Feb 1971	6.6	22	240	130	27	23	5.3	9.7
2. Whittier	1 Oct 1987	5.9	41	160		8.7		1.8	
3. Whittier aft.	4 Oct 1987	5.3	38	37	52	1.4	2.2	0.3	0.3
4. Pasadena	3 Oct 1988	4.9	32	54	36	1.6	0.9	0.3	0.2
5. Malibu	19 Jan 1989	5.0	36	15	22	0.9	1.0	0.2	0.2
6. Montebello	12 Jun 1989	4.1	34	21	22	0.8	0.8	0.2	0.2
7. Sierra Madre	28 Jun 1991	5.8	44	56	62	4.6	2.8	1.0	
8. Landers	28 Jun 1992	7.5	190	41	41	12	11	6.1	4.9
9. Big Bear	28 Jun 1992	6.5	150	25	23	3.6	3.6	0.9	1.0
10. Northridge	17 Jan 1994	6.7	7.2	390	440	40	51	12	7.9
11. Northridge aft.	20 Mar 1994	5.2	1.2	270	140	7.5	4.8	0.6	0.6
12. Northridge aft.	6 Dec 1994	4.5	11	57	60	3.0	2.4	0.5	0.2

A.2 DAMAGE IN 1994 NORTHRIDGE EARTHQUAKE

Shaking, structural response, and damage in the 1994 Northridge earthquake were more severe than in the San Fernando earthquake. As noted in Table A.2, peak acceleration at the ground floor was 440 cm/sec² in the longitudinal direction, 390 cm/sec² transversely. The 5%-damped acceleration response spectra for the motion recorded by instruments 16 and 14 are shown in Figure A.4 (calculated using Bispec [Hachem, 2000]). Assuming a fundamental period of 1.5 to 2.0 sec and 5% viscous damping, the building experienced damped elastic spectral acceleration of approximately 0.3 to 0.5g.

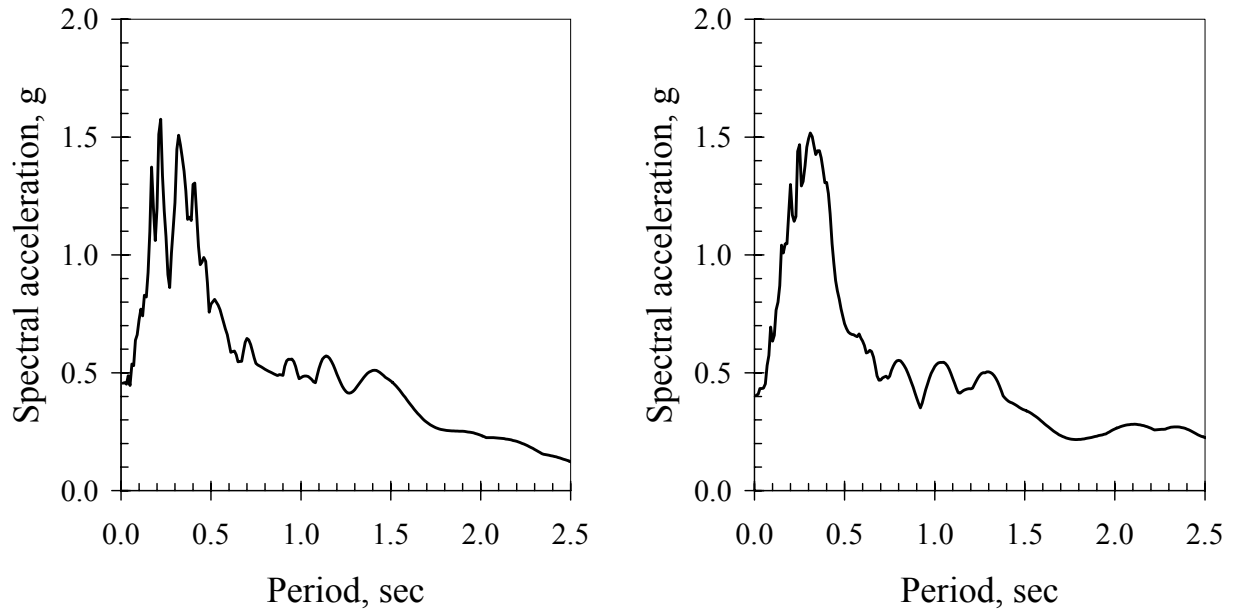


Fig. A.4 Spectral acceleration of ground-floor motions, 1994 longitudinal (left) and transverse (right)

Islam (1996) reports structural response in the Northridge earthquake in terms of relative displacements and transient interstory drift ratios, as shown in Table A.3. Several authors have estimated peak responses at the other floors; Table A.3 shows estimates by Li and Jirsa (1998) and Browning et al. (2000). The table shows fair agreement among the estimates: transient drift ratios reached approximately 2% in the 1st through 4th stories, decreasing to 0.5% toward the 7th story.

Table A.3 Recorded peak displacements and story drift ratios

Floor	Max rel. displacement (Islam, 1996)	Transient drift ratio relative to floor below		
		Recorded (Islam, 1996)	Calc., Li & Jirsa (1998)	Calc., Browning et al. (2000)
Longitudinal				
Roof	9.2 in.		0.3%	0.5%
7			0.6%	0.7%
6	8.2		0.9%	1.3%
5			1.9%	1.9%
4			1.7%	1.9%
3	3.6	1.9%	1.9%	1.0%
2	1.6	1.0%	1.8%	0.4%
Transverse				
R, east	6.9 in.			
R, west	9.0			
6, east	6.0			
3, east	2.9	1.6%		
3, west	3.4	1.3%		
2, east	1.6	1.1%		
2, west	1.9	1.2%		

Trifunac et al. (1999) and Trifunac and Hao (2001) present the results of two thorough damage surveys performed on February 4, 1994, and April 19, 1994. They report extensive structural damage, in the form of shear failure of columns and beam-column joints in the perimeter moment frame. The failures include spalling of the cover concrete over longitudinal bars, buckling of the longitudinal bars and through-cracks up to several inches wide. Damage to the south frame occurred at six locations on the 5th floor (column lines A-3, 4, 5, 7, 8, and 9) and one at the 3rd-floor level (column line A-9), as shown in Figure A.5. Damage to the north frame occurred in the full-height infill masonry walls at the 1st story, and at the base of the short columns at the 1st story in column lines D-2, D-3, and D-4. Damage to the north frame also occurred at or within the beam-column joint at 12 other locations at the 2nd through 5th floors, as shown in Figure A.6. The interested reader is referred to Trifunac et al. (1999) and Trifunac and Hao (2001) for additional detail, including photos of the damage.

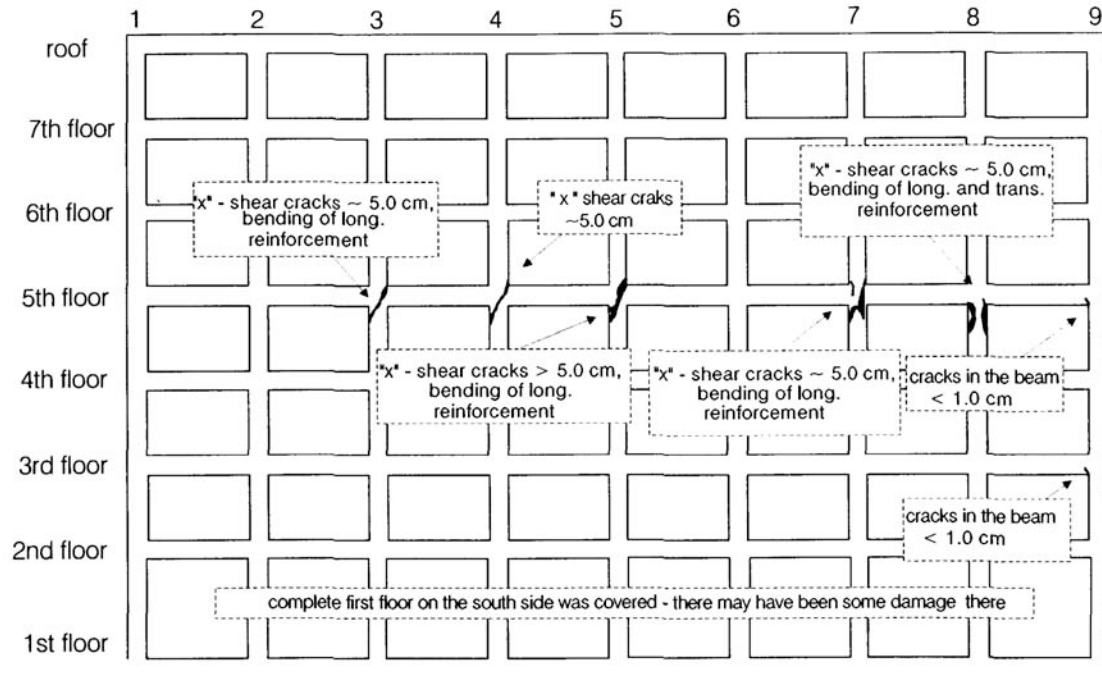


Fig. A.5 Structural damage in 1994 Northridge earthquake, south frame (Trifunac et al., 1999)

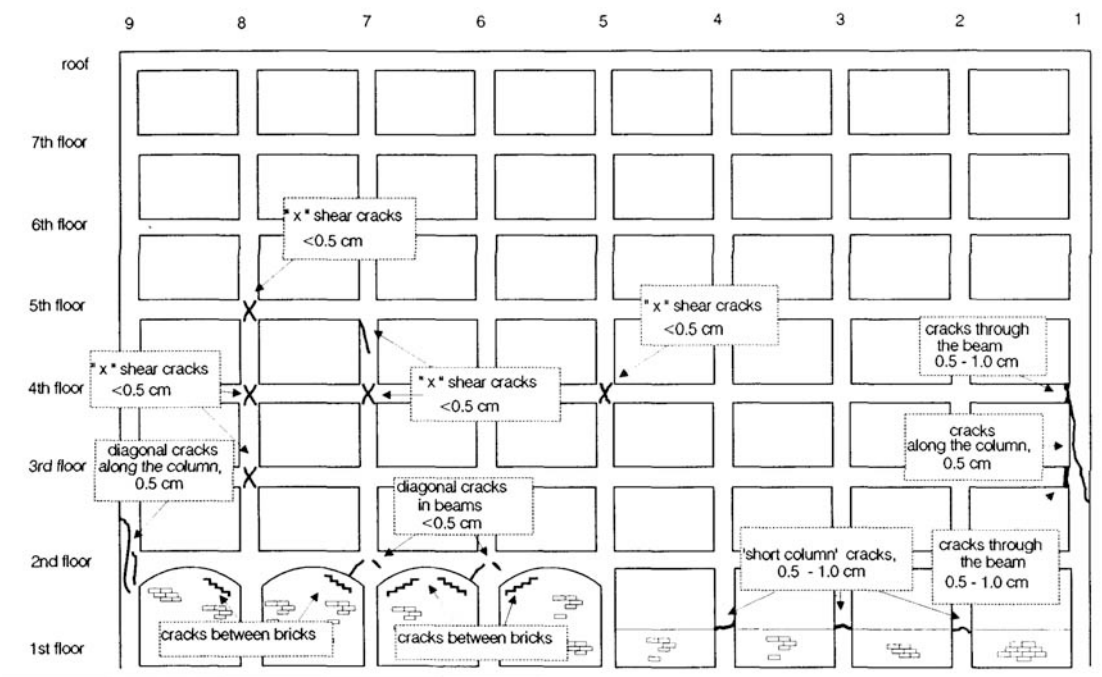


Fig. A.6 Structural damage in 1994 Northridge earthquake, north frame (Trifunac et al., 1999)

Structural repairs after the 1994 Northridge earthquake involved the addition of shearwalls at three columns of the south frame (3, 7, and 8) and four columns of the north frame (3, 5, 7, and 8), and at several interior column lines. Base fixity is provided to the new shearwalls by the addition of grade beams spanning between pier groups. Figure A.7 shows the building as it appeared in March 2001. However, consideration of the testbed building after this seismic strengthening effort is beyond the scope of the present project.

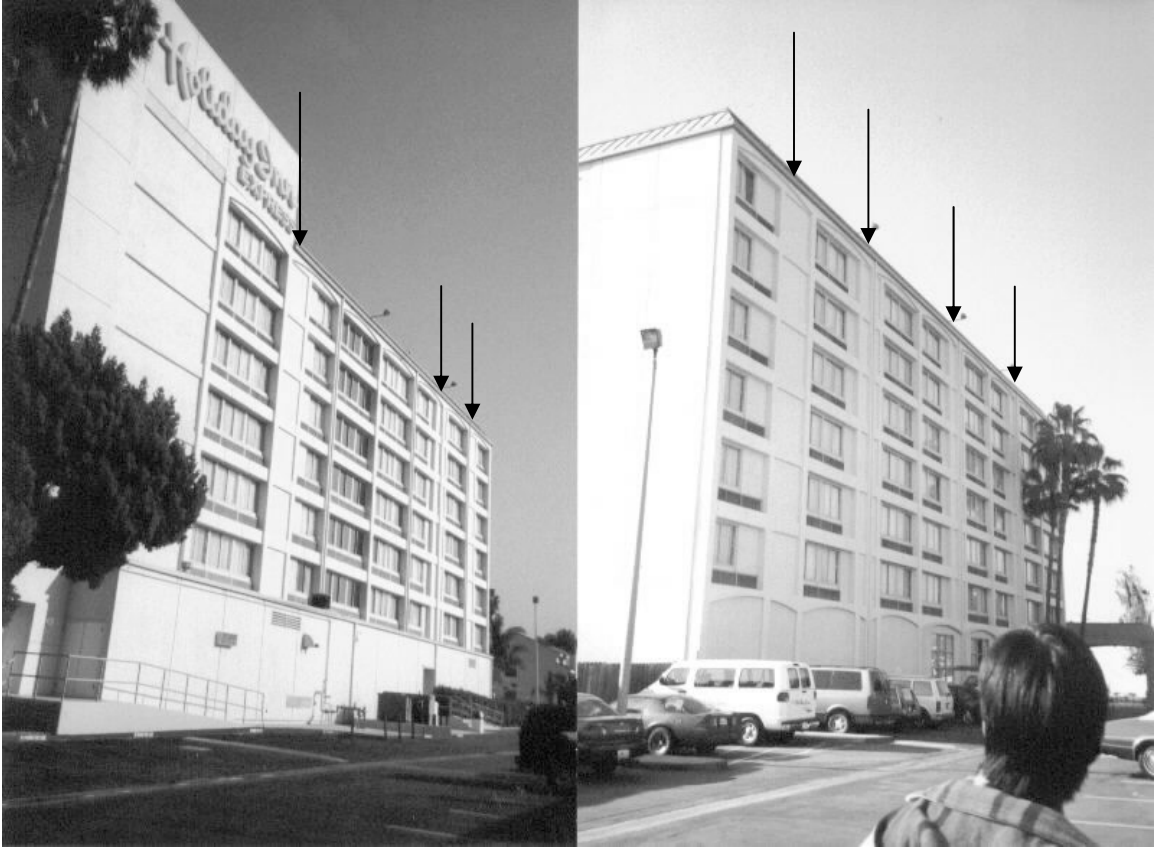


Fig. A.7 Shearwalls added to south (left) and north frames (right) after the 1994 Northridge earthquake. (Left: lines A-3, 7 and 8 from near to far. Right: lines D-8, 7, 5, and 3).

Appendix B: Component Fragility Functions

Authors: E. Miranda, H. Aslani

This appendix summarizes fragility functions for structural and non-structural components in the Van Nuys testbed structure. Damage states associated with repairs or replacement of structural or non-structural components are identified, and fragility functions for each of these damage states are developed using results from experimental research.

B.1 FRAGILITY FUNCTIONS FOR STRUCTURAL COMPONENTS

Four different groups of structural components were identified for the Van Nuys testbed; slab-column connections, columns, interior beam-column connections and exterior beam-column connections. For each group, damage states associated with different repair actions were identified. Fragility functions for each damage state were then developed using the results from experimental results available in the literature. Table B.1 summarizes the damage states that were used for each group of components.

Analysis of the results of various damage states indicates that fragility functions can be assumed to have a lognormal distribution (Aslani and Miranda 2003). Therefore, only two parameters, namely logarithmic mean and logarithmic standard deviation of the *EDP*, were required to define the fragility function corresponding to a certain damage state. The engineering demand parameter used in fragility functions of structural components is the interstory drift ratio, IDR. Similarly, loss functions are developed by estimating the cost of each itemized repair action at defined damage states. The cost of each itemized repair action was assessed either from information obtained from subcontractors specialized in repair or concrete structures or by using available data in R.S. Means (2002), FEMA 308 or Hazus (1999) documents.

Table B.1 Definition of damage measures, *DM*, for structural components

Damage Measures	Damage State	Repair Action	Fragility Surface
<i>Slab-column connections</i>			
DM ₁	Initial cracking	Patching and/or painting of the cracks	No
DM ₂	Significant cracking	Epoxy injection	No
DM ₃	Punching shear failure	Spall repair	Yes
DM ₄	LVCC*	Partial or total collapse	Yes
<i>Columns</i>			
DM ₁	Significant cracking	Epoxy injection	No
DM ₂	Shear failure	Crack stitching and spall repair	Yes
DM ₃	Axial failure (LVCC)	Partial or total collapse	Yes
<i>Interior beam-column connections</i>			
DM ₁	Beam or column cracking	Epoxy injection	No
DM ₂	Joint cracking	Epoxy injection	No
DM ₃	Spalling	Spall repair	No
DM ₄	LVCC	Partial or total collapse	No
<i>Exterior beam-column connections</i>			
DM ₁	Beam or column cracking	Epoxy injection	No
DM ₂	Joint cracking	Epoxy injection	No
DM ₃	Spalling	Spall repair	No
DM ₄	LVCC	Partial or total collapse	No

* Loss of vertical carrying capacity

B.1.1 Slab-Column Connections

Table B.1 shows that four damage states were defined for slab-column connections. The first damage state corresponds to the initial cracking in the component. The required repair task is patching and painting the cracks. The second damage state occurs when significant cracking is observed in the component that cannot be repaired by patching and painting. Epoxy injection of the cracks is required to repair the element. The third damage state corresponds to punching shear failure of the connection. At this stage the spalled concrete should be replaced and some reinforcement may need to be replaced in the connection. The last damage state occurs when the connection loses its vertical carrying capacity.

Table B.2 summarizes the median and dispersion (standard deviation of the log of the data) of the lognormal distribution fitted to the fragility and loss data of each slab-column connection damage state. Information presented in Table B.2 is based on experimental results summarized in Aslani and Miranda (2003). Figure B.1 presents the fragility functions developed for the first two states of damage in slab-column connections.

Table B.2 Statistical parameters for fragility and loss functions of slab-column connections

Damage Measure (DM)	Description of DM	Fragility parameters		Loss parameters	
		median	Dispersion	median	Dispersion
1	Initial cracking that can be repaired with pasting, taping, repasting and painting	0.004	0.40	0.10	0.65
2	Significant cracking that can be repaired with epoxy injection, pasting and painting	0.009	0.22	0.40	0.70
3	Punching shear failure that can be repaired with spall repair, epoxy injection, pasting and painting	$G(IDR, V_g/V_0)$		1.00	0.75
4	Loss of vertical carrying capacity that leads to partial or total collapse of the building	$G(IDR, V_g/V_0)$		-	-

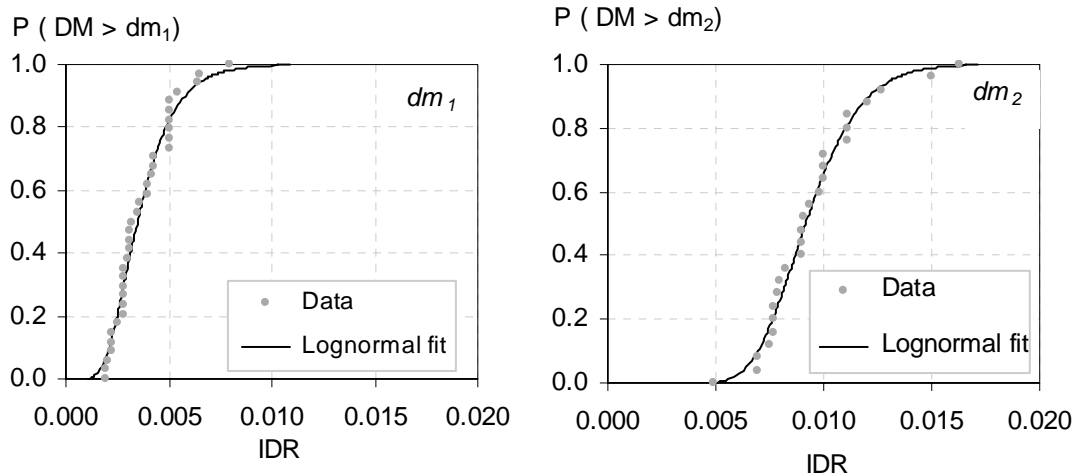


Fig. B.1 Fragility functions corresponding to damage measures dm_1 and dm_2 in slab-column connections

As discussed in Section 5.2, fragility surfaces were developed for the last two damage states in slab-column connections. Figure B.2 presents the fragility surface developed for the punching shear failure damage state, DM_3 .

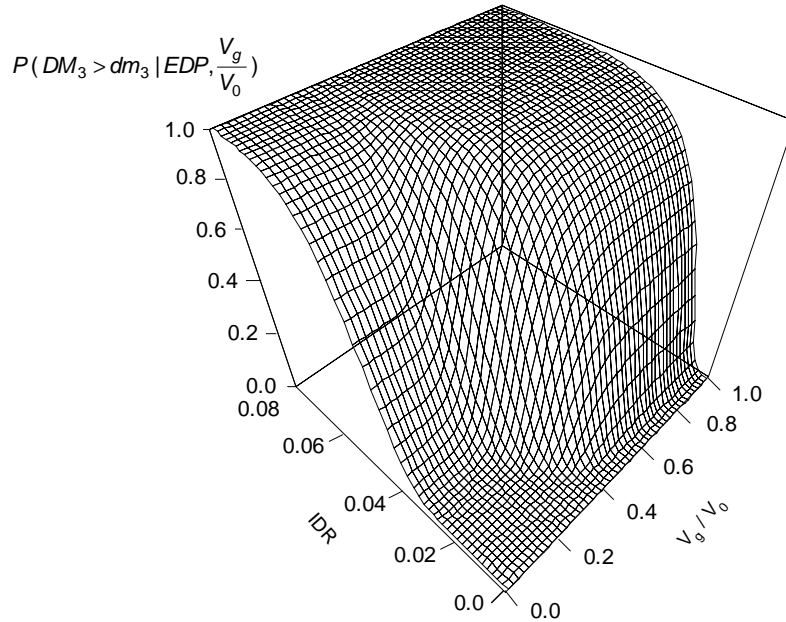


Fig. B.2 Fragility surface for punching shear failure in slab-column connection as a function of the interstory drift ratio and normalized gravity shear force

B.1.2 Columns

Three damage states were defined for columns: cracking, shear failure, and axial failure. Required repair actions for each state are presented in Table B.1. Table B.3 presents the statistical parameters to develop fragility and loss functions for columns. Information on the median and dispersion of the lognormal distribution that correspond to cracking was estimated on the basis of 1000 experimental results (Panagiotakos et al., 2001). The fragility curve for this damage state is presented in Figure B.3.

As indicated in Table B.3, fragility surfaces were developed for the last two damage states, namely shear failure and axial failure in columns. The fragility surface for the axial failure of columns is presented in Figure B.4.

Table B.3 Statistical parameters for fragility and loss functions of columns

Damage Measure (DM)	Description of DM	Fragility parameters		Loss parameters	
		median	Dispersion	median	Dispersion
1	Significant cracking that can be repaired with epoxy injection, pasting, taping, and painting	0.009	0.40	0.50	0.70
2	Shear failure that can be repaired with crack stitching, spall repair, epoxy injection, pasting and painting	$G(IDR, \alpha_{col.})$		2.00	0.75
3	Axial failure (Loss of vertical carrying capacity) that leads to partial or total collapse of the building	$G(IDR, \alpha_{col.})$		-	-

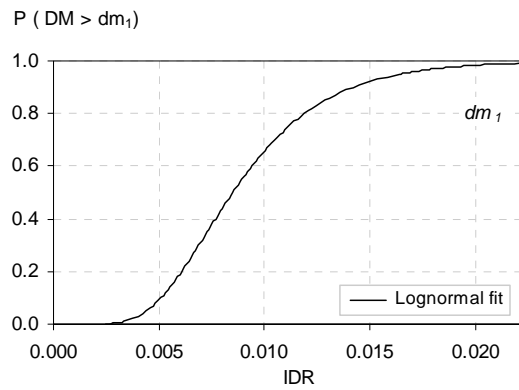


Fig. B.3 Fragility function corresponding to damage measure dm1 in columns

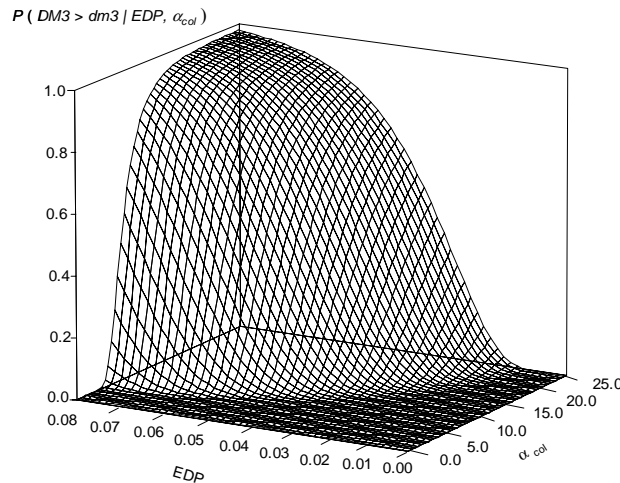


Fig. B.4 Fragility surface for axial failure in columns

B.1.3 Interior Beam-Column Connections

Four damage states are defined for interior beam-column connections. The first two damage states, beam or column cracking and joint cracking, can be repaired with epoxy injection. The third damage state corresponds to spalling of concrete in the connection. The required course of action to repair this damage state is to remove the spalled concrete, clean the edges, and pour new concrete. The last damage state, loss of vertical carrying capacity, is very unlikely to be observed in interior connections. Table B.4 provides a summary of the statistical parameters of fragility and loss functions corresponding to the four damage states of interior beam-column connections. Figure B.5 presents the fragility functions developed based on the results of different experiments (Panagiotakos et al. 2001, Aslani and Miranda 2003).

Table B.4 Statistical parameters for fragility and loss functions of interior beam-column connections

Damage Measure (DM)	Description of DM	Fragility parameters		Loss parameters	
		median	Dispersion	median	Dispersion
1	Beam or column cracking that can be repaired with epoxy injection, pasting, taping and painting	0.007	0.36	0.25	0.65
2	Joint cracking that can be repaired with epoxy injection, pasting and painting	0.015	0.37	0.40	0.70
3	Concrete spalling that can be repaired with spall repair, epoxy injection, pasting and painting	0.028	0.25	1.00	0.75
4	Loss of vertical carrying capacity that leads to partial or total collapse of the building	0.070	0.25	-	-

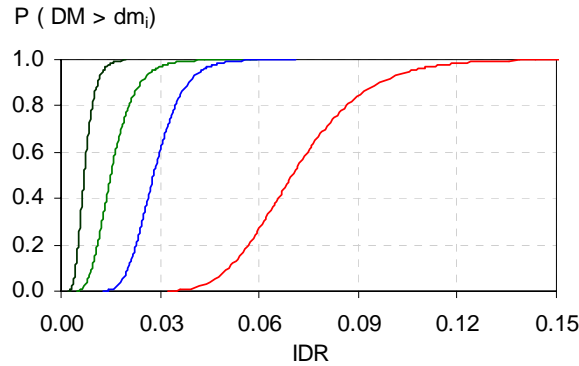


Fig. B.5 Fragility functions corresponding to damage measures in interior beam-column connections

B.1.4 Exterior Beam-Column Connections

Similar to interior beam-column connections, four damage states are defined for exterior beam-column connections. Table B.5 provides a summary of the required statistical parameters to develop fragility functions for damage states in exterior beam-column connections. Further, Figure B.6, presents the fragility functions developed based on the results of different experiments (Panagiotakos et al. 2001; Aslani and Miranda 2003).

Table B.5 Statistical parameters for fragility functions of interior beam-column connections

Damage Measure (DM)	Description of DM	Fragility parameters		Loss parameters	
		median	Dispersion	median	Dispersion
1	Beam or column cracking that can be repaired with epoxy injection, pasting, taping and painting	0.007	0.36	0.25	0.65
2	Joint cracking that can be repaired with epoxy injection, pasting and painting	0.014	0.46	0.40	0.70
3	Concrete spalling that can be repaired with spall repair, epoxy injection, pasting and painting	0.03	0.20	1.00	0.75
4	Loss of vertical carrying capacity that leads to partial or total collapse of the building	0.06	0.30	-	-

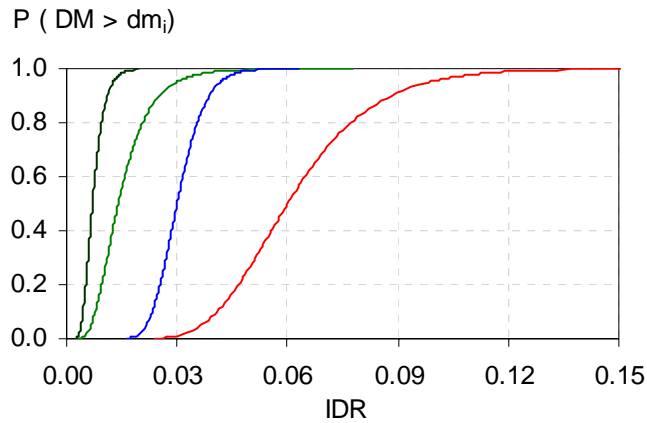


Fig. B.6 Fragility functions corresponding to damage measures in interior beam-column connections

B.2 FRAGILITY FUNCTIONS FOR NONSTRUCTURAL COMPONENTS

Nonstructural components in the Van Nuys testbed structure were identified from the architectural drawings. All components were classified according to the taxonomy of nonstructural components proposed by Taghavi and Miranda (2003). Table B.6 shows a list of the main nonstructural components in the building.

Table B.6 List of main nonstructural components in the testbed building

Nonstructural Components			
Bath tub	Floor finishes	Partitions	Suspended ceiling
Cooling	Handrail	Piping	Toilet
Doors	Heating	Plaster ceiling	Urinals
Ducts	HVAC	Plumbing	Vents
Elevator	Insulation	Power outlet	Wall finishes
Façade	Light fixtures	Pump	Walls
Fire Protection System	Light Switch	Sink	Windows

Non-structural components were classified according to their sensitivity into three categories: (i) Drift sensitive, (ii) Acceleration sensitive, (iii) Rugged. Figure B.7 shows that about 44, 53 and 3 percent of the cost corresponds to acceleration sensitive, drift sensitive and rugged components, respectively.

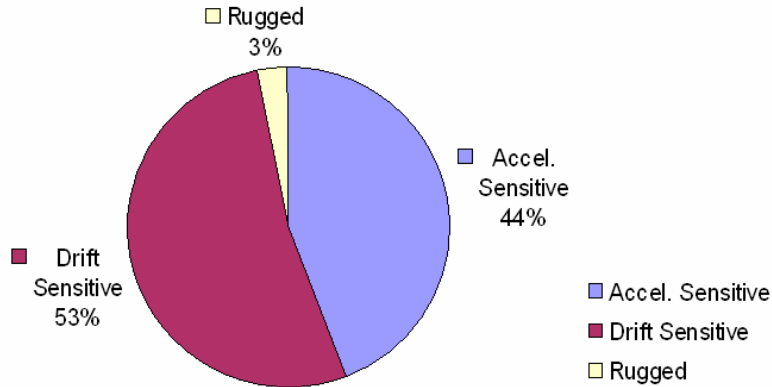


Fig. B.7 Sensitivity chart of nonstructural components in Van Nuys building

B.2.1 Fragility Functions for Partitions

The data points used to generate fragility functions for metal stud partitions are based on four experimental research programs (Freeman 1971, Nakata et al. 1984, Rihal 1982, Rihal and Granneman 1984). Damage states and repair actions associated with each damage state are shown in Table B.7. A total of 31, 25 and 1 damage–motion pairs were obtained for the first, second and third damage state, respectively. As shown in Figure B.8, data points of the first and second damage states follow a lognormal distribution relatively well with geometric mean and logarithmic standard deviation listed in Table B.7.

Table B.7 Parameters of fragility and loss functions of gypsum-board partitions

Damage Measure (DM)	Description of DM	Fragility parameters		Loss parameters	
		median	Dispersion	median	Dispersion
1	Visible damage and small cracks in gypsum boards that can be repaired with taping, pasting and painting	0.004	0.56	0.12	0.20
2	Extensive crack in gypsum boards that can be repaired with replacing the gypsum boards, taping, pasting and painting	0.008	0.27	0.60	0.20
3	Damage to panels and also frames that can be repaired with replacing gypsum boards and frames, taping, pasting and painting	0.011	0.25	1.2	0.20

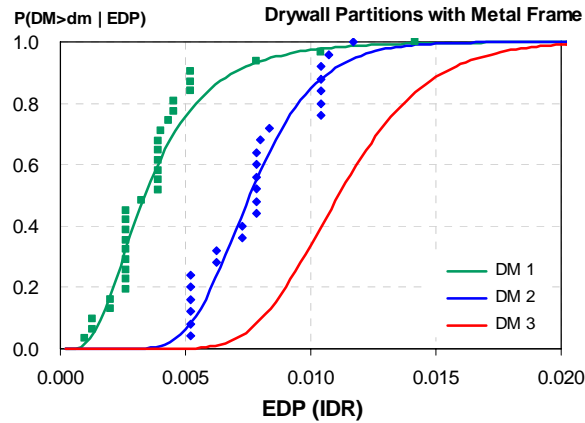


Fig. B.8 Fragility functions of metal stud gypsum board partitions

B.2.2 Fragility Functions for Windows

Fragility curves for windows were provided based on the damage-motion pairs of four experimental studies (Behr and Worrell 1998, Bouwkamp 1960, King and Lim 1991, Wight 1983). A total number of 88 experiments were considered including 62 experiments that caused cracking in glass panels and 26 that caused glass fallout. Based on the recommendation by Czarnecki (1973), the first damage state causing minor damages in frame was considered to be triggered at 50 percent of the drift needed to produce the second damage state. The data points and fitted curves are shown in Figure B.9. Parameters and description of each damage state are listed on Table B.8.

Table B.8 Parameters of fragility and loss functions for sliding windows

Damage Measure (DM)	Description of DM	Fragility parameters		Loss parameters	
		median	Dispersion	median	Dispersion
1	Some minor damages around the frame that can be repaired with realignment of window	0.016	0.29	0.12	0.20
2	Cracking occurs at glass panels but no fallout that can be repaired with replacing of glass panel	0.032	0.29	0.60	0.20
3	Part of glass panels falls out of the frame that can be repaired with replacing of glass panel	0.036	0.27	1.2	0.20

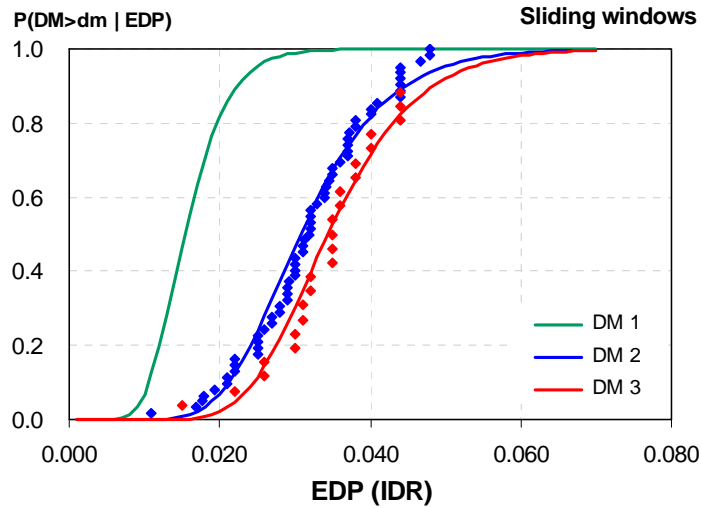


Fig. B.9 Fragility curves of sliding windows

It should be noted that although damage states 2 and 3 have the same repair action and therefore can be assumed as a single damage state, they have been recognized as two damage states because the consequences of damage are different.

B.2.3 Fragility Functions of Suspended Acoustical Ceilings

The fragility curves for acoustical suspended ceilings were developed based on two experimental studies (Rihal and Granneman 1984, Anco 1983). The fragility functions are based on a total of 24 points corresponding to three damage states. Parameters and description of the three damage states are given in Table B.9 and a comparison of the data points with fitted lognormal distribution is shown in Figure B.10.

Table B.9 Description and parameters of fragility curves of acoustical ceilings

Damage Measure (DM)	Description of DM	Fragility parameters		Loss parameters	
		median	Dispersion	Median	Dispersion
1	Hanging wires are splayed and few panels fall down that can be repaired with fixing the hanging wires and replacing the fallen panel	0.27g	0.40	0.12	0.20
2	Damage to some of main runners and cross tee bars in addition to hanging wires that can be repaired with replacing the damaged parts of grid, fallen panels and damaged hanging wires	0.65g	0.50	0.36	0.20
3	Ceiling grid tilts downward (near collapse) that can be repaired with replacing the ceiling and panels	1.28g	0.55	1.2	0.20

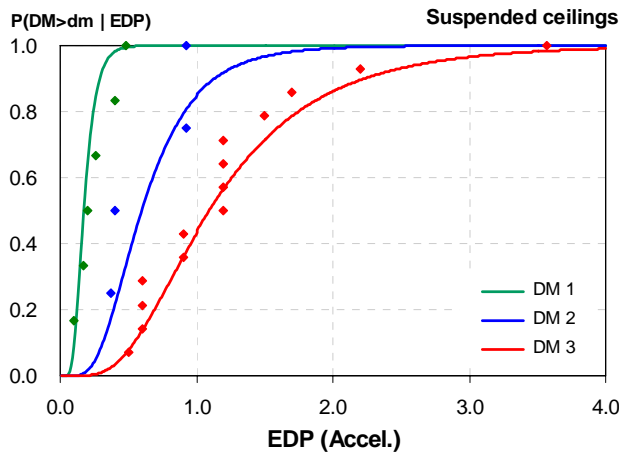


Fig. B.10 Fragility curves of acoustical suspended ceilings

B.2.4 General Fragility Curves for Drift and Acceleration Sensitive Components

Since there is only a very limited number of experimental studies on nonstructural components and many of them do not provide enough information for developing fragility curves, for some of the components of the Van Nuys testbed, two generic fragility curves recommended for nonstructural components in HAZUS (1999) were used. A family of curves is used for

acceleration-sensitive components and a different family of curves is used for drift-sensitive components. Table B.10 summarizes the parameters of the fragility curves for drift sensitive components while parameters for fragility and loss functions for acceleration-sensitive components are given in Table B.11.

Table B.10 Statistical parameters for fragility and loss functions of generic nonstructural drift sensitive components

Damage Measure (DM)	Description of DM	Fragility parameters		Loss parameters	
		median	Dispersion	median	Dispersion
1	Slight damage	0.004	0.50	0.03	0.20
2	Moderate damage	0.008	0.50	0.12	0.20
3	Extensive damage	0.025	0.50	0.60	0.20
4	Complete damage	0.050	0.50	1.20	0.20

Table B.11 Statistical parameters for fragility and loss functions of generic nonstructural acceleration sensitive components

Damage Measure (DM)	Description of DM	Fragility parameters		Loss parameters	
		median	Dispersion	median	Dispersion
1	Slight damage	0.25g	0.60	0.02	0.20
2	Moderate damage	0.50g	0.60	0.12	0.20
3	Extensive damage	1.00g	0.60	0.36	0.20
4	Complete damage	2.00g	0.60	1.20	0.20

Appendix C: Summary of Loss Estimation Methodology

Authors: E. Miranda, H. Aslani

This appendix summarizes the methodology used to estimate the seismic performance of structures quantitatively by continuous variables in terms of economic losses. As described in Section 5.3, the methodology permits the estimation of various different measures of economic losses that can occur in a building.

C.1 EXPECTED LOSS IN A GIVEN SCENARIO

Using the total probability theorem the expected value of the total economic loss in a building conditioned on a ground motion intensity im , $E[L_T | IM = im]$, can be computed as the weighted sum of the expected value of losses when collapse does not occur and of the expected value of losses when collapse occurs, as follows:

$$E[L_T | IM = im] = E[L_T | NC, IM = im] \cdot P(NC | IM = im) + E[L_T | C] \cdot P(C | IM = im) \quad (C.1)$$

where $E[L_T | NC, IM = im]$ is the expected value of the total loss in the building provided that collapse does not occur at a ground motion intensity level im , $P(NC | IM = im)$ is the probability of non-collapse conditioned on IM , $E[L_T | C]$ is the expected loss in the building when global collapse occurs, and $P(C | IM = im)$ is the probability that the structure collapses under a ground motion with a level of intensity im . Since collapse and non-collapse are mutually exclusive damage states, the probability of non-collapse is simply equal to one minus the probability of collapse.

The total economic loss in a building, L_T , is defined as the sum of the loss in the individual components of the building:

$$L_T = LC_1 + LC_2 + LC_3 + LC_4 + LC_5 + LC_6 + LC_7 + \dots + LC_{N-1} + LC_N = \sum_{i=1}^N LC_i \quad (C.2)$$

where LC_i is the loss in the i^{th} component and N is the total number of damageable components in the building. The loss in the i^{th} component, LC_i , can be expressed as:

$$LC_i = a_i \cdot L_i \quad (C.3)$$

where a_i is the mean value of the cost of the i^{th} component and L_i is the cost of repair or replacement of the i^{th} component normalized by a_i . Substituting (C.3) in (C.2), the total economic loss in a building is then computed as:

$$L_T = \sum_{i=1}^N a_i L_i \quad (C.4)$$

Using Equation (C.4), the expected value of the total loss in the building under an earthquake with intensity im at the site and provided that no collapse occurs, $E[L_T | NC, IM = im]$, is given by:

$$E[L_T | NC, IM = im] = E \left[\sum_{i=1}^N (a_i \cdot L_i | NC, IM = im) \right] = \sum_{i=1}^N a_i \cdot E[L_i | NC, IM = im] \quad (C.5)$$

where $E[L_i | NC, IM = im]$ is the expected normalized loss in the i^{th} component given that global collapse has not occurred at the intensity level im .

The expected loss in a given component when no collapse occurs, $E[L_i | NC, IM = im]$, depends on the seismic demands ($EDPs$) imposed to the component and can be computed as:

$$E[L_i | NC, IM = im] = \int_0^{\infty} E[L_i | EDP_i = edp_i] \cdot \left| dP(EDP_i > edp_i | NC, IM = im) \right| \quad (C.6)$$

where $E[L_i | EDP_i = edp_i]$ is the expected loss in the i^{th} component conditioned on the level of imposed demand edp_i , $P(EDP_i > edp_i | NC, IM = im)$ is the probability of exceeding edp_i , in the i^{th}

component given that global collapse has not occurred at the intensity level im . The expected loss in the i^{th} component conditioned on edp , $E[L_i | EDP_i = edp_i]$ is computed as:

$$E[L_i | EDP_i = edp_i] = \sum_{k=1}^m E[L_i | DM_k = dm_k] \cdot P(DM_k = dm_k | EDP_i = edp_i) \quad (C.7)$$

where m is the number of damage states in the i^{th} component (without including loss of vertical carrying capacity), $E[L_i | DM_k = dm_k]$ is the expected value of the normalized cost due to repairs or replacements corresponding to the k^{th} damage state in the i^{th} component and $P(DM_k = dm_k | EDP_i = edp_i)$ is the probability of the i^{th} component being in its k^{th} damage state, dm_k , given that it is subjected to an EDP demand of edp_i .

Various studies (e.g., Aslani and Miranda, 2003) have shown that $P(EDP_i > edp_i | NC, IM = im)$ can be assumed to be lognormally distributed with parameters $\mu_{\ln[EDP_i | IM = im]}$ and $\sigma_{\ln[EDP_i | IM = im]}$. Therefore, it can be written as:

$$P(EDP_i > edp_i | NC, IM = im) = \Phi \left[\frac{\ln(EDP_i) - \mu_{\ln[EDP_i | IM = im]}}{\sigma_{\ln[EDP_i | IM = im]}} \right] \quad (C.8)$$

where $\Phi[]$ is the cumulative normal distribution function, parameter $\mu_{\ln[EDP_i | IM = im]}$ is the median of the EDP conditioned on IM , and $\sigma_{\ln[EDP_i | IM = im]}$ is a measure of dispersion of the EDP conditioned on IM . A robust procedure to estimate $\mu_{\ln[EDP_i | IM = im]}$ and $\sigma_{\ln[EDP_i | IM = im]}$ from simulation results is presented in Miranda and Aslani (2003).

The probability that the i^{th} component will be in the k^{th} damage state given that component has been subjected to an EDP equal to edp is computed as:

$$P(DM_k = dm_k | EDP_i = edp_i) = \begin{cases} P(DM_k > dm_k | EDP_i = edp_i) - P(DM_{k+1} > dm_{k+1} | EDP_i = edp_i) & \text{for } k < m \\ P(DM_k > dm_k | EDP_i = edp_i) & \text{for } k = m \end{cases} \quad (C.9)$$

where $P(DM_k > dm_k | EDP_i = edp_i)$ is the probability of exceeding damage state k in the i^{th} component given that it has been subjected to an EDP equal to edp , $P(DM_{k+1} > dm_{k+1} | EDP_i = edp_i)$ is the probability of exceeding damage state $k+1$ in i^{th} component

given that it has been subjected to an EDP equal to edp . Functions $P(DM_k > dm_k | EDP_i = edp_i)$ and $P(DM_{k+1} > dm_{k+1} | EDP_i = edp_i)$ correspond to the k^{th} and $k^{\text{th}+1}$ fragility functions of the i^{th} component as a function of EDP , which describe the vulnerability or damageability of the i^{th} component with increasing levels of EDP .

The fragility function for the k^{th} damage state in the i^{th} component is assumed to follow a cumulative lognormal distribution with parameters $\mu_{\ln[DM_k|EDP_i]}$, the logarithmic mean of the $EDPs$ associated with the k^{th} damage state in the i^{th} component, and $\sigma_{\ln[DM_k|EDP_i]}$, the logarithmic standard deviation of the $EDPs$. These parameters depend on the damage state and on the type of component.

C.2 EXPECTED ANNUAL LOSS

The expected annual loss in the building, $E[L_T]$, can be computed by integrating $E[L_T | IM = im]$, equation (C.1) over all possible levels of intensity, using the total probability theorem:

$$E[L_T] = \int_0^t \int_0^\infty e^{-\lambda\tau} E[L_T | IM = im] \cdot \left| \frac{dv(IM)}{dIM} \right| dIM d\tau \quad (C.10)$$

where $e^{-\lambda\tau}$ is the discounted factor of the loss over a reference time t , λ is the discount rate per year, $dv(IM)/dIM$ is the derivative of the seismic hazard curve at the site. The time period t can correspond to the design life of a new structure, the remaining life of an existing structure or another reference time period.

C.3 PROBABILITY OF LOSING A CERTAIN DOLLAR AMOUNT IN A GIVEN SCENARIO

The probability of losing a certain dollar amount in a given scenario, $P(L_T > l_T | IM = im)$, can be computed, using the total probability theorem as follows:

$$P(L_T > l_T | IM = im) = P(L_T > l_T | NC, IM = im) \cdot P(NC | IM = im) + P(L_T > l_T | C) \cdot P(C | IM = im) \quad (C.11)$$

where $P(L_T > l_T | NC, IM = im)$ is the probability of exceeding a certain dollar amount l_T , in the building given that collapse has not occurred when the ground motion intensity is equal to im ,

$P(L_T > l_T | C)$ is the probability of exceeding l_T given that global collapse has occurred in the building, and $P(NC | IM = im)$ and $P(C | IM = im)$ are the probability of non-collapse and of collapse, respectively.

As shown in equation (C.11) computing the probability of losing a certain dollar amount conditioned on a ground motion intensity im , requires knowledge of the probability distribution function of the total loss conditioned on non-collapse and IM and of the probability distribution of the total loss when collapse occurs. Although these distributions are, in general, unknown, in many cases, relatively good approximations of $P(L_T > l_T | IM = im)$ can be obtained by making assumptions on its probability distribution, provided that the first and second moments are known. The first and second moments of $P(L_T > l_T | IM = im)$ can be computed as a function of the first and second moments of $P(L_T > l_T | NC, IM = im)$ and $P(L_T > l_T | C)$. In particular, the first moment of $P(L_T > l_T | IM = im)$ can be obtained using equation (C.1) and the variance can be computed as:

$$\begin{aligned} \sigma^2(L_T > l_T | IM = im) &= \sigma^2(L_T | NC, IM = im) \cdot P(NC | IM = im) + \sigma^2(L_T | C) \cdot P(C | IM = im) \\ &+ \{E[L_T | NC, IM = im] - E[L_T | IM = im]\}^2 \cdot P(NC | IM = im) \\ &+ \{E[L_T | C] - E[L_T | IM = im]\}^2 \cdot P(C | IM = im) \end{aligned} \quad (C.12)$$

Alternatively, one can make assumptions on the probability distribution of $P(L_T > l_T | NC, IM = im)$ and on the probability distribution of $P(L_T > l_T | C)$ and compute $P(L_T > l_T | IM = im)$ using (C.11). As shown in Chapter 5, both approaches have been used as part of this investigation with almost identical results.

C.4 DISPERSION OF THE TOTAL LOSS CONDITIONED ON IM

The dispersion of the total loss in the building provided that collapse has not occurred at intensity level im , $\sigma_{[L_T|NC,IM=im]}$, can be computed as a function of the dispersion in the losses of individual components as follows:

$$\sigma_{[L_T | NC, IM = im]} = \left[\sum_{i=1}^N a_i^2 \cdot \sigma_{L_i|NC,IM}^2 + \sum_{i=1}^N \sum_{\substack{j=1 \\ j \neq i}}^N a_i \cdot a_j \cdot \rho_{L_i, L_j|NC,IM} \cdot \sigma_{L_i|NC,IM} \sigma_{L_j|NC,IM} \right]^{1/2} \quad (C.13)$$

where $\sigma_{L_i|NC,IM}^2$ is the variance of the loss in the i^{th} component when collapse has not occurred at intensity level im , and $\rho_{L_i, L_j|NC,IM}$ is the correlation coefficient between the losses in the i^{th} and j^{th} components conditioned on IM when collapse has not occurred.

The variance of the loss in the i^{th} component when collapse has not occurred at intensity level im , is given:

$$\sigma_{L_i|NC,IM}^2 = E[L_i^2 | NC, IM = im] - (E[L_i | NC, IM = im])^2 \quad (C.14)$$

In equation (C.14), the expected loss of the i^{th} component conditioned on non-collapse and IM , $E[L_i | NC, IM = im]$, is computed using equation (C.6), while $E[L_i^2 | NC, IM = im]$ is computed as:

$$E[L_i^2 | NC, IM = im] = \int_0^{\infty} E[L_i^2 | EDP_i = edp_i] \cdot |dP(EDP_i > edp_i | NC, IM = im)| \quad (C.15)$$

Using the total probability theorem, $E[L_i^2 | EDP_i = edp_i]$ can be evaluated in terms of the damage states of i^{th} component using:

$$E[L_i^2 | EDP_i = edp_i] = \sum_{k=1}^m E[L_i^2 | DM_k = dm_k] \cdot P(DM_k = dm_k | EDP_i = edp_i) \quad (C.16)$$

where $E[L_i^2 | DM_k = dm_k]$ can be expanded as:

$$E[L_i^2 | DM_k = dm_k] = \sigma^2 [L_i | DM_k = dm_k] + (E[L_i | DM_k = dm_k])^2 \quad (C.17)$$

where $\sigma^2 [L_i | DM_k = dm_k]$ is the variance of the normalized cost of repairs or replacement corresponding to the k^{th} damage state in i^{th} component.

C.4.1 Dispersion of the Total Loss When Components Losses Are Uncorrelated

If the losses in individual components are assumed to be uncorrelated, then the correlation factors $\rho_{L_i, L_j | NC, IM}$ are equal to zero and the dispersion of the total loss conditioned on IM , (Equation C.13) simplifies to:

$$\sigma[L_T | NC, IM = im] = \left[\sum_{i=1}^N a_i^2 \cdot \sigma_{L_i | NC, IM}^2 \right]^{1/2} \quad (C.18)$$

C.4.2 Dispersion of the Total Loss When Components Losses Are Correlated

If the losses in individual components are assumed to be correlated, then the correlation between the losses in two individual components conditioned on a given intensity level, $\rho_{L_i, L_j | NC, IM}$, should be computed. This correlation coefficient depends on three aspects: (1) the correlation between the losses in two components conditioned on a damage state, $\rho_{L_i, L_j | DM_{ki}, DM_{kj}}$; (2) the correlation between damage states of two components conditioned on a level of structural response, $\rho_{DM_{ki}, DM_{kj} | EDP_i, EDP_j}$; and (3) the correlation between the structural responses (EDPs) that affect both components for a given level of earthquake intensity, $\rho_{EDP_i, EDP_j | IM}$.

The correlation between the losses in two individual components conditioned on a given intensity level, $\rho_{L_i, L_j | NC, IM}$, can be written as:

$$\rho_{L_i, L_j | NC, IM} = \frac{\sigma_{L_i L_j | NC, IM}}{\sigma_{L_i | NC, IM} \sigma_{L_j | NC, IM}} \quad (C.19)$$

where $\sigma_{L_i L_j | NC, IM}$ is the covariance of the loss between the i^{th} and j^{th} components conditioned on IM , when collapse has not occurred. $\sigma_{L_i L_j | NC, IM}$ can be expanded as:

$$\begin{aligned} \sigma_{L_i L_j | NC, IM} \approx & \frac{1}{2} \left[\frac{dE[L_i | EDP_i = edp_i]}{dEDP_i} \right]_{E[EDP_i | NC, IM = im]} \times \left[\frac{dE[L_j | EDP_j = edp_j]}{dEDP_j} \right]_{E[EDP_j | NC, IM = im]} \\ & \times \rho_{EDP_i, EDP_j | NC, IM} \sigma_{EDP_i | NC, IM} \sigma_{EDP_j | NC, IM} + \left[\sigma_{L_i, L_j | EDP_i, EDP_j} \right]_{E[EDP_i | NC, IM = im], E[EDP_j | NC, IM = im]} \end{aligned} \quad (C.20)$$

where $dE[L_i | EDP_i = edp_i] / dEDP_i$ evaluated at $E[EDP_i | NC, IM = im]$, $dE[L_j | EDP_j = edp_j] / dEDP_j$ evaluated at $E[EDP_j | NC, IM = im]$, and $\rho_{EDP_i, EDP_j | NC, IM}$ are obtained using simulation results and the covariance $\sigma_{L_i, L_j | EDP_i, EDP_j}$ is given by:

$$\begin{aligned} \sigma_{L_i, L_j | EDP_i, EDP_j} = & \sum_{ki=1}^{mi} \sum_{kj=1}^{mj} \left\{ \left(\rho_{L_i, L_j | DM_{ki}, DM_{kj}} \sigma_{L_i | DM_{ki}} \sigma_{L_j | DM_{kj}} + E[L_i | DM_{ki} = dm_{ki}] E[L_j | DM_{kj} = dm_{kj}] \right) \right. \\ & \times P(DM_{ki} = dm_{ki}, DM_{kj} = dm_{kj} | EDP_i = edp_i, EDP_j = edp_j) \left. \right\} \\ & - \left\{ \sum_{ki=1}^{mi} E[L_i | DM_{ki} = dm_{ki}] P(DM_{ki} = dm_{ki} | EDP_i = edp_i) \right\} \\ & \times \left\{ \sum_{kj=1}^{mj} E[L_j | DM_{kj} = dm_{kj}] P(DM_{kj} = dm_{kj} | EDP_j = edp_j) \right\} \end{aligned} \quad (C.21)$$

As shown in equation (C.21), estimation of the covariance $\sigma_{L_i, L_j | EDP_i, EDP_j}$ requires knowledge of the correlation between the losses in two components conditioned on a damage state, $\rho_{L_i, L_j | DM_{ki}, DM_{kj}}$, and of the joint probability distribution of DM given EDP , $P(DM_{ki} = dm_{ki}, DM_{kj} = dm_{kj} | EDP_i = edp_i, EDP_j = edp_j)$. In this investigation $\rho_{L_i, L_j | DM_{ki}, DM_{kj}}$ is obtained from the correlation of construction costs of different subcontractors. In order to estimate the joint probability distribution of damage in two different components conditioned on EDP , two extreme cases are considered. The damages to components that are identical are assumed to be fully correlated while the damages to components that are not identical are assumed to be uncorrelated. The effects of intermediate levels of correlation at the damage given EDP level are currently also being investigated (Aslani and Miranda 2004).

C.4.2.1 Joint Probability of Damage in Components That Are Not Identical

This case includes those components that are of different types and are subjected to either different levels of EDP or same levels of EDP . For example, a slab-column connection in the third story and a window in the third story, or a slab-column connection in the third story and a window in the fourth story. For these components it is assumed that the probability of the i^{th} component being at a damage state DM_{ki} , conditioned on EDP_i is not correlated with the probability of the j^{th} component being at a damage state DM_{kj} , conditioned on EDP_j . Therefore, the joint probability distribution of DM given EDP can be computed as:

$$P(DM_{ki}=dm_{ki}, DM_{kj}=dm_{kj} | EDP_i=edp_i, EDP_j=edp_j) = P(DM_{ki}=dm_{ki} | EDP_i=edp_i) \times P(DM_{kj}=dm_{kj} | EDP_j=edp_j) \quad (C.22)$$

Substituting equation (C.22) in (C.21) the covariance of the loss between components i and j conditioned on EDP can then be computed as:

$$\sigma_{L_i, L_j | EDP_i, EDP_j} = \sum_{ki=1}^{mi} \sum_{kj=1}^{mj} \left\{ \rho_{L_i, L_j | DM_{ki}, DM_{kj}} \sigma_{L_i | DM_{ki}} \sigma_{L_j | DM_{kj}} \right. \\ \left. \times P(DM_{ki}=dm_{ki} | EDP_i=edp_i) P(DM_{kj}=dm_{kj} | EDP_j=edp_j) \right\} \quad (C.23)$$

C.4.2.2 Joint Probability of Damage in Identical Components

This case includes those components that are of the same type with exactly the same damage states and precisely the same fragility parameters at each damage state, imposed to the same levels of EDP . For example, the damage in two interior columns that have exactly the same gravity load, geometry, concrete strength and reinforcement, located in the third story are considered to be in the *fully correlated* category. For this category, we assume that the joint probability of the i^{th} component being at a damage state DM_{ki} conditioned on EDP_i and the j^{th} component being at a damage state DM_{kj} conditioned on EDP_j , when k^i is not equal to k^j , is 0.

On the basis of the above assumptions, we can simplify the joint probability distribution $P(DM_{ki}=dm_{ki}, DM_{kj}=dm_{kj} | EDP_i=edp_i, EDP_j=edp_j)$ as:

$$P(DM_{ki}=dm_{ki}, DM_{kj}=dm_{kj} | EDP_i=edp_i, EDP_j=edp_j) = \begin{cases} P & \text{if } ki=kj=k \\ 0 & \text{if } ki \neq kj \end{cases} \quad (C.24)$$

where

$$P = P(DM_{ki}=dm_{ki} | EDP_i=edp_i) = P(DM_{kj}=dm_{kj} | EDP_j=edp_j) \quad (C.25)$$

Substituting (C.24) and (C.25) in the right-hand side of (C.21), the covariance of the loss between components i and j conditioned on EDP for identical components is given by:

$$\begin{aligned} \sigma_{L_i, L_j | EDP_i, EDP_j} = & \sum_{k=1}^m \left(\sigma_{L_i | DM_k}^2 + (E[L_i | DM_k = dm_k])^2 \right) P(DM_k = dm_k | EDP_i = edp_i) \\ & - \left(\sum_{k=1}^m E[L_i | DM_k = dm_k] P(DM_k = dm_k | EDP_i = edp_i) \right)^2 \end{aligned} \quad (C.26)$$

It should be noted that correlation coefficients $\rho_{L_i, L_j | DM_{ki}, DM_{kj}}$ and $\rho_{EDP_i, EDP_j | NC, IM}$ are typically positive, therefore it can be seen from equations (C.13), (C.20) and (C.21) that the effect of correlations between the losses in individual components will typically produce an increase in dispersion of the total loss.

C.5 PROBABILITY OF LOSING A CERTAIN DOLLAR AMOUNT IN ANY GIVEN YEAR

The mean annual frequency (MAF) of a certain dollar loss can be computed by integrating $P[L_T > l_T | IM = im]$, equation (C.11), over all possible levels of intensity as follows:

$$v[L_T > l_T] = \int_0^{\infty} P[L_T > l_T | IM = im] \cdot \left| \frac{dv(IM)}{dIM} \right| \cdot dIM \quad (C.27)$$

For values smaller than 0.01, the mean annual frequency of exceedance of a loss l_T is approximately equal to the probability of losing more than a certain dollar amount l_T in any given year, $P[L_T > l_T]$. Hence, (C.27) can be rewritten as:

$$P[L_T > l_T] \approx \int_0^{\infty} P[L_T > l_T | IM = im] \cdot \left| \frac{dv(IM)}{dIM} \right| \cdot dIM \quad (C.28)$$

Appendix D: Fatality Model for Non-ductile Concrete Frame Structures Developed from Gölcük Population Survey Data

Authors: K. Shoaf, H. Seligson, M. Ramirez, M. Kano

This appendix describes the development of a fatality model for non-ductile concrete frame structures, similar to the Van Nuys Test Bed, from population-based survey data collected in Gölcük, Turkey, following the Kocaeli Earthquake of August 17, 1999. Fatalities are a key decision variable (DV) included in the PEER methodology, and their estimation is dependent on the damage measure (DM) defined as “building collapse.”

D.1 DATA COLLECTION

Data were gathered by Ms. Marla Petal of the Bagazici University, Kandilli Observatory and Earthquake Research Institute. A survey of households was conducted utilizing a standardized questionnaire designed by the UCLA Center for Public Health and Disasters and adapted for local use by Ms. Petal. The questionnaire was designed to gather information from an affected population in a format that would be usable by both epidemiology and engineering researchers in loss estimation modeling. Data were gathered by interviewing the most knowledgeable person in the household (usually the mother). Interviews were conducted by trained graduate students between March and June 2001, 19–21 months after the earthquake.

The questionnaire included questions about the household and all of the individuals living in that household. Categories of questions include damage to the household and neighborhood; injuries sustained by members of the household; activity of members of the household at the time of the earthquake; and demographic characteristics of the household.

A representative sample of 453 households were selected from the city of Gölcük. The sample was selected using random sampling methodologies from each of two locations. About half of the sample (204 households) came from the temporary housing provided for those families from Gölcük whose homes had been classified as damaged beyond repair. The remaining 53% of the households were sampled from buildings within the city that had either been continuously occupied since the earthquake, or had been repaired and re-occupied.

D.1.1 Characteristics of the Survey Sample

The 453 households in the sample include 1,861 individuals. The average household size was four (4), with 7% of the households having only one member and 12% having 6 or more members. The mean age of household members was 29.6, with respondents (heads of households) having a mean age of 40.8 and other household members being younger (mean = 26.8 years). Household members' ages ranged from 0 – 92 years, with 31% of the individuals being 18 years of age and under and 4% being 65 years of age and older (see Table D.1). Slightly more than half of the sample (51%) was female. Respondents were more likely to be female, 66% of those who responded as the “most knowledgeable” for the rest of the household were female.

Table D.1 Age distribution of individuals in sample

Age category	Frequency	Percent
18 and under	577	31.0
19–64	1090	58.6
65 and over	75	4.0
Missing	119	6.4
Total	1861	100.0

The majority of households (80.1%) reported that they lived in concrete buildings (Table D.2). The average age of the buildings in which these households resided was 18.5 years, with the newest buildings having been constructed in 1999 and the oldest having been built 148 years earlier. Concrete buildings were significantly newer than other types, with the average age of

concrete buildings being 14.7 years. Wood construction was the oldest type, with the average age of wood buildings being 58.4 years. About 45% of families lived in buildings that had four or fewer floors, with the tallest buildings having 10 floors. Concrete buildings were more likely to have 5 or more floors, with 67% of those in concrete buildings reporting their buildings as having 5 or more floors. Only 7% of those in masonry, and 13% of those in wood buildings reported that the building had 5 or more floors.

Table D.2 Distribution of construction of buildings

Type of construction	Frequency	Percent
Wood	16	3.5
Steel	4	0.9
Concrete	363	80.1
Bricks/Masonry	70	15.5
Total	453	100.0

D.1.2 Impact of the Earthquake on the Survey Sample

Close to 80% of households reported damage to their homes as a result of the earthquake. Those households in brick (81%) and concrete buildings (83%) were most likely to report damage to their homes, with slightly more than 50% of those in wood, and 26% of those in steel buildings reporting damage. Overall, 30% of families reported damage that was classified as partial or total collapse of the building. When looking at type of building, those in concrete buildings were more likely to report damage that was classified as partial or total collapse of the building. Thirty-five percent (35%) of those families in concrete buildings reported collapse, whereas 25% of those in wood and steel buildings reported collapse and only 7% of those in masonry buildings. Taller buildings were also more likely to suffer collapse, with 76% of those buildings with 5 or more floors having collapse and only 47% of shorter buildings. In a report on the earthquake, Sahin and Tari [2000] reported 12,310 collapsed or heavily damaged housing units, 7,789 moderately damaged housing units, and 9,299 slightly damaged housing units in Golcuk.

In 1999, there were approximately 80,000 residents living in Golcuk. This suggests that all households suffered damage to their home, with about a third suffering collapse or heavy damage, similar to that which is demonstrated here in this study.

In total, 38 individuals (2.0% of individuals) died in 22 households (4.9% of households). An additional 251 individuals were reported injured (13.5%) in 147 households (32.5%). Thirteen households reported one member of the family had died in the earthquake, five households reported two deaths, three reported three deaths, and one household had six members of the family die in the earthquake. Those under the age of 18 were more likely to die than either those 19-64 or those over the age of 65. Those aged 19–64 had a higher injury rate than those younger or older than them (Table D.3). Sahin and Tari [2000] reported that 5025 people died in Gölcük during the earthquake, this translates to a mortality rate of about 6%. This study produces a mortality rate of about 2% of individuals. However, approximately 5% of households suffered one or more deaths. Since this study obviously could not interview members of households where all of the members died, any analyses here will be a low estimate of mortality.

Table D.3 Distribution of injury/death across age categories

Age category	Frequency of injured or killed			Total
	Not injured/killed	Injured	Killed	
18 and under	522 (90.5%)	36 (6.2%)	19 (3.3%)	577 (100.0%)
19-64	908 (83.3%)	167 (15.3%)	15 (1.4%)	1090 (100.0%)
65 and over	65 (86.7%)	9 (12.0%)	1 (1.3%)	75 (100.0%)
Total*	1495 (85.8%)	212 (12.2%)	35 (2.0%)	1742 (100.0%)

**n*=119 excluded for missing information on injury or death status.

D.2 METHODS

The study population for our analyses was defined as individuals who were reportedly in concrete buildings that either partially or totally collapsed during the earthquake (*n*=517). This represents 28% (517/1861) of the total survey sample. Some of the individuals belonged to the same household, so that the 517 individuals used in our analyses represent 128 households. Information is not available on how many buildings were in the survey sample.

To create multivariate causal models of fatality, two levels of information on the subjects were taken from the surveys: individual characteristics and building characteristics. Individual characteristics included demographics, such as age and gender, behavior during the earthquake, physical location within damaged buildings, and physical injury or death due to the earthquake. Building characteristics included building height and extent of collapse. Information about the members of the household, except for the household respondent, was obtained indirectly from the household respondent. Thus, while the demographic information provided by the household respondent is expected to be accurate, the information regarding behavior and physical location within the building during the earthquake may not be as accurate. In addition, households in which all members had died are not represented in our sample because no respondent was available for those households.

Buildings were characterized according to number of floors and extent of building collapse. Building collapse was defined as either “partial collapse” or “total collapse, ” depending on responses to a series of questions in the interview about damage to the respondent’s building. The respondents were asked to respond “yes” or “no” to each questionnaire item addressing each of the following damage descriptors (with collapse-related damage descriptors indicated with an asterisk):

1. Personal property broken
2. Entire building destroyed *
3. Foundation destroyed
4. Building off foundation
5. House walls damaged
6. House walls collapsed *
7. Chimney damaged
8. Chimney collapsed
9. Ceiling/roof damaged
10. Ceiling/roof collapsed *
11. Water pipes broke
12. Water heater damaged/destroyed
13. Gas lines broken
14. Floors damaged

- 15. Floors collapsed *
- 16. Patio/porch damaged
- 17. Fences/fence wall damaged
- 18. Driveway damaged/destroyed
- 19. Garage damaged/destroyed

Various combinations of “yes” responses were used to identify respondents in buildings considered to have suffered partial or total collapse, as given in Table D.4. It should be noted that in order for the building to be assumed to have suffered “total collapse,” the respondent must have responded yes to the item “Entire building destroyed,” but could also answer yes to the other collapse-related questions. It was also assumed that foundation destruction, in the absence of other reported collapse damage, could occur due to fault rupture or ground failure, and was therefore not assumed to be indicative of either total or partial collapse when reported on its own. Because the typical wall construction was masonry infill, wall collapse was also not assumed to be indicative of either total or partial collapse when reported on its own.

Table D.4 Survey responses used to categorize buildings as having suffered “Partial Collapse” and “Total Collapse”

Partial Collapse	Total Collapse
“Ceiling/roof collapsed”	“Entire building destroyed”
“Ceiling/roof collapsed” + “Foundation destroyed”	“Entire building destroyed” + “Foundation destroyed”
“Floors collapsed”	“Entire building destroyed” + “Ceiling/roof collapsed”
“Floors collapsed” + “Foundation destroyed”	“Entire building destroyed” + “Foundation destroyed” + “Ceiling/roof collapsed”
“Ceiling/roof collapsed” + “Floors collapsed”	“Entire building destroyed” + “Foundation destroyed” + “Floors collapsed”
“Ceiling/roof collapsed” + “Floors collapsed” + “Foundation destroyed”	“Entire building destroyed” + “Ceiling/roof collapsed” + “Floors collapsed”
	“Entire building destroyed” + “Foundation destroyed” + “Ceiling/roof collapsed” + “Floors collapsed”

D.2.1 Cases and Fatality Rate Calculations

Cases were defined as subjects who were reported to have died from physical trauma sustained during the earthquake. Fatality rates were calculated by dividing the number of cases, a , by the population at risk, n . Assuming the rate is a good estimate of the risk, when the outcome is rare, this measurement can be interpreted as a probability or risk of death. For example, to estimate the fatality rate in partially collapsed building structures, we divided the number of fatalities reported in partially collapsed buildings by the total number of subjects reported to have lived in a building that sustained partial collapse during the earthquake:

$$a/n = 3/200 = 0.015 \quad (\text{D.1})$$

This figure, 0.015, can then be multiplied by 100 to obtain a rate of 1.5 fatalities per 100 people.

Because of small sample sizes, we could not separately model rates of injury for every age and building category. Therefore, we grouped subjects into four age categories, 0–9, 10–19, 20–39, 40 and above, and examined fatality rates across these age groups. We found no substantial differences in the rates between the 0–9 and 10–19 groups, and between the 20–39 and 40 and above groups. Therefore, we present rates in two age categories, 19 or younger and 20 or older. We also estimated rates separately for buildings with one to four floors and for buildings with five to ten floors. These two categories of floors were selected because of prior knowledge that construction differences by number of floors impact building collapse patterns.

D.2.2 Modeling a Rate Multiplier

We present two methods to calculate a rate multiplier for death.

The first method involves use of stratified analysis to analyze rate ratios. We separated data into several strata of interest and calculated rates within each stratum. Then, we divided the rate in one stratum (the index stratum) with the rate in another (the reference stratum). If, for example, we are interested in calculating the rate ratio comparing gender groups, and the rate for females is 3/100 and the rate for males is 1.4/100, the rate ratio is then 2.14, meaning the rate of females is more than twice the rate of males.

The second method involves the estimates of odds ratios (ORs), which are epidemiologic measures of association between a variable of interest, for example, gender, and an outcome, in

this study, death. If the outcome is rare, (i.e., less than 10%), then the ORs can estimate the rate ratio. So, for a rare outcome, an odds ratio of 2 for gender, using males as the reference group, means that females have twice the death rate of males.

To estimate rate ratios, we used conventional logistic regression to model a binary outcome (fatal vs non-fatal) comparing age groups. This model fits a logistic curve to the outcome using predictor variables. The exponentiated value of the beta estimate from this regression model is the estimated odds ratio. Ninety-five percent confidence intervals were also calculated as measurements of the precision of our estimates. All regression models were calculated using SPSS v.11.5.

By modeling, we can adjust for multiple confounders, which are variables that may distort odds ratio estimates. This bias occurs because confounders are risk factors for the outcome, but are also mathematically associated with the primary predictor variable. For example, suppose we estimate a death rate ratio of 2 comparing females to males. Suppose age is an independent risk factor for death (i.e., older people are at higher risk for death than younger people) and in our study sample we have more older women than men. If we do not account for the distribution of age in our model, we are not sure if our estimate of 2 reflects the effect of age or the effect of gender or a combination of both. In regression modeling, we can adjust analytically for age and gender in the same analysis and estimate separate independent effects.

Conversely, we can use the rate multiplier for gender to solve for rate estimates specific for males and females. For example, we estimate the fatality rate of males to be 1.5/100. Then, we can multiply the male fatality rate by the rate ratio (a rate multiplier) for gender, 2 in our example, and calculate the rate for females, i.e., $1.5 \times 2 = 3.0$.

This algebraic solution is appropriate if all estimates originated from the same population or the populations share similar causal pathways to death.

D.3 RESULTS

D.3.1 Characteristics of the Analysis Sample

Table D.5 shows the characteristics of the sample subset used for analyses. It includes 517 individuals belonging to 128 households that were in concrete buildings that suffered partial or

total collapse as a result of the earthquake. The unit of analysis for the following analyses is the individual ($n = 517$).

Table D.5 Characteristics of the sample subset ($n = 517$)

Parameter	Categories	% (n)
Age	0-9	13.2 (68)
	10-19	20.7 (107)
	20-39	28.9 (149)
	40-59	25.5 (132)
	60+	4.8 (25)
	Missing	7.0 (36)
Gender	Female	51.8 (268)
	Male	48.2 (249)
	Missing	0.0 (0)
Event outcome	Fatal	7.2 (37)
	Non-fatal	92.8 (480)
	Missing	0.0 (0)
Occupant's movement during earthquake	Moved	28.6 (148)
	Did not move	59.4 (307)
	Missing	12.0 (62)
Type of building collapse	Partial collapse	38.7 (200)
	Total collapse	61.3 (317)
	Missing	0.0 (0)
Building height	1-4 floors	21.1 (109)
	5-10 floors	78.9 (408)
	Missing	0.0 (0)
Occupant's floor location within building	Ground floor	15.7 (81)
	Upper floor	58.6 (303)
	Missing	25.7 (133)

The majority of the sample (62.8%) was younger than 40 years old. The gender distribution was about equal. Those who were reported to have sustained fatal injuries during the earthquake comprised 7.2% of the sample. Those who reportedly moved during the earthquake were 28.6% of the sample. In terms of building characteristics, 61.3% of the sample had been in buildings that suffered total collapse as a result of the earthquake, 78.9% had been in buildings with a height of 5 or more floors, and 58.6% had been in the upper floors of the buildings, as opposed to the ground floor.

D.3.2 Fatality Rates Associated with Partial or Total Building Collapse

Table D.6 shows the fatality rates by type of building collapse. The rates are for per 100 people at risk, the cases are the actual number of fatalities that were reported, and the *n* indicates the number of people who were at risk under each specified condition.

Table D.6 Fatality rates by partial or total building collapse

	Rate per 100	Cases	<i>n</i>
Partial collapse	1.5	3	200
Total collapse	10.7	34	317

The fatality rate in buildings that suffered partial collapse was 1.5 per 100 compared to 10.7 per 100 in buildings that suffered total collapse.

D.3.3 Fatality Rates Associated with Demographic Characteristics

Table 7 shows the fatality rates by gender, conditional on building collapse. In buildings that suffered partial collapse, the fatality rate among females was 3.2 per 100 compared to 0 per 100 among males. In buildings that suffered total collapse, the fatality rate among females was 11 per 100 compared to 10.4 per 100 among males. Overall, the fatality rate among females was 8.2 per 100 compared to 6.0 per 100 among males.

Table D.7 Fatality rates by gender and type of building collapse

	Partial collapse			Total collapse			Total		
	Rate per 100	Cases	<i>n</i>	Rate per 100	Cases	<i>n</i>	Rate per 100	Cases	<i>n</i>
Female	3.2	3	95	11.0	19	173	8.2	22	268
Male	0.0	0	105	10.4	15	144	6.0	15	249

Table D.8 shows the fatality rates by age group conditional on type of building collapse. In buildings that partially collapsed, the fatality rate was 0 per 100 regardless of age group. In buildings that totally collapsed, the fatality rate was 19.6 per 100 among children and adolescents 0–19 years old, compared to 6.5 per 100 among adults 20 years and older. Overall, people 19 and younger had a fatality rate of 12.6 per 100 compared to 3.9 per 100 among adults of ages 20 and over.

Table D.8 Fatality rates by age group and type of building collapse*

	Partial collapse			Total collapse			Total		
	Rate per 100	Cases	<i>n</i>	Rate per 100	Cases	<i>n</i>	Rate per 100	Cases	<i>n</i>
0-19	0.0	0	63	19.6	22	112	12.6	22	175
20+	0.0	0	122	6.5	12	184	3.9	12	306

**n*=36 excluded from analyses for missing data on age.

D.3.4 Fatality Rates Associated with Movement during the Earthquake

Table D.9 shows the fatality rates by occupant’s movement during the earthquake conditional on type of building collapse. In buildings that partially collapsed, the fatality rate was 0 per 100 for those who reportedly moved during the earthquake compared to 2.2 per 100 for those who reportedly did not or could not move during the earthquake. In buildings that totally collapsed,

the fatality rate was 4.9 per 100 for those who reportedly moved, compared to 12.8 per 100 for those who reportedly did not move. Overall, those who reportedly moved during the earthquake had a fatality rate of 2.7 per 100 compared to 9.1 per 100 for those who reportedly did not move.

Table D.9 Fatality rates by movement during the earthquake and type of building collapse*

	Partial collapse			Total collapse			Total		
	Rate per 100	Cases	<i>n</i>	Rate per 100	Cases	<i>n</i>	Rate per 100	Cases	<i>n</i>
Moved	0.0	0	80	4.0	4	100	2.2	4	180
Did not move	2.7	3	112	12.8	25	195	9.1	28	307

**n*=30 excluded from analyses for missing data on movement during earthquake

Of those who reportedly moved when the earthquake started, the majority reported moving within the building (e.g., to a different room, to a doorway, under furniture), while only about a fifth of them (41/179) reported moving outside of the building. Table D.10 shows the fatality rates by whether the occupant moved outside the building or not, conditional on the occupant's floor location within the building and type of building collapse.

Table D.10 Fatality rates by movement during the earthquake and type of building collapse*

	Partial collapse			Total collapse		
	Rate per 100	Cases	<i>n</i>	Rate per 100	Cases	<i>n</i>
Ground floor						
Moved outside	0.0	0	8	0.0	0	11
Stayed inside	0.0	0	3	6.9	4	58
Upper floor						
Moved outside	0.0	0	12	0.0	0	7
Stayed inside	0.0	0	128	15.6	20	128

**n*=162 excluded listwise for missing data

Among those people who reported moving outside of the building, none of them had a fatal outcome. About 24% (19/80) of those who were on the ground floor moved outside the building, while only 7% (19/275) of those on the upper floors moved outside. The fatality rate for those who stayed on the upper floors of totally collapsed buildings was 15.6 per 100, compared to 6.9 per 100 for those who stayed on the ground floor of totally collapsed buildings.

D.3.5 Fatality Rates Associated with Building Height

Table D.11 shows the fatality rates by the height of the buildings conditional on the type of building collapse. The fatality rates in buildings with 1–4 floors were 0 per 100, regardless of the type of building collapse. In buildings with 5–10 floors, the fatality rate was 2 per 100 in partially collapsed buildings, 13.1 per 100 in totally collapsed buildings, and 9.1 per 100 overall.

Table D.11 Fatality rates by building height and by type of building collapse

	Partial collapse			Total collapse			Total		
	Rate per 100	Cases	<i>n</i>	Rate per 100	Cases	<i>n</i>	Rate per 100	Cases	<i>n</i>
1-4 floors	0.0	0	51	0.0	0	58	0.0	0	109
5-10 floors	2.0	3	149	13.1	34	259	9.1	37	408

Table D.12 shows the fatality rates by the occupant’s floor location within the building conditional on the type of building collapse.

Table D.12 Fatality rates by occupant’s floor location within building and type of building collapse*

	Partial collapse			Total collapse			Total		
	Rate per 100	Cases	<i>n</i>	Rate per 100	Cases	<i>n</i>	Rate per 100	Cases	<i>n</i>
Ground floor	0.0	0	11	5.7	4	70	4.9	4	81
Upper floors	0.0	0	149	16.2	25	154	8.3	25	303

**n*=133 excluded for missing data on occupant’s floor location within building

In buildings that suffered partial collapse, the fatality rates were 0 per 100 regardless of the occupant’s floor location within the building. In buildings that suffered total collapse, the fatality rate was 5.7 per 100 for those who had been on the ground floor, and 16.2 per 100 for those who had been on the upper floors. Overall, the fatality rate for those who had been on the ground floor was 4.9 per 100, and 8.3 per 100 for those who had been on upper floors.

D.3.6 Multi-Parameter Model of Fatality Rates

The parameters included in the final model are extent of building collapse (total vs. partial collapse), building height (1–4 vs. 5–10 floors), and the floor location of the occupant (ground floor vs. upper floors). Although movement during the earthquake was found to have a protective effect against death, it is not included in the final model because there are not enough data to support the definition of movements that tend to be protective. Table D.13 shows the fatality rates according to the parameters included in the final model, that is, fatality rates by occupant’s floor location within the building, conditional on building height and type of building collapse.

Table D.13 Fatality rates by occupant’s floor location, conditional on building height and type of building collapse

	Partial collapse			Total collapse		
	Rate per 100	Cases	<i>n</i>	Rate per 100	Cases	<i>n</i>
1-4 floor building						
Ground floor	0.0	0	7	0.0	0	12
Upper floors	0.0	0	3	0.0	0	19
5-10 floor building						
Ground floor	0.0	0	4	6.9	4	58
Upper floors	0.0	0	113	18.5	25	135

**n*=133 excluded listwise for missing data

In buildings that suffered partial collapse, the fatality rates were 0 per 100 regardless of the occupant’s floor location within the building or the height of the building. Similarly, the fatality rate in buildings with 1–4 floors that suffered total collapse was also 0 per 100, regardless of the occupant’s floor location or the type of building collapse. In buildings with 5–10 floors that totally collapsed, the fatality rate was 6.9 per 100 for those who had been on the ground floor, compared to 18.5 for those who had been on the upper floors of those buildings.

D.3.7 Odds Ratios

As the difference in fatality risks by age group was quite large, we calculated an odds ratio for age that can be applied to fatality rates to account for the age-related risks. Table D.14 shows the fatality odds ratio for age, comparing 0–19 year-olds to those 20 and above.

Table D.14 Fatality odds ratio for age*

<i>Parameter (Indicator category)</i>	<i>n</i>	<i>Odds Ratio</i>	<i>95% Confidence Interval</i>	
Age group (0-19 year-olds)	481*	3.5	1.70	7.31

**n*=36 excluded for missing data on age

The crude odds ratio of 3.5 for age, with the 0–19 year-old group as the indicator category, means that 0–19 year-olds have 3.5 times the fatality rate of those who are 20 years or older, not accounting for other factors. This odds ratio can be used to multiply the fatality rates for 20+ year-olds to estimate the fatality rates for those who are 19 years old or younger, under the same specified conditions.

For example, Table D.15 shows the fatality rates for 0–19 year-olds and for those 20 and above, conditional on occupant’s floor location in a 5–10 floor building that totally collapsed. The fatality rates for the 0-19 year-old group is approximately 3 to 3.5 times the fatality rates for the 20+ year-old group across all conditions.

Table D.15 Fatality rates by age group conditional on occupant’s floor location within a 5–10 floor building that totally collapsed

	Totally collapsed buildings with 5-10 floors								
	Ground floor			Upper floor			Total		
	Rate per 100	Cases	<i>n</i>	Rate per 100	Cases	<i>n</i>	Rate per 100	Cases	<i>n</i>
0-19 years old	14.3	2	14	30.9	17	55	27.5	19	69
20+ years old	4.5	2	44	10.0	8	80	8.1	10	124

D.4 COMPARISON TO OTHER CASUALTY MODELS

The fatality model developed from the Golcuk survey data may be compared to previously published engineering-based casualty estimation models, such as those in ATC-13 and those incorporated into the HAZUS software.

The casualty estimation model presented in *ATC-13: Earthquake Damage Evaluation Data for California* [ATC, 1985] consists of tabulated injury and death rates related to a building’s level of damage, or damage state — an approach first proposed by Whitman [see Whitman et al., 1974]. The ATC-13 rates, given in Table D.16 with the ATC-13 damage state definitions, represent a combination of the historic statistics (updated from earlier NOAA work), other engineering models (Whitman), and “judgmental evaluation” [ATC, 1985]. The rates as tabulated appear to rely heavily on the earlier NOAA work, reflecting the 4:1 ratio of serious injuries to deaths, and 30:1 ratio of minor injuries to deaths used by the NOAA loss estimation studies [NOAA, 1972 and NOAA, 1973]. It should be noted that the casualty rates are independent of structural type (with the exception of a rate reduction for wood and light steel structures), and depend solely on the building’s damage state. It is also interesting to note that the ATC-13 model assumes that all occupants of “Destroyed” buildings suffer at least minor injury (i.e., the rates for minor and serious injuries and deaths sum to 1.0), but that only 35% of occupants of buildings suffering “Major” damage will be injured or killed, leaving 65% unharmed.

Table D.16 ATC-13 injury and death rates* (after Table 9.3, ATC, 1985)

	Damage State	Range	Minor Injuries	Serious Injuries	Dead
1	None	0	0	0	0
2	Slight	0-1	3/100,000	1/250,000	1/1,000,000
3	Light	1-10	3/10,000	1/25,000	1/100,000
4	Moderate	10-30	3/1,000	1/2,500	1/10,000
5	Heavy	30-60	3/100	1/250	1/1,000
6	Major	60-100	3/10	1/25	1/100
7	Destroyed	100	2/5	2/5	1/5

* For light steel and wood-frame construction, multiply all numerators by 0.1.

For comparison with the survey fatality model for non-ductile concrete frame (NDCF) structures, the ATC-13 damage states “Major” and “Destroyed” are of interest. Here we assume that our definition of partial collapse would roughly correspond to “Major” damage, while total collapse would correspond to “Destroyed.” The overall fatality rates for partial and total collapse of NDCF structures, as reported in Table D.6, are 1.5% and 10.7% respectively, regardless of building height or occupant location. When building height is considered, the fatality rate for total collapse increases to 13.1% (Table D.11) for mid-rise structures, and when occupant location is included, the rate increases further to 16.2% for occupants of upper floors of mid-rise structures (Table D.12). The survey-based fatality rate for partial collapse (1.5%) agrees well with the equivalent ATC-13 rate for “Major” damage (1%), while the fatality rate for total collapse (10.7% to 16.2%) is slightly lower but of the same order of magnitude as the equivalent rate for “Destroyed” (20%). (This rate comparison is summarized in Table D.19.)

The casualty estimation model within HAZUS® (the standardized, nationally applicable earthquake loss estimation methodology and software developed by NIBS for FEMA) also relates casualty rates to building damage state, although with its own unique definitions for both injury severity and damage state. HAZUS® estimates building damage expressed in terms of the probability of a building being in any of four damage states; Slight, Moderate, Extensive and Complete, with a range of damage factors (repair cost divided by replacement cost) associated with each damage state (see Table D.17).

**Table D.17 HAZUS® Earthquake loss estimation methodology casualty rates
(HAZUS®99, SR-2)**

Damage State	Damage Factor	CASUALTY SEVERITY LEVEL			
		Severity 1 (%)	Severity 2 (%)	Severity 3 (%)	Severity 4 (%)
Slight	0-5%	0.05	0	0	0
Moderate	5-20%	0.2 – 0.25 (URM* = 0.35)	0.025 – 0.030 (URM = 0.40)	0 (URM = 0.001)	0 (URM = 0.001)
Extensive	20-50%	1.0 (URM = 2.0)	0.1 (URM = 0.2)	0.001 (URM = 0.002)	0.001 (URM = 0.002)
Complete (No Collapse)	50-100%	5.0 (URM = 10.0)	1.0 (URM = 2.0)	0.01 (URM = 0.02)	0.01 (URM = 0.02)
Complete (With Collapse)	50-100%	40.0	20.0	5.0 (LRWF* = 3.0, MH* = 3.0, SLF* = 3.0)	10.0 (LRWF = 5.0, MH = 5.0, SLF = 5.0)

Notes: URM = unreinforced masonry
 LRWF = low-rise wood frame
 MH = mobile home
 SLF = steel, light frame structures

Four severity levels are used to categorize injuries [NIBS/FEMA, 2002], as described in Table D.18.

Table D.18 HAZUS® Earthquake loss estimation methodology injury severity class definitions (HAZUS®99, SR-2)

Severity	Description
Severity 1	“Injuries requiring basic medical aid that could be administered by paraprofessionals. These types of injuries would require bandages or observation. Some examples are: a sprain, a severe cut requiring stitches, a minor burn (first degree or second degree on a small part of the body), or a bump on the head without loss of consciousness. Injuries of lesser severity that could be self treated are not estimated by HAZUS.”

Severity 2	“Injuries requiring a greater degree of medical care and use of medical technology such as x-rays or surgery, but not expected to progress to a life threatening status. Some examples are third degree burns or second degree burns over large parts of the body, a bump on the head that causes loss of consciousness, fractured bone, dehydration or exposure.”
Severity 3	“Injuries that pose an immediate life threatening condition if not treated adequately and expeditiously. Some examples are: uncontrolled bleeding, punctured organ, other internal injuries, spinal cord injuries, or crush syndrome.”
Severity 4	“Instantaneously killed or mortally injured”

For implementation within the HAZUS® software, casualty rates are tabulated for indoor casualties at each injury severity level by structural/building type and damage state (outdoor casualty rates are also provided, but are not considered here). In addition, the casualty estimation module considers the impact of building collapse in the “Complete” damage state. For each model building type, the description of the “Complete” damage state indicates the fraction of total floor area that is likely to collapse, based on judgment and limited available data. (The associated injury model is then applied to just that fraction). For reinforced concrete frame structures, the collapse fraction is assumed to be 13% (low-rise), 10% (mid-rise) and 5%(high-rise).

It should be noted that within the most recent version of HAZUS® [HAZUS® 99 SR-2, 2002], the indoor casualty rates for injury severity levels 3 and 4 do not show much variation across building types, with the exception of unreinforced masonry and a few other types of structures (wood frame, light steel frame and mobile homes). The HAZUS® casualty rates are based on available U.S. and worldwide casualty data. However, during model development, it was noted that the available data are not of the best quality and often have insufficient information about the type of structures where injuries occurred, and the mechanism of the injury [NIBS/FEMA, 1999]. The HAZUS® 99 SR-2 casualty rates and damage state definitions are provided in Table D.17.

For comparison with the survey-based fatality model for non-ductile concrete frame (NDCF) structures, the HAZUS® damage states of “Extensive” and “Complete (with Collapse)”

are of interest. By definition, concrete frame structures (HAZUS® class C1 – reinforced concrete moment resisting frames) in the “extensive” damage state may suffer partial collapse, and although just 10% of the mid-rise concrete frame structures are expected to collapse, the rates for the “Complete (with collapse)” are relevant here.

Accordingly, we assume that our definition of partial collapse corresponds to the “Extensive” damage state, while rates for total collapse correspond to “Complete (with collapse)”. The survey NDCF fatality rate for partial collapse (1.5%) exceeds the equivalent HAZUS rate for “extensive” damage (0.001%), but the fatality rates for total collapse (10.7 – 16.2%) agrees well with and slightly exceeds the equivalent rate for “Complete (with collapse)” (10%). These comparisons are summarized in Table D.19, along with the comparison for the ATC-13 fatality model.

Table D.19 Comparison of PEER NDCF fatality model to published models

Published Model	Published Model		Proposed PEER Survey-based NDCF Fatality Model	
	Damage Category	Fatality Rate	Damage Description	Fatality Rate
ATC-13 [ATC, 1985]	“Major”	1%	Partial Collapse	1.5% (overall NDCF)
	“Destroyed”	20%	Total Collapse	10.7% (overall NDCF) 13.1% (mid-rise NDCF) 16.2% (upper floors of mid-rise NDCF structures)
HAZUS®9 9 SR-2 [NIBS/FE MA, 2002]	“Extensive”	0.001%	Partial Collapse	1.5% (overall NDCF)
	“Complete (With Collapse)”	10%	Total Collapse	10.7% (overall NDCF) 13.1% (mid-rise NDCF) 16.2% (upper floors of mid-rise NDCF structures)

References

- Abrahamson, N. A. and W. J. Silva (1997). "Empirical Response Spectral Attenuation Relations for Shallow Crustal Earthquakes." *Seismological Research Letters* 68(1): 94-126.
- ACI 318. (2002). *Building Code Requirements for Structural Concrete and Commentary*, American Concrete Institute, Farmington Hills, MI.
- ACI 318 (1999). *Building Code Requirements for Structural Concrete and Commentary*, American Concrete Institute, Detroit, MI.
- ASCE 31 (2002). *Seismic Evaluation of Existing Buildings*, American Society of Civil Engineers, Reston, VA.
- ATC-13 (1985). *Earthquake Damage Evaluation Data for California*, Applied Technology Council Report Number ATC-13, Redwood City, California.
- ATC-40. (1996). *Seismic Evaluation and Retrofit of Existing Concrete Buildings, Volume 2 – Appendices*, Applied Technology Council, Redwood City, CA.
- API. (1993). *Recommended Practice for planning, designing and constructing fixed offshore platforms*, API RP 2A-WSD, 20th Ed., American Petroleum Institute, Washington, D.C.
- Applied Technology Council. (2003). *Proceedings of FEMA-Funded Workshop on Communicating Earthquake Risk*, Report ATC-58-1, Applied Technology Council, Redwood City, California.
- Anco Engineers Inc. Technical Staff. (1983). *Seismic hazard assessment of nonstructural ceiling components-Phase I*, Culver City, California
- Aslani, H. and Miranda, E. (2003). "Probabilistic damage assessment for building-specific loss estimation" *Report PEER 2002/16*, Pacific Earthquake Engineering Research (PEER) Center, Richmond, CA.

- Aslani, H. and Miranda, E. (2003). "Probabilistic Assessment of Building Response During Earthquakes" *Proc. Ninth International Conference on Application of Statistics and Probability in Civil Engineering*, San Francisco, CA, Vol. 2, 1441-1448.
- Aslani, H. and Miranda, E. (2004), "Investigation of the effects of correlation for building-specific loss estimation" *Report in preparation*, Pacific Earthquake Engineering Research (PEER) Center, Richmond, CA
- Atkinson, G.M. and Silva, W. (2000). "Stochastic Modeling of California Ground Motions" *Bulletin of the Seismological Society of America*, 90 (2), 255-274.
- Au, S.K. and Beck, J.L. (2001). "Estimation of small failure probabilities in high dimensions by subset simulation" *Probabilistic Engineering Mechanics*, 16 (4), 263-277.
- Au, S.K., Beck, J.L. and Jalayer, F. (2004) (expected). "Subset simulation: an efficient tool for probabilistic performance assessment" accepted Dec 2003 for publication in *Computer-Aided Civil and Infrastructure Engineering*, Blackwell Publishers, Boston, MA
- Baker, J. and Cornell, C.A. (2003). "Uncertainty specification and propagation for loss estimation using FOSM methods" *Report PEER 2003/07*, Pacific Earthquake Engineering Research (PEER) Center, Richmond, CA.
- Baker, J.W. and Cornell, C.A. (2003). "Uncertainty specification and propagation for loss estimation using FOSM methods," *Proc. Ninth International Conference on Applications of Statistics and Probability in Civil Engineering (ICASP9)*, San Francisco, CA.
- Baron, J., Hershey, J.C. and Kunreuther, H. (2000), "Determinants of Priority for Risk Reduction: The Role of Worry" *Risk Analysis*, 20(4), 413-427.
- Barin B., Pincheria J.A. (2002). *Influence of modeling parameters and assumptions on the seismic response of an existing RC building*, Dept. of Civil and Environmental Engineering, University of Wisconsin, Madison
- Bazzurro, P. and Cornell, C.A. (2002). "Vector-Valued Probabilistic Seismic Hazard Analysis (VPSHA)," *Proceedings 7th U.S. National Conference on Earthquake Engineering*, Boston, MA.
- Beck, J.L., Porter, K.A., Shaikhutdinov, R.S., Moroi, T., Tsukada, Y., Masuda, M. (in press). "Impact of Seismic Risk on Lifetime Property Values" *Final Report, CUREE-Kajima Joint Research Program Phase IV, Consortium of Universities for Earthquake Engineering Research*, Richmond, CA

- Beck, J.L. (1982), "System identification applied to strong motion records from structures" *American Society of Mechanical Engineers*, New York, 109-133
- Behr, R.A., Worrell, C.L. (1998). "Limit states for architectural glass under simulated seismic loadings" *ATC 29-1, Proceedings of Seminar on Seismic Design, Retrofit, and Performance of Nonstructural Components*, Applied Technology Council, Redwood City, California, 229-240
- Bernal, D. (1994). "Viscous damping in inelastic structural response," *Journal of Structural Engineering*, Vol. 120, no. 4, 1240-1254
- Bouwkamp, J.G. (1960), "Behavior of Window Panels Under In-Plane Forces" *UCB/SESM-1960/07*, Berkeley, Dept. of Civil Engrg., University of California
- Bray, J. (2002). "Summary of IM Meetings," <http://www.peertestbeds.net/Crosscutting.htm>
- Browning, J., Li, Y.R., Lynn, A., Moehle, J.P. (2000). "Performance assessment for a reinforced concrete frame building" *Earthquake Spectra* 16 (3): 541-555.
- Building Seismic Safety Council (BSSC). (2001). *NEHRP Recommended Provisions for Seismic Regulations for New Buildings and Other Structures*, Federal Emergency Management Agency, Washington D.C.
- California Strong Motion Instrumentation Program. (2001). *Van Nuys 7-Story Hotel, CSMIP Station No. 24386*, California Division of Mines and Geology, Sacramento, CA.
<ftp://ftp.consrv.ca.gov/pub/dmg/csmip/BuildingPages/BLD24386.HTM>
- Camarillo, H.R. (2003). "Evaluation of Shear Strength Methodologies for Reinforced Concrete Columns." *M.S Thesis*. University of Washington, Seattle. 137 p.
- Camelo, V.S., Beck, J.L., and Hall, J.F. (2001). "Dynamic Characteristics of Woodframe Structures" *Consortium of Universities for Research in Earthquake Engineering*, Richmond, CA
- California Geosystems. (1994), *Foundation Soils Investigation, Existing Holiday Inn Building, Roscoe Blvd and Orion Ave, Van Nuys, CA*, Glendale, CA.
- Chang, S.E. (2003). "Transportation planning for disasters: an accessibility approach" *Environment and Planning*, 35(06), 1051-1072.
- Charles, C., Gafni, A., and Whelan, T. (1997). "Shared decision-making in the medial encounter: what does it mean?" *Social Science and Medicine*, 44(5), 681-692.

- Charles, C., Gafni, A., and Whelan, T. (1999). "Decision-making in the physician-patient encounter: revisiting the shared treatment decision-making model" *Social Science and Medicine*, 49, 651-661.
- Chopra A.K. (2000) *Dynamics of Structures: Theory and Applications to Earthquake Engineering*, Upper Saddle River, NJ: Prentice Hall.
- City of Los Angeles Dept of Building and Safety. (1966). *Application for Inspection of New Building and for Certificate of Occupancy, for 8244 Orion Ave.*, Sepulveda, Los Angeles.
- Cordova, P.P., Deierlein, G.G., Mehanna, S.S.F., and Cornell, C.A. (2000). "Development of a two-parameter seismic intensity measure and probabilistic assessment procedure" *Proceedings of the 2nd U.S.-Japan Workshop on Performance-Based Seismic Earthquake Engineering Methodology for Reinforced Concrete Building Structures*, Sapporo, Japan, 195-214.
- Corley (1966). "Rotational Capacity of Reinforced Concrete Beams." *Journal of Structural Engineering*, ASCE 92 (ST5): 121-14.
- Cornell, C.A. (1996). "Calculating building seismic performance reliability; a basis for multi-level design norms" *Proc. 11th WCEE*, Acapulco, Mexico.
- Cornell, C.A. and Krawinkler, H. (2000). "Progress and challenges in seismic performance assessment." *PEER News*, April 2000.
- Cornell, C.A., Jalayer, F. Hamburger, R.O. and Foutch, D.A. (2002). "The Probabilistic Basis for the 2000 SAC/FEMA Steel Moment Frame Guidelines," *Journal of Structural Engineering*, Vol. 128, No. 4, 526-533.
- Czarnecki, R.M. (1973). "Earthquake damage to tall buildings" R73-8, Dept. of Civil Engineering, Massachusetts Inst. of Technology, Cambridge.
- Darendeli, M.B. (2001), "Development of a new family of normalized modulus reduction and material damping curves," *Ph.D. dissertation*, University of Texas, Austin, 362 pp.
- Deierlein, G.G., Krawinkler, H. and Cornell, C.A. (2003). "A framework for performance-based earthquake engineering." *Proceedings of 2003 Pacific Conference on Earthquake Engineering*.
- Eberhard, M.O., Mookerjee, A. and Parrish, M. (2001), "Uncertainties in Performance Estimates for RC Columns" *Pacific Earthquake Engineering Research Center*, Richmond, CA: <http://ce.washington.edu/~peera1>.

- EERI. (1998). *Incentives and Impediments to Improving the Seismic Performance of Buildings*, Earthquake Engineering Research Institute, Oakland, CA
- Earthquake Engineering Research Institute (EERI). (1994). "Northridge Earthquake January 17, 1994, Preliminary Reconnaissance Report," *Publication 94-01*, Oakland, CA, 96 pp.
- Ellingwood, B., Galambos, T.V., MacGregor, J.G., and Cornell, C.A. (1980) "Development of a Probability-Based Load Criterion for American National Standard A58" *National Bureau of Standards*, Washington, DC, 222 pp.
- Elwood, K.J., Moehle, J.P. (2003). "Shake table tests and analytical studies on the gravity load collapse of reinforced concrete frames" *Report PEER 2003/01*, Pacific Earthquake Engineering Research (PEER) Center, Richmond, CA.
- Epstein, H.L. (1965), *Holiday Inn of America, Orion Ave, Van Nuys, CA, Structural Calculations*, Los Angeles, CA, 183 pp.
- Federal Emergency Management Agency, FEMA (2003). *Improved inelastic seismic analysis procedures*, FEMA 440, Washington D.C.
- FEMA 156. (1988). *Typical Costs for Seismic Rehabilitation of Existing Buildings*, Federal Emergency Management Agency, Washington, D.C.
- FEMA 273. (1997). *NEHRP Guidelines for the Seismic Rehabilitation of Buildings*, Federal Emergency Management Agency, Washington, D.C.
- FEMA 308, (1998). "Repair of earthquake damaged concrete and masonry wall buildings." Prepared by the *Applied Technology Council (ATC-43 Project)* for the Federal Emergency Management Agency, Washington, D.C, 65 pages.
- FEMA 310 (1998). *Handbook for the Seismic Evaluation of Buildings – A Prestandard*, Federal Emergency Management Agency, Washington, D.C.
- FEMA 355F (2000). *State of the Art Report on Performance Prediction and Evaluation of Steel Moment-Frame Buildings*. SAC Joint Venture, Federal Emergency Management Agency, Washington D.C.
- FEMA 356 (2000). *Prestandard and Commentary for the Seismic Rehabilitation of Buildings*, Federal Emergency Management Agency, Washington, D.C.
- Frankel, A., Mueller, C., Barnhard, T., Perkins, D., Leyendecker, E.V., Dickman, N., Hanson, S., and Hopper, M. (1997). *National 1996 Seismic Hazard Maps: U.S. Geological Survey, Open-File Report 97-131*.

- Frankel, A., and Leyendecker, E.V. (2001). *Uniform Hazard Response Spectra and Seismic Hazard Curves for the United States*, US Geological Survey, Menlo Park, CA
- Freeman, S.A. (1971), "Third progress report on racking tests of wall panels," *Blume (John A.) and Assoc., S.F. Research Div.*, San Francisco
- Gentle J.E. (2003). *Random number generation and Monte Carlo methods*, Springer-Verlag, New York.
- GeoSystems (1994). *Foundation Soils Investigation, Existing Holiday Inn Building, Roscoe Boulevard and Orion Avenue, Van Nuys, California*, Report by GeoSystems Environmental and Geotechnical Consultants to Holiday Inn, 8 August 1994.
- Gilmartin, U.M., Freeman, S.A., and Rihal, S.S. (1998). "Using Earthquake Strong Motion Records to Assess the Structural and Nonstructural Response of the 7-Story Van Nuys Hotel to The Northridge Earthquake of January 17, 1994" *Proceedings of the 6th National Conference on Earthquake Engineering*, Seattle, WA.
- Giovenale, P., Cornell, C.A., and Esteva, L. (2004). "Efficient Comparison of Alternative Ground Motion Intensity Measures: Transforming Conditional Distributions of Non-Linear Structural Response," Submitted to *Structural Dynamics and Earthquake Engineering*.
- Graham, J.R. and Harvey, C.R. (2001) "The theory and practice of corporate finance: evidence from the field," *Journal of Financial Economics*, 60, 187-243.
- Hart, G.C. (1975). "Earthquake design of buildings: damping." *Journal of the structural division, ASCE*.
- Hausas, T. and Der Kiureghian, A. (2003). "Developments in Finite Element Reliability and Sensitivity Analysis of Nonlinear Structures," *Proc. Ninth International Conference on Applications of Statistics and Probability in Civil Engineering (ICASP9)*, San Francisco, CA.
- HAZUS 99 Technical Manual (1999). Federal Emergency Management Agency, Washington, D.C.
- Huber, P. (1990). *Liability: The Legal Revolution and Its Consequences*, NY: Basic Books.
- Ibarra, L. (2003). "Global Collapse of Frame Structures Under Seismic Excitations" *Ph.D. dissertation*, Stanford University.
- Ince, U. and Meszaros, J. (2003). "Seismic Hazard Mitigation Decisions Using PBEE: Financial Metrics and a Case Study," Working Paper, University of Washington, Bothell.

- Ince, U. and Meszaros, J. (2003), "Performance-based seismic hazard mitigation: financial metrics, a decision model and a case study" Working paper.
- International Code Council. (2000). *International Building Code*, Whittier, CA: International Conference of Building Officials, 756 pp.
- Islam, M.S., (1996). "Analysis of the Response of an Instrumented 7-story Nonductile Concrete Frame Building Damaged During the Northridge Earthquake," *Proceedings of the 1996 Annual Meeting of the Los Angeles Tall Buildings Structural Council, May 10, 1996, Los Angeles, CA*.
- Islam, M.S. (1994). "Holiday Inn, Orion Avenue, Van Nuys." *Proceedings of the 63rd Annual SEAOC Convention*, Structural Engineers Association of California.
- Islam, M.S. (1996a) "Analysis of the Northridge Earthquake Response of a Damaged Nonductile Concrete Frame Building" *The Structural Design of Tall Buildings*, Vol. 5, 151-182.
- Islam, M.S., (1996b), "Holiday Inn," *1994 Northridge Earthquake Buildings Case Study Project Proposition 122: Product 3.2*, Seismic Safety Commission, Sacramento CA, 189-233.
- Islam, M.S., Gupta, M. and Kenneth, B. (1998). "Critical Review of The State-Of-The-Art Analytical Tools and Acceptance Criterion in Light of Observed Response of an Instrumented Nonductile Concrete Frame Building" *Proceedings, Sixth US National Conference on Earthquake Engineering, Seattle, Washington, May 31-June 4, 1998*, Earthquake Engineering Research Institute, Oakland CA, 11 pp.
- Jalayer, F. (2003). "Direct Probabilistic Seismic Analysis: Implementing Non-Linear Dynamic Assessments," *Ph. D. dissertation*, CE&E Dept., Stanford University.
- Jalayer, F. and Cornell, C.A. (2003). "A Technical Framework for Probability-based Demand and Capacity Factor Design (DCFD) Seismic Formats," *Report PEER 2003/08*, Pacific Earthquake Engineering Research (PEER) Center, Richmond, CA.
- Jennings, P.C. (1971). "Engineering Features of the San Fernando Earthquake of February 9, 1971" *Report EERL 71 – 02*, California Institute of Technology, Pasadena, CA
- John A. Blume & Associates, Engineers (1973). "Holiday Inn (29)" *San Fernando, California, Earthquake of February 9, 1971*, vol. 1, part a, National Oceanographic and Aviation Administration, Washington, DC, 359-393

- Jones, A.L., Kramer, S.L. and Arduino, P. (2002). "Estimation of Uncertainty in Geotechnical Properties for Performance-Based Earthquake Engineering," *Report PEER 2002/16*, Pacific Earthquake Engineering Research (PEER) Center, Richmond, CA.
- Kennedy, R.P., Cornell, C.A., Campbell, R.D., Kaplan, S. and Perla H.F. (1980). "Probabilistic Seismic Safety Study of an Existing Nuclear Power Plant," *Nuclear Engineering and Design*, Vol. 59, No. 2, 315-338.
- Kennedy, R.P. and Short, S.A. (1994). "Basis for seismic provisions of DOE-STD-1020." UCRL-CR-111478 and BNL-52418, Lawrence Livermore National Laboratory and Brookhaven National Laboratory.
- King, A.B., Lim, K. Y. S. (1991), "The behavior of external glazing systems under seismic in-plane racking," *Pacific Conference on Earthquake Engineering*, New Zealand Natl. Society for Earthquake Engineering, Auckland, 315-326, Vol. 2
- Kowalsky M.J, Priestley M.J.N (2000): "Improved analytical model for shear strength of circular reinforced concrete columns in seismic regions." *ACI Structural Journal*, 97(3): 388-396.
- Kramer, S.L. (2003). Personal communication
- Kramer, S.L. (1996). *Geotechnical Earthquake Engineering*, Prentice Hall, Upper Saddle River, NJ.
- Krawinkler, H. (2002). "A general approach to seismic performance assessment," *Proceedings, International Conference on Advances and New Challenges in Earthquake Engineering Research, ICANCEER 2002*, Hong Kong, August 19-20.
- Krawinkler, H., Medina, R., and Alavi, B. (2003). "Seismic Drift and Ductility Demands and Their Dependence on Ground Motions," *Journal of Engineering Structures*, Vol. 25, No. 5, 637 - 653.
- Krawinkler, H., and Miranda, E. (2004). "Performance-based earthquake engineering," Chapter 9 of *Earthquake engineering: from engineering seismology to performance-based engineering*, Y. Bozorgnia and V.V. Bertero, Editors, CRC Press.
- Krawinkler, H., and Ibarra, L. (2004). "Sidesway Collapse of Frames with Deteriorating Properties" *Proceedings of the SEAONC Convention 2004*.
- Kunreuther, H. and Schade, C. (2001). "Worry and Mental Accounting with Protective Measures" Working Paper, The Wharton School, University of Pennsylvania.

- Lehman, D.E. (1994). "Towards a Consistent Formulation of the Plastic Hinge Length Method." *CE 299 Report*. University of California, Berkeley.
- Li, Y.R., and Jirsa, J.O. (1998). "Nonlinear Analyses of an Instrumented Structure Damaged in the 1994 Northridge Earthquake" *Earthquake Spectra*, 14(2), Earthquake Engineering Research Institute, Oakland, CA, 245-264.
- Luco, N., and Cornell, C. A. (1998). "Seismic Drift Demands for two SMRF structures with brittle connections," *Structural Engineering World Wide 1998*, Elsevier Science Ltd., Oxford, England, 1998. Paper T158-3.
- Luco, N. and Cornell, C.A. (2004). "Structure-Specific Scalar Intensity Measures for Near Source and Ordinary Earthquake Ground Motions," *Earthquake Spectra*, Submitted.
- Luo, Y.H., Durrani, A.J. and Conte, J.P. (1994). "Equivalent Frame Analysis of Flat Plate Buildings for Seismic Loading." *Journal of Structural Engineering*, Vol. 120, No. 7, American Society of Civil Engineers, Reston, VA.
- Lynn, A.C., Moehle, J.P., Mahin, S.A., Holmes, W.T. (1996). "Seismic evaluation of existing reinforced concrete building columns." *Earthquake Spectra* 12(4): 715-739.
- May, P. (2003). *Performance-based Regulatory Regimes: The Saga of Leaky Buildings*, Law and Society Association Meeting, Pittsburgh, PA.
- Means (2002). "Building construction cost data. 60th annual edition." R.S. Means Company, Inc. Kingston, MA. 694 pages.
- McVerry, G.H. (1979). "Frequency Domain Identification of Structural Models for Earthquake Records" *Report No. EERL 79-02*, California Institute of Technology, Pasadena, CA, <http://caltecheerl.library.caltech.edu/documents/disk0/00/00/02/23/00000223-00/7902.pdf>,
- Melek, M., and Wallace, J. (2004). "Cyclic Behavior of Columns with Short Lap Splices" *ACI Structural Journal* 101 (6): 802-811.
- Menegotto, M. and Pinto, P. (1973). "Method of Analysis of Cyclically Loaded Reinforced Concrete Plane Frames Including Changes in Geometry and Nonelastic Behavior of Elements Under Combined Normal Geometry and Nonelastic Behavior of Elements Under Combined Normal Force and Bending." *Proceedings of the IABSE Symposium on the Resistance and Ultimate Deformability of Structures Acted on by Well-Defined Repeated Loads*. Lisbon.

- Medina, R. and Krawinkler, H. (2003). "Seismic Demands for Nondeteriorating Frame Structures and Their Dependence on Ground Motions," PEER Report 2003/15.
- Melchers, R. E (1999). *Structural Reliability Analysis and Prediction*. John Wiley and Sons, Chichester.
- Meszaros, J. and Fiegner, M. (2003). *Learning from a Rare Event: Organizations' Lessons from the Nisqually Earthquake in Washington State*, National Academy of Management Conference, Seattle, WA.
- Meszaros, J., Francisco, S., and Lehman, D. (2003). "Structural engineers' insights regarding performance-based engineering adoption" Working Paper, University of Washington, Bothell.
- Mileti, D.S. (1999). *Disasters by Design: A Reassessment of Natural Hazards in the United States*, Washington, D.C.: Joseph Henry Press.
- Miranda, E. and Aslani, H. (2003). "Probabilistic response assessment for building-specific loss estimation." *Report PEER 2003/03*, Pacific Earthquake Engineering Research (PEER) Center, Richmond, CA.
- Moehle, J.P., and Deierlein, G.G. (2004). "A framework for performance-based earthquake engineering" *Proceedings of 13th World Conference on Earthquake Engineering*, #679, Vancouver, CA.
- Nakata, S. et al. (1984). "U.S.-Japan cooperative research on r/c full-scale building test: Part 3 -- Installation on nonstructural elements and repair works, damage aspects and hysteretic properties after repair" *Proceedings of the Eighth World Conference on Earthquake Engineering*, Prentice-Hall, Inc., Englewood Cliffs, New Jersey, Vol. VI, pages 611-618.
- NIBS/FEMA, 1999. *HAZUS@99 Earthquake Loss Estimation Methodology, Service Release 1 (SR1) Technical Manual*, Developed by the Federal Emergency Management Agency through agreements with the National Institute of Building Sciences, Washington, D.C.
- NIBS/FEMA, 2002. *HAZUS@99 Earthquake Loss Estimation Methodology, Service Release 2 (SR2) Technical Manual*, Developed by the Federal Emergency Management Agency through agreements with the National Institute of Building Sciences, Washington, D.C.
- Newmark N.M., Hall W.J. (1982). "Earthquake spectra and design," *Engineering monographs on earthquake criteria, structural design, and strong motion records v. 3*, Berkeley: Earthquake Engineering Research Institute.

- NOAA, (1972). *A Study of Earthquake Losses in the San Francisco Bay Area; Data and Analysis*, prepared for the Office of Emergency Preparedness by the National Oceanic & Atmospheric Administration.
- NOAA, (1973). *A Study of Earthquake Losses in the Los Angeles, California Area*, prepared for the Federal Disaster Assistance Administration, Department of Housing & Urban Development by the National Oceanic & Atmospheric Administration, Washington, D.C.
- Ohta, Y. and Goto, N. (1976) "Estimation of s-wave velocity in terms of characteristic indices of soil" *Butsuri-Tanku*, Vol. 29, No. 4, 34-41
- Palm, R. and Carroll, J. (1998). *Illusions of Safety: Culture and Earthquake Hazard Response In California and Japan*, Boulder, CO: Westview Press.
- Panagiotakos, T.B. and Fardis, M.N. (2001). "Deformations of reinforced concrete members at yielding and ultimate" *ACI Structural Journal*, 98 (2), pp. 135-148
- Parsons, T. (1951), *The Social System*, Glencoe, IL: Free Press.
- Paspuleti, C. (2002). "Seismic analysis of an older reinforced concrete frame structure," *M.S. Thesis*, CE&E Dept., University of Washington.
- Porter, K.A., Beck, J.L., and Shaikhutdinov, R. (in progress) "Sensitivity of Building Loss to Major Uncertain Variables," for submission to *Earthquake Spectra*, Earthquake Engineering Research Institute, Oakland, CA
- Porter, K.A., and Kiremidjian, A.S. (2001). "Assembly-Based Vulnerability and its Uses in Seismic Performance Evaluation and Risk-Management Decision-Making" *Report No. 139*, John A. Blume Earthquake Engineering Center, Stanford, CA, 214 pp.,
- Porter, K.A., Kiremidjian, A.S., and LeGrue, J.S. (2001). "Assembly-based vulnerability of buildings and its use in performance evaluation," *Earthquake Spectra*, 17(2), 291-312.
- Porter, K.A., Beck, J.L., and Shaikhutdinov, R.V. (2002a), "Sensitivity of Building Loss Estimates to Major Uncertain Variables," *Earthquake Spectra*, 18(4), 719-743.
- Porter, K.A., Beck, J.L., and Shaikhutdinov, R.V. (2004) (expected), "Simplified Estimation of Economic Seismic Risk for Buildings," accepted Jan 2004 for publication in *Earthquake Spectra*, Earthquake Engineering Research Institute, Oakland, CA
- Porter, K.A., Beck, J.L., Seligson, H.A., Scawthorn, C.R., Tobin, L.T., and Boyd, T. (2002b). *Improving Loss Estimation for Woodframe Buildings*, Consortium of Universities for Research in Earthquake Engineering, Richmond, CA, 136 pp.

<http://resolver.caltech.edu/caltechEERL:2002.EERL-2002-01> (main report)

<http://resolver.caltech.edu/caltechEERL:2002.EERL-2002-02> (appendices)

- Prakhash, V., Powell, G.H., and Filippou, F.C. (1992). "DRAIN-2DX: Base program user guide" *Report No. UCB/SEMM-92/29*, Department of Civil Engineering, University of California, Berkeley, CA.
- Rihal, S. S. (1982). "Behavior of non-structural building partitions during earthquakes" *Seventh Symposium on Earthquake Engineering*, Sarita Prakashan, Meerut, India, pages 267-277, Vol. 1
- Rihal, S. S.; Granneman, G. (1984), "Experimental investigation of the dynamic behavior of building partitions and suspended ceilings during earthquakes," *ARCE R84-1*, Architectural Engineering Dept., California Polytechnic State Univ., San Luis Obispo
- Rissman and Rissman Associates. (1965). *Holiday Inn Van Nuys Structural Drawings*, Pacific Palisades, CA
- SEAOC. (1997). *The One Page Green Book of Existing Building Structural Evaluation and Seismic Retrofit*, Structural Engineers Association of California, CA
- Sahin, M & Tari, E. (2000). "The August 17 Kocaeli and the November 12 Duzce earthquakes in Turkey" *Earth Planets Space*, 52,753–757.
- Scholl, R.E., Kustu, O., Perry, C.L., and Zanetti, J.M. (1982). "Seismic Damage Assessment for High-Rise Buildings" *URS/JAB 8020*, URS/John A. Blume & Associates, Engineers, San Francisco, CA, 321 pp.
- Scholl, R.E. (1981). "Seismic Damage Assessment for Highrise Buildings" *Annual Technical Report, Open-file Report 81-381*, Menlo Park, CA: US Geological Survey, 143 pp.
- Seligson, H.A., Shoaf, K.I., Peek-Asa, C., and Mahue-Giangreco, M. (2002). "Engineering-Based Earthquake Casualty Modeling: Past, Present and Future," *Proc. 7th U.S. National Conference on Earthquake Engineering, July 21-25, 2002*, Boston, MA, Earthquake Engineering Research Institute, Oakland, CA
- Shome, N. (1999). "Probabilistic Demand Analysis of Nonlinear Structures," *Ph. D. dissertation*, Department of C&EE, Stanford University.
- Shome, N., Cornell, C.A., Bazzurro, P., and Carballo, J.E. (1998). "Earthquakes, Records and Nonlinear Responses," *Earthquake Spectra*, Vol. 14, No. 3, 469-500.

- Silva, W. (2000). *PEER Strong Motion Database*, Pacific Earthquake Engineering Research (PEER) Center, Berkeley, CA, <http://peer.berkeley.edu/smcat/index.html>
- Somerville, P. and Collins, N. (2002). *Ground Motion Time Histories For The Van Nuys Building*, Prepared for the PEER Methodology Testbeds Project, URS Corporation, Pasadena, CA. <http://www.peertestbeds.net/VNY/PrelimVanNuysHazardReport.pdf>
- Somerville, P., Smith, N., Punyamurthula, S., and Sun, S. (1997). "Development of Ground Motion Time Histories for Phase 2 of the FEMA/SAC Steel Project" *Background Document Report No. SAC/BD-97/04*, SAC Joint Venture.
- Stewart, J. P., Fenves, G.L., and Seed, R.B. (1999). "Seismic soil-structure interaction in buildings. II: Empirical findings" *J. Geotech. & Geoenv. Engrg., ASCE*, 125, 38-48.
- Structural Engineers Association of California. (1999). *Recommended Lateral Force Requirements and Commentary, 7th Edition*, Sacramento, CA, 440 pp.
- Taghavi, S. and Miranda, E. (2003), "Response assessment of nonstructural building elements" *Report PEER 2003/05*, Pacific Earthquake Engineering Research (PEER) Center, Richmond, CA.
- Taghavi, S. and Aslani, H. (2003), "Probabilistic Study of Peak Floor Acceleration Demands on Linear and Nonlinear Structures," *Proc. Ninth International Conference on Application of Statistics and Probability in Civil Engineering, July 6-9, 2003*, San Francisco, California.
- Theiss, A. (2005), "The impact of beam-column joint damage on the response of an older reinforced concrete frame building" *M.S. Thesis*, CE&E Dept., University of Washington.
- Tinsley, J.C., and Fumal, T.E. (1985), "Mapping Quaternary Sedimentary Deposits for Areal Variations in Shaking Response" *Evaluating Earthquake Hazards in the Los Angeles*
- Trifunac, M.D., Ivanovic, S.S. and Todorovska, M.I. (1999). "Instrumented 7-Storey Reinforced Concrete Building in Van Nuys, California: Description of the Damage from the 1994 Northridge Earthquake and Strong Motion Data" *Report CE 99-02*, University of Southern California Department of Civil Engineering, Los Angeles, CA.
- Trifunac, M.D., and Hao, T.Y. (2001). "7-Storey Reinforced Concrete Building in Van Nuys, California: Photographs of the Damage from the 1994 Northridge Earthquake" *Report CE 01-05*, University of Southern California Department of Civil Engineering, Los Angeles, CA.
- Trifunac, M.D., Ivanovic, S.S. and Todorovska, M.I. (2001). "Apparent Periods of A Building. I: Fourier Analysis" *Journal of Structural Engineering, ASCE* 127(5): 517-537.

- Vanderbilt, M.D. and Corley, W.G. (1983). "Frame Analysis of Concrete Buildings" *Concrete International*, American Concrete Institute, December 1983.
- Wight, James K. (1983). *U.S.-Japan Cooperative Research Program: construction of the full scale reinforced concrete test structure*, University of Michigan. Dept. of Civil Engineering, Ann Arbor
- Webb, G.R., Tierney, K.J. and Dahlhamer, J. (2000): "Businesses and disasters: Empirical patterns and unanswered questions" *Natural Hazards Review*,1(2), 83-90.
- Whitman, R.V., Biggs, J.M., Brennan III, J., Cornell, C.A., de Neufville, R., Vanmarcke E.M. (1974). "Seismic design decision analysis: methodology and pilot application," Massachusetts Institute of Technology, Department of Civil Engineering, Cambridge, Massachusetts, *Report MIT-CE-R74-15, Structures Publication No. 385*.

PEER REPORTS

PEER reports are available from the National Information Service for Earthquake Engineering (NISEE). To order PEER reports, please contact the Pacific Earthquake Engineering Research Center, 1301 South 46th Street, Richmond, California 94804-4698. Tel.: (510) 231-9468; Fax: (510) 231-9 461.

- PEER 2005/11** *Van Nuys Hotel Building Testbed Report: Exercising Seismic Performance Assessment.* Helmut Krawinkler, editor. October 2005.
- PEER 2005/06** *Global Collapse of Frame Structures under Seismic Excitations.* Luis F. Ibarra and Helmut Krawinkler. September 2005.
- PEER 2005/01** *Empirical Characterization of Site Conditions on Strong Ground Motion.* Jonathan P. Stewart, Yoojoong Choi, and Robert W. Graves. June 2005.
- PEER 2004/09** *Electrical Substation Equipment Interaction: Experimental Rigid Conductor Studies.* Christopher Stearns and André Filiatrault. February 2005.
- PEER 2004/08** *Seismic Qualification and Fragility Testing of Line Break 550-kV Disconnect Switches.* Shakhzod M. Takhirov, Gregory L. Fenves, and Eric Fujisaki. January 2005.
- PEER 2004/07** *Ground Motions for Earthquake Simulator Qualification of Electrical Substation Equipment.* Shakhzod M. Takhirov, Gregory L. Fenves, Eric Fujisaki, and Don Clyde. January 2005.
- PEER 2004/06** *Performance-Based Regulation and Regulatory Regimes.* Peter J. May and Chris Koski. September 2004.
- PEER 2004/05** *Performance-Based Seismic Design Concepts and Implementation: Proceedings of an International Workshop.* Peter Fajfar and Helmut Krawinkler, editors. September 2004.
- PEER 2004/04** *Seismic Performance of an Instrumented Tilt-up Wall Building.* James C. Anderson and Vitelmo V. Bertero. July 2004.
- PEER 2004/03** *Evaluation and Application of Concrete Tilt-up Assessment Methodologies.* Timothy Graf and James O. Malley. October 2004.
- PEER 2004/02** *Analytical Investigations of New Methods for Reducing Residual Displacements of Reinforced Concrete Bridge Columns.* Junichi Sakai and Stephen A. Mahin. August 2004.
- PEER 2004/01** *Seismic Performance of Masonry Buildings and Design Implications.* Kerri Anne Taeko Tokoro, James C. Anderson, and Vitelmo V. Bertero. February 2004.
- PEER 2003/18** *Performance Models for Flexural Damage in Reinforced Concrete Columns.* Michael Berry and Marc Eberhard. August 2003.
- PEER 2003/17** *Predicting Earthquake Damage in Older Reinforced Concrete Beam-Column Joints.* Catherine Pagni and Laura Lowes. October 2004.
- PEER 2003/16** *Seismic Demands for Performance-Based Design of Bridges.* Kevin Mackie and Božidar Stojadinovi . August 2003.
- PEER 2003/15** *Seismic Demands for Nondeteriorating Frame Structures and Their Dependence on Ground Motions.* Ricardo Antonio Medina and Helmut Krawinkler. May 2004.
- PEER 2003/14** *Finite Element Reliability and Sensitivity Methods for Performance-Based Earthquake Engineering.* Terje Haukaas and Armen Der Kiureghian. April 2004.
- PEER 2003/13** *Effects of Connection Hysteretic Degradation on the Seismic Behavior of Steel Moment-Resisting Frames.* Janise E. Rodgers and Stephen A. Mahin. March 2004.
- PEER 2003/12** *Implementation Manual for the Seismic Protection of Laboratory Contents: Format and Case Studies.* William T. Holmes and Mary C. Comerio. October 2003.
- PEER 2003/11** *Fifth U.S.-Japan Workshop on Performance-Based Earthquake Engineering Methodology for Reinforced Concrete Building Structures.* February 2004.
- PEER 2003/10** *A Beam-Column Joint Model for Simulating the Earthquake Response of Reinforced Concrete Frames.* Laura N. Lowes, Nilanjan Mitra, and Arash Altoontash. February 2004.

- PEER 2003/09** *Sequencing Repairs after an Earthquake: An Economic Approach.* Marco Casari and Simon J. Wilkie. April 2004.
- PEER 2003/08** *A Technical Framework for Probability-Based Demand and Capacity Factor Design (DCFD) Seismic Formats.* Fatemeh Jalayer and C. Allin Cornell. November 2003.
- PEER 2003/07** *Uncertainty Specification and Propagation for Loss Estimation Using FOSM Methods.* Jack W. Baker and C. Allin Cornell. September 2003.
- PEER 2003/06** *Performance of Circular Reinforced Concrete Bridge Columns under Bidirectional Earthquake Loading.* Mahmoud M. Hachem, Stephen A. Mahin, and Jack P. Moehle. February 2003.
- PEER 2003/05** *Response Assessment for Building-Specific Loss Estimation.* Eduardo Miranda and Shahram Taghavi. September 2003.
- PEER 2003/04** *Experimental Assessment of Columns with Short Lap Splices Subjected to Cyclic Loads.* Murat Melek, John W. Wallace, and Joel Conte. April 2003.
- PEER 2003/03** *Probabilistic Response Assessment for Building-Specific Loss Estimation.* Eduardo Miranda and Hesameddin Aslani. September 2003.
- PEER 2003/02** *Software Framework for Collaborative Development of Nonlinear Dynamic Analysis Program.* Jun Peng and Kincho H. Law. September 2003.
- PEER 2003/01** *Shake Table Tests and Analytical Studies on the Gravity Load Collapse of Reinforced Concrete Frames.* Kenneth John Elwood and Jack P. Moehle. November 2003.
- PEER 2002/24** *Performance of Beam to Column Bridge Joints Subjected to a Large Velocity Pulse.* Natalie Gibson, André Filiatrault, and Scott A. Ashford. April 2002.
- PEER 2002/23** *Effects of Large Velocity Pulses on Reinforced Concrete Bridge Columns.* Greg L. Orozco and Scott A. Ashford. April 2002.
- PEER 2002/22** *Characterization of Large Velocity Pulses for Laboratory Testing.* Kenneth E. Cox and Scott A. Ashford. April 2002.
- PEER 2002/21** *Fourth U.S.-Japan Workshop on Performance-Based Earthquake Engineering Methodology for Reinforced Concrete Building Structures.* December 2002.
- PEER 2002/20** *Barriers to Adoption and Implementation of PBEE Innovations.* Peter J. May. August 2002.
- PEER 2002/19** *Economic-Engineered Integrated Models for Earthquakes: Socioeconomic Impacts.* Peter Gordon, James E. Moore II, and Harry W. Richardson. July 2002.
- PEER 2002/18** *Assessment of Reinforced Concrete Building Exterior Joints with Substandard Details.* Chris P. Pantelides, Jon Hansen, Justin Nadauld, and Lawrence D. Reaveley. May 2002.
- PEER 2002/17** *Structural Characterization and Seismic Response Analysis of a Highway Overcrossing Equipped with Elastomeric Bearings and Fluid Dampers: A Case Study.* Nicos Makris and Jian Zhang. November 2002.
- PEER 2002/16** *Estimation of Uncertainty in Geotechnical Properties for Performance-Based Earthquake Engineering.* Allen L. Jones, Steven L. Kramer, and Pedro Arduino. December 2002.
- PEER 2002/15** *Seismic Behavior of Bridge Columns Subjected to Various Loading Patterns.* Asadollah Esmaeily-Gh. and Yan Xiao. December 2002.
- PEER 2002/14** *Inelastic Seismic Response of Extended Pile Shaft Supported Bridge Structures.* T.C. Hutchinson, R.W. Boulanger, Y.H. Chai, and I.M. Idriss. December 2002.
- PEER 2002/13** *Probabilistic Models and Fragility Estimates for Bridge Components and Systems.* Paolo Gardoni, Armen Der Kiureghian, and Khalid M. Mosalam. June 2002.
- PEER 2002/12** *Effects of Fault Dip and Slip Rake on Near-Source Ground Motions: Why Chi-Chi Was a Relatively Mild M7.6 Earthquake.* Brad T. Aagaard, John F. Hall, and Thomas H. Heaton. December 2002.
- PEER 2002/11** *Analytical and Experimental Study of Fiber-Reinforced Strip Isolators.* James M. Kelly and Shakhzod M. Takhirov. September 2002.
- PEER 2002/10** *Centrifuge Modeling of Settlement and Lateral Spreading with Comparisons to Numerical Analyses.* Sivapalan Gajan and Bruce L. Kutter. January 2003.

- PEER 2002/09** *Documentation and Analysis of Field Case Histories of Seismic Compression during the 1994 Northridge, California, Earthquake.* Jonathan P. Stewart, Patrick M. Smith, Daniel H. Whang, and Jonathan D. Bray. October 2002.
- PEER 2002/08** *Component Testing, Stability Analysis and Characterization of Buckling-Restrained Unbonded Braces™.* Cameron Black, Nicos Makris, and Ian Aiken. September 2002.
- PEER 2002/07** *Seismic Performance of Pile-Wharf Connections.* Charles W. Roeder, Robert Graff, Jennifer Soderstrom, and Jun Han Yoo. December 2001.
- PEER 2002/06** *The Use of Benefit-Cost Analysis for Evaluation of Performance-Based Earthquake Engineering Decisions.* Richard O. Zerbe and Anthony Falit-Baiamonte. September 2001.
- PEER 2002/05** *Guidelines, Specifications, and Seismic Performance Characterization of Nonstructural Building Components and Equipment.* André Filiatrault, Constantin Christopoulos, and Christopher Stearns. September 2001.
- PEER 2002/04** *Consortium of Organizations for Strong-Motion Observation Systems and the Pacific Earthquake Engineering Research Center Lifelines Program: Invited Workshop on Archiving and Web Dissemination of Geotechnical Data, 4–5 October 2001.* September 2002.
- PEER 2002/03** *Investigation of Sensitivity of Building Loss Estimates to Major Uncertain Variables for the Van Nuys Testbed.* Keith A. Porter, James L. Beck, and Rustem V. Shaikhutdinov. August 2002.
- PEER 2002/02** *The Third U.S.-Japan Workshop on Performance-Based Earthquake Engineering Methodology for Reinforced Concrete Building Structures.* July 2002.
- PEER 2002/01** *Nonstructural Loss Estimation: The UC Berkeley Case Study.* Mary C. Comerio and John C. Stallmeyer. December 2001.
- PEER 2001/16** *Statistics of SDF-System Estimate of Roof Displacement for Pushover Analysis of Buildings.* Anil K. Chopra, Rakesh K. Goel, and Chatpan Chintanapakdee. December 2001.
- PEER 2001/15** *Damage to Bridges during the 2001 Nisqually Earthquake.* R. Tyler Ranf, Marc O. Eberhard, and Michael P. Berry. November 2001.
- PEER 2001/14** *Rocking Response of Equipment Anchored to a Base Foundation.* Nicos Makris and Cameron J. Black. September 2001.
- PEER 2001/13** *Modeling Soil Liquefaction Hazards for Performance-Based Earthquake Engineering.* Steven L. Kramer and Ahmed-W. Elgamal. February 2001.
- PEER 2001/12** *Development of Geotechnical Capabilities in OpenSees.* Boris Jeremi . September 2001.
- PEER 2001/11** *Analytical and Experimental Study of Fiber-Reinforced Elastomeric Isolators.* James M. Kelly and Shakhzod M. Takhirov. September 2001.
- PEER 2001/10** *Amplification Factors for Spectral Acceleration in Active Regions.* Jonathan P. Stewart, Andrew H. Liu, Yoojoong Choi, and Mehmet B. Baturay. December 2001.
- PEER 2001/09** *Ground Motion Evaluation Procedures for Performance-Based Design.* Jonathan P. Stewart, Shyh-Jeng Chiou, Jonathan D. Bray, Robert W. Graves, Paul G. Somerville, and Norman A. Abrahamson. September 2001.
- PEER 2001/08** *Experimental and Computational Evaluation of Reinforced Concrete Bridge Beam-Column Connections for Seismic Performance.* Clay J. Naito, Jack P. Moehle, and Khalid M. Mosalam. November 2001.
- PEER 2001/07** *The Rocking Spectrum and the Shortcomings of Design Guidelines.* Nicos Makris and Dimitrios Konstantinidis. August 2001.
- PEER 2001/06** *Development of an Electrical Substation Equipment Performance Database for Evaluation of Equipment Fragilities.* Thalia Agnanos. April 1999.
- PEER 2001/05** *Stiffness Analysis of Fiber-Reinforced Elastomeric Isolators.* Hsiang-Chuan Tsai and James M. Kelly. May 2001.
- PEER 2001/04** *Organizational and Societal Considerations for Performance-Based Earthquake Engineering.* Peter J. May. April 2001.
- PEER 2001/03** *A Modal Pushover Analysis Procedure to Estimate Seismic Demands for Buildings: Theory and Preliminary Evaluation.* Anil K. Chopra and Rakesh K. Goel. January 2001.

- PEER 2001/02** *Seismic Response Analysis of Highway Overcrossings Including Soil-Structure Interaction.* Jian Zhang and Nicos Makris. March 2001.
- PEER 2001/01** *Experimental Study of Large Seismic Steel Beam-to-Column Connections.* Egor P. Popov and Shakhzod M. Takhirov. November 2000.
- PEER 2000/10** *The Second U.S.-Japan Workshop on Performance-Based Earthquake Engineering Methodology for Reinforced Concrete Building Structures.* March 2000.
- PEER 2000/09** *Structural Engineering Reconnaissance of the August 17, 1999 Earthquake: Kocaeli (Izmit), Turkey.* Halil Sezen, Kenneth J. Elwood, Andrew S. Whittaker, Khalid Mosalam, John J. Wallace, and John F. Stanton. December 2000.
- PEER 2000/08** *Behavior of Reinforced Concrete Bridge Columns Having Varying Aspect Ratios and Varying Lengths of Confinement.* Anthony J. Calderone, Dawn E. Lehman, and Jack P. Moehle. January 2001.
- PEER 2000/07** *Cover-Plate and Flange-Plate Reinforced Steel Moment-Resisting Connections.* Taejin Kim, Andrew S. Whittaker, Amir S. Gilani, Vitelmo V. Bertero, and Shakhzod M. Takhirov. September 2000.
- PEER 2000/06** *Seismic Evaluation and Analysis of 230-kV Disconnect Switches.* Amir S. J. Gilani, Andrew S. Whittaker, Gregory L. Fenves, Chun-Hao Chen, Henry Ho, and Eric Fujisaki. July 2000.
- PEER 2000/05** *Performance-Based Evaluation of Exterior Reinforced Concrete Building Joints for Seismic Excitation.* Chandra Clyde, Chris P. Pantelides, and Lawrence D. Reaveley. July 2000.
- PEER 2000/04** *An Evaluation of Seismic Energy Demand: An Attenuation Approach.* Chung-Che Chou and Chia-Ming Uang. July 1999.
- PEER 2000/03** *Framing Earthquake Retrofitting Decisions: The Case of Hillside Homes in Los Angeles.* Detlof von Winterfeldt, Nels Roselund, and Alicia Kitsuse. March 2000.
- PEER 2000/02** *U.S.-Japan Workshop on the Effects of Near-Field Earthquake Shaking.* Andrew Whittaker, ed. July 2000.
- PEER 2000/01** *Further Studies on Seismic Interaction in Interconnected Electrical Substation Equipment.* Armen Der Kiureghian, Kee-Jeung Hong, and Jerome L. Sackman. November 1999.
- PEER 1999/14** *Seismic Evaluation and Retrofit of 230-kV Porcelain Transformer Bushings.* Amir S. Gilani, Andrew S. Whittaker, Gregory L. Fenves, and Eric Fujisaki. December 1999.
- PEER 1999/13** *Building Vulnerability Studies: Modeling and Evaluation of Tilt-up and Steel Reinforced Concrete Buildings.* John W. Wallace, Jonathan P. Stewart, and Andrew S. Whittaker, editors. December 1999.
- PEER 1999/12** *Rehabilitation of Nonductile RC Frame Building Using Encasement Plates and Energy-Dissipating Devices.* Mehrdad Sasani, Vitelmo V. Bertero, James C. Anderson. December 1999.
- PEER 1999/11** *Performance Evaluation Database for Concrete Bridge Components and Systems under Simulated Seismic Loads.* Yael D. Hose and Frieder Seible. November 1999.
- PEER 1999/10** *U.S.-Japan Workshop on Performance-Based Earthquake Engineering Methodology for Reinforced Concrete Building Structures.* December 1999.
- PEER 1999/09** *Performance Improvement of Long Period Building Structures Subjected to Severe Pulse-Type Ground Motions.* James C. Anderson, Vitelmo V. Bertero, and Raul Bertero. October 1999.
- PEER 1999/08** *Envelopes for Seismic Response Vectors.* Charles Menun and Armen Der Kiureghian. July 1999.
- PEER 1999/07** *Documentation of Strengths and Weaknesses of Current Computer Analysis Methods for Seismic Performance of Reinforced Concrete Members.* William F. Cofer. November 1999.
- PEER 1999/06** *Rocking Response and Overturning of Anchored Equipment under Seismic Excitations.* Nicos Makris and Jian Zhang. November 1999.
- PEER 1999/05** *Seismic Evaluation of 550 kV Porcelain Transformer Bushings.* Amir S. Gilani, Andrew S. Whittaker, Gregory L. Fenves, and Eric Fujisaki. October 1999.
- PEER 1999/04** *Adoption and Enforcement of Earthquake Risk-Reduction Measures.* Peter J. May, Raymond J. Burby, T. Jens Feeley, and Robert Wood.
- PEER 1999/03** *Task 3 Characterization of Site Response General Site Categories.* Adrian Rodriguez-Marek, Jonathan D. Bray, and Norman Abrahamson. February 1999.

- PEER 1999/02** *Capacity-Demand-Diagram Methods for Estimating Seismic Deformation of Inelastic Structures: SDF Systems.* Anil K. Chopra and Rakesh Goel. April 1999.
- PEER 1999/01** *Interaction in Interconnected Electrical Substation Equipment Subjected to Earthquake Ground Motions.* Armen Der Kiureghian, Jerome L. Sackman, and Kee-Jeung Hong. February 1999.
- PEER 1998/08** *Behavior and Failure Analysis of a Multiple-Frame Highway Bridge in the 1994 Northridge Earthquake.* Gregory L. Fenves and Michael Ellery. December 1998.
- PEER 1998/07** *Empirical Evaluation of Inertial Soil-Structure Interaction Effects.* Jonathan P. Stewart, Raymond B. Seed, and Gregory L. Fenves. November 1998.
- PEER 1998/06** *Effect of Damping Mechanisms on the Response of Seismic Isolated Structures.* Nicos Makris and Shih-Po Chang. November 1998.
- PEER 1998/05** *Rocking Response and Overturning of Equipment under Horizontal Pulse-Type Motions.* Nicos Makris and Yiannis Roussos. October 1998.
- PEER 1998/04** *Pacific Earthquake Engineering Research Invitational Workshop Proceedings, May 14–15, 1998: Defining the Links between Planning, Policy Analysis, Economics and Earthquake Engineering.* Mary Comerio and Peter Gordon. September 1998.
- PEER 1998/03** *Repair/Upgrade Procedures for Welded Beam to Column Connections.* James C. Anderson and Xiaojing Duan. May 1998.
- PEER 1998/02** *Seismic Evaluation of 196 kV Porcelain Transformer Bushings.* Amir S. Gilani, Juan W. Chavez, Gregory L. Fenves, and Andrew S. Whittaker. May 1998.
- PEER 1998/01** *Seismic Performance of Well-Confined Concrete Bridge Columns.* Dawn E. Lehman and Jack P. Moehle. December 2000.